

THE BELL SYSTEM TECHNICAL JOURNAL

DEVOTED TO THE SCIENTIFIC AND ENGINEERING
ASPECTS OF ELECTRICAL COMMUNICATION

Volume 50

December 1971

Number 10

Copyright © 1971, American Telephone and Telegraph Company. Printed in U.S.A.

Statistics of a General Class of Avalanche Detectors With Applications to Optical Communication

By S. D. PERSONICK

(Manuscript received June 29, 1971)

Previous results on the statistics of avalanche detectors are generalized to the case where electrons and holes suffer collision ionizations with unequal probability. It is assumed here that the ratio of collision ionization probabilities per unit length of weaker-to-stronger carrier is a constant k independent of position in the high-field region. The moment-generating function of the random avalanche gain G is obtained as a function of k and the average gain \bar{G} , and is used to obtain Chernov bounds on error rates of digital optical receivers employing avalanche detectors. It is shown the required energy per pulse to achieve a given error rate decreases as k decreases for fixed \bar{G} . For each $k > 0$, there is an optimal mean gain \bar{G}_{opt} resulting in minimum required energy per pulse. At $k = 0.1$, $\bar{G}_{opt} \approx 100$ and the required energy is within 10 dB of that required with very high gains (a few thousand) at $k = 0$.

I. INTRODUCTION

In a previous paper¹ results on the statistics of two particular avalanche detectors with applications to optical communication were

presented. It was required either that only one carrier suffer collision ionizations in the high-field region (unilateral gain) or that both carriers suffer collision ionizations with equal probability per unit length in the high-field region. The present work allows for more general unequal ionization probabilities per unit length with the requirement only that the ratio of the two quantities be constant throughout the high-field region. The moment-generating function of the random gain is obtained as a function of this ratio and the average gain. The results are consistent with unpublished conjectures of R. J. McIntyre.² The moment-generating functions are used to obtain Chernov bounds on the error rates of digital optical receivers employing avalanche detectors and using either coherent or incoherent light. Results on avalanche statistics are summarized in Section V. Numerical results on the Chernov bounds are given in Section VI (6.5) and Section VII.

II. MODEL OF THE AVALANCHE DETECTOR

The avalanche detector is a device in which thermally or optically generated hole-electron pairs generate additional hole-electron pairs through collision ionizations. Within the device there is a "high-field region" where holes have probability $\beta(x)$ per unit length (which depends

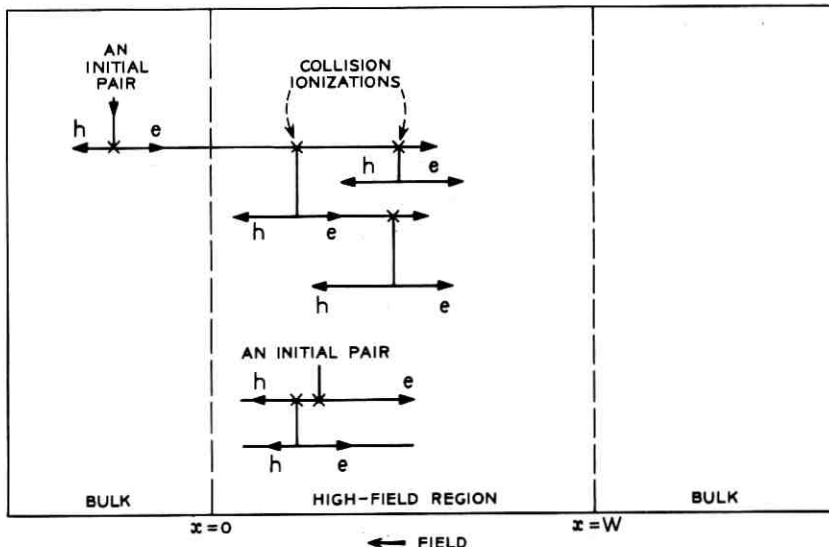


Fig. 1—Avalanche detector.

upon the position x) of suffering a collision ionization as they travel to the left under the influence of the electron field (see Fig. 1). Electrons traveling to the right have a probability $\alpha(x)$ per unit length of collision ionization. Carriers can be created within the high-field region due to thermal effects or due to the presence of incident light. Carriers can also drift into the region if they are generated outside of the region. It is assumed that all collision ionizations are independent. This requires that the mean distance between ionizing collisions be large compared to the distance over which a carrier can randomize its momentum after a collision.³ Hole-electron pairs created through collision ionization can in turn generate additional pairs by the same mechanism. This is the avalanche process.

III. THE STATISTICS

We seek the statistics of the random total number of hole-electron pairs which result ultimately through collision ionizations when an initial hole-electron pair is injected into the high field at some position x . Define $p_v(n, x)$ as the probability that n pairs ultimately result including the initially injected pair. The moment-generating function of the number of pairs $M_v(s)$ is therefore⁴

$$M_v(s, x) = \sum_1^{\infty} p_v(n, x) e^{sn}. \quad (1)$$

We shall derive $M_v(s, x)$. Before proceeding we must review some well known results which will be needed in that derivation.

If $\{x_i\}$ are random variables which are independent, then the moment-generating function of the sum of the $\{x_i\}$ is the product of the individual moment-generating functions.⁴ The semi-invariant moment-generating function SIMGF of a random variable X having probability density $p_X(x)$ is the natural logarithm of the moment-generating function of X

$$\psi_X(s) \equiv \ln [M_X(s)] = \ln \left[\sum_{-\infty}^{\infty} p_X(x) e^{sx} \right]. \quad (2)$$

The SIMGF of a sum of n independent random variables is the sum of the individual SIMGF's.

We can now proceed to derive $M_v(s, x)$. Divide the high-field region into K intervals of width $dX = W/K$. See Fig. 2. Label these intervals 1, 2, 3, ..., j , ..., K . If a hole-electron pair is injected into interval j , define, as above, the probability density of the total number of pairs ultimately resulting in the avalanche process (including the initial pair)

as $p_g(n, x)$ where x is taken as the center of interval j . The hole of the initial pair moves to the left and the electron to the right toward $x = 0$ or $x = W$ respectively. As they pass through their respective intervals, new pairs may be created in each through collision ionization. We shall assume that the interval width dX is sufficiently narrow so that the initial pair carriers create either one or no new pairs in each interval. If the initial hole or electron generates a new pair in some interval k , then that new pair will ultimately generate N_k pairs including itself through the avalanche process. Thus with each interval we can associate a number of pairs N_k . This number equals zero if the appropriate initial pair carrier suffers no collision ionizations in interval k . This number equals one or more if the appropriate initial pair carrier suffers a collision ionization in interval k . The total number of pairs ultimately generated through the avalanche process including the initial pair is one plus the sum of the $\{N_k\}$. Since collision ionizations are all independent, all the N_k are independent. Thus we have the SIMGF of the total number of pairs given by

$$\psi_g(s, x) = s + \sum_{k=1}^{W/dX} \psi_{N_k}(s) \quad (3)$$

where s is the SIMGF of the deterministic initial pair and $\psi_{N_k}(s)$ is the SIMGF of N_k .

The SIMGF of N_k is obtained as follows. The probability that

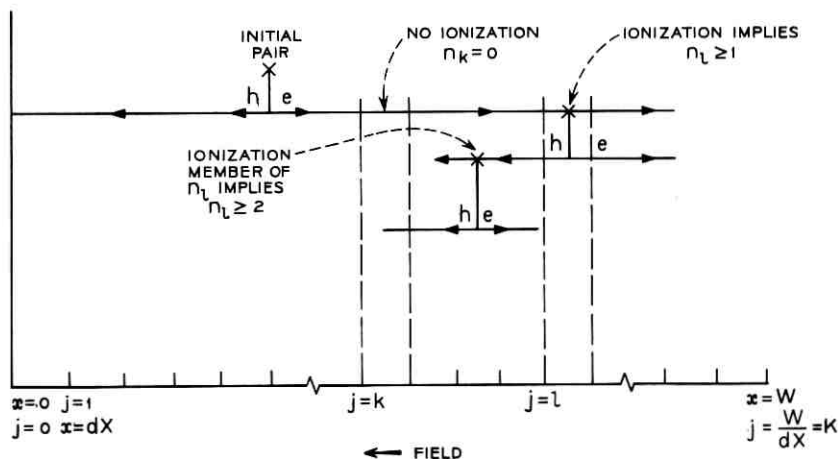


Fig. 2—Avalanche process.

$N_k = 0$ is $1 - \gamma dX$ where $\gamma = \alpha(x)$ if interval k is to the right of interval j where the initial pair enters, $\gamma = \beta(x)$ if k is to the left of j . (x is evaluated at the center of interval k .) The probability that $N_k = Z > 0$ is the probability of a collision ionization in interval k times the probability that a new pair created at interval k ultimately results in Z pairs including itself. That is

$$\Pr(N_k = Z) = \gamma dX p_\nu(Z, x) \quad \text{for } Z > 0 \quad (4)$$

with x evaluated at the center of interval k . Thus

$$\begin{aligned} \psi_{N_k}(s) &= \ln \left[\sum_{Z=0}^{\infty} \Pr(N_k = Z) e^{sZ} \right] \\ &= \ln \left[(1 - \gamma dX) e^{s^0} + \sum_{Z=1}^{\infty} \gamma dX p_\nu(Z, x) e^{sZ} \right] \\ &= \ln [1 - \gamma dX + \gamma dX M_\nu(s, x)] \\ &= \ln [1 - \gamma dX + \gamma dX e^{\psi_\nu(s, x)}] \end{aligned} \quad (5)$$

where

$$\gamma = \alpha(x) \quad \text{if } k > j$$

$$\gamma = \beta(x) \quad \text{if } k < j$$

x = center of interval k .

Using (3) and (5) and taking the limit as dX gets infinitely small, one obtains

$$\begin{aligned} \psi_\nu(s, x) &= s + \int_0^x \beta(x') [e^{\psi_\nu(s, x')} - 1] dx' \\ &\quad + \int_x^w \alpha(x') (e^{\psi_\nu(s, x')} - 1) dx'. \end{aligned} \quad (6)$$

Equation (6) is the critical equation for determining $\psi_\nu(s, x)$, and thus $M_\nu(s, x) = \exp[\psi_\nu(s, x)]$. Using Leibnitz's rule for differentiation of integrals one obtains

$$\frac{\partial}{\partial x} \psi_\nu(s, x) = [\beta(x) - \alpha(x)] (e^{\psi_\nu(s, x)} - 1). \quad (7)$$

The solution of (7) is

$$\psi_\nu(s, x) = \ln \left[\frac{1}{1 - C \exp \left(\int_0^x [\beta(x') - \alpha(x')] dx' \right)} \right] \quad (8)$$

where $C = (e^{\psi_0(s,0)} - 1)/e^{\psi_0(s,0)}$ which can be checked by substitution.

Substituting (8) into (6) one obtains the particular result

$$\psi_0(s, 0)$$

$$= s + \int_0^W \alpha(x') \left[\frac{1}{1 - C \exp \left(\int_0^{x'} [\beta(x'') - \alpha(x'')] dx'' \right)} - 1 \right] dx'. \quad (9)$$

If one makes the *assumption*³ that at each point in the high-field region

$$\beta(x) = k \cdot \alpha(x) \quad (10)$$

where k is a constant, one can solve (9) to obtain

$$\begin{aligned} \psi_0(s, 0) &= s - \delta + \frac{1}{k-1} \ln \left[\frac{e^{(k-1)\delta}}{M_0(s, 0) - e^{(k-1)\delta}[M_0(s, 0) - 1]} \right] \\ &= s + \frac{1}{1-k} \ln [M_0(s, 0) - e^{(k-1)\delta}[M_0(s, 0) - 1]] \end{aligned} \quad (11)$$

where

$$M_0(s, 0) = e^{\psi_0(s, 0)} \quad \text{and} \quad \delta = \int_0^W \alpha(x) dx.$$

One can write (11) in another way by making a substitution.* Define $\delta'(s)$ implicitly by

$$e^{\delta'(s)} = M_0(s, 0) e^{\delta-s}, \quad (12)$$

that is,

$$e^{\psi_0(s, 0)} = M_0(s, 0) = e^{s-\delta+\delta'(s)}. \quad (13)$$

Using (12) in (11) one obtains the implicit equation

$$e^{-k\delta'(s)} - e^{-\delta'(s)} = e^s [e^{-k\delta} - e^{-\delta}] \quad (14)$$

which determines $\delta'(s)$ and thus $M_0(s, 0)$ through (13).

Equation (14) is still not explicit. A numerical technique for solution is discussed in the next section. One can use (11) [or (14)] and (8) to obtain $\psi_0(s, x)$ or $M_0(s, x)$ for any x . Recall that x is the point of entry of the initial pair. In the applications we shall be concerned with $x = 0$ or $x = W$. That is, pairs are generated in a drift region outside the high-field region with carriers drifting into the high-field region.

* Equation (14) will follow from (11) and (12) by tedious algebra. Further, (14) will not be used in the following results except to compare with McIntyre's work in Appendix A.

The equation (14) is consistent with some unpublished conjectures of McIntyre given in Appendix A.

IV. NUMERICAL SOLUTIONS

Equations (11) through (14) can be solved numerically. One technique is to differentiate (11) to obtain the result

$$\frac{\partial}{\partial s} M_\nu(s, 0) = M_\nu(s, 0) \left(\frac{k-1}{k} \right) \left[1 - \frac{1}{k} (M_\nu(s, 0) e^{-s} e^\delta)^{k-1} \right]^{-1} \quad (15)$$

where $M_\nu(0, 0) = 1$.

Equation (15) can be integrated with a computer to obtain $M_\nu(s, 0)$ explicitly.

V. SUMMARY OF ANALYTIC RESULTS ON AVALANCHE STATISTICS

From Sections I through IV and a previous paper by this author,¹ we obtained the following:

Assumptions:

Holes travel toward $x = 0$, electrons toward $x = W$.

Hole ionization probability per unit length = $\beta(x)$.

Electron ionization probability per unit length = $\alpha(x)$.

$\beta(x) = k \cdot \alpha(x)$, k a constant for all x .

High-field region width = W .

Definitions:

$$\delta \equiv \int_0^W \alpha(x) dx,$$

$p_\nu(n, x)$ = probability that if an initial pair enters the high-field region at point x , n pairs will ultimately result through the avalanche process including the initial pair,

$$\tilde{G}(x) = \text{mean avalanche gain} = \sum_1^\infty n p_\nu(n, x),$$

$M_\nu(s, x) \equiv$ moment-generating function of $p_\nu(n, x)$

$$= \sum_{n=1}^\infty p_\nu(n, x) e^{sn}.$$

Results:

$$1. M_v(s, x) = \left[1 - \frac{(M_v(s, 0) - 1)}{M_v(s, 0)} \exp \left[(k - 1) \int_0^x \alpha(x') dx' \right] \right]^{-1} \quad \text{for all } k. \quad (16)$$

For $k = 0$ (Unilateral Gain)

$$2a. M_v(s, 0) = [1 - e^\delta [1 - e^{-s}]]^{-1} \quad \text{where} \quad \tilde{G}(0) = e^\delta. \quad (17)$$

$$2b. p_v(n, 0) = \frac{1}{G} \left(\frac{G - 1}{G} \right)^{n-1} \quad \text{where} \quad G = \tilde{G}(0). \quad (18)$$

For $k \neq 0, k \neq 1$

$$3. \frac{\partial}{\partial s} M_v(s, 0) = M_v(s, 0) \left(\frac{k-1}{k} \right) \left[1 - \frac{1}{k} (M_v(s, 0) e^{-s} e^\delta)^{k-1} \right]^{-1},$$

where

$$M_v(0, 0) = 1 \quad (19)$$

where

$$\tilde{G}(0) = \left(\frac{k-1}{k} \right) \left[1 - \frac{1}{k} e^{\delta(k-1)} \right]^{-1}.$$

For $k = 1$ (Equal Ionization)

$$4. \frac{\partial}{\partial s} M_v(s, 0) = M_v(s, 0) \left[1 - \left(\frac{G-1}{G} \right) M_v(s, 0) \right]^{-1}$$

$$M_v(0, 0) = 1$$

where

$$G = \tilde{G}(0). \quad (20)$$

VI. APPLICATIONS TO RECEIVERS USING AVALANCHE DETECTORS

6.1 General Comments

We shall next apply the results of Section V to obtain bounds on the error rates of digital receivers. The receivers to be discussed here are the single- and twin-channel systems described below. We shall upper-bound the power required at the receiver to obtain a desired error rate using the Chernov bounds.

6.2 The Receivers

The twin-channel receiver is shown in Fig. 3. Depending on the state of a binary information source, one of two channels has optical output

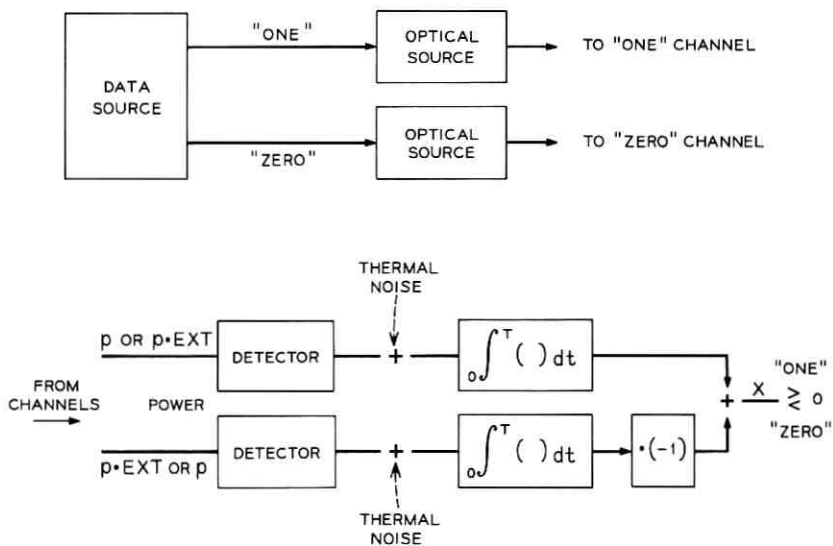


Fig. 3—Twin-channel system.

power p for duration T while the other has output power $p \cdot EXT$ for duration T . EXT signifies extinction. EXT would ideally be zero, but is left finite and less than unity for practical reasons. The optical power falling on an avalanche photo diode causes the emission of photo-electrons which are multiplied along with the detector "dark current" through the avalanche gain mechanism. The detector outputs (multiplied counts) are integrated in devices having thermal noises referred to their respective inputs. The integrator outputs are subtracted and the difference X is compared to a threshold of zero to decide what the information state was.

The single-channel system is essentially half the twin-channel system as shown in Fig. 4. The single integrator output X is compared to a threshold γ to decide upon the information state.

6.3 The Chernov Bounds

The Chernov bound is a useful tool for bounding the probability that a random variable X will lie above or below a given threshold γ . It is given as follows⁵

$$\Pr(X > \gamma) \leq e^{\psi_X(s) - s\psi'_X(s)} \Big|_{\gamma = \psi'_X(s)}$$

provided $s > 0$,

$$\Pr(X < \gamma) \leq e^{\psi_x(s) - s\psi'_x(s)} \Big|_{\gamma = \psi'_x(s)}$$

provided $s < 0$, (21)

where

$$\psi_x(s) = \text{SIMGF of } X \equiv \ln \left[\int_{-\infty}^{\infty} p_x(x) e^{sx} dx \right]$$

and

$$\psi'_x(s) = \frac{\partial}{\partial s} \psi_x(s).$$

6.4 Chernov Bounds for the Two Systems

6.4.1 Preliminaries

We wish to determine the required power p to achieve a desired decision error probability for each of the receivers discussed in Section 6.2 with various types of detectors and various values of other system parameters such as dark current and thermal noise in the integrators. To apply the Chernov bounds we will need the SIMGF's of the variables X at the outputs of the receivers. (See Figs. 3 and 4.)

An important result needed here is the following:

Lemma: If C is integer-valued and greater than or equal to zero; and if $U = \sum_i^C g_i$, where the g_i are independent, identically distributed random variables (that is, each "count" produced by the C process independently



POWER = p OR $p \cdot \text{EXT}$

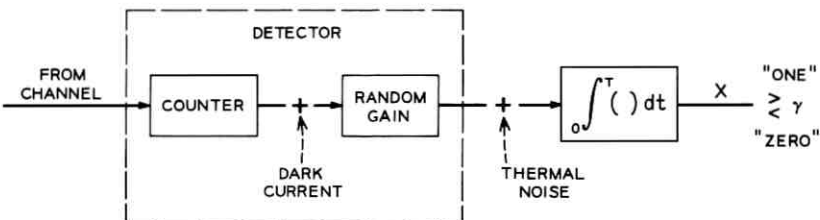


Fig. 4—Single-channel system.

generates g_i contributions to the U process through some gain mechanism); then the SIMGF of U is¹

$$\psi_U(s) = \psi_c(\psi_g(s)) \quad (22)$$

where $\psi_g(s)$ is the SIMGF of the identically distributed random variables g_i .

One can model an avalanche photodiode as a photon counter followed by a random avalanche multiplier. Each photon counter output "count" produces a random number of "counts" at the multiplier output. Thus, since we know from Section V the SIMGF of a random multiplier which corresponds to $\psi_g(s)$ in (22), and since we seek the SIMGF of the photodiode output which corresponds to $\psi_U(s)$ in (22), it follows that we need the SIMGF of the number of counts emitted by a photon counter with light incident upon it, which corresponds to $\psi_c(s)$ in (22).

6.4.2 Photon Counter Statistics

6.4.2.1 Coherent Light. If the light incident upon the photon counter is coherent, then it is well known that the SIMGF of the total counts emitted in an interval T is given by⁶ (see Appendix B)

$$\psi_c(s) = [LAMSIG + LAMD] [e^s - 1] \quad (23)$$

where

$LAMSIG$ = Total incident light energy $\cdot \eta/\hbar\Omega$

η = Detector quantum efficiency

$\hbar\Omega$ = Energy of photon at optical frequency used

$LAMD$ = Mean number of dark current counts before avalanche gain in an interval T .

6.4.2.2 Incoherent Light. If the incident light is incoherent with H independent spatial-temporal "degrees of freedom," then the SIMGF of the total counts emitted by the photon counter in interval T is (see Appendix B)

$$\psi_c = LAMD[e^s - 1] + \ln \left[\left[1 - \frac{LAMSIG}{H} (e^s - 1) \right]^{-H} \right] \quad (24)$$

where $LAMSIG$ is the average total incident energy times $\eta/\hbar\Omega$. Clearly (24) is the same as (23) as H approaches infinity, which is a well known result.

6.4.3 Final Calculations

6.4.3.1 Twin-Channel System. Since, for the twin-channel receiver, X consists of the difference of two random integrator outputs, we need

the following well known result.⁴ If $X = X_1 - X_2$, and if X_1 and X_2 are independent, then the SIMGF of X is

$$\psi_x(s) = \psi_{x_1}(s) + \psi_{x_2}(-s). \quad (25)$$

Each integrator output contains the sum of the counts emitted by its detector and the integral of its thermal noise. The SIMGF of the random variable N obtained when Gaussian thermal noise spectral height N_0 is integrated over an interval T is well known to be

$$\psi_N(s) = \frac{s^2}{2} N_0 T. \quad (26)$$

Using (22) through (26) we obtain for the SIMGF of the twin-channel receiver output X when the information is in state "one", and the optical source is coherent,

$$\begin{aligned} \psi_x(s) = s^2 N_0 T &+ \left[\frac{p \cdot T \cdot \eta}{\hbar \Omega} + LAMD \right] [M_\sigma(s) - 1] \\ &+ \left[\frac{p \cdot T \cdot EXT \cdot \eta}{\hbar \Omega} + LAMD \right] [M_\sigma(-s) - 1] \end{aligned} \quad (27)$$

where

$LAMD$ = mean number of dark current counts before avalanche gain in an interval T

N_0 = spectral height of the thermal noises referred to the integrator inputs.

$M_\sigma(s)$ is obtained from (16) through (20) depending upon the particular gain mechanism. If the optical source is incoherent, we have

$$\begin{aligned} \psi_x(s) = s^2 N_0 T &+ LAMD[M_\sigma(s) + M_\sigma(-s) - 2] \\ &+ \ln \left[\left[1 - \frac{p \cdot T \cdot \eta}{H \hbar \Omega} [M_\sigma(s) - 1] \right]^{-H} \right] \\ &+ \ln \left[\left[1 - \frac{p \cdot T \cdot EXT \cdot \eta}{H \hbar \Omega} [M_\sigma(-s) - 1] \right]^{-H} \right]. \end{aligned} \quad (28)$$

We seek the probability that when the information is in state "one", X is less than zero, and we therefore decide that the information state was "zero." That is, we seek the error probability. One can use (27) or (28) and the Chernov bound of (21) to determine the required value of $LAMSIG \equiv p \cdot T \cdot \eta / (\hbar \Omega)$ to achieve a desired error probability. Since the twin-channel receiver is symmetric, the error probability

when the information is in state "zero" is the same as when it is in state "one."

6.4.3.2 Single-Channel System. For the single-channel receiver, we need the SIMGF of X under both information states. Call X_1 the random variable X when the information is in the state "one." Call X_0 the random variable X when the information is in state zero. Using results of Section 6.4, one obtains for coherent light

$$\begin{aligned}\psi_{X_1}(s) &= \frac{s^2 N_0 T}{2} + \left[LAMD + \frac{p \cdot T \cdot \eta}{\hbar \Omega} \right] [M_\sigma(s) - 1] \\ \psi_{X_0}(s) &= \frac{s^2 N_0}{2} + \left[LAMD + \frac{p \cdot T \cdot EXT \cdot \eta}{\hbar \Omega} \right] [M_\sigma(s) - 1].\end{aligned}\quad (29)$$

For incoherent light

$$\begin{aligned}\psi_{X_1}(s) &= \frac{s^2 N_0 T}{2} + LAMD [M_\sigma(s) - 1] \\ &\quad + \ln \left[\left[1 - \frac{p \cdot T \cdot \eta}{H \hbar \Omega} [M_\sigma(s) - 1] \right]^{-H} \right] \\ \psi_{X_0}(s) &= \frac{s^2 N_0}{2} + LAMD [M_\sigma(s) - 1] \\ &\quad + \ln \left[\left[1 - \frac{p \cdot T \cdot EXT \cdot \eta}{H \cdot \hbar \Omega} [M_\sigma(s) - 1] \right]^{-H} \right].\end{aligned}\quad (30)$$

One can then use the results of (29) and (30) along with the Chernov bounds of (21) to simultaneously find values of $LAMSIG = p \cdot T \cdot \eta / (\hbar \Omega)$ and the threshold γ (see Fig. 4) to ensure some desired error probability (which for convenience here will be the same for either information state).

6.5 Numerical Results

The Chernov bounds described above were evaluated numerically. The results are displayed on the attached figures described below. The range of parameter values is realistic and practical, to the best of this author's knowledge. The curves presented are those deemed most interesting by the author. Other calculations can of course be made. Parameters used are defined as follows:^{*}

$LAMSIG$ = Required mean number of detected photons per pulse in the "on" channel of the twin-channel

* SIG , EXT , G , K , H , and $LAMD$ are input parameters to the program which calculates $LAMSIG$ for a desired error rate.

receiver or in the "one" state of the single-channel receiver.

LAMSIG-EXT = Mean number of detected counts per pulse in the "off" channel of the twin-channel receiver or in the "zero" state of the single-channel receiver.

SIG = Normalized thermal noise standard deviation

$$= \{4k\theta T/[R e^2]\}^{\frac{1}{2}} = \{4k\theta C/e^2\}^{\frac{1}{2}}$$

where e = electron charge, $k\theta$ = Boltzmann's constant · absolute temperature, R = equivalent noise resistance at integrator input, T = pulse duration, $C = T/R$ = integrator equivalent input capacitance. For the results to follow, a reasonable value of *SIG* was chosen to be 6000.

G = Mean avalanche gain.

H = Temporal-spatial diversity for incoherent carrier case.

k = Ratio of ionization probability per unit length of weaker and stronger ionizing carriers.*

LAMD = Dark current counts per interval T before avalanche gain.

Fig. 5

LAMSIG vs *G* is plotted for the twin-channel case with *k* as parameter. *SIG* was set at 6000, the error rate is 10^{-9} , *LAMD* was set at 5 counts and *EXT* = 0.01. *H* = 10,000 which is equivalent to assuming a coherent carrier.

Fig. 6

The value at optimal gain of *LAMSIG* vs *k* is plotted. Points are tagged with the optimal *G*. The receiver is a twin-channel system with *SIG* = 6000, *EXT* = 0.01, *LAMD* = 5. *H* is 10,000 which is equivalent to assuming a coherent carrier. The error rate is 10^{-9} .

Fig. 7

LAMSIG vs *G* is plotted for two values of error rate 10^{-9} and 10^{-5} for

* For these calculations it was assumed that the detector is designed so that the stronger ionizing carriers generated optically or associated with dark current enter the high-field region from a drift region outside the high-field region. This corresponds to initial pairs entering the gain mechanism of $x = 0$ or $x = W$ as discussed in Section III.

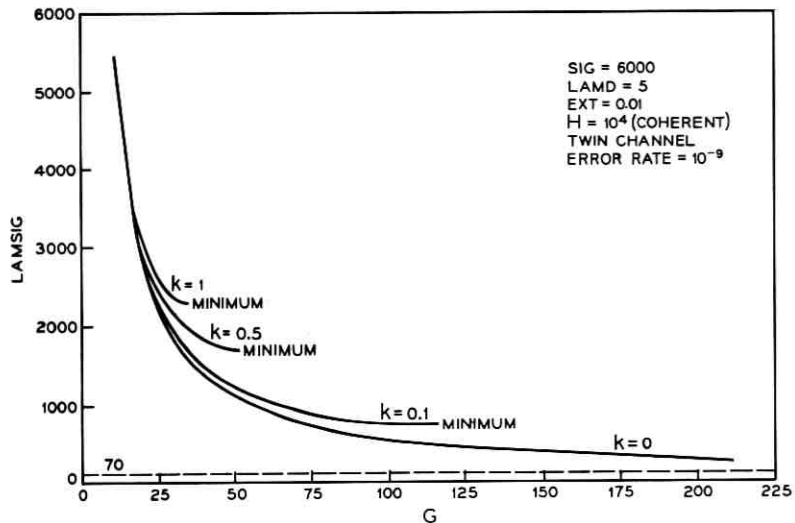
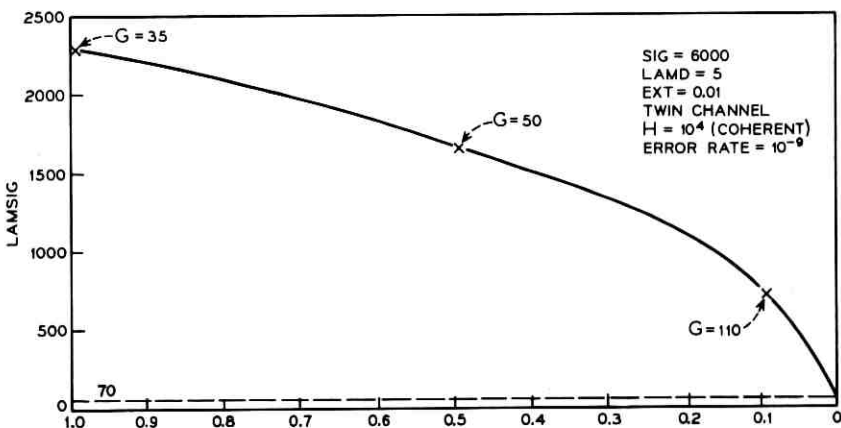


Fig. 5—LAMSIG versus gain.

Fig. 6—LAMSIG at optimal gain versus k .

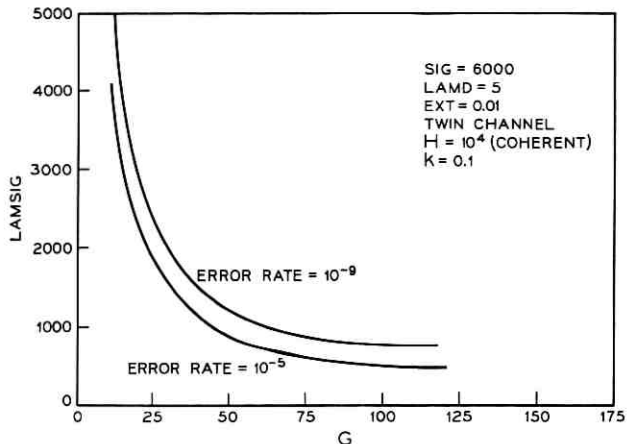


Fig. 7—LAMSIG versus gain.

a twin-channel system with $SIG = 6000$, $EXT = 0.01$, $H = 10,000$ $LAMD = 5$, $k = 0.1$.

Fig. 8

Single- and twin-channel systems are compared. $LAMSIG$ vs G is plotted for $SIG = 6000$, $EXT = 0.01$, $LAMD = 5$, $H = 10,000$, error rate = 10^{-9} , $k = 0$. Note that from an average power viewpoint the single-channel system is 3 dB better than shown if the binary information source is random, since $LAMSIG$ is the energy in "one" state.

Fig. 9

Same as Fig. 8 except $k = 1$. Note the scale change.

Fig. 10

$LAMSIG$ vs G for $H = 100$ and $H = 10,000$ for twin-channel system. $SIG = 6000$, $EXT = 0.01$, $LAMD = 5$, $k = 0$, error rate = 10^{-9} .

6.6 Further Comments

When systems were investigated for sensitivity to the choice $LAMD = 5$, $EXT = 0.01$, it was found that insignificant changes in $LAMSIG$ vs G occurred when various combinations of $LAMD = 5$ or 50, $EXT = 0.01$ or 0.001 were tried.

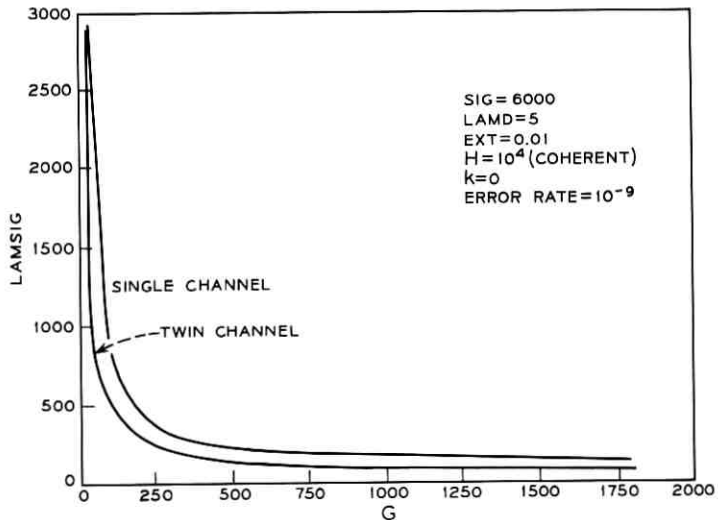


Fig. 8—LAMSIG versus gain.

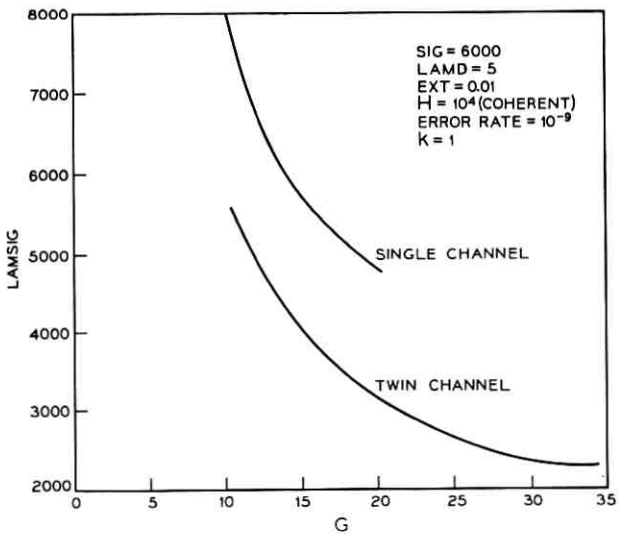


Fig. 9—LAMSIG versus gain.

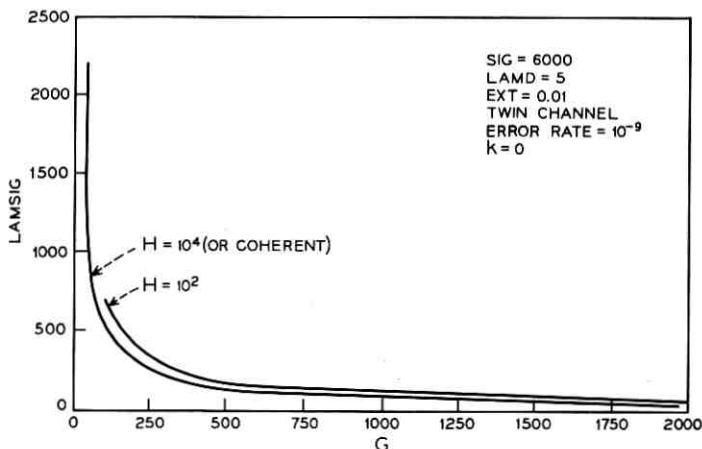


Fig. 10—LAMSIG versus gain.

VII. CONCLUSIONS ON APPLICATIONS

If one assumes that the Chernov bounds are sufficiently tight so that actual energy required per bit to achieve specified error rates can be compared for various system parameters by comparing the bounds,* then one can conclude the following.

- (i) Define k as the ratio of the collision ionization probabilities per unit length of the weaker-ionizing to the stronger-ionizing carrier (carriers are of course holes and electrons). Assume that the detector is designed "well" such that optically and thermally generated carriers enter the high-field region from a drift region outside. From the bounds, one obtains the result that the required energy per pulse to achieve a desired error rate decreases as k decreases for fixed average avalanche gain. A value $k = 0$ is best; but a value $k = 0.1$ will allow one to operate with energy within 10 dB of that required at very high gains with a $k = 0$ device. For each value of k except zero there is an optimal gain resulting in minimum required energy per pulse. The optimal gain is larger for smaller k . At $k = 0.1$, the optimal gain is about 100. At $k = 0$, the optimal gain is infinite, but a gain of a few thousand allows

* For simple cases where both the bounds and actual energy requirements can be obtained (for instance for the $k = 0$ case) the two results differ by a few dB or less.

close to optimal required energy per pulse. One can conclude that a silicon device with $k = 0.1$ and a gain of about 100 would be a good choice for an optical detector. This is true since a detector with k less than 0.1 and yet having gain significantly higher than 100 is not available at this time.

(ii) The required energy per pulse for systems using incoherent optical sources differs from that for systems using coherent sources by less than a few dB provided the product of the source bandwidth and the pulse duration exceeds 100. This is true even if there is no spatial incoherence of the light at the detector.

(iii) For reasonable parameter values, and assuming a random information stream, the single-channel receiver requires about 1.5 dB less energy per pulse to achieve a desired error rate than the twin-channel receiver.

(iv) The required energy per pulse is insensitive to reasonable values of dark current and extinction ratios.

(v) For a particular system, a change in the desired error rate from 10^{-9} to 10^{-5} results in a change in the required energy per pulse of 1 to 3 dB, depending upon the avalanche gain. This shows that the required energy per pulse is fairly insensitive to the error rate. On the other hand, this means that poor error rates will result if insufficient loss margin is provided. That is, a small lowering of the received energy can greatly increase the error rate.

APPENDIX A

In an unpublished work, McIntyre conjectures (from special case calculations) that the probability density of the random gain, defined here as $p_o(n, 0)$ is given by

$$p_o(n, 0) = \frac{\Gamma\left(\frac{n}{1-k} + 1\right) e^{-\delta} (e^{-k\delta} - e^{-\delta})^{n-1}}{n! \Gamma\left(\frac{n}{1-k} + 2 - n\right)}$$

where k and δ are the same as in (10) through (13).

If one makes the assumption that the conjectured $p_o(n, 0)$ has sum over n normalized to unity for each value of k and for each δ , then one obtains the result of (14) by using the definition of the moment-generating function and the normalization property.

APPENDIX B

If light of *known* intensity falls upon a photon counter during an interval T , then the probability density of the total number of counts emitted is well known⁶ to be Poisson distributed as follows

$$p_c(n) = [\Lambda + LAMD]^n \frac{e^{-(LAMD+\Lambda)}}{n!}. \quad (31)$$

Where Λ^* is the total energy incident in the interval T times $\eta/\hbar\Omega$, $LAMD$ is the mean number of dark current counts per second times the interval T , and $\eta/\hbar\Omega$ is the detector quantum efficiency divided by the energy in a photon.

The moment-generating function of the distribution of (31) is given by

$$M_c(s) = \exp [[\Lambda + LAMD][e^s - 1]]. \quad (32)$$

If the incident light is a stochastic process, then the moment-generating function of the output count distribution is obtained by averaging (32) over the probability density of the stochastic total energy incident in the interval T

$$M_c(s) = \int_0^\infty \exp ([\Lambda + LAMD][e^s - 1]) p(\Lambda) d\Lambda. \quad (33)$$

An incoherent light field is normally taken to mean that the complex envelope of the classical field is a complex Gaussian random process. That is, such a field incident on the photon counter plane can be written as

$$\begin{aligned} E(\rho, t) &= \sqrt{2} \operatorname{re}\{\epsilon(\rho, t)e^{i\Omega t}\} \\ \rho &\in \text{counter plane} \\ t &\in (0, T) \end{aligned} \quad (34)$$

where $\epsilon(\rho, t)$ is a complex Gaussian random process.

If one expands $\epsilon(\rho, t)$ in its Karhunen-Loeve eigenfunctions,⁵ one obtains

$$\begin{aligned} \epsilon(\rho, t) &= \sum e_k \phi_k(\rho, t) \\ \rho &\in \text{counter plane} \\ t &\in (0, T) \end{aligned} \quad (35)$$

* In the text, Λ is called *LAMSIG*.

where

$$\int_{\text{counter plane}} \int_0^T \phi_k(\rho, t) \phi_i^*(\rho, t) d^2\rho dt = \delta_{k,i}$$

and the coefficients e_k are independent complex Gaussian random variables satisfying

$$\begin{aligned} \langle e_k e_j^* \rangle &= \gamma_k \delta_{k,j} \\ \langle e_k e_i \rangle &= 0. \end{aligned} \quad (36)$$

The energy incident upon the photon counter is

$$\frac{\hbar\Omega}{\eta} \Lambda = \int \epsilon(\rho, t) \epsilon^*(\rho, t) d^2\rho dt = \sum |e_k|^2. \quad (37)$$

If one assumes an equal distribution of average energy in roughly H "modes,"

$$\begin{aligned} \gamma_k &= \gamma, \quad 1 \leq k \leq H \\ &= 0, \quad k > H \end{aligned} \quad (38)$$

then it follows that from (33) and the complex Gaussian statistics of the e_k that

$$M_C(s) = \exp [LAMD(e^* - 1)] \cdot \left[1 - \frac{\eta}{\hbar\Omega} \gamma(e^* - 1) \right]^{-H}. \quad (39)$$

Assumption (38) implies that the energy of the incoherent light is roughly equally distributed in H degrees of freedom.

REFERENCES

1. Personick, S. D., "New Results on Avalanche Multiplication Statistics with Applications to Optical Detection," BSTJ, 50, No. 1 (January 1971), pp. 167-189.
2. McIntyre, R. J., unpublished work (see Appendix A).
3. McIntyre, R. J., "Multiplication Noise in Uniform Avalanche Diodes," IEEE Trans. Elec. Dev., ED-13, No. 1 (January 1966), pp. 164-168.
4. Davenport, W., and Root, W., *Random Signals and Noise*, New York: John Wiley & Sons, 1958.
5. Van Trees, H. L., *Detection Estimation and Modulation, I*, New York: John Wiley & Sons, 1967.
6. Glauber, R. J., *Quantum Optics and Electronics, Les Honches 1964*, Lecture Notes at Session of the Summer School of Theoretical Physics at the Univ. of Grenoble, Ed. De Witt, New York: Gordon and Breach, 1965, p. 64.

THE BELL SYSTEM TECHNICAL JOURNAL

DEVOTED TO THE SCIENTIFIC AND ENGINEERING
ASPECTS OF ELECTRICAL COMMUNICATION

Volume 50

December 1971

Number 10

Copyright © 1971, American Telephone and Telegraph Company. Printed in U.S.A.

Statistics of a General Class of Avalanche Detectors With Applications to Optical Communication

By S. D. PERSONICK

(Manuscript received June 29, 1971)

Previous results on the statistics of avalanche detectors are generalized to the case where electrons and holes suffer collision ionizations with unequal probability. It is assumed here that the ratio of collision ionization probabilities per unit length of weaker-to-stronger carrier is a constant k independent of position in the high-field region. The moment-generating function of the random avalanche gain G is obtained as a function of k and the average gain \bar{G} , and is used to obtain Chernov bounds on error rates of digital optical receivers employing avalanche detectors. It is shown the required energy per pulse to achieve a given error rate decreases as k decreases for fixed \bar{G} . For each $k > 0$, there is an optimal mean gain \bar{G}_{opt} resulting in minimum required energy per pulse. At $k = 0.1$, $\bar{G}_{opt} \approx 100$ and the required energy is within 10 dB of that required with very high gains (a few thousand) at $k = 0$.

I. INTRODUCTION

In a previous paper¹ results on the statistics of two particular avalanche detectors with applications to optical communication were

presented. It was required either that only one carrier suffer collision ionizations in the high-field region (unilateral gain) or that both carriers suffer collision ionizations with equal probability per unit length in the high-field region. The present work allows for more general unequal ionization probabilities per unit length with the requirement only that the ratio of the two quantities be constant throughout the high-field region. The moment-generating function of the random gain is obtained as a function of this ratio and the average gain. The results are consistent with unpublished conjectures of R. J. McIntyre.² The moment-generating functions are used to obtain Chernov bounds on the error rates of digital optical receivers employing avalanche detectors and using either coherent or incoherent light. Results on avalanche statistics are summarized in Section V. Numerical results on the Chernov bounds are given in Section VI (6.5) and Section VII.

II. MODEL OF THE AVALANCHE DETECTOR

The avalanche detector is a device in which thermally or optically generated hole-electron pairs generate additional hole-electron pairs through collision ionizations. Within the device there is a "high-field region" where holes have probability $\beta(x)$ per unit length (which depends

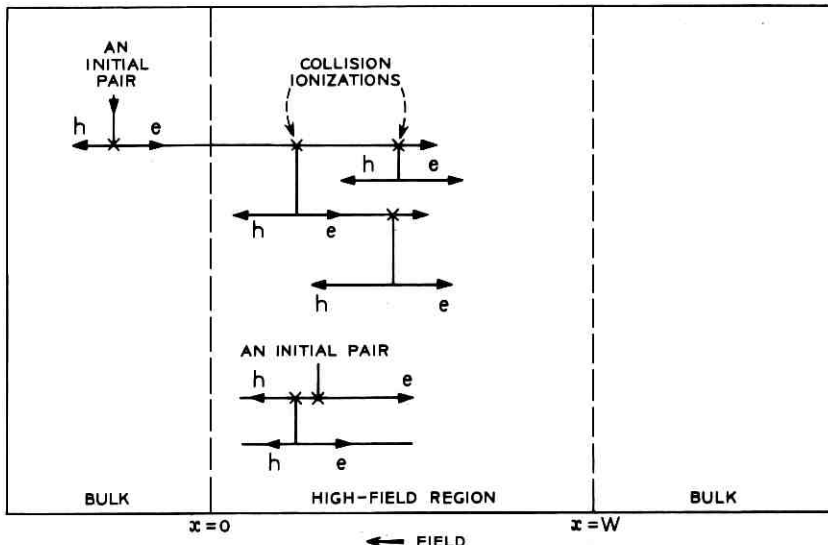


Fig. 1—Avalanche detector.

upon the position x) of suffering a collision ionization as they travel to the left under the influence of the electron field (see Fig. 1). Electrons traveling to the right have a probability $\alpha(x)$ per unit length of collision ionization. Carriers can be created within the high-field region due to thermal effects or due to the presence of incident light. Carriers can also drift into the region if they are generated outside of the region. It is assumed that all collision ionizations are independent. This requires that the mean distance between ionizing collisions be large compared to the distance over which a carrier can randomize its momentum after a collision.³ Hole-electron pairs created through collision ionization can in turn generate additional pairs by the same mechanism. This is the avalanche process.

III. THE STATISTICS

We seek the statistics of the random total number of hole-electron pairs which result ultimately through collision ionizations when an initial hole-electron pair is injected into the high field at some position x . Define $p_g(n, x)$ as the probability that n pairs ultimately result including the initially injected pair. The moment-generating function of the number of pairs $M_g(s)$ is therefore⁴

$$M_g(s, x) = \sum_1^{\infty} p_g(n, x) e^{sn}. \quad (1)$$

We shall derive $M_g(s, x)$. Before proceeding we must review some well known results which will be needed in that derivation.

If $\{x_i\}$ are random variables which are independent, then the moment-generating function of the sum of the $\{x_i\}$ is the product of the individual moment-generating functions.⁴ The semi-invariant moment-generating function SIMGF of a random variable X having probability density $p_X(x)$ is the natural logarithm of the moment-generating function of X

$$\psi_X(s) \equiv \ln [M_X(s)] = \ln \left[\sum_{-\infty}^{\infty} p_X(x) e^{sx} \right]. \quad (2)$$

The SIMGF of a sum of n independent random variables is the sum of the individual SIMGF's.

We can now proceed to derive $M_g(s, x)$. Divide the high-field region into K intervals of width $dX = W/K$. See Fig. 2. Label these intervals 1, 2, 3, ..., j , ..., K . If a hole-electron pair is injected into interval j , define, as above, the probability density of the total number of pairs ultimately resulting in the avalanche process (including the initial pair)

as $p_o(n, x)$ where x is taken as the center of interval j . The hole of the initial pair moves to the left and the electron to the right toward $x = 0$ or $x = W$ respectively. As they pass through their respective intervals, new pairs may be created in each through collision ionization. We shall assume that the interval width dX is sufficiently narrow so that the initial pair carriers create either one or no new pairs in each interval. If the initial hole or electron generates a new pair in some interval k , then that new pair will ultimately generate N_k pairs including itself through the avalanche process. Thus with each interval we can associate a number of pairs N_k . This number equals zero if the appropriate initial pair carrier suffers no collision ionizations in interval k . This number equals one or more if the appropriate initial pair carrier suffers a collision ionization in interval k . The total number of pairs ultimately generated through the avalanche process including the initial pair is one plus the sum of the $\{N_k\}$. Since collision ionizations are all independent, all the N_k are independent. Thus we have the SIMGF of the total number of pairs given by

$$\psi_o(s, x) = s + \sum_{k=1}^{W/dX} \psi_{N_k}(s) \quad (3)$$

where s is the SIMGF of the deterministic initial pair and $\psi_{N_k}(s)$ is the SIMGF of N_k .

The SIMGF of N_k is obtained as follows. The probability that

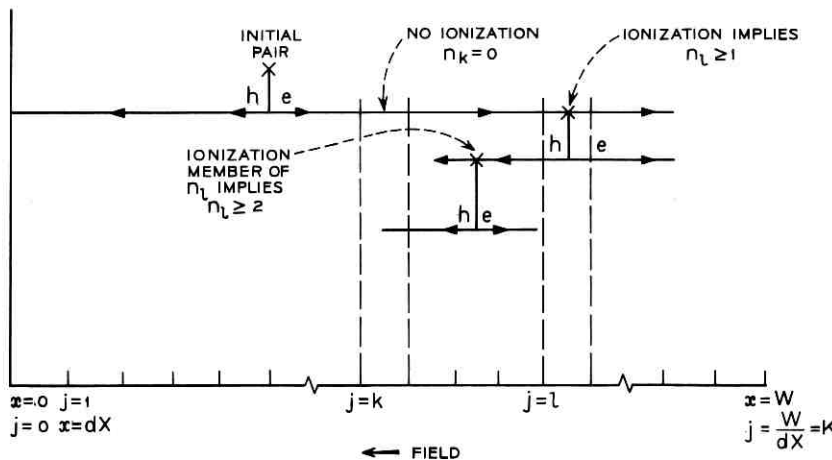


Fig. 2—Avalanche process.

$N_k = 0$ is $1 - \gamma dX$ where $\gamma = \alpha(x)$ if interval k is to the right of interval j where the initial pair enters, $\gamma = \beta(x)$ if k is to the left of j . (x is evaluated at the center of interval k .) The probability that $N_k = Z > 0$ is the probability of a collision ionization in interval k times the probability that a new pair created at interval k ultimately results in Z pairs including itself. That is

$$\Pr(N_k = Z) = \gamma dX p_g(Z, x) \quad \text{for } Z > 0 \quad (4)$$

with x evaluated at the center of interval k . Thus

$$\begin{aligned} \psi_{N_k}(s) &= \ln \left[\sum_{Z=0}^{\infty} \Pr(N_k = Z) e^{sZ} \right] \\ &= \ln \left[(1 - \gamma dX) e^{s^0} + \sum_{Z=1}^{\infty} \gamma dX p_g(Z, x) e^{sZ} \right] \\ &= \ln [1 - \gamma dX + \gamma dX M_g(s, x)] \\ &= \ln [1 - \gamma dX + \gamma dX e^{\psi_g(s, x)}] \end{aligned} \quad (5)$$

where

$$\gamma = \alpha(x) \quad \text{if } k > j$$

$$\gamma = \beta(x) \quad \text{if } k < j$$

$$x = \text{center of interval } k.$$

Using (3) and (5) and taking the limit as dX gets infinitely small, one obtains

$$\begin{aligned} \psi_g(s, x) &= s + \int_0^x \beta(x') [e^{\psi_g(s, x')} - 1] dx' \\ &\quad + \int_x^w \alpha(x') [e^{\psi_g(s, x')} - 1] dx'. \end{aligned} \quad (6)$$

Equation (6) is the critical equation for determining $\psi_g(s, x)$, and thus $M_g(s, x) = \exp[\psi_g(s, x)]$. Using Leibnitz's rule for differentiation of integrals one obtains

$$\frac{\partial}{\partial x} \psi_g(s, x) = [\beta(x) - \alpha(x)] (e^{\psi_g(s, x)} - 1). \quad (7)$$

The solution of (7) is

$$\psi_g(s, x) = \ln \left[\frac{1}{1 - C \exp \left(\int_0^x [\beta(x') - \alpha(x')] dx' \right)} \right] \quad (8)$$

where $C = (e^{\psi_v(s, 0)} - 1)/e^{\psi_v(s, 0)}$ which can be checked by substitution.

Substituting (8) into (6) one obtains the particular result

$$\psi_v(s, 0)$$

$$= s + \int_0^W \alpha(x') \left[\frac{1}{1 - C \exp \left(\int_0^{x'} [\beta(x'') - \alpha(x'')] dx'' \right)} - 1 \right] dx'. \quad (9)$$

If one makes the *assumption*³ that at each point in the high-field region

$$\beta(x) = k \cdot \alpha(x) \quad (10)$$

where k is a constant, one can solve (9) to obtain

$$\begin{aligned} \psi_v(s, 0) &= s - \delta + \frac{1}{k-1} \ln \left[\frac{e^{(k-1)\delta}}{M_v(s, 0) - e^{(k-1)\delta}[M_v(s, 0) - 1]} \right] \\ &= s + \frac{1}{1-k} \ln [M_v(s, 0) - e^{(k-1)\delta}[M_v(s, 0) - 1]] \end{aligned} \quad (11)$$

where

$$M_v(s, 0) = e^{\psi_v(s, 0)} \quad \text{and} \quad \delta = \int_0^W \alpha(x) dx.$$

One can write (11) in another way by making a substitution.* Define $\delta'(s)$ implicitly by

$$e^{\delta'(s)} = M_v(s, 0) e^{\delta-s}, \quad (12)$$

that is,

$$e^{\psi_v(s, 0)} = M_v(s, 0) = e^{s-\delta+\delta'(s)}. \quad (13)$$

Using (12) in (11) one obtains the implicit equation

$$e^{-k\delta'(s)} - e^{-\delta'(s)} = e^s [e^{-k\delta} - e^{-\delta}] \quad (14)$$

which determines $\delta'(s)$ and thus $M_v(s, 0)$ through (13).

Equation (14) is still not explicit. A numerical technique for solution is discussed in the next section. One can use (11) [or (14)] and (8) to obtain $\psi_v(s, x)$ or $M_v(s, x)$ for any x . Recall that x is the point of entry of the initial pair. In the applications we shall be concerned with $x = 0$ or $x = W$. That is, pairs are generated in a drift region outside the high-field region with carriers drifting into the high-field region.

* Equation (14) will follow from (11) and (12) by tedious algebra. Further, (14) will not be used in the following results except to compare with McIntyre's work in Appendix A.

The equation (14) is consistent with some unpublished conjectures of McIntyre given in Appendix A.

IV. NUMERICAL SOLUTIONS

Equations (11) through (14) can be solved numerically. One technique is to differentiate (11) to obtain the result

$$\frac{\partial}{\partial s} M_g(s, 0) = M_g(s, 0) \left(\frac{k-1}{k} \right) \left[1 - \frac{1}{k} (M_g(s, 0) e^{-s} e^{\delta})^{k-1} \right]^{-1} \quad (15)$$

where $M_g(0, 0) = 1$.

Equation (15) can be integrated with a computer to obtain $M_g(s, 0)$ explicitly.

V. SUMMARY OF ANALYTIC RESULTS ON AVALANCHE STATISTICS

From Sections I through IV and a previous paper by this author,¹ we obtained the following:

Assumptions:

Holes travel toward $x = 0$, electrons toward $x = W$.

Hole ionization probability per unit length = $\beta(x)$.

Electron ionization probability per unit length = $\alpha(x)$.

$\beta(x) = k \cdot \alpha(x)$, k a constant for all x .

High-field region width = W .

Definitions:

$$\delta \equiv \int_0^W \alpha(x) dx,$$

$p_g(n, x)$ = probability that if an initial pair enters the high-field region at point x , n pairs will ultimately result through the avalanche process including the initial pair,

$$\bar{G}(x) = \text{mean avalanche gain} = \sum_1^\infty n p_g(n, x),$$

$M_g(s, x) \equiv \text{moment-generating function of } p_g(n, x)$

$$= \sum_{n=1}^\infty p_g(n, x) e^{sn}.$$

Results:

$$1. M_\nu(s, x) = \left[1 - \frac{(M_\nu(s, 0) - 1)}{M_\nu(s, 0)} \exp \left[(k - 1) \int_0^x \alpha(x') dx' \right] \right]^{-1}$$

for all k . (16)

For $k = 0$ (Unilateral Gain)

$$2a. M_\nu(s, 0) = [1 - e^\delta [1 - e^{-s}]]^{-1} \quad \text{where} \quad \tilde{G}(0) = e^\delta. \quad (17)$$

$$2b. p_\nu(n, 0) = \frac{1}{G} \left(\frac{G - 1}{G} \right)^{n-1} \quad \text{where} \quad G = \tilde{G}(0). \quad (18)$$

For $k \neq 0, k \neq 1$

$$3. \frac{\partial}{\partial s} M_\nu(s, 0) = M_\nu(s, 0) \left(\frac{k-1}{k} \right) \left[1 - \frac{1}{k} (M_\nu(s, 0) e^{-s} e^\delta)^{k-1} \right]^{-1},$$

where

$$M_\nu(0, 0) = 1 \quad (19)$$

where

$$\tilde{G}(0) = \left(\frac{k-1}{k} \right) \left[1 - \frac{1}{k} e^{\delta(k-1)} \right]^{-1}.$$

For $k = 1$ (Equal Ionization)

$$4. \frac{\partial}{\partial s} M_\nu(s, 0) = M_\nu(s, 0) \left[1 - \left(\frac{G-1}{G} \right) M_\nu(s, 0) \right]^{-1}$$

$$M_\nu(0, 0) = 1$$

where

$$G = \tilde{G}(0). \quad (20)$$

VI. APPLICATIONS TO RECEIVERS USING AVALANCHE DETECTORS

6.1 General Comments

We shall next apply the results of Section V to obtain bounds on the error rates of digital receivers. The receivers to be discussed here are the single- and twin-channel systems described below. We shall upper-bound the power required at the receiver to obtain a desired error rate using the Chernov bounds.

6.2 The Receivers

The twin-channel receiver is shown in Fig. 3. Depending on the state of a binary information source, one of two channels has optical output

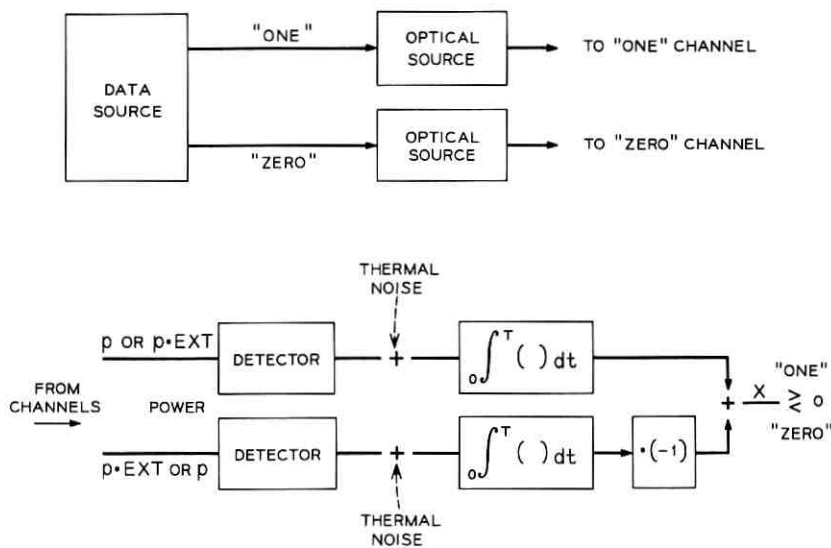


Fig. 3—Twin-channel system.

power p for duration T while the other has output power $p \cdot EXT$ for duration T . EXT signifies extinction. EXT would ideally be zero, but is left finite and less than unity for practical reasons. The optical power falling on an avalanche photo diode causes the emission of photo-electrons which are multiplied along with the detector "dark current" through the avalanche gain mechanism. The detector outputs (multiplied counts) are integrated in devices having thermal noises referred to their respective inputs. The integrator outputs are subtracted and the difference X is compared to a threshold of zero to decide what the information state was.

The single-channel system is essentially half the twin-channel system as shown in Fig. 4. The single integrator output X is compared to a threshold γ to decide upon the information state.

6.3 The Chernov Bounds

The Chernov bound is a useful tool for bounding the probability that a random variable X will lie above or below a given threshold γ . It is given as follows⁵

$$\Pr(X > \gamma) \leq e^{\psi_X(s) - s\psi'_X(s)} \Big|_{\gamma = \psi'_X(s)}$$

provided $s > 0$,

$$\Pr(X < \gamma) \leq e^{\psi_X(s) - s\psi'_X(s)} \Big|_{\gamma = \psi'_X(s)}$$

provided $s < 0$, (21)

where

$$\psi_X(s) = \text{SIMGF of } X \equiv \ln \left[\int_{-\infty}^{\infty} p_X(x) e^{sx} dx \right]$$

and

$$\psi'_X(s) = \frac{\partial}{\partial s} \psi_X(s).$$

6.4 Chernov Bounds for the Two Systems

6.4.1 Preliminaries

We wish to determine the required power p to achieve a desired decision error probability for each of the receivers discussed in Section 6.2 with various types of detectors and various values of other system parameters such as dark current and thermal noise in the integrators. To apply the Chernov bounds we will need the SIMGF's of the variables X at the outputs of the receivers. (See Figs. 3 and 4.)

An important result needed here is the following:

Lemma: If C is integer-valued and greater than or equal to zero; and if $U = \sum_i^C g_i$, where the g_i are independent, identically distributed random variables (that is, each "count" produced by the C process independently



POWER = p OR $p \cdot \text{EXT}$

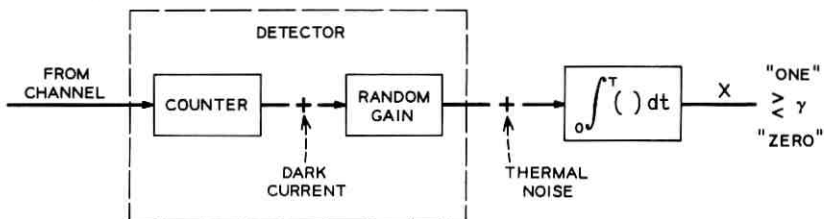


Fig. 4—Single-channel system.

generates g_i contributions to the U process through some gain mechanism); then the SIMGF of U is¹

$$\psi_U(s) = \psi_c(\psi_g(s)) \quad (22)$$

where $\psi_g(s)$ is the SIMGF of the identically distributed random variables g_i .

One can model an avalanche photodiode as a photon counter followed by a random avalanche multiplier. Each photon counter output "count" produces a random number of "counts" at the multiplier output. Thus, since we know from Section V the SIMGF of a random multiplier which corresponds to $\psi_g(s)$ in (22), and since we seek the SIMGF of the photodiode output which corresponds to $\psi_U(s)$ in (22), it follows that we need the SIMGF of the number of counts emitted by a photon counter with light incident upon it, which corresponds to $\psi_c(s)$ in (22).

6.4.2 Photon Counter Statistics

6.4.2.1 Coherent Light. If the light incident upon the photon counter is coherent, then it is well known that the SIMGF of the total counts emitted in an interval T is given by⁶ (see Appendix B)

$$\psi_c(s) = [LAMSIG + LAMD] [e^s - 1] \quad (23)$$

where

$LAMSIG$ = Total incident light energy $\cdot \eta / \hbar\Omega$

η = Detector quantum efficiency

$\hbar\Omega$ = Energy of photon at optical frequency used

$LAMD$ = Mean number of dark current counts before avalanche gain in an interval T .

6.4.2.2 Incoherent Light. If the incident light is incoherent with H independent spatial-temporal "degrees of freedom," then the SIMGF of the total counts emitted by the photon counter in interval T is (see Appendix B)

$$\psi_c = LAMD[e^s - 1] + \ln \left[\left[1 - \frac{LAMSIG}{H} (e^s - 1) \right]^{-H} \right] \quad (24)$$

where $LAMSIG$ is the average total incident energy times $\eta / \hbar\Omega$. Clearly (24) is the same as (23) as H approaches infinity, which is a well known result.

6.4.3 Final Calculations

6.4.3.1 Twin-Channel System. Since, for the twin-channel receiver, X consists of the difference of two random integrator outputs, we need

the following well known result.⁴ If $X = X_1 - X_2$, and if X_1 and X_2 are independent, then the SIMGF of X is

$$\psi_x(s) = \psi_{x_1}(s) + \psi_{x_2}(-s). \quad (25)$$

Each integrator output contains the sum of the counts emitted by its detector and the integral of its thermal noise. The SIMGF of the random variable N obtained when Gaussian thermal noise spectral height N_0 is integrated over an interval T is well known to be

$$\psi_N(s) = \frac{s^2}{2} N_0 T. \quad (26)$$

Using (22) through (26) we obtain for the SIMGF of the twin-channel receiver output X when the information is in state "one", and the optical source is coherent,

$$\begin{aligned} \psi_x(s) = s^2 N_0 T &+ \left[\frac{p \cdot T \cdot \eta}{\hbar \Omega} + LAMD \right] [M_\sigma(s) - 1] \\ &+ \left[\frac{p \cdot T \cdot EXT \cdot \eta}{\hbar \Omega} + LAMD \right] [M_\sigma(-s) - 1] \end{aligned} \quad (27)$$

where

$LAMD$ = mean number of dark current counts before avalanche gain in an interval T

N_0 = spectral height of the thermal noises referred to the integrator inputs.

$M_\sigma(s)$ is obtained from (16) through (20) depending upon the particular gain mechanism. If the optical source is incoherent, we have

$$\begin{aligned} \psi_x(s) = s^2 N_0 T &+ LAMD[M_\sigma(s) + M_\sigma(-s) - 2] \\ &+ \ln \left[\left[1 - \frac{p \cdot T \cdot \eta}{H \hbar \Omega} [M_\sigma(s) - 1] \right]^{-H} \right] \\ &+ \ln \left[\left[1 - \frac{p \cdot T \cdot EXT \cdot \eta}{H \hbar \Omega} [M_\sigma(-s) - 1] \right]^{-H} \right]. \end{aligned} \quad (28)$$

We seek the probability that when the information is in state "one", X is less than zero, and we therefore decide that the information state was "zero." That is, we seek the error probability. One can use (27) or (28) and the Chernov bound of (21) to determine the required value of $LAMSIG \equiv p \cdot T \cdot \eta / (\hbar \Omega)$ to achieve a desired error probability. Since the twin-channel receiver is symmetric, the error probability

when the information is in state "zero" is the same as when it is in state "one."

6.4.3.2 Single-Channel System. For the single-channel receiver, we need the SIMGF of X under both information states. Call X_1 the random variable X when the information is in the state "one." Call X_0 the random variable X when the information is in state zero. Using results of Section 6.4, one obtains for coherent light

$$\begin{aligned}\psi_{X_1}(s) &= \frac{s^2 N_0 T}{2} + \left[LAMD + \frac{p \cdot T \cdot \eta}{\hbar \Omega} \right] [M_\sigma(s) - 1] \\ \psi_{X_0}(s) &= \frac{s^2 N_0}{2} + \left[LAMD + \frac{p \cdot T \cdot EXT \cdot \eta}{\hbar \Omega} \right] [M_\sigma(s) - 1].\end{aligned}\quad (29)$$

For incoherent light

$$\begin{aligned}\psi_{X_1}(s) &= \frac{s^2 N_0 T}{2} + LAMD [M_\sigma(s) - 1] \\ &\quad + \ln \left[\left[1 - \frac{p \cdot T \cdot \eta}{H \hbar \Omega} [M_\sigma(s) - 1] \right]^{-H} \right] \\ \psi_{X_0}(s) &= \frac{s^2 N_0 T}{2} + LAMD [M_\sigma(s) - 1] \\ &\quad + \ln \left[\left[1 - \frac{p \cdot T \cdot EXT \cdot \eta}{H \cdot \hbar \Omega} [M_\sigma(s) - 1] \right]^{-H} \right].\end{aligned}\quad (30)$$

One can then use the results of (29) and (30) along with the Chernov bounds of (21) to simultaneously find values of $LAMSIG = p \cdot T \cdot \eta / (\hbar \Omega)$ and the threshold γ (see Fig. 4) to ensure some desired error probability (which for convenience here will be the same for either information state).

6.5 Numerical Results

The Chernov bounds described above were evaluated numerically. The results are displayed on the attached figures described below. The range of parameter values is realistic and practical, to the best of this author's knowledge. The curves presented are those deemed most interesting by the author. Other calculations can of course be made. Parameters used are defined as follows:^{*}

$LAMSIG$ = Required mean number of detected photons per pulse in the "on" channel of the twin-channel

* SIG , EXT , G , K , H , and $LAMD$ are input parameters to the program which calculates $LAMSIG$ for a desired error rate.

receiver or in the "one" state of the single-channel receiver.

LAMSIG·EXT = Mean number of detected counts per pulse in the "off" channel of the twin-channel receiver or in the "zero" state of the single-channel receiver.

SIG = Normalized thermal noise standard deviation

$$= \{4k\theta T/[Re^2]\}^{1/2} = \{4k\theta C/e^2\}^{1/2}$$

where e = electron charge, $k\theta$ = Boltzmann's constant · absolute temperature, R = equivalent noise resistance at integrator input, T = pulse duration, $C = T/R$ = integrator equivalent input capacitance. For the results to follow, a reasonable value of *SIG* was chosen to be 6000.

G = Mean avalanche gain.

H = Temporal-spatial diversity for incoherent carrier case.

k = Ratio of ionization probability per unit length of weaker and stronger ionizing carriers.*

LAMD = Dark current counts per interval T before avalanche gain.

Fig. 5

LAMSIG vs *G* is plotted for the twin-channel case with *k* as parameter. *SIG* was set at 6000, the error rate is 10^{-9} , *LAMD* was set at 5 counts and *EXT* = 0.01. *H* = 10,000 which is equivalent to assuming a coherent carrier.

Fig. 6

The value at optimal gain of *LAMSIG* vs *k* is plotted. Points are tagged with the optimal *G*. The receiver is a twin-channel system with *SIG* = 6000, *EXT* = 0.01, *LAMD* = 5. *H* is 10,000 which is equivalent to assuming a coherent carrier. The error rate is 10^{-9} .

Fig. 7

LAMSIG vs *G* is plotted for two values of error rate 10^{-9} and 10^{-5} for

* For these calculations it was assumed that the detector is designed so that the stronger ionizing carriers generated optically or associated with dark current enter the high-field region from a drift region outside the high-field region. This corresponds to initial pairs entering the gain mechanism of $x = 0$ or $x = W$ as discussed in Section III.

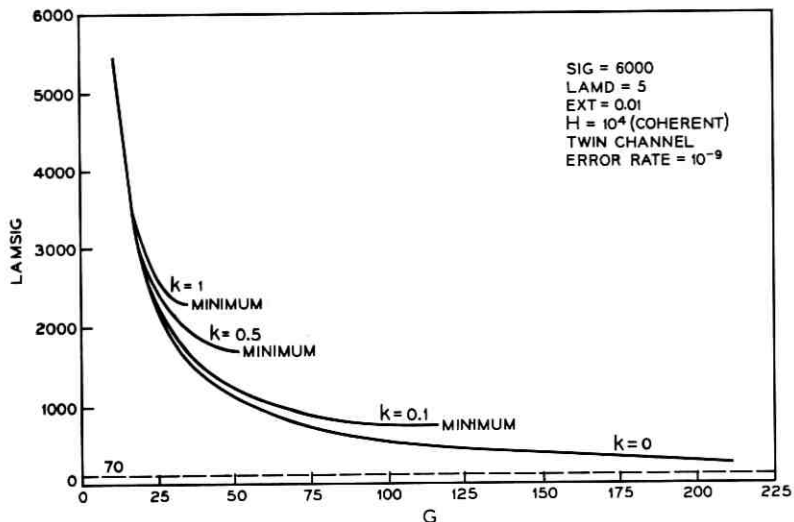
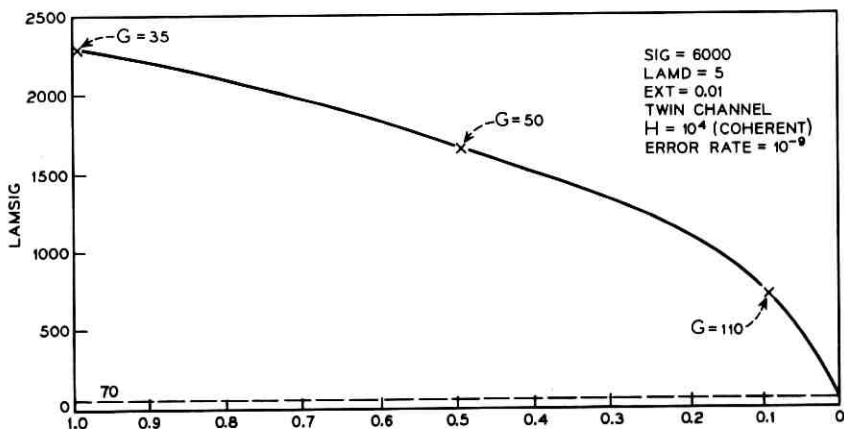


Fig. 5—LAMSIG versus gain.

Fig. 6—LAMSIG at optimal gain versus k .

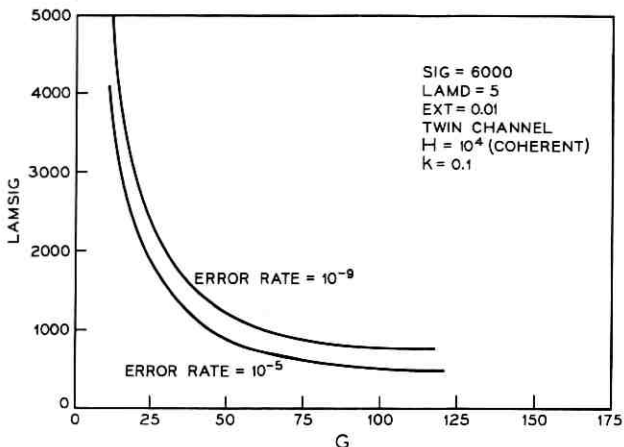


Fig. 7—LAMSIG versus gain.

a twin-channel system with $SIG = 6000$, $EXT = 0.01$, $H = 10,000$ $LAMD = 5$, $k = 0.1$.

Fig. 8

Single- and twin-channel systems are compared. $LAMSIG$ vs G is plotted for $SIG = 6000$, $EXT = 0.01$, $LAMD = 5$, $H = 10,000$, error rate = 10^{-9} , $k = 0$. Note that from an average power viewpoint the single-channel system is 3 dB better than shown if the binary information source is random, since $LAMSIG$ is the energy in "one" state.

Fig. 9

Same as Fig. 8 except $k = 1$. Note the scale change.

Fig. 10

$LAMSIG$ vs G for $H = 100$ and $H = 10,000$ for twin-channel system. $SIG = 6000$, $EXT = 0.01$, $LAMD = 5$, $k = 0$, error rate = 10^{-9} .

6.6 Further Comments

When systems were investigated for sensitivity to the choice $LAMD = 5$, $EXT = 0.01$, it was found that insignificant changes in $LAMSIG$ vs G occurred when various combinations of $LAMD = 5$ or 50, $EXT = 0.01$ or 0.001 were tried.

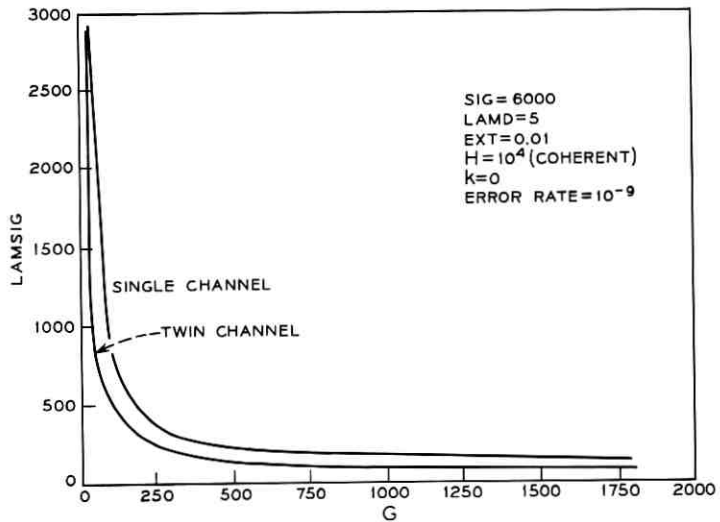


Fig. 8—LAMSIG versus gain.

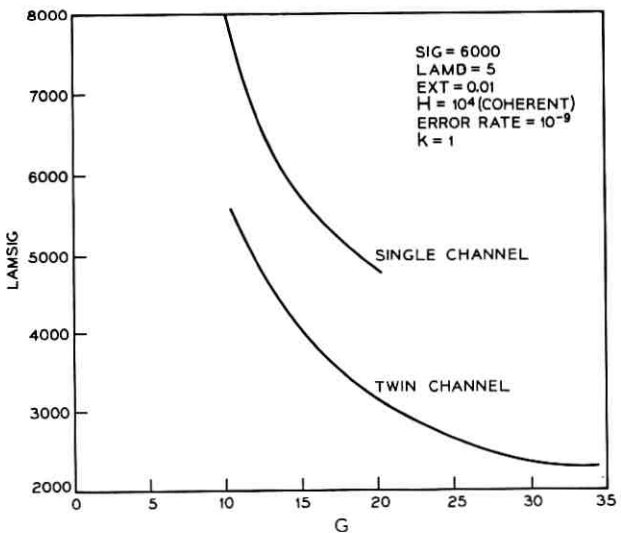


Fig. 9—LAMSIG versus gain.

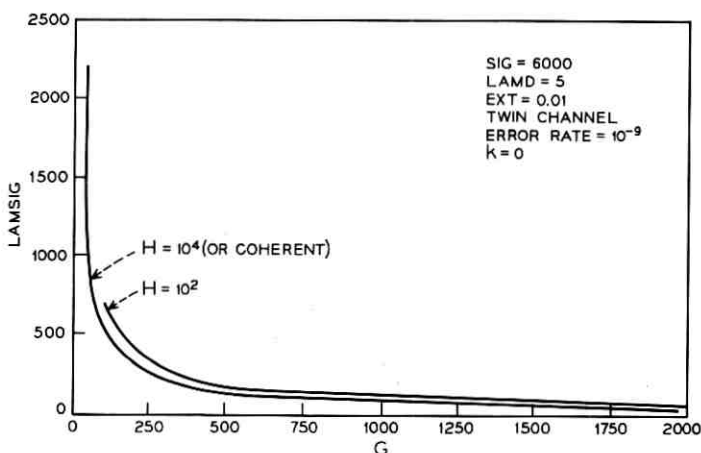


Fig. 10—LAMSIG versus gain.

VII. CONCLUSIONS ON APPLICATIONS

If one assumes that the Chernov bounds are sufficiently tight so that actual energy required per bit to achieve specified error rates can be compared for various system parameters by comparing the bounds,* then one can conclude the following.

- (i) Define k as the ratio of the collision ionization probabilities per unit length of the weaker-ionizing to the stronger-ionizing carrier (carriers are of course holes and electrons). Assume that the detector is designed "well" such that optically and thermally generated carriers enter the high-field region from a drift region outside. From the bounds, one obtains the result that the required energy per pulse to achieve a desired error rate decreases as k decreases for fixed average avalanche gain. A value $k = 0$ is best; but a value $k = 0.1$ will allow one to operate with energy within 10 dB of that required at very high gains with a $k = 0$ device. For each value of k except zero there is an optimal gain resulting in minimum required energy per pulse. The optimal gain is larger for smaller k . At $k = 0.1$, the optimal gain is about 100. At $k = 0$, the optimal gain is infinite, but a gain of a few thousand allows

* For simple cases where both the bounds and actual energy requirements can be obtained (for instance for the $k = 0$ case) the two results differ by a few dB or less.

close to optimal required energy per pulse. One can conclude that a silicon device with $k = 0.1$ and a gain of about 100 would be a good choice for an optical detector. This is true since a detector with k less than 0.1 and yet having gain significantly higher than 100 is not available at this time.

(ii) The required energy per pulse for systems using incoherent optical sources differs from that for systems using coherent sources by less than a few dB provided the product of the source bandwidth and the pulse duration exceeds 100. This is true even if there is no spatial incoherence of the light at the detector.

(iii) For reasonable parameter values, and assuming a random information stream, the single-channel receiver requires about 1.5 dB less energy per pulse to achieve a desired error rate than the twin-channel receiver.

(iv) The required energy per pulse is insensitive to reasonable values of dark current and extinction ratios.

(v) For a particular system, a change in the desired error rate from 10^{-9} to 10^{-5} results in a change in the required energy per pulse of 1 to 3 dB, depending upon the avalanche gain. This shows that the required energy per pulse is fairly insensitive to the error rate. On the other hand, this means that poor error rates will result if insufficient loss margin is provided. That is, a small lowering of the received energy can greatly increase the error rate.

APPENDIX A

In an unpublished work, McIntyre conjectures (from special case calculations) that the probability density of the random gain, defined here as $p_s(n, 0)$ is given by

$$p_s(n, 0) = \frac{\Gamma\left(\frac{n}{1-k} + 1\right) e^{-\delta} (e^{-k\delta} - e^{-\delta})^{n-1}}{n! \Gamma\left(\frac{n}{1-k} + 2 - n\right)}$$

where k and δ are the same as in (10) through (13).

If one makes the assumption that the conjectured $p_s(n, 0)$ has sum over n normalized to unity for each value of k and for each δ , then one obtains the result of (14) by using the definition of the moment-generating function and the normalization property.

APPENDIX B

If light of *known* intensity falls upon a photon counter during an interval T , then the probability density of the total number of counts emitted is well known⁶ to be Poisson distributed as follows

$$p_c(n) = [\Lambda + LAMD]^n \frac{e^{-(\Lambda + LAMD)}}{n!}. \quad (31)$$

Where Λ^* is the total energy incident in the interval T times $\eta/\hbar\Omega$, $LAMD$ is the mean number of dark current counts per second times the interval T , and $\eta/\hbar\Omega$ is the detector quantum efficiency divided by the energy in a photon.

The moment-generating function of the distribution of (31) is given by

$$M_c(s) = \exp [[\Lambda + LAMD][e^s - 1]]. \quad (32)$$

If the incident light is a stochastic process, then the moment-generating function of the output count distribution is obtained by averaging (32) over the probability density of the stochastic total energy incident in the interval T

$$M_c(s) = \int_0^\infty \exp ([\Lambda + LAMD][e^s - 1]) p(\Lambda) d\Lambda. \quad (33)$$

An incoherent light field is normally taken to mean that the complex envelope of the classical field is a complex Gaussian random process. That is, such a field incident on the photon counter plane can be written as

$$\begin{aligned} E(\rho, t) &= \sqrt{2} \operatorname{re}\{\epsilon(\rho, t)e^{i\Omega t}\} \\ &\rho \in \text{counter plane} \\ &t \in (0, T) \end{aligned} \quad (34)$$

where $\epsilon(\rho, t)$ is a complex Gaussian random process.

If one expands $\epsilon(\rho, t)$ in its Karhunen-Loeve eigenfunctions,⁵ one obtains

$$\begin{aligned} \epsilon(\rho, t) &= \sum e_k \phi_k(\rho, t) \\ &\rho \in \text{counter plane} \\ &t \in (0, T) \end{aligned} \quad (35)$$

* In the text, Λ is called *LAMSIG*.

where

$$\int_{\text{counter plane}} \int_0^T \phi_k(\rho, t) \phi_i^*(\rho, t) d^2\rho dt = \delta_{k,i}$$

and the coefficients e_k are independent complex Gaussian random variables satisfying

$$\begin{aligned} \langle e_k e_i^* \rangle &= \gamma_k \delta_{k,i} \\ \langle e_k e_i \rangle &= 0. \end{aligned} \quad (36)$$

The energy incident upon the photon counter is

$$\frac{\hbar\Omega}{\eta} \Lambda = \int \epsilon(\rho, t) \epsilon^*(\rho, t) d^2\rho dt = \sum |e_k|^2. \quad (37)$$

If one assumes an equal distribution of average energy in roughly H "modes,"

$$\begin{aligned} \gamma_k &= \gamma, \quad 1 \leq k \leq H \\ &= 0, \quad k > H \end{aligned} \quad (38)$$

then it follows that from (33) and the complex Gaussian statistics of the e_k that

$$M_c(s) = \exp [LAMD(e^* - 1)] \cdot \left[1 - \frac{\eta}{\hbar\Omega} \gamma(e^* - 1) \right]^{-H}. \quad (39)$$

Assumption (38) implies that the energy of the incoherent light is roughly equally distributed in H degrees of freedom.

REFERENCES

1. Personick, S. D., "New Results on Avalanche Multiplication Statistics with Applications to Optical Detection," BSTJ, 50, No. 1 (January 1971), pp. 167-189.
2. McIntyre, R. J., unpublished work (see Appendix A).
3. McIntyre, R. J., "Multiplication Noise in Uniform Avalanche Diodes," IEEE Trans. Elec. Dev., ED-13, No. 1 (January 1966), pp. 164-168.
4. Davenport, W., and Root, W., *Random Signals and Noise*, New York: John Wiley & Sons, 1958.
5. Van Trees, H. L., *Detection Estimation and Modulation, I*, New York: John Wiley & Sons, 1967.
6. Glauber, R. J., *Quantum Optics and Electronics, Les Honches 1964*, Lecture Notes at Session of the Summer School of Theoretical Physics at the Univ. of Grenoble, Ed. De Witt, New York: Gordon and Breach, 1965, p. 64.

Design of Digital Filter Banks for Speech Analysis

By R. W. SCHAFER and L. R. RABINER

(Manuscript received June 22, 1971)

A bank of bandpass filters is often used in performing short-time spectrum analysis of speech signals. This paper is concerned with the analysis and design of digital filter banks composed of equally spaced bandpass filters. It is shown that significant improvement in the composite filter bank response can be achieved by proper choice of the relative phases of the bandpass filters. The results are extended to more general filter bank configurations.

I. INTRODUCTION

Many speech processing systems are based on the concept of short-time spectrum analysis.^{1,2} Spectrum analyzers for such systems often consist of a set of bandpass filters whose combined passbands cover a desired frequency range. Although continuous-time filters have traditionally been used in filter banks for speech analysis, hardware realizations of digital filters are now available,³ and the advantages which digital filters offer should be exploited in filter bank design. These advantages include: flexibility of design of the individual bandpass filters, precision of realization, stability of digital hardware, and the efficiency of realization of the filter bank afforded by the possibility of multiplexing the digital hardware. Thus it is important to consider design techniques for filter banks composed of digital bandpass filters.

To focus on the basic concepts in filter bank design, it is useful to define an *ideal filter bank* spectrum analyzer. Figure 1 depicts such a filter bank composed of digital filters whose impulse responses are denoted by $h_k(nT)$, $k = 0, 1, \dots, M$, where $1/T$ is the sampling frequency of the input signal.* Such a filter bank constitutes an ideal spectrum analyzer if the input $x(nT)$ (with possibly further band limiting) can be synthesized exactly (within some fixed delay) by a linear

* The filter $h_0(nT)$ is a lowpass filter which is included for completeness although this band is usually not analyzed in practical speech analysis systems.

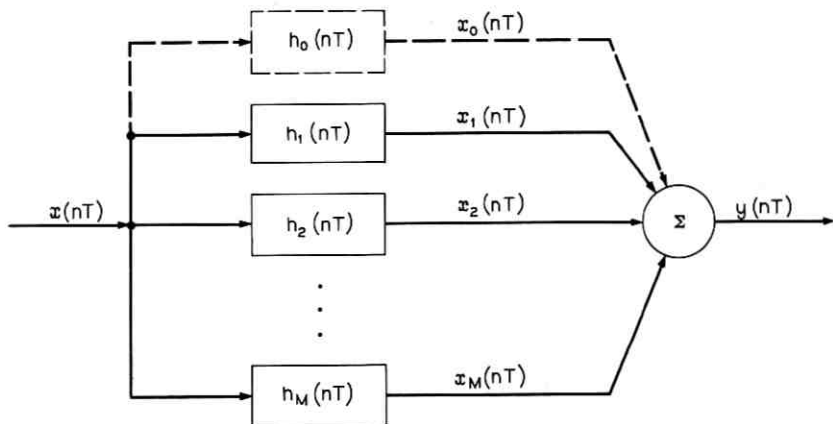


Fig. 1—Bank of digital bandpass filters.

combination of the bandpass filter outputs $x_k(nT)$. An example of such a system would be one in which the filters are ideal rectangular bandpass filters with the same constant gain and linear phase in their passbands and zero gain outside. If the filter bandwidths are such that the frequency range

$$\frac{-\pi}{T} \leq \omega \leq \frac{\pi}{T}$$

is completely covered without overlap, then the input can be synthesized exactly by adding together the outputs of the bandpass filters.

The essential characteristics of the ideal spectrum analyzer are that the frequency response of the combined outputs must exhibit a flat magnitude response and a linear phase, and therefore the combined impulse response must be a delayed digital impulse (unit sample). Causal digital filters (filters whose impulse responses are zero for $n < 0$) cannot have the desired ideal gain characteristics and may not have linear phase.* Therefore a filter bank composed of such filters cannot achieve the ideal characteristics of flat magnitude response and linear phase. In this paper we will describe an approach to the design of filter banks that approximate the ideal spectrum analyzer. First we present a detailed analysis of a filter bank configuration in which equally spaced, equal-bandwidth digital filters are used. This analysis suggests a technique for optimizing the filter bank characteristics and

* Finite duration impulse response digital filters can have precisely linear phase.

also suggests how the results can be used where nonuniform bandwidths are desired. The results are illustrated with examples.

II. ANALYSIS OF UNIFORM FILTER BANKS

Assume that the bandpass filters in Fig. 1 have impulse responses of the form

$$h_k(nT) = 2 | D_k | h(nT) \cos(\omega_k nT + \Phi_k) \quad k = 1, 2, \dots, M \quad (1)$$

$$h_0(nT) = | D_0 | h(nT)$$

where $\omega_k = \omega_1 + (k - 1) \Delta\omega$, and $h(nT)$ is the impulse response of a prototype lowpass filter. (When the $k = 0$ lowpass filter is used, $\omega_1 = \Delta\omega$ and $\omega_0 = 0$.) The system functions for this set of bandpass filters are

$$H_k(z) = | D_k | e^{j\Phi_k} H(ze^{-j\omega_k T}) + | D_k | e^{-j\Phi_k} H(ze^{j\omega_k T}) \quad k = 1, 2, \dots, M$$

$$H_0(z) = | D_0 | H(z). \quad (2)$$

The frequency response of these filters is obtained after substituting $z = e^{j\omega T}$ in (2) as

$$H_k(e^{j\omega T}) = | D_k | e^{j\Phi_k} H(e^{j(\omega - \omega_k)T}) + | D_k | e^{-j\Phi_k} H(e^{j(\omega + \omega_k)T}), \quad k = 1, 2, \dots, M, \quad (3)$$

$$H_0(e^{j\omega T}) = | D_0 | H(e^{j\omega T}).$$

If the frequency response of prototype lowpass filter, $H(e^{j\omega T})$, drops off sharply, then it can be seen from (3) that

$$\begin{aligned} | H_k(e^{j\omega T}) | &\approx | D_k | | H(e^{j(\omega - \omega_k)T}) | \quad 0 \leq \omega \leq \pi/T \\ &\approx | D_k | | H(e^{j(\omega + \omega_k)T}) | \quad -\pi/T \leq \omega \leq 0. \end{aligned}$$

In this case the filter bank consists of a set of $(M + 1)$ equally spaced bandpass filters with identical magnitude responses around their respective center frequencies. We have chosen this method of designing bandpass filters from lowpass prototypes for analytical convenience and because of the importance of spectrum analysis systems of this form.^{1,2} The results to be discussed apply for other bandpass transformations in so far as they yield a set of uniformly spaced bandpass filters with identical frequency characteristics.

Our objective is to choose the prototype lowpass filter and the parameters $| D_k |$, ω_1 , $\Delta\omega$, and Φ_k so that the filter bank will closely approximate the characteristics of the ideal spectrum analyzer. To do this we must consider the response of the composite filter bank. First,

however, it is useful to interpret the individual bandpass filter outputs in terms of spectrum analysis considerations.

The individual filter outputs are of the form

$$x_k(nT) = \sum_{r=-\infty}^n 2x(rT) | D_k | h(nT - rT) \cos [\omega_k(nT - rT) + \Phi_k], \quad (4)$$

$$x_0(nT) = \sum_{r=-\infty}^n x(rT) | D_0 | h(nT - rT)$$

which can be expressed as

$$\begin{aligned} x_k(nT) &= 2 \operatorname{Re} \{ D_k X(\omega_k, n) e^{j\omega_k n T} \} \\ x_0(nT) &= \operatorname{Re} \{ D_0 X(0, n) \} \end{aligned} \quad (5)$$

where D_k is the complex constant defined by

$$\begin{aligned} D_k &= | D_k | e^{j\Phi_k} \quad k = 1, 2, \dots, M \\ D_0 &= | D_0 |, \end{aligned} \quad (6)$$

and

$$X(\omega_k, n) = \sum_{r=-\infty}^n x(rT) h(nT - rT) e^{-j\omega_k r T}. \quad (7)$$

The quantity $X(\omega_k, n)$ is the discrete-time version of the short-time Fourier transform⁴ of $x(nT)$. Thus, (5) serves to relate the bandpass filter outputs $x_k(nT)$ to the short-time Fourier transform.

The frequency response and impulse response of the composite filter bank are obtained from

$$y(nT) = \sum_{k=0}^M x_k(nT). \quad (8)$$

After substituting (5) into (8) and noting that if $x(nT)$ is real, $X(-\omega_k, n)$ is the complex conjugate of $X(\omega_k, n)$, we obtain

$$y(nT) = \sum_{k=-M}^M D_k X(\omega_k, n) e^{j\omega_k n T} \quad (9)$$

where $\omega_{-k} = -\omega_k$, and D_{-k} is the complex conjugate of D_k . Substituting (7) into (9) and interchanging the order of summations results in

$$y(nT) = \sum_{r=-\infty}^n x(rT) \left[h(nT - rT) \cdot \sum_{k=-M}^M D_k e^{j\omega_k (nT - rT)} \right]. \quad (10)$$

Defining

$$d(nT) = \sum_{k=-M}^M D_k e^{j\omega_k n T}, \quad (11)$$

we observe from (10) that the combined impulse response of the filter bank can be expressed as

$$\tilde{h}(nT) = h(nT) d(nT). \quad (12)$$

Equations (11) and (12) are the basic results of the analysis. (Note that they could have been obtained directly by summing the impulse responses $h_k(nT)$, with the sacrifice of the interpretation of the filter bank outputs in terms of the short-time spectrum.)

Equation (12) shows that the filter bank impulse response is the product of the prototype lowpass filter impulse response $h(nT)$, and the sequence $d(nT)$ defined by (11). The choice of lowpass filter depends on both the desired frequency resolution and the requirement of obtaining flat magnitude and linear phase response in the composite filter bank. The sequence $d(nT)$ is independent of the prototype lowpass filter and is a function of the frequency spacing, the relative gains and phases, and the number of bandpass filters. Thus, for a given choice of prototype lowpass filter, the parameters of $d(nT)$ can be adjusted to achieve the best approximation to the ideal spectrum analyzer. To see how this occurs, we shall first examine in detail the characteristics of the sequence $d(nT)$.

As will be shown in the remainder of this section, a particularly useful choice of the complex coefficients D_k in (11) is

$$D_k = e^{j\omega_k n_0 T} \quad k = \pm 1, \pm 2, \dots, \pm M. \quad (13)$$

$$D_0 = 1,$$

where n_0 is an integer. That is,

$$\Phi_k = \omega_k n_0 T, \quad \text{and} \quad |D_k| = 1.$$

(The condition $D_0 = 1$ implies that the band around $\omega = 0$ is included in the filter bank; $D_0 = 0$ implies that it is not.) It can be shown that for this choice of D_k , (11) becomes

$$d(nT) = D_0 + \frac{2 \sin [M \Delta\omega(nT + n_0 T)/2]}{\sin [\Delta\omega(nT + n_0 T)/2]} \cos [\omega_a(nT + n_0 T)] \quad (14)$$

where $\omega_a = \omega_1 + (M - 1) \Delta\omega/2$, and D_0 is 1 or 0 depending on whether or not the lowpass channel is included.

The properties of the sequence $d(nT)$ determine the character of

the impulse response of the filter bank. Some of these properties are summarized below:

- (i) The parameter n_0 shifts the sequence $d(nT)$ by n_0 samples with respect to $h(nT)$.
- (ii) The sequence $d(nT)$ is even about the sample $n = -n_0$; i.e., $d(nT - n_0T) = d(-nT - n_0T)$.
- (iii) The maximum value of $d(nT)$ occurs at $n = -n_0$. This value is $d(-n_0T) = 2M + D_0$.
- (iv) If $2\pi/(\Delta\omega T)$ and $\omega_1/\Delta\omega$ are both integers, then the sequence $d(nT)$ is periodic with period $2\pi/\Delta\omega$. Otherwise, $d(nT)$ will be an almost periodic sequence which will peak up at time intervals of $2\pi/\Delta\omega$.

Insight into the properties of $d(nT)$ can be gained by considering a simple example. Assume that $\omega_1 = \Delta\omega$ and $2\pi/(\Delta\omega T) = N$ where N is an odd integer. That is, the entire frequency range $-\pi/T \leq \omega \leq \pi/T$, is divided into N equal bands. If $M = (N - 1)/2$, the entire frequency range is covered. Under these conditions (14) can be written

$$d(nT) = \frac{\sin \left[\left(\frac{2M+1}{2} \right) \Delta\omega(nT + n_0T) \right]}{\sin [\Delta\omega(nT + n_0T)/2]} - 1 \quad \text{if } D_0 = 0 \quad (15a)$$

$$= \frac{\sin \left[\left(\frac{2M+1}{2} \right) \Delta\omega(nT + n_0T) \right]}{\sin [\Delta\omega(nT + n_0T)/2]} \quad \text{if } D_0 = 1. \quad (15b)$$

(If N is even, the $k = 0$ filter is not used, i.e., $D_0 = 0$, and ω_1 is $\Delta\omega/2$.) It is clear from (15b) that for these conditions $d(nT)$ is a periodic sequence with period $NT = 2\pi/\Delta\omega$. In fact, $d(nT)$ may be thought of as samples of a continuous-time periodic Dirichlet kernel as shown in Fig. 2a. If $M = (N - 1)/2$ and $D_0 = 1$, $d(nT)$ is a periodic discrete-time impulse train with impulses occurring at multiples of NT . This is because the sample points on the periodic Dirichlet kernel occur at the maxima and the zero crossings, as indicated by the small circles in Fig. 2a.

The conditions for $d(nT)$ to be periodic are that both $\omega_1/\Delta\omega$ and $2\pi/(\Delta\omega T)$ be equal to integers. To see this, we must examine (14) in detail. If $2\pi/(\Delta\omega T)$ is an integer, and M is an odd integer, the sequence $2 \sin [M \Delta\omega(nT + n_0T)/2]/\sin [\Delta\omega(nT + n_0T)/2]$ is periodic with period $NT = 2\pi/\Delta\omega$. If $\omega_1/\Delta\omega$ is an integer and M is odd, the sequence $\cos [(\omega_1 + (M - 1) \Delta\omega/2)(nT + n_0T)]$ is also periodic with a period

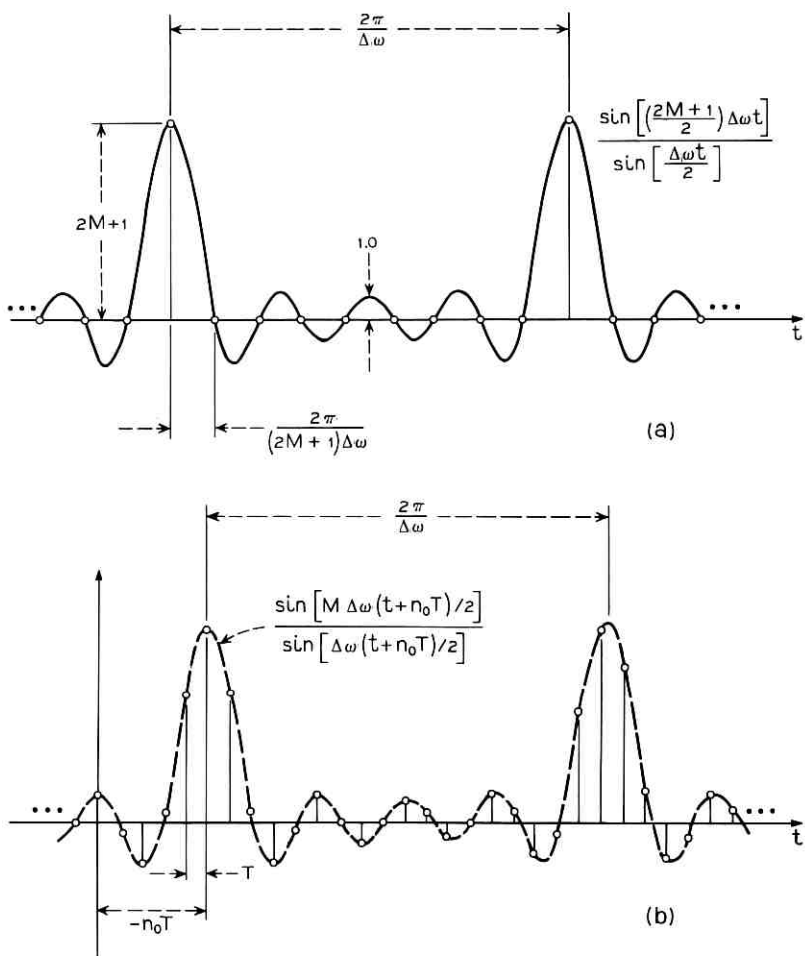


Fig. 2—(a) Periodic continuous-time Dirichlet kernel, (b) continuous-time envelope and sequence $d(nT)$ when either $\omega_1/\Delta\omega$ or $2\pi/(\Delta\omega T)$ are not integers.

that is an integer multiple of $2\pi/\Delta\omega$. Thus the product of these two sequences is periodic with period $2\pi/\Delta\omega$. The identical result holds for M an even integer and $2\pi/\Delta\omega$ and $\omega_1/\Delta\omega$ integers although the interaction between the component sequences is slightly different.

If either $2\pi/(\Delta\omega T)$ or $\omega_1/\Delta\omega$ are not integers, $d(nT)$ will not be periodic, but will still peak up at time intervals of $2\pi/\Delta\omega$. Such a case is depicted in Fig. 2b where the samples $d(nT)$ are marked by the

small circles and the dotted curve shows the factor

$$\sin [M \Delta\omega(nT + n_0 T)/2]/\sin [\Delta\omega(nT + n_0 T)/2]$$

when M is odd. As shown in Fig. 2b, $d(nT)$ will always have even symmetry about sample $n = -n_0$.

III. DESIGN OF UNIFORM FILTER BANKS USING BESSSEL FILTERS

In the preceding section we presented a detailed analysis of a filter bank composed of equally spaced equal-bandwidth filters. In this section we will show how the results of that analysis can be employed in filter bank design.

The objective of flat amplitude response and linear phase is most easily achieved with bandpass filters having these same properties. For this reason, Bessel (maximally flat delay) filters are often used in filter banks.⁵ In the examples shown in this paper, we have used digital filters obtained from Bessel prototype designs using impulse invariance.⁶ It should be noted that the digital filters obtained this way do not have the maximally flat delay property. J. P. Thiran⁷ has shown that the denominator of the system function of maximally flat delay digital filters is a Gauss hypergeometric function. It is reasonable to expect however, that for the narrow-band filters of interest here, the differences should be negligible.

As an example a digital filter derived from a sixth-order Bessel lowpass filter with asymptotic cutoff frequency of 60 Hz is shown in Fig. 3. The impulse response is shown in Fig. 3a, and the amplitude and phase responses are shown in Fig. 3b and Fig. 3c. The filter shown in Fig. 3 was used in a filter bank* with the following choice of parameters: $D_0 = 0$, $T = 10^{-4}$ sec, $\Delta\omega = 2\pi(100)$, $\omega_1 = 2\pi(100)$, $n_0 = 0$, and $M = 30$. The resulting filter bank characteristics are shown in Fig. 4. The filter bank impulse response, $\tilde{h}(nT)$, is shown in Fig. 4a along with the prototype lowpass impulse response $h(nT)$. For the above choice of parameters, $d(nT)$ is obtained from (15a) as

$$d(nT) = \frac{\sin [0.61\pi n]}{\sin [0.01\pi n]} - 1, \quad (16)$$

which is periodic with period 100 samples (10 msec), with peaks occurring at $nT = 0, \pm 10, \pm 20, \dots$ msec. From Fig. 4a, it can be seen that in the product $h(nT) \cdot d(nT)$, the peak of $d(nT)$ at $nT = 0$ will be attenuated since $h(nT)$ is small around $nT = 0$. On the other hand,

* Note that the resulting bandpass filters are twelfth order.

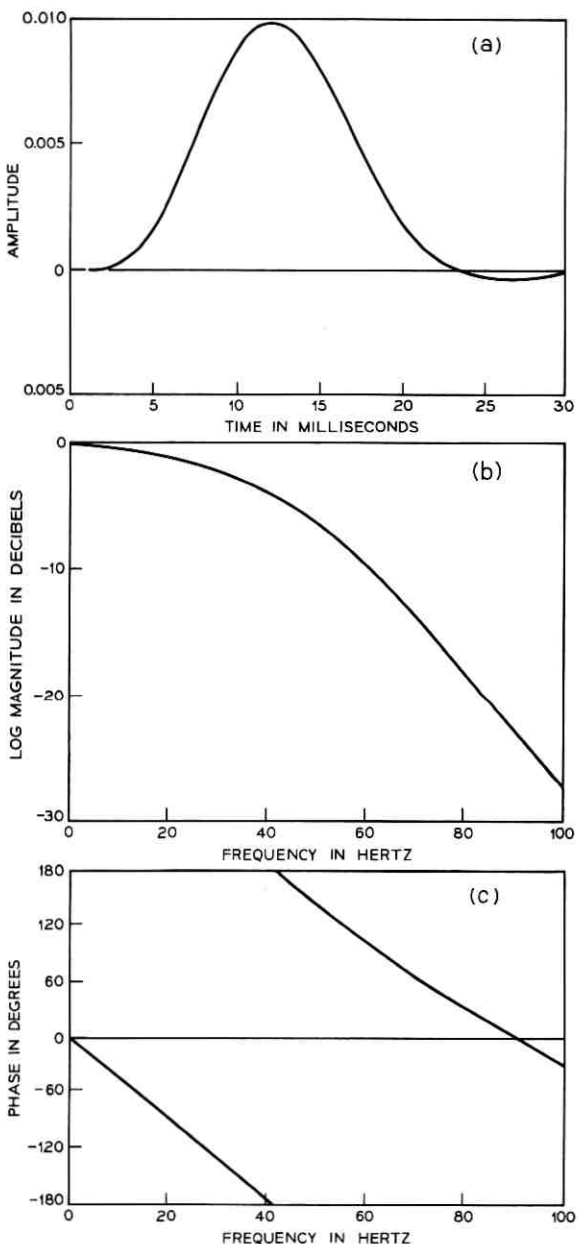


Fig. 3—Sixth-order Bessel filter characteristics. (a) Impulse response, (b) magnitude response, (c) phase response.

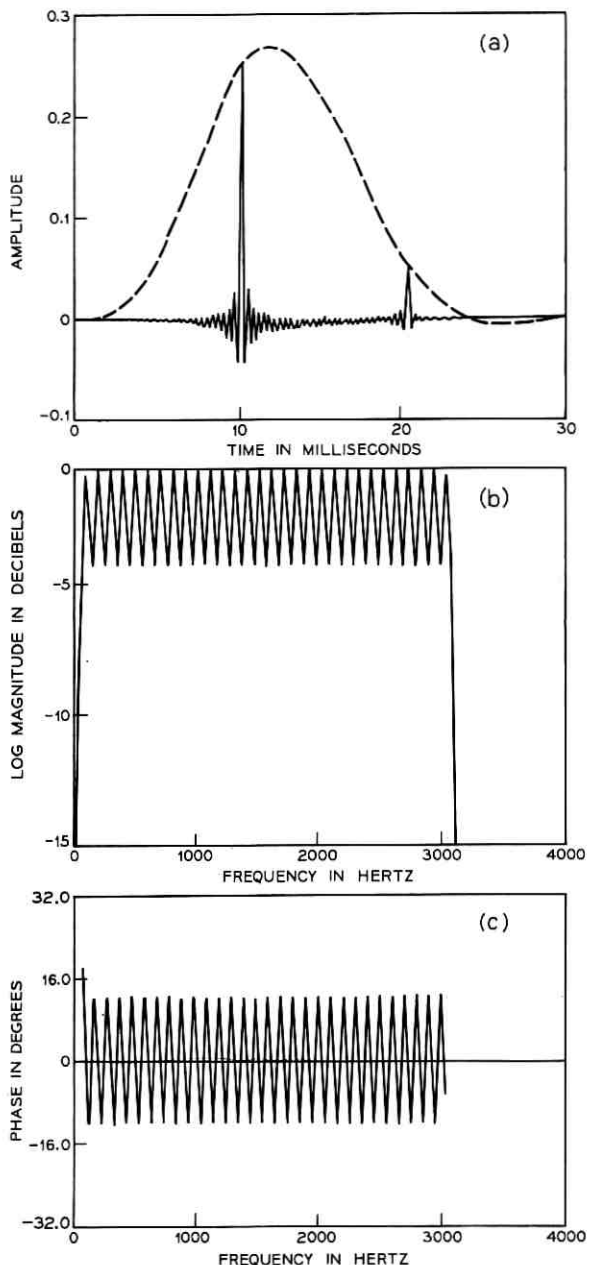


Fig. 4—Characteristics of 30-channel filter bank. (a) Impulse response (dotted curve is the impulse response of the prototype lowpass filter in Fig. 3), (b) composite magnitude response, (c) composite phase response after subtracting 10-msec delay.

the peak of $d(nT)$ at $nT = 10$ msec occurs at approximately the peak of $h(nT)$, and at $nT = 20$ msec, $h(nT)$ is large enough to produce a significant echo in the impulse response of the filter bank. As is shown in Fig. 4b and 4c, this corresponds to a 3.9-dB ripple in the amplitude response and a 25.5-degree peak-to-peak ripple in the phase response (after removing a linear phase component corresponding to a 10-msec or 100-sample delay). To decrease this amplitude and phase ripple, we should attempt to eliminate the echo in the impulse response. Furthermore, the phase ripple will be eliminated if the impulse response $h(nT)$ has even symmetry about some delay time $n_D T$. One approach is to broaden the filter bandwidths, or equivalently reduce the spacing $\Delta\omega$, so that $h(nT)$ is contracted relative to the spacing of pulses in $d(nT)$. This is generally not an acceptable solution since $h(nT)$ and $\Delta\omega$ are usually fixed by some frequency resolution criterion. However, if we refer to the properties of $d(nT)$ which were previously summarized, we note that a negative value of n_0 will shift $d(nT)$ to the right relative to $h(nT)$ so that $d(nT)$ will have even symmetry about time $n_D T = -n_0 T$. If n_0 can be chosen so that $\tilde{h}(nT) = h(nT) \cdot d(nT)$ has approximately even symmetry and consists of only one significant pulse, then the amplitude and phase ripple will be small. The manner in which this is achieved is shown in Fig. 5 where it is assumed for simplicity that $d(nT)$ is a train of digital impulses as would be the case for $M = (N - 1)/2$. Figure 5a depicts the case where $n_0 = 0$. Figure 5b shows the situation where n_0 was chosen to shift the impulse which was at $nT = 0$ in Fig. 5a to the right and into the vicinity of the peak of $h(nT)$. If it is assumed that only three impulses have nonzero amplitudes ($\alpha_1, \alpha_2, \alpha_3$) such that $4|\alpha_1| \cdot |\alpha_3| < |\alpha_1 + \alpha_3| \cdot |\alpha_2|$, then it can be shown (see Appendix) that the peak-to-peak amplitude ripple of the filter bank is

$$R_A = 20 \log_{10} \left[\frac{|\alpha_2 + \alpha_1 + \alpha_3|}{|\alpha_2 - \alpha_1 - \alpha_3|} \right]. \quad (17)$$

Similarly, if $|\alpha_1 + \alpha_3| < |\alpha_2|$, the peak-to-peak phase ripple about a linear phase corresponding to a delay of $-n_0 T$ is given by

$$R_P = 2 \tan^{-1} \left[\frac{\alpha_1 - \alpha_3}{(\alpha_2^2 - (\alpha_1 + \alpha_3)^2)^{1/2}} \right]. \quad (18)$$

The conditions for (17) and (18) to hold are satisfied when α_1 and α_3 are small relative to α_2 , which is the normal situation. It can be seen from (18) and (17) that the phase ripple will be zero if $\alpha_1 = \alpha_3$, and the amplitude ripple will be small if $(\alpha_1 + \alpha_3)/\alpha_2$ is small.

Although these results were derived for the idealized case when $d(nT)$

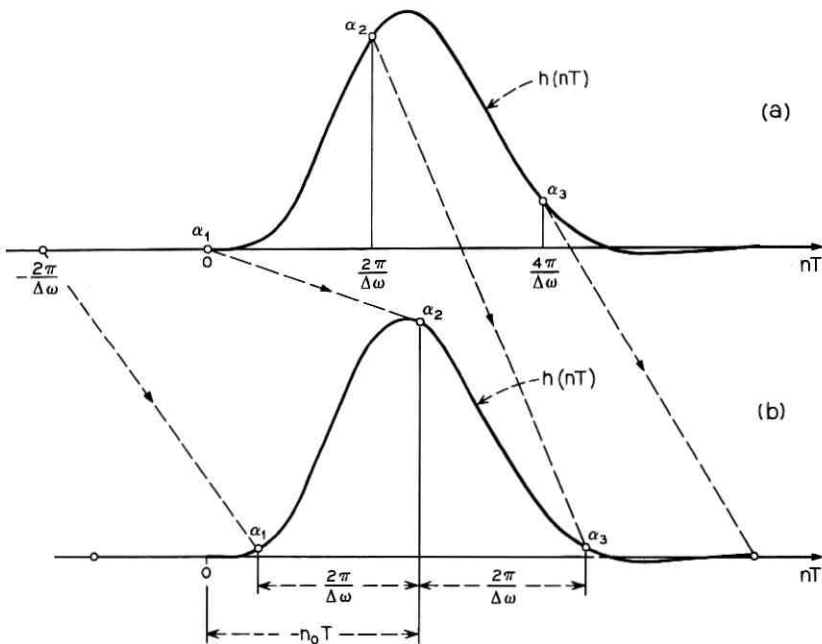


Fig. 5—Illustration of how to adjust the parameter n_0 . (a) Composite impulse response for $n_0 = 0$, (b) n_0 chosen to minimize magnitude and phase ripple (dotted lines indicate movement of individual pulses in $d(nT)$).

is an impulse train, we have found that amplitude and phase ripple can be determined quite accurately using (17) and (18) in more general situations. With the foregoing principles in mind we have written an interactive computer program for filter bank design. Using this program we can design a filter bank with low amplitude and phase ripple by the following process:

- Choose ω_1 , $\Delta\omega$, and M to cover the desired analysis band and choose $h(nT)$ to provide desired frequency resolution. This results in an $h(nT)$ that has a duration of approximately $4\pi/\Delta\omega$ as shown in Fig. 5.
- Evaluate $h(nT)$ and determine n_0 such that $\alpha_1 \approx \alpha_3$ as in Fig. 5b.
- If the resulting filter bank is not satisfactory, steps i and ii are repeated.

In cases where $\omega_1/\Delta\omega$ is not an integer, it is important to choose n_0

so that the point of even symmetry in $d(nT)$ is shifted into the vicinity of the peak of $h(nT)$. Otherwise, it may be impossible to achieve a very good approximation to linear phase. An example of the improvement gained by proper choice of n_0 is shown in Fig. 6. In this example all the parameters were the same as in the example of Fig. 4 except a value of $n_0 = -129$ was chosen by the above process. In this case the in-band amplitude ripple is 0.8 dB and the phase ripple is 0.6 degree, as compared to 3.8 dB and 25.5 degrees when $n_0 = 0$.

R. M. Golden⁵ has shown that inverting the sign of alternating channels often significantly improves the characteristics of a filter bank. This technique has a simple interpretation in terms of our results. It can be shown that inverting the sign of alternating channels is equivalent to delaying the sequence $d(nT)$ by $n_0 = -\pi/(\Delta\omega T)$ samples. This amount of delay may be nearly correct if the duration of $h(nT)$ is approximately $3\pi/\Delta\omega$; however for the situation shown in Fig. 4a, such a delay would produce a worse filter bank than no delay at all ($n_0 = 0$). Also, to achieve linear phase when $\omega_1/\Delta\omega$ is not an integer, the point of even symmetry in $d(nT)$ should be delayed to the vicinity of the peak of $h(nT)$. This does not occur when the signs of alternate channels are inverted.

IV. DESIGN OF NONUNIFORM BANDWIDTH FILTER BANKS

In speech applications it is common to take advantage of the frequency resolution characteristics of the ear^{4,5} by using increasing bandwidth filters at higher frequencies. The previously discussed techniques can be applied to this situation if the filter bank consists of several sub-banks, each with different resolution. Each sub-bank can be designed as discussed above, with care being taken to ensure that the entire frequency band of interest is covered by the combination of the sub-banks. It may be necessary to equalize the delay between sub-banks by providing additional delay for all but one of the sub-banks.* This is depicted in Fig. 7 for three sub-banks with increasing-bandwidth sixth-order Bessel filters. Figure 7a shows the lowpass prototype impulse response and shifted $d(nT)$ sequence[†] for the first sub-bank. The lowpass asymptotic cutoff used was 78 Hz, the spacing of filters was $\Delta\omega_1 = 2\pi(125)$, the first filter was centered at $\omega_{11} = 2\pi(250)$, and a value of $n_{01} = -100$ (10-msec delay) was required to

* Golden⁵ has shown that the delays can be approximately equalized by increasing the order of the lowpass prototype in direct proportion to the increase in bandwidth.

[†] The sequence $d(nT)$ is shown as an impulse train for convenience in plotting. The actual sequences would look like those in Fig. 4 and Fig. 6.

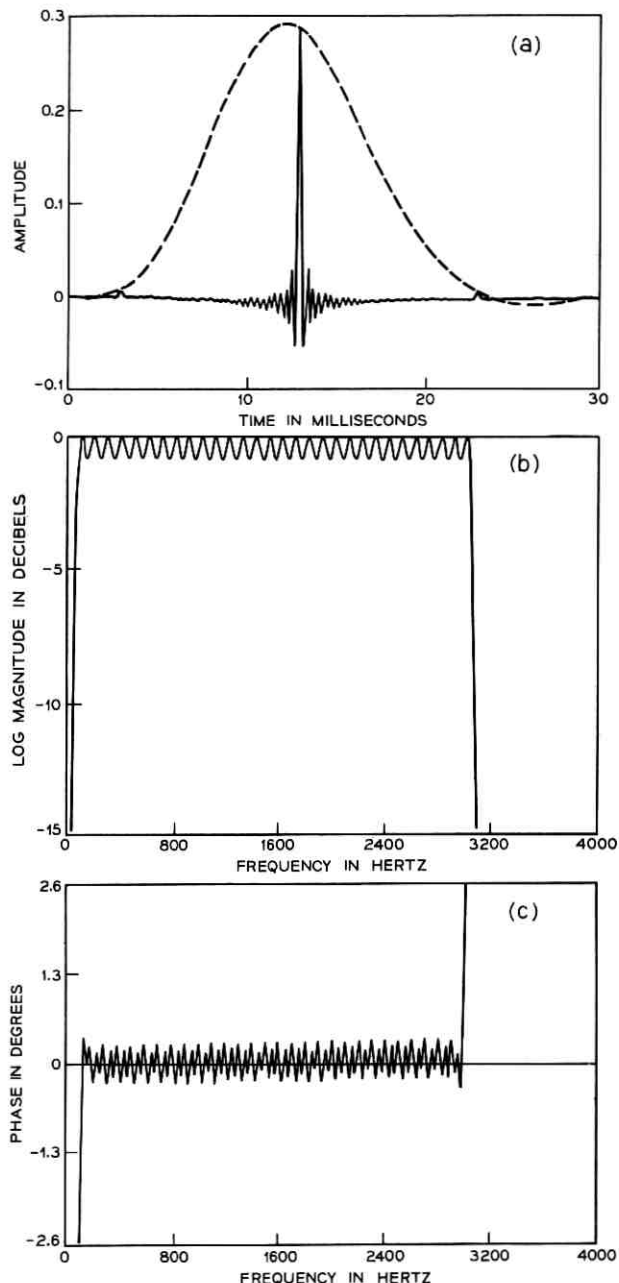


Fig. 6—Characteristics of 30-channel filter bank. (a) Impulse response for $n_0 = -129$ (dotted curve is the impulse response in Fig. 3), (b) composite magnitude response, (c) composite phase response after subtracting 12.9-msec delay.

minimize the amplitude and phase ripple. Figure 7b shows the second sub-band in which the basic parameters were: lowpass asymptotic cutoff 136 Hz, $\Delta\omega_2 = 2\pi(218)$, $\omega_{12} = 2\pi(1296.5)$, and $n_{02} = -57$ (5.7-msec delay). To line up the central peaks, an additional delay of $n_2 = 43$ samples (4.3 msec) was required. Figure 7c shows the third sub-band where the lowpass cutoff was 192 Hz, $\Delta\omega_3 = 2\pi(307)$, $\omega_{13} = 2\pi(2213)$, and $n_{03} = -40$ (4-msec delay). A value of $n_3 = 60$ samples (6.0 msec) is required to line up the central peak with those in Fig. 7a and 7b. The response of the combination of these three sub-banks is shown in Fig. 8. Figure 8a shows the impulse response, Fig. 8b shows the amplitude response, and Fig. 8c shows the phase after a linear phase corresponding to 10-msec delay has been subtracted. It can be

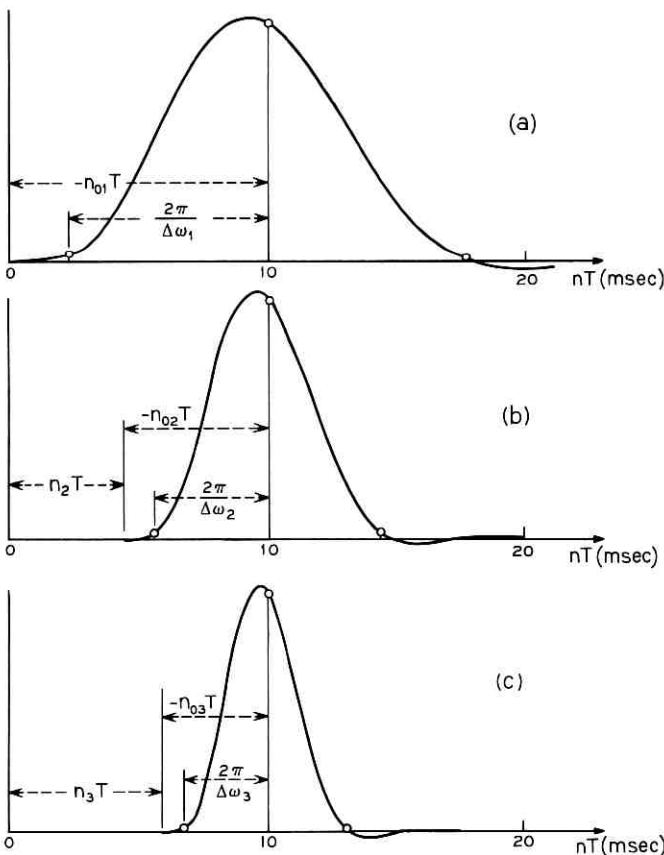


Fig. 7—Illustration of the design of nonuniform filter banks: (a) impulse response for narrow bandwidth filters, (b) impulse response for intermediate bandwidth filters, (c) impulse response for wide bandwidth filters.

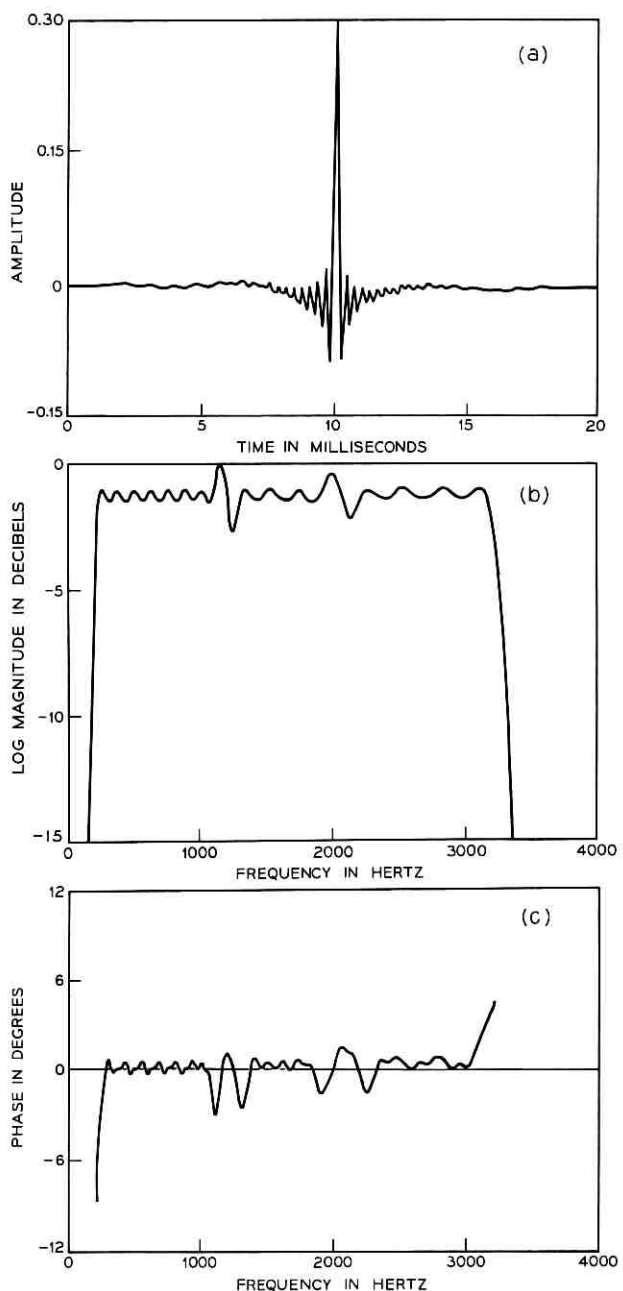


Fig. 8—Composite filter bank characteristics with three different sub-banks: (a) impulse response, (b) magnitude response, (c) phase response after subtracting 10-msec delay.

seen in Fig. 8b and 8c that the ripple in the sub-banks is quite low as would be expected from Fig. 7. At the boundary between sub-banks, however, the ripple increases significantly due to the fact that the last filter in the lower sub-bank drops off more rapidly than the first filter in the next sub-bank. This excessive variation at the boundary between sub-banks can be eliminated to some extent by using increasingly higher-order filters in the sub-banks. Alternatively, nonuniform resolution can be obtained by using equal-bandwidth filters and adding together groups of two or more of their outputs to achieve the desired bandwidth. Such an approach would require increased computation but would produce filter bank characteristics comparable to those in Fig. 6.

V. CONCLUSION

We have discussed the analysis and design of digital filter banks and have shown how the incorporation of a linearly increasing phase shift in each bandpass filter can significantly improve the overall filter bank characteristics. We also showed how the techniques can be used in nonuniform bandwidth filter banks.

The examples which we gave were based on Bessel lowpass prototypes which have impulse responses of desirable shape but rather poor amplitude response. Recent results in the design of finite duration impulse response filters⁸ offer attractive possibilities for filter bank design. Such filters can have precisely linear phase and can be designed using iterative techniques with constraints on both the impulse response shape and the amplitude response. The use of such filters, together with the basic principles discussed in this paper, should yield filter banks with excellent properties.

APPENDIX

Derivation of Magnitude and Phase Ripple Formulas

Assume an impulse response sequence

$$\begin{aligned}
 h(n) &= \alpha_1 & n = 0 \\
 &= \alpha_2 & n = n_p \\
 &= \alpha_3 & n = 2n_p \\
 &= 0 & \text{elsewhere.}
 \end{aligned} \tag{19}$$

The system function of this system is

$$H(e^{j\omega T}) = \alpha_1 + \alpha_2 e^{-j\omega n_p T} + \alpha_3 e^{-j\omega 2n_p T}. \tag{20}$$

The squared magnitude response is

$$|H(e^{j\omega T})|^2 = [\alpha_2 + (\alpha_1 + \alpha_3) \cos(\omega n_p T)]^2 + (\alpha_1 - \alpha_3)^2 \sin^2(\omega n_p T), \quad (21)$$

and the phase response is

$$\arg[H(e^{j\omega T})] = \tan^{-1} \left[\frac{(\alpha_1 - \alpha_3) \sin(\omega n_p T)}{\alpha_2 + (\alpha_1 + \alpha_3) \cos(\omega n_p T)} \right] \quad (22)$$

where a linear phase component $-\omega n_p T$ has been removed. Clearly, both (21) and (22) are periodic functions of ω with period $2\pi/n_p T$. To determine the amplitude and phase ripple, we must locate the maxima and minima of (21) and (22).

If we differentiate (21) with respect to ω , we find that the maxima and minima occur for values of ω satisfying

$$\sin(\omega n_p T) = 0 \quad (23a)$$

$$\cos(\omega n_p T) = -\alpha_2 \frac{(\alpha_1 + \alpha_3)}{4\alpha_1\alpha_3}. \quad (23b)$$

The second equation is satisfied by a real value of ω if and only if

$$|\alpha_1| \cdot |\alpha_3| > |\alpha_1 + \alpha_2| \cdot |\alpha_2|. \quad (24)$$

In a good filter bank design, α_1 and α_3 will be positive and much smaller than α_2 , and (24) will not be satisfied. Evaluating the second derivative shows that in this case the maxima and minima of $|H(e^{j\omega T})|$ will alternate and occur at values of ω satisfying (23a); i.e., $\omega = 0, \pm\pi/n_p T, \pm 2\pi/n_p T, \dots$. In this case the amplitude ripple in dB is given by

$$R_A = 20 \log_{10} \left[\frac{|\alpha_2 + \alpha_1 + \alpha_3|}{|\alpha_2 - \alpha_1 - \alpha_3|} \right]. \quad (25)$$

If (22) is differentiated with respect to ω , we find that the maxima and minima occur at values of ω satisfying

$$\cos \omega n_p T = -\left(\frac{\alpha_1 + \alpha_3}{\alpha_2} \right). \quad (26)$$

Equation (26) is satisfied by real values of ω if $|\alpha_1 + \alpha_3| < |\alpha_2|$. In this case the maxima and minima again alternate, and the peak-to-peak phase ripple is

$$R_p = 2 \tan^{-1} \left[\frac{\alpha_1 - \alpha_3}{(\alpha_2^2 - (\alpha_1 + \alpha_3)^2)^{1/2}} \right]. \quad (27)$$

If $|\alpha_1 + \alpha_3| > |\alpha_2|$, the phase curve will be discontinuous with a jump of 2π radians occurring at $\omega = \pm\pi/n_p T, \pm 3\pi/n_p T, \dots$.

REFERENCES

1. Flanagan, J. L., and Golden, R. M., "Phase Vocoder," B.S.T.J., 45, No. 9 (November 1966), pp. 1493-1509.
2. Flanagan, J. L., and Lummis, R. C., "Signal Processing to Reduce Multipath Distortion in Small Rooms," J. Acoust. Soc. Am., 47, No. 1 (June 1970), pp. 1475-1481.
3. Jackson, L. B., Kaiser, J. F., and McDonald, H. S., "An Approach to the Implementation of Digital Filters," IEEE Trans. Audio and Electroacoust., AU-16, No. 3 (September 1968), pp. 413-421.
4. Flanagan, J. L., *Speech Analysis, Synthesis and Perception*, New York: Academic Press, 1965.
5. Golden, R. M., "Vocoder Filter Design: Practical Considerations," J. Acoust. Soc. Am., 43, (December 1967) pp. 803-810.
6. Gold, B., and Rader, C. M., *Digital Processing of Signals*, New York: McGraw-Hill Book Co., 1969.
7. Thiran, J. P., "Recursive Digital Filters with Maximally Flat Group Delay," IEEE Trans. Ckt. Theory, CT-18, No. 4 (November 1971).
8. Rabiner, L. R., "Techniques for Designing Finite Duration Impulse Response Digital Filters," IEEE Trans. Com. Tech., COM-19, No. 2 (April 1971), pp. 188-195.

The Preference of Slope Overload to Granularity in the Delta Modulation of Speech

By N. S. JAYANT and A. E. ROSENBERG

(Manuscript received June 18, 1971)

A preference study was made to assess the relative annoyance values of slope-overload distortion and granular noise in delta-modulated speech. A recently described adaptive delta modulator was simulated at frequencies of 20 and 40 kHz, and controlled amounts of the two types of degradation were introduced into samples of a 2-second utterance. Rankings were obtained for these samples on the basis of preference judgments of nine listeners, each of whom assessed the samples, pairwise, in a tournament-type strategy. Results indicate that the speech sample exhibiting the minimum degradation on an objective, overall-noise-power basis is not subjectively the most preferred sample. Furthermore, the subjectively optimum delta modulator exhibits greater overload and lesser granularity than the objectively optimum device.

I. INTRODUCTION

The principle of delta modulation¹ has been widely described in the literature. Briefly, delta modulation is a digital encoding strategy which uses a simple feedback mechanism to produce a "staircase" approximation to an input signal. A block diagram of the simplest form of delta modulation appears in Fig. 1. The input sequence $\{X_r\}$ is usually band-limited and suitably oversampled. The "staircase" sequence Y_r is generated according to the equations

$$C_r = \text{sgn} (X_r - Y_{r-1}) \quad (1)$$

$$Y_r - Y_{r-1} = m_r = \Delta_r \cdot C_r. \quad (2)$$

The step-size Δ_r is assumed to be a constant in conventional (linear) delta modulation. "Adaptive" delta modulation, on the other hand, allows for modifications of Δ_r in accordance with the changing slope

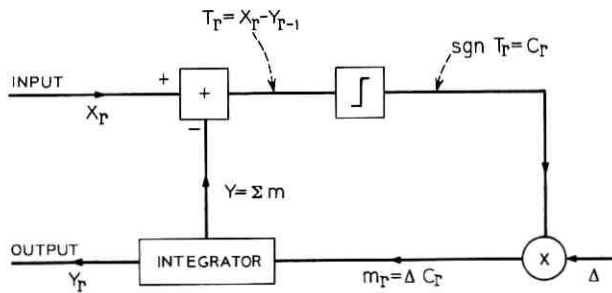


Fig. 1—Schematic diagram of a linear delta modulator.

characteristics of the input signal. Such adaptation results in better encoding, and several types of adaptive delta modulation have been described in the literature.^{2,3,4}

Figure 2 illustrates the mechanism of an adaptive delta modulator and demonstrates how suitable increases and decreases of step size facilitate better encoding during steep and flat regions of the input signal waveform. Such adaptations can be effected by observations on a "recent" segment of the binary sequence $\{C_r\}$; this is illustrated by equation (5) in the sequel.

Figure 2 also brings out the distinction between two types of encoding error in delta modulation, viz., "granular noise" and "slope-overload"

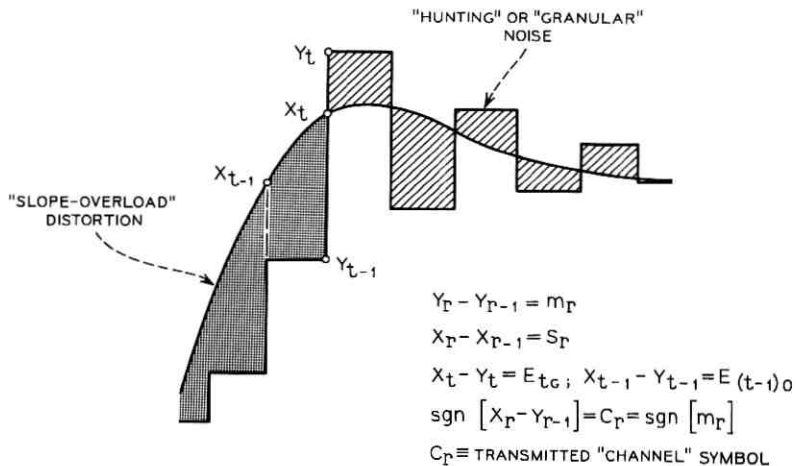


Fig. 2—Illustration of adaptive delta modulation.

distortion. A given error sample

$$E_r = X_r - Y_r \quad (3)$$

can be defined to fall into the granular or slope-overload category, depending on whether the corresponding step m_r crosses the input waveform or not. Thus, in Fig. 2, there is a 'granular' error E_{tG} at the sampling instant t , and an 'overload' error $E_{(t-1)O}$ at the sampling instant $(t-1)$. As a matter of definition, we will note that $E_{tO} = E_{(t-1)G} = 0$.

The signal output $\{Z_r\}$ of the delta modulator is actually obtained by filtering the staircase sequence $\{Y_r\}$ to the input signal band. Let $\{X_r^F\}$ be the result of passing $\{X_r\}$ through the same lowpass filter. A perceptually relevant measure of signal degradation is accordingly defined by the encoding error

$$e_r = X_r^F - Z_r \quad (4)$$

As with the quantity E_r in (3), one can distinguish samples of granularity and slope overload, e_{rG} and e_{rO} , in the error sequence $\{e_r\}$. Referring to Fig. 2 once more it can be seen that a physical distinction between the two types of error is suggested. Granularity can be described as a "signal-uncorrelated" random noise-type of phenomenon. It is characterized by alternation of signs and tends to be independent of signal amplitude. Slope overload, on the other hand, can be described as a "signal-correlated" distortion, since its sign and magnitude are related to the slope of the signal. This physical difference between slope overload and granularity suggests a corresponding perceptual distinction and raises the question of the relative annoyance values of the two forms of signal degradation in delta modulation. The present paper describes a study of the above question as referred to the delta modulation of a speech signal.

Earlier work in this subject is in the form of a perceptual experiment⁵ in which H. Levitt, et al., characterized the perceptibility of slope-overload distortion as such. As mentioned earlier, our paper will seek to answer the complementary question of the relative perceptibilities of slope overload and granularity when they occur simultaneously in delta-modulated speech, as they usually do.

The approach we used was to vary the relative amount of slope overload and granularity introduced into samples of a test utterance, and to evaluate these samples on the basis of both objective and perceptual criteria; and then to interpret these evaluations with specific reference to the overload-granularity dichotomy.

Section II summarizes the salient features of a computer-simulated adaptive delta modulator that was utilized in the present study. This adaptive encoder has been recently described and shown to provide toll-quality speech reproduction at bit rates of practical importance.⁴

Section III defines the objective measures of speech quality used in our study, while Section IV defines a subjective measure of preference and describes an underlying perceptual experiment.

II. DESCRIPTION OF THE DELTA MODULATOR

Figure 3 is a schematic block diagram of the adaptive delta modulator utilized in the present study. This encoder is defined by the basic equations (1) and (2), and by the adaptation rule

$$\left. \begin{aligned} \Delta_r &= P \cdot \Delta_{r-1} & \text{if } C_r = C_{r-1} \\ &= \frac{1}{P} \cdot \Delta_{r-1} & \text{if } C_r \neq C_{r-1} \end{aligned} \right\} ; \quad P \geq 1. \quad (5)$$

Notice that a conventional (linear) delta modulator corresponds to the special case of $P = 1$. In our study the value of P was a variable parameter; different (delta-modulated) speech samples corresponded to different suitably spaced values of P , and thereby to different mixtures of slope-overload and granularity.

The original speech sample X was a 2-second male utterance of "Have you seen Bill?" that had been band-limited to 3.3 kHz. The delta modulation was performed at sampling rates of 20 and 40 kHz. The latter frequency provides speech reproduction that approaches telephone

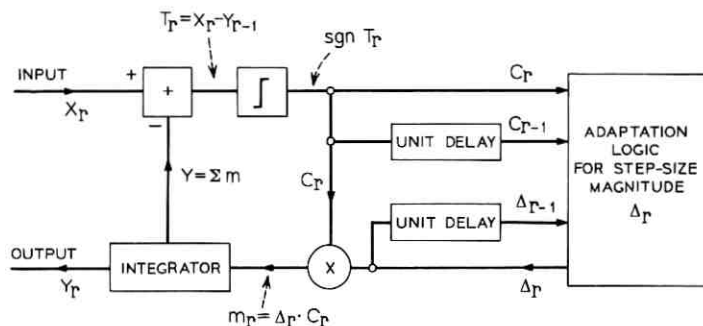


Fig. 3—Schematic diagram of an adaptive delta modulator.

Design of Digital Filter Banks for Speech Analysis

By R. W. SCHAFER and L. R. RABINER

(Manuscript received June 22, 1971)

A bank of bandpass filters is often used in performing short-time spectrum analysis of speech signals. This paper is concerned with the analysis and design of digital filter banks composed of equally spaced bandpass filters. It is shown that significant improvement in the composite filter bank response can be achieved by proper choice of the relative phases of the bandpass filters. The results are extended to more general filter bank configurations.

I. INTRODUCTION

Many speech processing systems are based on the concept of short-time spectrum analysis.^{1,2} Spectrum analyzers for such systems often consist of a set of bandpass filters whose combined passbands cover a desired frequency range. Although continuous-time filters have traditionally been used in filter banks for speech analysis, hardware realizations of digital filters are now available,³ and the advantages which digital filters offer should be exploited in filter bank design. These advantages include: flexibility of design of the individual bandpass filters, precision of realization, stability of digital hardware, and the efficiency of realization of the filter bank afforded by the possibility of multiplexing the digital hardware. Thus it is important to consider design techniques for filter banks composed of digital bandpass filters.

To focus on the basic concepts in filter bank design, it is useful to define an *ideal filter bank* spectrum analyzer. Figure 1 depicts such a filter bank composed of digital filters whose impulse responses are denoted by $h_k(nT)$, $k = 0, 1, \dots, M$, where $1/T$ is the sampling frequency of the input signal.* Such a filter bank constitutes an ideal spectrum analyzer if the input $x(nT)$ (with possibly further band limiting) can be synthesized exactly (within some fixed delay) by a linear

* The filter $h_0(nT)$ is a lowpass filter which is included for completeness although this band is usually not analyzed in practical speech analysis systems.

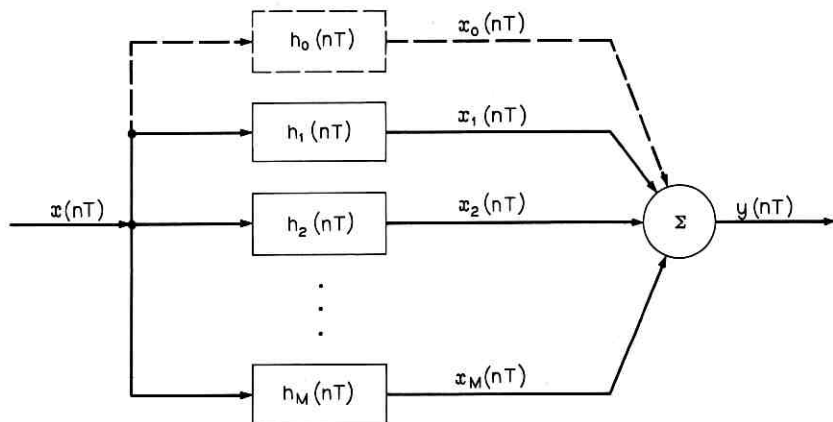


Fig. 1—Bank of digital bandpass filters.

combination of the bandpass filter outputs $x_k(nT)$. An example of such a system would be one in which the filters are ideal rectangular bandpass filters with the same constant gain and linear phase in their passbands and zero gain outside. If the filter bandwidths are such that the frequency range

$$\frac{-\pi}{T} \leq \omega \leq \frac{\pi}{T}$$

is completely covered without overlap, then the input can be synthesized exactly by adding together the outputs of the bandpass filters.

The essential characteristics of the ideal spectrum analyzer are that the frequency response of the combined outputs must exhibit a flat magnitude response and a linear phase, and therefore the combined impulse response must be a delayed digital impulse (unit sample). Causal digital filters (filters whose impulse responses are zero for $n < 0$) cannot have the desired ideal gain characteristics and may not have linear phase.* Therefore a filter bank composed of such filters cannot achieve the ideal characteristics of flat magnitude response and linear phase. In this paper we will describe an approach to the design of filter banks that approximate the ideal spectrum analyzer. First we present a detailed analysis of a filter bank configuration in which equally spaced, equal-bandwidth digital filters are used. This analysis suggests a technique for optimizing the filter bank characteristics and

* Finite duration impulse response digital filters can have precisely linear phase.

also suggests how the results can be used where nonuniform bandwidths are desired. The results are illustrated with examples.

II. ANALYSIS OF UNIFORM FILTER BANKS

Assume that the bandpass filters in Fig. 1 have impulse responses of the form

$$h_k(nT) = 2 | D_k | h(nT) \cos(\omega_k nT + \Phi_k) \quad k = 1, 2, \dots, M \quad (1)$$

$$h_0(nT) = | D_0 | h(nT)$$

where $\omega_k = \omega_1 + (k - 1) \Delta\omega$, and $h(nT)$ is the impulse response of a prototype lowpass filter. (When the $k = 0$ lowpass filter is used, $\omega_1 = \Delta\omega$ and $\omega_0 = 0$.) The system functions for this set of bandpass filters are

$$H_k(z) = | D_k | e^{i\Phi_k} H(ze^{-i\omega_k T}) + | D_k | e^{-i\Phi_k} H(ze^{i\omega_k T}) \quad k = 1, 2, \dots, M$$

$$H_0(z) = | D_0 | H(z). \quad (2)$$

The frequency response of these filters is obtained after substituting $z = e^{i\omega T}$ in (2) as

$$H_k(e^{i\omega T}) = | D_k | e^{i\Phi_k} H(e^{i(\omega - \omega_k)T}) + | D_k | e^{-i\Phi_k} H(e^{i(\omega + \omega_k)T}), \quad k = 1, 2, \dots, M, \quad (3)$$

$$H_0(e^{i\omega T}) = | D_0 | H(e^{i\omega T}).$$

If the frequency response of prototype lowpass filter, $H(e^{i\omega T})$, drops off sharply, then it can be seen from (3) that

$$\begin{aligned} | H_k(e^{i\omega T}) | &\approx | D_k | | H(e^{i(\omega - \omega_k)T}) | \quad 0 \leq \omega \leq \pi/T \\ &\approx | D_k | | H(e^{i(\omega + \omega_k)T}) | - \pi/T \leq \omega \leq 0. \end{aligned}$$

In this case the filter bank consists of a set of $(M + 1)$ equally spaced bandpass filters with identical magnitude responses around their respective center frequencies. We have chosen this method of designing bandpass filters from lowpass prototypes for analytical convenience and because of the importance of spectrum analysis systems of this form.^{1,2} The results to be discussed apply for other bandpass transformations in so far as they yield a set of uniformly spaced bandpass filters with identical frequency characteristics.

Our objective is to choose the prototype lowpass filter and the parameters $| D_k |$, ω_1 , $\Delta\omega$, and Φ_k so that the filter bank will closely approximate the characteristics of the ideal spectrum analyzer. To do this we must consider the response of the composite filter bank. First,

however, it is useful to interpret the individual bandpass filter outputs in terms of spectrum analysis considerations.

The individual filter outputs are of the form

$$x_k(nT) = \sum_{r=-\infty}^n x(rT) | D_k | h(nT - rT) \cos [\omega_k(nT - rT) + \Phi_k], \quad (4)$$

$$x_0(nT) = \sum_{r=-\infty}^n x(rT) | D_0 | h(nT - rT)$$

which can be expressed as

$$\begin{aligned} x_k(nT) &= 2 \operatorname{Re} \{ D_k X(\omega_k, n) e^{j \omega_k n T} \} \\ x_0(nT) &= \operatorname{Re} \{ D_0 X(0, n) \} \end{aligned} \quad (5)$$

where D_k is the complex constant defined by

$$\begin{aligned} D_k &= | D_k | e^{j \Phi_k} \quad k = 1, 2, \dots, M \\ D_0 &= | D_0 |, \end{aligned} \quad (6)$$

and

$$X(\omega_k, n) = \sum_{r=-\infty}^n x(rT) h(nT - rT) e^{-j \omega_k r T}. \quad (7)$$

The quantity $X(\omega_k, n)$ is the discrete-time version of the short-time Fourier transform⁴ of $x(nT)$. Thus, (5) serves to relate the bandpass filter outputs $x_k(nT)$ to the short-time Fourier transform.

The frequency response and impulse response of the composite filter bank are obtained from

$$y(nT) = \sum_{k=0}^M x_k(nT). \quad (8)$$

After substituting (5) into (8) and noting that if $x(nT)$ is real, $X(-\omega_k, n)$ is the complex conjugate of $X(\omega_k, n)$, we obtain

$$y(nT) = \sum_{k=-M}^M D_k X(\omega_k, n) e^{j \omega_k n T} \quad (9)$$

where $\omega_{-k} = -\omega_k$, and D_{-k} is the complex conjugate of D_k . Substituting (7) into (9) and interchanging the order of summations results in

$$y(nT) = \sum_{r=-\infty}^n x(rT) \left[h(nT - rT) \cdot \sum_{k=-M}^M D_k e^{j \omega_k (nT - rT)} \right]. \quad (10)$$

Defining

$$d(nT) = \sum_{k=-M}^M D_k e^{j\omega_k n T}, \quad (11)$$

we observe from (10) that the combined impulse response of the filter bank can be expressed as

$$\tilde{h}(nT) = h(nT) d(nT). \quad (12)$$

Equations (11) and (12) are the basic results of the analysis. (Note that they could have been obtained directly by summing the impulse responses $h_k(nT)$, with the sacrifice of the interpretation of the filter bank outputs in terms of the short-time spectrum.)

Equation (12) shows that the filter bank impulse response is the product of the prototype lowpass filter impulse response $h(nT)$, and the sequence $d(nT)$ defined by (11). The choice of lowpass filter depends on both the desired frequency resolution and the requirement of obtaining flat magnitude and linear phase response in the composite filter bank. The sequence $d(nT)$ is independent of the prototype lowpass filter and is a function of the frequency spacing, the relative gains and phases, and the number of bandpass filters. Thus, for a given choice of prototype lowpass filter, the parameters of $d(nT)$ can be adjusted to achieve the best approximation to the ideal spectrum analyzer. To see how this occurs, we shall first examine in detail the characteristics of the sequence $d(nT)$.

As will be shown in the remainder of this section, a particularly useful choice of the complex coefficients D_k in (11) is

$$D_k = e^{j\omega_k n_0 T} \quad k = \pm 1, \pm 2, \dots, \pm M. \quad (13)$$

$$D_0 = 1,$$

where n_0 is an integer. That is,

$$\Phi_k = \omega_k n_0 T, \quad \text{and} \quad |D_k| = 1.$$

(The condition $D_0 = 1$ implies that the band around $\omega = 0$ is included in the filter bank; $D_0 = 0$ implies that it is not.) It can be shown that for this choice of D_k , (11) becomes

$$d(nT) = D_0 + \frac{2 \sin [M \Delta\omega(nT + n_0 T)/2]}{\sin [\Delta\omega(nT + n_0 T)/2]} \cos [\omega_a(nT + n_0 T)] \quad (14)$$

where $\omega_a = \omega_1 + (M - 1) \Delta\omega/2$, and D_0 is 1 or 0 depending on whether or not the lowpass channel is included.

The properties of the sequence $d(nT)$ determine the character of

the impulse response of the filter bank. Some of these properties are summarized below:

- (i) The parameter n_0 shifts the sequence $d(nT)$ by n_0 samples with respect to $h(nT)$.
- (ii) The sequence $d(nT)$ is even about the sample $n = -n_0$; i.e., $d(nT - n_0T) = d(-nT - n_0T)$.
- (iii) The maximum value of $d(nT)$ occurs at $n = -n_0$. This value is $d(-n_0T) = 2M + D_0$.
- (iv) If $2\pi/(\Delta\omega T)$ and $\omega_1/\Delta\omega$ are both integers, then the sequence $d(nT)$ is periodic with period $2\pi/\Delta\omega$. Otherwise, $d(nT)$ will be an almost periodic sequence which will peak up at time intervals of $2\pi/\Delta\omega$.

Insight into the properties of $d(nT)$ can be gained by considering a simple example. Assume that $\omega_1 = \Delta\omega$ and $2\pi/(\Delta\omega T) = N$ where N is an odd integer. That is, the entire frequency range $-\pi/T \leq \omega \leq \pi/T$, is divided into N equal bands. If $M = (N - 1)/2$, the entire frequency range is covered. Under these conditions (14) can be written

$$d(nT) = \frac{\sin \left[\left(\frac{2M+1}{2} \right) \Delta\omega(nT + n_0T) \right]}{\sin [\Delta\omega(nT + n_0T)/2]} - 1 \quad \text{if } D_0 = 0 \quad (15a)$$

$$= \frac{\sin \left[\left(\frac{2M+1}{2} \right) \Delta\omega(nT + n_0T) \right]}{\sin [\Delta\omega(nT + n_0T)/2]} \quad \text{if } D_0 = 1. \quad (15b)$$

(If N is even, the $k = 0$ filter is not used, i.e., $D_0 = 0$, and ω_1 is $\Delta\omega/2$.) It is clear from (15b) that for these conditions $d(nT)$ is a periodic sequence with period $NT = 2\pi/\Delta\omega$. In fact, $d(nT)$ may be thought of as samples of a continuous-time periodic Dirichlet kernel as shown in Fig. 2a. If $M = (N - 1)/2$ and $D_0 = 1$, $d(nT)$ is a periodic discrete-time impulse train with impulses occurring at multiples of NT . This is because the sample points on the periodic Dirichlet kernel occur at the maxima and the zero crossings, as indicated by the small circles in Fig. 2a.

The conditions for $d(nT)$ to be periodic are that both $\omega_1/\Delta\omega$ and $2\pi/(\Delta\omega T)$ be equal to integers. To see this, we must examine (14) in detail. If $2\pi/(\Delta\omega T)$ is an integer, and M is an odd integer, the sequence $2 \sin [M \Delta\omega(nT + n_0T)/2]/\sin [\Delta\omega(nT + n_0T)/2]$ is periodic with period $NT = 2\pi/\Delta\omega$. If $\omega_1/\Delta\omega$ is an integer and M is odd, the sequence $\cos [(\omega_1 + (M - 1) \Delta\omega/2)(nT + n_0T)]$ is also periodic with a period

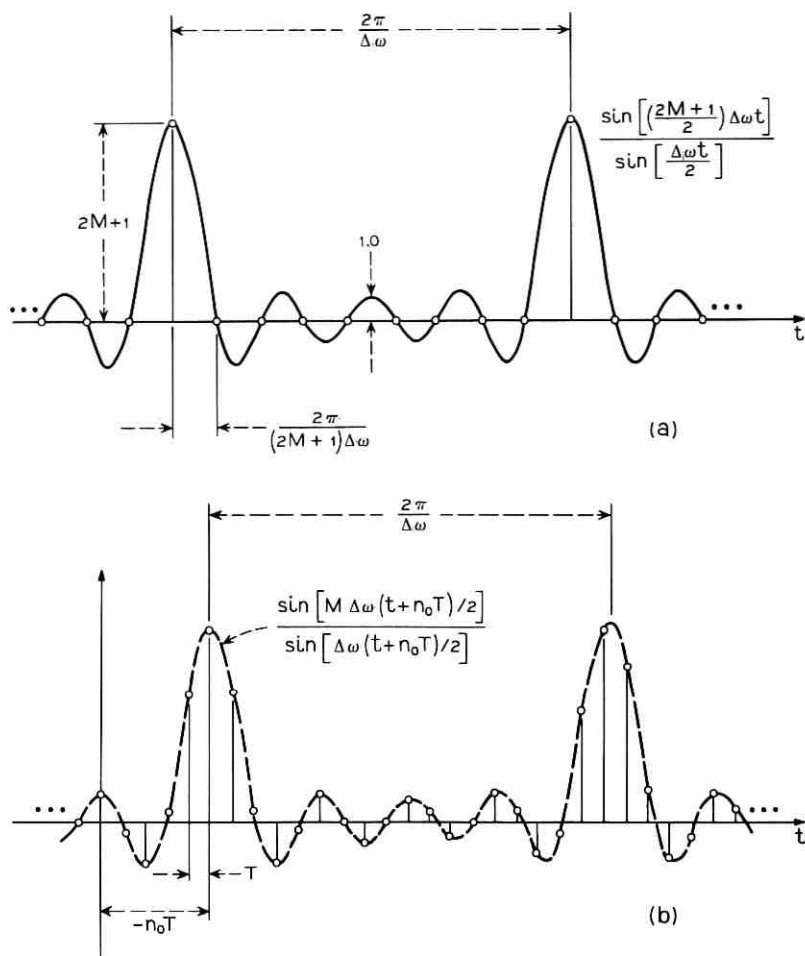


Fig. 2—(a) Periodic continuous-time Dirichlet kernel, (b) continuous-time envelope and sequence $d(nT)$ when either $\omega_1/\Delta\omega$ or $2\pi/(\Delta\omega T)$ are not integers.

that is an integer multiple of $2\pi/\Delta\omega$. Thus the product of these two sequences is periodic with period $2\pi/\Delta\omega$. The identical result holds for M an even integer and $2\pi/\Delta\omega$ and $\omega_1/\Delta\omega$ integers although the interaction between the component sequences is slightly different.

If either $2\pi/(\Delta\omega T)$ or $\omega_1/\Delta\omega$ are not integers, $d(nT)$ will not be periodic, but will still peak up at time intervals of $2\pi/\Delta\omega$. Such a case is depicted in Fig. 2b where the samples $d(nT)$ are marked by the

small circles and the dotted curve shows the factor

$$\sin [M \Delta\omega(nT + n_0 T)/2]/\sin [\Delta\omega(nT + n_0 T)/2]$$

when M is odd. As shown in Fig. 2b, $d(nT)$ will always have even symmetry about sample $n = -n_0$.

III. DESIGN OF UNIFORM FILTER BANKS USING BESSSEL FILTERS

In the preceding section we presented a detailed analysis of a filter bank composed of equally spaced equal-bandwidth filters. In this section we will show how the results of that analysis can be employed in filter bank design.

The objective of flat amplitude response and linear phase is most easily achieved with bandpass filters having these same properties. For this reason, Bessel (maximally flat delay) filters are often used in filter banks.⁵ In the examples shown in this paper, we have used digital filters obtained from Bessel prototype designs using impulse invariance.⁶ It should be noted that the digital filters obtained this way do not have the maximally flat delay property. J. P. Thiran⁷ has shown that the denominator of the system function of maximally flat delay digital filters is a Gauss hypergeometric function. It is reasonable to expect however, that for the narrow-band filters of interest here, the differences should be negligible.

As an example a digital filter derived from a sixth-order Bessel lowpass filter with asymptotic cutoff frequency of 60 Hz is shown in Fig. 3. The impulse response is shown in Fig. 3a, and the amplitude and phase responses are shown in Fig. 3b and Fig. 3c. The filter shown in Fig. 3 was used in a filter bank* with the following choice of parameters: $D_0 = 0$, $T = 10^{-4}$ sec, $\Delta\omega = 2\pi(100)$, $\omega_1 = 2\pi(100)$, $n_0 = 0$, and $M = 30$. The resulting filter bank characteristics are shown in Fig. 4. The filter bank impulse response, $\tilde{h}(nT)$, is shown in Fig. 4a along with the prototype lowpass impulse response $h(nT)$. For the above choice of parameters, $d(nT)$ is obtained from (15a) as

$$d(nT) = \frac{\sin [0.61\pi n]}{\sin [0.01\pi n]} - 1, \quad (16)$$

which is periodic with period 100 samples (10 msec), with peaks occurring at $nT = 0, \pm 10, \pm 20, \dots$ msec. From Fig. 4a, it can be seen that in the product $h(nT) \cdot d(nT)$, the peak of $d(nT)$ at $nT = 0$ will be attenuated since $h(nT)$ is small around $nT = 0$. On the other hand,

* Note that the resulting bandpass filters are twelfth order.

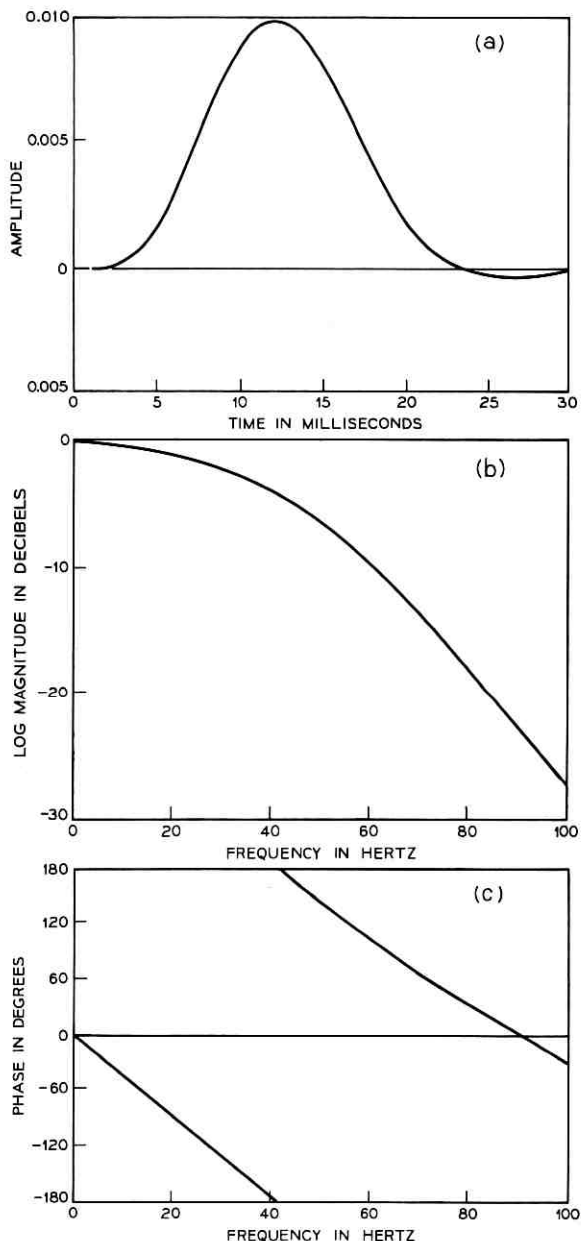


Fig. 3—Sixth-order Bessel filter characteristics. (a) Impulse response, (b) magnitude response, (c) phase response.

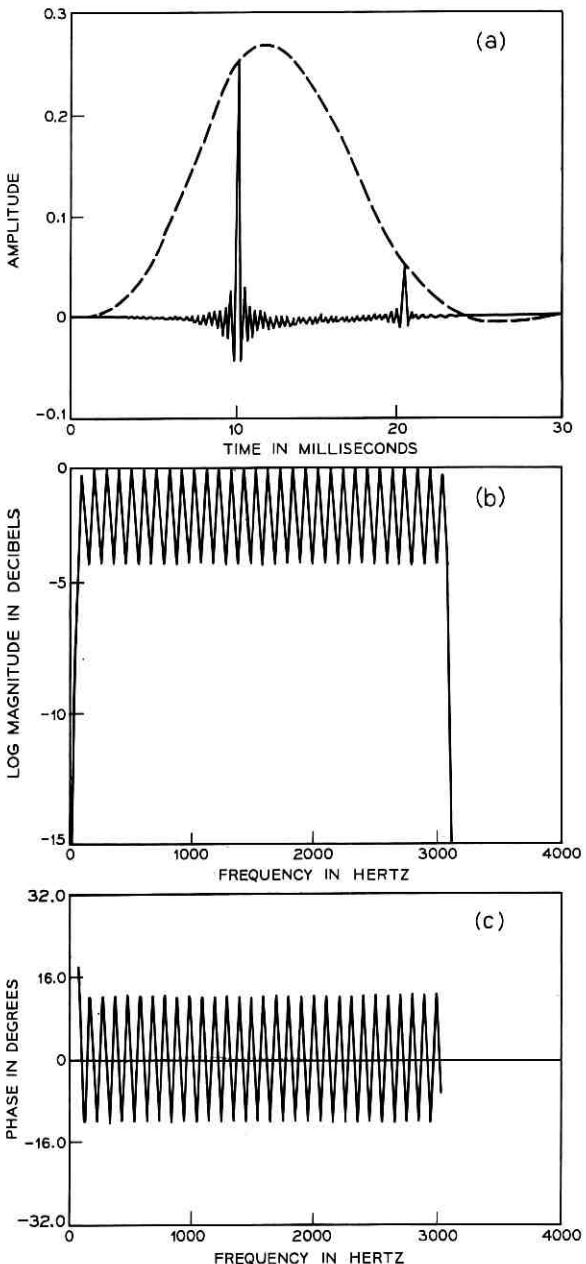


Fig. 4—Characteristics of 30-channel filter bank. (a) Impulse response (dotted curve is the impulse response of the prototype lowpass filter in Fig. 3), (b) composite magnitude response, (c) composite phase response after subtracting 10-msec delay.

the peak of $d(nT)$ at $nT = 10$ msec occurs at approximately the peak of $h(nT)$, and at $nT = 20$ msec, $h(nT)$ is large enough to produce a significant echo in the impulse response of the filter bank. As is shown in Fig. 4b and 4c, this corresponds to a 3.9-dB ripple in the amplitude response and a 25.5-degree peak-to-peak ripple in the phase response (after removing a linear phase component corresponding to a 10-msec or 100-sample delay). To decrease this amplitude and phase ripple, we should attempt to eliminate the echo in the impulse response. Furthermore, the phase ripple will be eliminated if the impulse response $h(nT)$ has even symmetry about some delay time $n_D T$. One approach is to broaden the filter bandwidths, or equivalently reduce the spacing $\Delta\omega$, so that $h(nT)$ is contracted relative to the spacing of pulses in $d(nT)$. This is generally not an acceptable solution since $h(nT)$ and $\Delta\omega$ are usually fixed by some frequency resolution criterion. However, if we refer to the properties of $d(nT)$ which were previously summarized, we note that a negative value of n_0 will shift $d(nT)$ to the right relative to $h(nT)$ so that $d(nT)$ will have even symmetry about time $n_D T = -n_0 T$. If n_0 can be chosen so that $\tilde{h}(nT) = h(nT) \cdot d(nT)$ has approximately even symmetry and consists of only one significant pulse, then the amplitude and phase ripple will be small. The manner in which this is achieved is shown in Fig. 5 where it is assumed for simplicity that $d(nT)$ is a train of digital impulses as would be the case for $M = (N - 1)/2$. Figure 5a depicts the case where $n_0 = 0$. Figure 5b shows the situation where n_0 was chosen to shift the impulse which was at $nT = 0$ in Fig. 5a to the right and into the vicinity of the peak of $h(nT)$. If it is assumed that only three impulses have nonzero amplitudes ($\alpha_1, \alpha_2, \alpha_3$) such that $4|\alpha_1| \cdot |\alpha_3| < |\alpha_1 + \alpha_3| \cdot |\alpha_2|$, then it can be shown (see Appendix) that the peak-to-peak amplitude ripple of the filter bank is

$$R_A = 20 \log_{10} \left[\frac{|\alpha_2 + \alpha_1 + \alpha_3|}{|\alpha_2 - \alpha_1 - \alpha_3|} \right]. \quad (17)$$

Similarly, if $|\alpha_1 + \alpha_3| < |\alpha_2|$, the peak-to-peak phase ripple about a linear phase corresponding to a delay of $-n_0 T$ is given by

$$R_P = 2 \tan^{-1} \left[\frac{\alpha_1 - \alpha_3}{(\alpha_2^2 - (\alpha_1 + \alpha_3)^2)^{1/2}} \right]. \quad (18)$$

The conditions for (17) and (18) to hold are satisfied when α_1 and α_3 are small relative to α_2 , which is the normal situation. It can be seen from (18) and (17) that the phase ripple will be zero if $\alpha_1 = \alpha_3$, and the amplitude ripple will be small if $(\alpha_1 + \alpha_3)/\alpha_2$ is small.

Although these results were derived for the idealized case when $d(nT)$

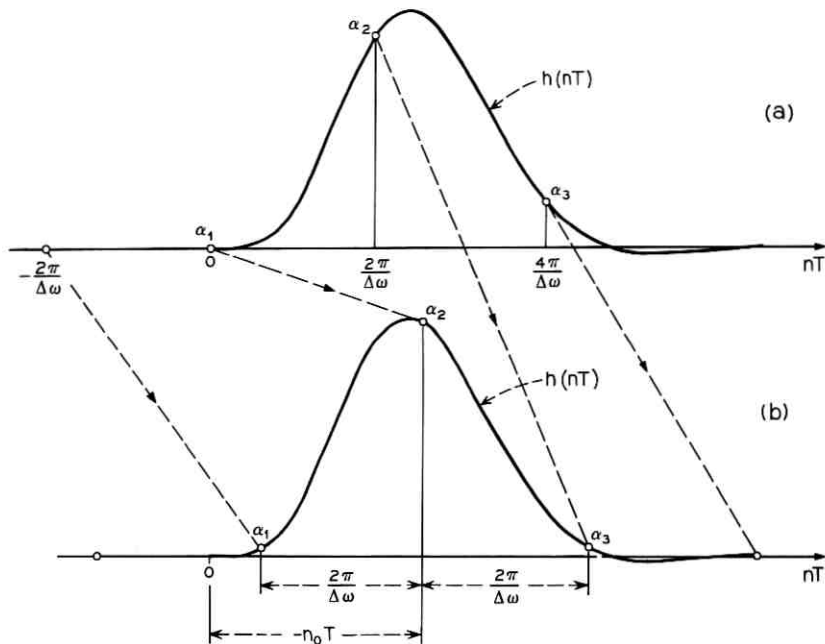


Fig. 5—Illustration of how to adjust the parameter n_0 . (a) Composite impulse response for $n_0 = 0$, (b) n_0 chosen to minimize magnitude and phase ripple (dotted lines indicate movement of individual pulses in $d(nT)$).

is an impulse train, we have found that amplitude and phase ripple can be determined quite accurately using (17) and (18) in more general situations. With the foregoing principles in mind we have written an interactive computer program for filter bank design. Using this program we can design a filter bank with low amplitude and phase ripple by the following process:

- (i) Choose ω_1 , $\Delta\omega$, and M to cover the desired analysis band and choose $h(nT)$ to provide desired frequency resolution. This results in an $h(nT)$ that has a duration of approximately $4\pi/\Delta\omega$ as shown in Fig. 5.
- (ii) Evaluate $h(nT)$ and determine n_0 such that $\alpha_1 \approx \alpha_3$ as in Fig. 5b.
- (iii) If the resulting filter bank is not satisfactory, steps *i* and *ii* are repeated.

In cases where $\omega_1/\Delta\omega$ is not an integer, it is important to choose n_0

so that the point of even symmetry in $d(nT)$ is shifted into the vicinity of the peak of $h(nT)$. Otherwise, it may be impossible to achieve a very good approximation to linear phase. An example of the improvement gained by proper choice of n_0 is shown in Fig. 6. In this example all the parameters were the same as in the example of Fig. 4 except a value of $n_0 = -129$ was chosen by the above process. In this case the in-band amplitude ripple is 0.8 dB and the phase ripple is 0.6 degree, as compared to 3.8 dB and 25.5 degrees when $n_0 = 0$.

R. M. Golden⁵ has shown that inverting the sign of alternating channels often significantly improves the characteristics of a filter bank. This technique has a simple interpretation in terms of our results. It can be shown that inverting the sign of alternating channels is equivalent to delaying the sequence $d(nT)$ by $n_0 = -\pi/(\Delta\omega T)$ samples. This amount of delay may be nearly correct if the duration of $h(nT)$ is approximately $3\pi/\Delta\omega$; however for the situation shown in Fig. 4a, such a delay would produce a worse filter bank than no delay at all ($n_0 = 0$). Also, to achieve linear phase when $\omega_1/\Delta\omega$ is not an integer, the point of even symmetry in $d(nT)$ should be delayed to the vicinity of the peak of $h(nT)$. This does not occur when the signs of alternate channels are inverted.

IV. DESIGN OF NONUNIFORM BANDWIDTH FILTER BANKS

In speech applications it is common to take advantage of the frequency resolution characteristics of the ear^{4,5} by using increasing bandwidth filters at higher frequencies. The previously discussed techniques can be applied to this situation if the filter bank consists of several sub-banks, each with different resolution. Each sub-bank can be designed as discussed above, with care being taken to ensure that the entire frequency band of interest is covered by the combination of the sub-banks. It may be necessary to equalize the delay between sub-banks by providing additional delay for all but one of the sub-banks.* This is depicted in Fig. 7 for three sub-banks with increasing-bandwidth sixth-order Bessel filters. Figure 7a shows the lowpass prototype impulse response and shifted $d(nT)$ sequence[†] for the first sub-bank. The lowpass asymptotic cutoff used was 78 Hz, the spacing of filters was $\Delta\omega_1 = 2\pi(125)$, the first filter was centered at $\omega_{11} = 2\pi(250)$, and a value of $n_{01} = -100$ (10-msec delay) was required to

* Golden⁵ has shown that the delays can be approximately equalized by increasing the order of the lowpass prototype in direct proportion to the increase in bandwidth.

[†] The sequence $d(nT)$ is shown as an impulse train for convenience in plotting. The actual sequences would look like those in Fig. 4 and Fig. 6.

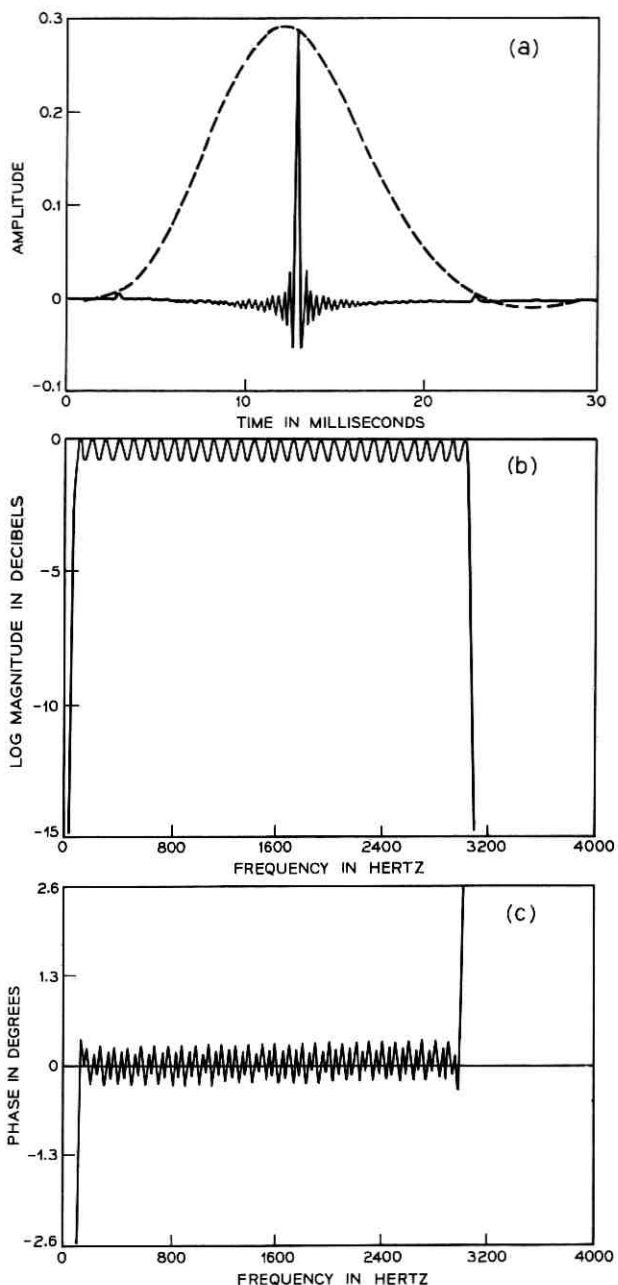


Fig. 6—Characteristics of 30-channel filter bank. (a) Impulse response for $n_0 = -129$ (dotted curve is the impulse response in Fig. 3), (b) composite magnitude response, (c) composite phase response after subtracting 12.9-msec delay.

minimize the amplitude and phase ripple. Figure 7b shows the second sub-bank in which the basic parameters were: lowpass asymptotic cutoff 136 Hz, $\Delta\omega_2 = 2\pi(218)$, $\omega_{12} = 2\pi(1296.5)$, and $n_{02} = -57$ (5.7-msec delay). To line up the central peaks, an additional delay of $n_2 = 43$ samples (4.3 msec) was required. Figure 7c shows the third sub-bank where the lowpass cutoff was 192 Hz, $\Delta\omega_3 = 2\pi(307)$, $\omega_{13} = 2\pi(2213)$, and $n_{03} = -40$ (4-msec delay). A value of $n_3 = 60$ samples (6.0 msec) is required to line up the central peak with those in Fig. 7a and 7b. The response of the combination of these three sub-banks is shown in Fig. 8. Figure 8a shows the impulse response, Fig. 8b shows the amplitude response, and Fig. 8c shows the phase after a linear phase corresponding to 10-msec delay has been subtracted. It can be

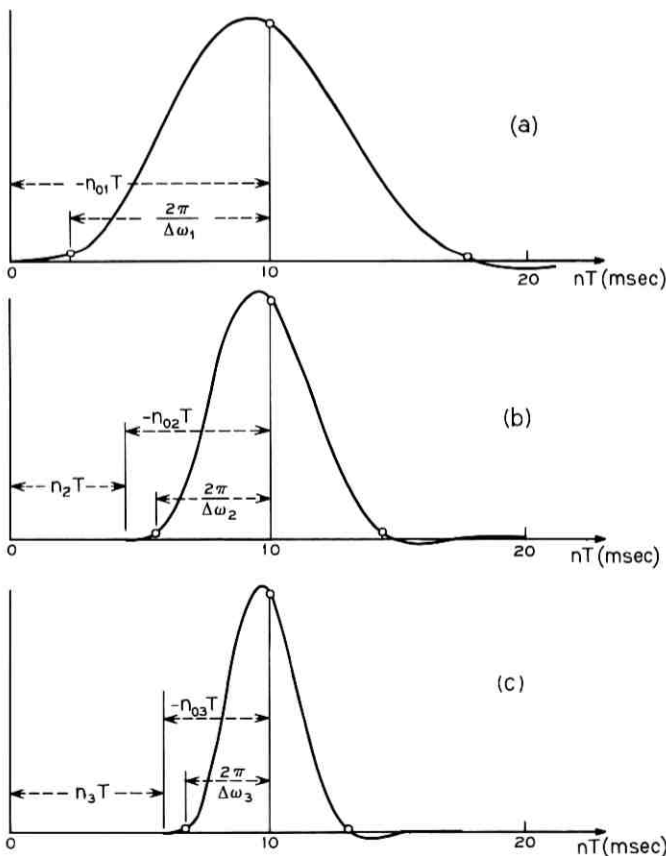


Fig. 7—Illustration of the design of nonuniform filter banks: (a) impulse response for narrow bandwidth filters, (b) impulse response for intermediate bandwidth filters, (c) impulse response for wide bandwidth filters.

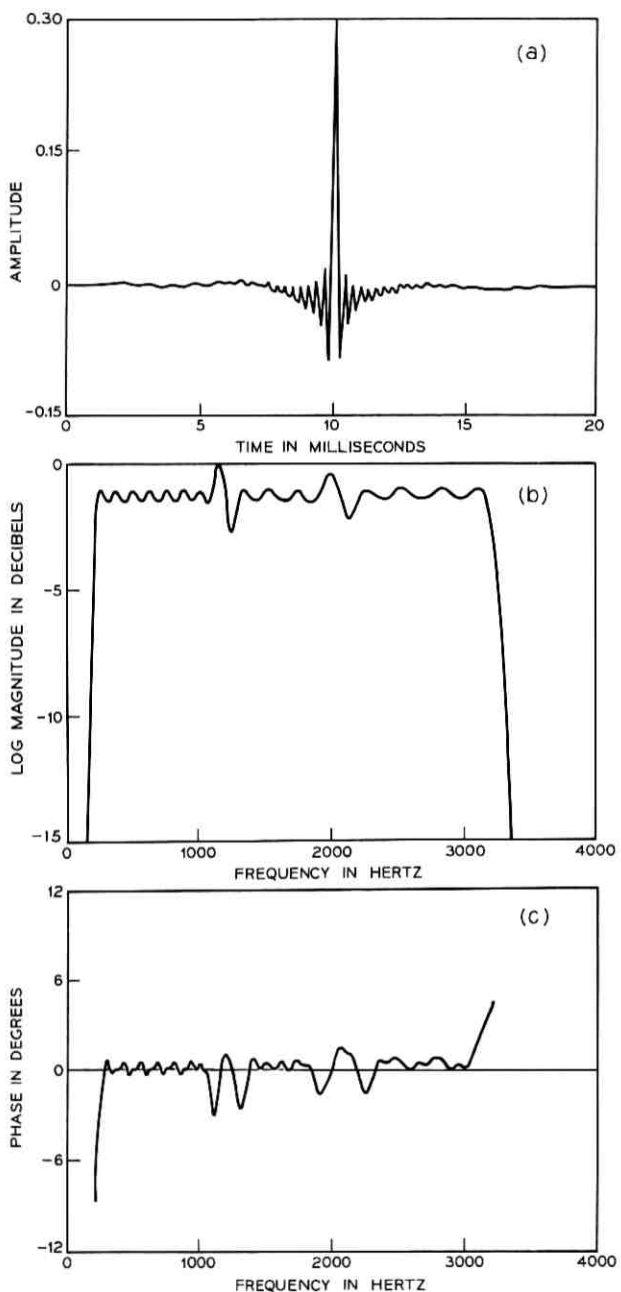


Fig. 8—Composite filter bank characteristics with three different sub-banks: (a) impulse response, (b) magnitude response, (c) phase response after subtracting 10-msec delay.

seen in Fig. 8b and 8c that the ripple in the sub-banks is quite low as would be expected from Fig. 7. At the boundary between sub-banks, however, the ripple increases significantly due to the fact that the last filter in the lower sub-bank drops off more rapidly than the first filter in the next sub-bank. This excessive variation at the boundary between sub-banks can be eliminated to some extent by using increasingly higher-order filters in the sub-banks. Alternatively, nonuniform resolution can be obtained by using equal-bandwidth filters and adding together groups of two or more of their outputs to achieve the desired bandwidth. Such an approach would require increased computation but would produce filter bank characteristics comparable to those in Fig. 6.

V. CONCLUSION

We have discussed the analysis and design of digital filter banks and have shown how the incorporation of a linearly increasing phase shift in each bandpass filter can significantly improve the overall filter bank characteristics. We also showed how the techniques can be used in nonuniform bandwidth filter banks.

The examples which we gave were based on Bessel lowpass prototypes which have impulse responses of desirable shape but rather poor amplitude response. Recent results in the design of finite duration impulse response filters⁸ offer attractive possibilities for filter bank design. Such filters can have precisely linear phase and can be designed using iterative techniques with constraints on both the impulse response shape and the amplitude response. The use of such filters, together with the basic principles discussed in this paper, should yield filter banks with excellent properties.

APPENDIX

Derivation of Magnitude and Phase Ripple Formulas

Assume an impulse response sequence

$$\begin{aligned}
 h(n) &= \alpha_1 & n = 0 \\
 &= \alpha_2 & n = n_p \\
 &= \alpha_3 & n = 2n_p \\
 &= 0 & \text{elsewhere.}
 \end{aligned} \tag{19}$$

The system function of this system is

$$H(e^{i\omega T}) = \alpha_1 + \alpha_2 e^{-i\omega n_p T} + \alpha_3 e^{-i\omega 2n_p T}. \tag{20}$$

The squared magnitude response is

$$|H(e^{j\omega T})|^2 = [\alpha_2 + (\alpha_1 + \alpha_3) \cos(\omega n_p T)]^2 + (\alpha_1 - \alpha_3)^2 \sin^2(\omega n_p T), \quad (21)$$

and the phase response is

$$\arg[H(e^{j\omega T})] = \tan^{-1} \left[\frac{(\alpha_1 - \alpha_3) \sin(\omega n_p T)}{\alpha_2 + (\alpha_1 + \alpha_3) \cos(\omega n_p T)} \right] \quad (22)$$

where a linear phase component $-\omega n_p T$ has been removed. Clearly, both (21) and (22) are periodic functions of ω with period $2\pi/n_p T$. To determine the amplitude and phase ripple, we must locate the maxima and minima of (21) and (22).

If we differentiate (21) with respect to ω , we find that the maxima and minima occur for values of ω satisfying

$$\sin(\omega n_p T) = 0 \quad (23a)$$

$$\cos(\omega n_p T) = -\alpha_2 \frac{(\alpha_1 + \alpha_3)}{4\alpha_1\alpha_3}. \quad (23b)$$

The second equation is satisfied by a real value of ω if and only if

$$4 |\alpha_1| \cdot |\alpha_3| > |\alpha_1 + \alpha_2| \cdot |\alpha_2|. \quad (24)$$

In a good filter bank design, α_1 and α_3 will be positive and much smaller than α_2 , and (24) will not be satisfied. Evaluating the second derivative shows that in this case the maxima and minima of $|H(e^{j\omega T})|$ will alternate and occur at values of ω satisfying (23a); i.e., $\omega = 0, \pm\pi/n_p T, \pm 2\pi/n_p T, \dots$. In this case the amplitude ripple in dB is given by

$$R_A = 20 \log_{10} \left[\frac{|\alpha_2 + \alpha_1 + \alpha_3|}{|\alpha_2 - \alpha_1 - \alpha_3|} \right]. \quad (25)$$

If (22) is differentiated with respect to ω , we find that the maxima and minima occur at values of ω satisfying

$$\cos \omega n_p T = -\left(\frac{\alpha_1 + \alpha_3}{\alpha_2} \right). \quad (26)$$

Equation (26) is satisfied by real values of ω if $|\alpha_1 + \alpha_3| < |\alpha_2|$. In this case the maxima and minima again alternate, and the peak-to-peak phase ripple is

$$R_p = 2 \tan^{-1} \left[\frac{\alpha_1 - \alpha_3}{(\alpha_2^2 - (\alpha_1 + \alpha_3)^2)^{1/2}} \right]. \quad (27)$$

If $|\alpha_1 + \alpha_3| > |\alpha_2|$, the phase curve will be discontinuous with a jump of 2π radians occurring at $\omega = \pm\pi/n_p T, \pm 3\pi/n_p T, \dots$.

REFERENCES

1. Flanagan, J. L., and Golden, R. M., "Phase Vocoder," *B.S.T.J.*, **45**, No. 9 (November 1966), pp. 1493-1509.
2. Flanagan, J. L., and Lummis, R. C., "Signal Processing to Reduce Multipath Distortion in Small Rooms," *J. Acoust. Soc. Am.*, **47**, No. 1 (June 1970), pp. 1475-1481.
3. Jackson, L. B., Kaiser, J. F., and McDonald, H. S., "An Approach to the Implementation of Digital Filters," *IEEE Trans. Audio and Electroacoust.*, *AU-16*, No. 3 (September 1968), pp. 413-421.
4. Flanagan, J. L., *Speech Analysis, Synthesis and Perception*, New York: Academic Press, 1965.
5. Golden, R. M., "Vocoder Filter Design: Practical Considerations," *J. Acoust. Soc. Am.*, **43**, (December 1967) pp. 803-810.
6. Gold, B., and Rader, C. M., *Digital Processing of Signals*, New York: McGraw-Hill Book Co., 1969.
7. Thiran, J. P., "Recursive Digital Filters with Maximally Flat Group Delay," *IEEE Trans. Ckt. Theory*, *CT-18*, No. 4 (November 1971).
8. Rabiner, L. R., "Techniques for Designing Finite Duration Impulse Response Digital Filters," *IEEE Trans. Com. Tech.*, *COM-19*, No. 2 (April 1971), pp. 188-195.

The Preference of Slope Overload to Granularity in the Delta Modulation of Speech

By N. S. JAYANT and A. E. ROSENBERG

(Manuscript received June 18, 1971)

A preference study was made to assess the relative annoyance values of slope-overload distortion and granular noise in delta-modulated speech. A recently described adaptive delta modulator was simulated at frequencies of 20 and 40 kHz, and controlled amounts of the two types of degradation were introduced into samples of a 2-second utterance. Rankings were obtained for these samples on the basis of preference judgments of nine listeners, each of whom assessed the samples, pairwise, in a tournament-type strategy. Results indicate that the speech sample exhibiting the minimum degradation on an objective, overall-noise-power basis is not subjectively the most preferred sample. Furthermore, the subjectively optimum delta modulator exhibits greater overload and lesser granularity than the objectively optimum device.

I. INTRODUCTION

The principle of delta modulation¹ has been widely described in the literature. Briefly, delta modulation is a digital encoding strategy which uses a simple feedback mechanism to produce a "staircase" approximation to an input signal. A block diagram of the simplest form of delta modulation appears in Fig. 1. The input sequence $\{X_r\}$ is usually band-limited and suitably oversampled. The "staircase" sequence Y_r is generated according to the equations

$$C_r = \text{sgn} (X_r - Y_{r-1}) \quad (1)$$

$$Y_r - Y_{r-1} = m_r = \Delta_r \cdot C_r. \quad (2)$$

The step-size Δ_r is assumed to be a constant in conventional (linear) delta modulation. "Adaptive" delta modulation, on the other hand, allows for modifications of Δ_r in accordance with the changing slope

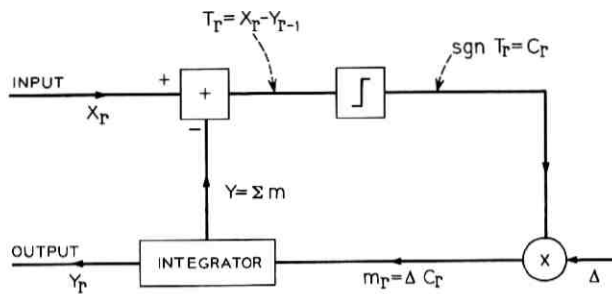


Fig. 1—Schematic diagram of a linear delta modulator.

characteristics of the input signal. Such adaptation results in better encoding, and several types of adaptive delta modulation have been described in the literature.^{2,3,4}

Figure 2 illustrates the mechanism of an adaptive delta modulator and demonstrates how suitable increases and decreases of step size facilitate better encoding during steep and flat regions of the input signal waveform. Such adaptations can be effected by observations on a "recent" segment of the binary sequence $\{C_r\}$; this is illustrated by equation (5) in the sequel.

Figure 2 also brings out the distinction between two types of encoding error in delta modulation, viz., "granular noise" and "slope-overload"

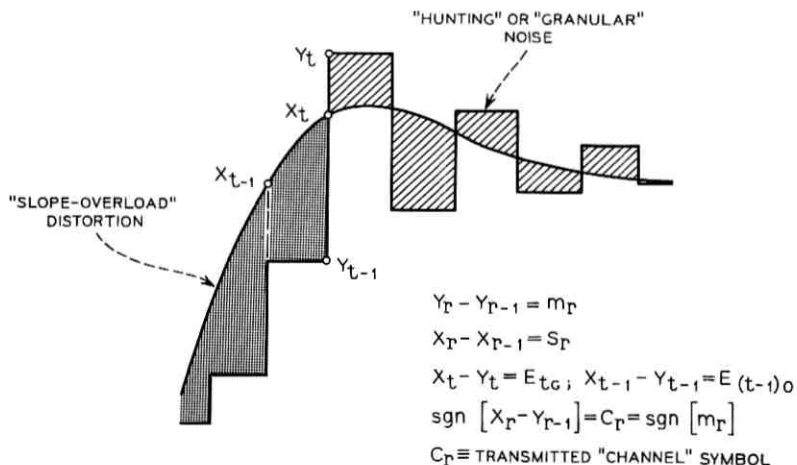


Fig. 2—Illustration of adaptive delta modulation.

distortion. A given error sample

$$E_r = X_r - Y_r \quad (3)$$

can be defined to fall into the granular or slope-overload category, depending on whether the corresponding step m_r crosses the input waveform or not. Thus, in Fig. 2, there is a 'granular' error $E_{r,G}$ at the sampling instant t , and an 'overload' error $E_{(t-1),O}$ at the sampling instant $(t-1)$. As a matter of definition, we will note that $E_{t,O} = E_{(t-1),G} = 0$.

The signal output $\{Z_r\}$ of the delta modulator is actually obtained by filtering the staircase sequence $\{Y_r\}$ to the input signal band. Let $\{X_r^F\}$ be the result of passing $\{X_r\}$ through the same lowpass filter. A perceptually relevant measure of signal degradation is accordingly defined by the encoding error

$$e_r = X_r^F - Z_r \quad (4)$$

As with the quantity E , in (3), one can distinguish samples of granularity and slope overload, $e_{r,G}$ and $e_{r,O}$, in the error sequence $\{e_r\}$. Referring to Fig. 2 once more it can be seen that a physical distinction between the two types of error is suggested. Granularity can be described as a "signal-uncorrelated" random noise-type of phenomenon. It is characterized by alternation of signs and tends to be independent of signal amplitude. Slope overload, on the other hand, can be described as a "signal-correlated" distortion, since its sign and magnitude are related to the slope of the signal. This physical difference between slope overload and granularity suggests a corresponding perceptual distinction and raises the question of the relative annoyance values of the two forms of signal degradation in delta modulation. The present paper describes a study of the above question as referred to the delta modulation of a speech signal.

Earlier work in this subject is in the form of a perceptual experiment⁵ in which H. Levitt, et al., characterized the perceptibility of slope-overload distortion as such. As mentioned earlier, our paper will seek to answer the complementary question of the relative perceptibilities of slope overload and granularity when they occur simultaneously in delta-modulated speech, as they usually do.

The approach we used was to vary the relative amount of slope overload and granularity introduced into samples of a test utterance, and to evaluate these samples on the basis of both objective and perceptual criteria; and then to interpret these evaluations with specific reference to the overload-granularity dichotomy.

Section II summarizes the salient features of a computer-simulated adaptive delta modulator that was utilized in the present study. This adaptive encoder has been recently described and shown to provide toll-quality speech reproduction at bit rates of practical importance.⁴

Section III defines the objective measures of speech quality used in our study, while Section IV defines a subjective measure of preference and describes an underlying perceptual experiment.

II. DESCRIPTION OF THE DELTA MODULATOR

Figure 3 is a schematic block diagram of the adaptive delta modulator utilized in the present study. This encoder is defined by the basic equations (1) and (2), and by the adaptation rule

$$\Delta_r = \begin{cases} P \cdot \Delta_{r-1} & \text{if } C_r = C_{r-1} \\ \frac{1}{P} \cdot \Delta_{r-1} & \text{if } C_r \neq C_{r-1} \end{cases}; \quad P \geq 1. \quad (5)$$

Notice that a conventional (linear) delta modulator corresponds to the special case of $P = 1$. In our study the value of P was a variable parameter; different (delta-modulated) speech samples corresponded to different suitably spaced values of P , and thereby to different mixtures of slope-overload and granularity.

The original speech sample X was a 2-second male utterance of "Have you seen Bill?" that had been band-limited to 3.3 kHz. The delta modulation was performed at sampling rates of 20 and 40 kHz. The latter frequency provides speech reproduction that approaches telephone

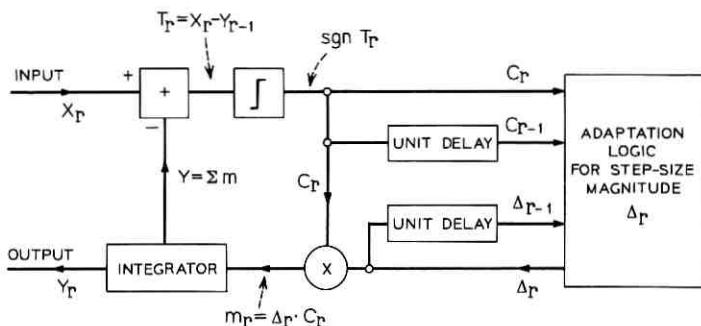


Fig. 3—Schematic diagram of an adaptive delta modulator.

quality.⁴ The lower sampling rate was included to provide a better demonstration of the annoyance properties of delta-modulated speech.

III. OBJECTIVE MEASURES OF SPEECH QUALITY

We recall the encoding error e_r , (4), and define the following measures of delta-modulator performance. (Summations are over the entire length of the speech utterance, and a nonzero granularity error at $r = t$ implies zero overload error, and vice versa.)

(i) The overload-noise energy in Z :

$$N_o = \sum e_{ro}^2 \quad (6)$$

(ii) The granular-noise energy in Z :

$$N_g = \sum e_{rg}^2 \quad (7)$$

(iii) The signal-to-noise ratio:

$$\text{SNR} = \frac{\sum X_r^2}{\sum e_{ro}^2 + \sum e_{rg}^2} \quad (8)$$

(iv) The signal-to-granular (overload)-noise ratio:

$$\text{SNR}_{g(o)} = \frac{\sum X_r^2}{\sum e_{rg(o)}^2} \quad (9)$$

IV. A SUBJECTIVE MEASURE OF SPEECH QUALITY

The perceptual evaluations of this paper are based on the pooled* judgments of nine listeners each of whom assessed speech stimuli† in six runs of a perceptual experiment. Each of these 54 experiments was a double-elimination tournament‡ (with a different, random, starting line-up). Matches in each tournament were between contending stimuli, playing two at a time. The result of each match was in the form of a binary preference judgment by the listener, while the result of a tournament was a set of scores awarded to each of the contesting speech stimuli on the basis of its record in the tournament. The actual scoring rule§ was one which, together with the double-elimination

* Intralistener variations were found to be less significant than the intrastimulus differences.

† The number of contending speech stimuli was also nine, at each sampling rate.

‡ The tournament ended when every losing contestant had lost twice.

§ In the course of each tournament a contestant accumulated a score as follows. No score was earned for a match that was lost; while, after every match that was won, the contestant's score was the sum of the accumulated scores, before the match, of the contestant and of the loser, plus one.

strategy, provided a useful alternative—as concluded from a separate simulation—to the more comprehensive testing procedure where every contending stimulus would be pitted against every other.

It was recognized, however, that both the scoring rule and the double-elimination strategy were empirical procedures. This was more so because they were applied to what was apparently a probabilistic environment: the binary preference-response of a listener to a given pair of contending stimuli can well be random, especially when the stimuli are not obviously different. It was, therefore, decided not to emphasize the actual scores obtained in the perceptual test. They were only used, instead, to extract a crude ranking information that would be less sensitive to the testing and scoring procedures.

Consequently, the following subjective preference value Q was assigned to each of M contesting speech stimuli:

$$Q = \frac{M - R}{M - 1}; \quad R = 1, 2, \dots, M \quad (10)$$

where R is the rank assigned to a stimulus on the basis of its accumulated score in the 54 runs of the perceptual test.

V. SUMMARY OF RESULTS

Figure 4 displays normalized values of the objective measures of quality SNR, SNR_G , and SNR_o , as well as the subjective preference function Q , as functions of the adaptation parameter P . The following observations emerge:

(i) The speech sample representing the minimum overall-noise-energy is not subjectively the most preferred sample. In fact, at both 20 and 40 Hz, the objective and subjective optima can be characterized by

$$P_{\text{OPT}}^{\text{SUBJ}} = 1.2 \quad (11)$$

$$P_{\text{OPT}}^{\text{OBJ}} = 1.5. \quad (12)$$

(ii) The approximate coincidence of the SNR and SNR_o curves indicates, by virtue of equations (6) through (9), that

$$N_o \gg N_G \quad (13)$$

for all considered values of P .

(iii) The relative disposition of the SNR_o , SNR_G , and Q curves—and of their maxima—demonstrates that, in spite of the preponderance (13) of overload in the overall-noise-energy, the granularity in a speech

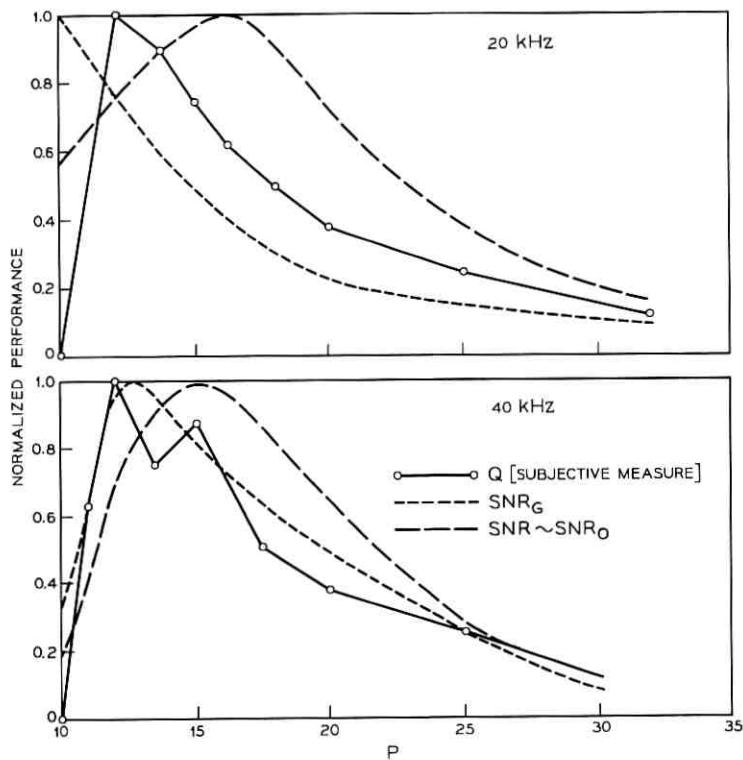


Fig. 4—Evaluations of delta-modulator performance.

stimulus has a strong influence on its subjective preference value.

Note that there is a double peak in the subjective preference curve, Q , for the 40-kHz case. This curve unambiguously ranks each of the experimental stimuli according to equation (10). However, the actual scores underlying this ranking show only a small difference between the stimulus with the secondary peak and the one immediately preceding it. What is probably indicated is a general broadening of the peak of the preference function for values of P between 1.2 and 1.5.

Table I lists, for the optimal characterizations (11) and (12), values of $N_{o(a)}$ (given as fractions of signal energy), SNR, and Q . Notice that the subjectively optimum delta modulator displays lesser granularity (N_a) and greater overload (N_o) than the objectively optimum modulator. It is again obvious that in perception, overload and granularity are not weighed in proportion to the respective noise energies N_o and N_a ;

TABLE I—CHARACTERISTIC OF OPTIMAL ADAPTIVE DELTA MODULATION
(N_o and N_g are entered as fractions of signal energy)

Sampling Frequency	P	N_o	N_g	SNR	Q
20 kHz	$P_{\text{SUBJ}}^{\text{OPT}} = 1.2$	0.0216	0.0003	43	1
	$P_{\text{OBJ}}^{\text{OPT}} = 1.5$	0.0158	0.0004	58	0.81
40 kHz	$P_{\text{SUBJ}}^{\text{OPT}} = 1.2$	0.0022	0.00003	450	1
	$P_{\text{OBJ}}^{\text{OPT}} = 1.5$	0.0016	0.00004	640	0.91

in fact, the perceptual preference of a speech sample seems to be determined very strongly by the extent of granularity in it, although the latter represents a very small fraction of the total noise energy.

Finally, Table I indicates that distinctions between objective and subjective assessments of speech quality appear to be less significant at the higher sampling rate of 40 kHz; thus, for example, the objectively best delta modulator has a greater value of subjective preference Q at 40 kHz than at 20 kHz.

VI. CONCLUSION

We have shown that in delta modulation, a speech sample exhibiting the minimum degradation on an objective, overall-noise-energy basis is not equivalent, in general, to the perceptually most preferred sample. We have also indicated that this distinction may be less significant in higher quality delta modulation than in a low-bit-rate encoder.

The subjectively optimum delta-encoder displays a greater overload N_o and lesser granularity N_g than the objectively best encoder. This feature, together with the fact that $N_o \gg N_g$ in either case, suggests the strong influence of granular noise on the perceptual assessment of a speech sample; equivalently, a lesser "annoyance value" is to be associated with slope-overload distortion.* A possible explanation of

* Companding in PCM exploits a similar but *not identical* subjective phenomenon, viz., the greater tolerance to encoding errors in regions of high input amplitude. (Notice however, that in delta modulation, slope overload is not confined to high-amplitude regions, nor is granularity associated only with low input amplitude.)

this observation would be the fact that granularity is explicitly perceivable by a listener as an "additive background noise," while slope-overload distortion exists only in relation to an original signal which is not known to the listener.

Finally, our observation that slope overload is "less annoying" than granularity is to be invoked with caution. Broadly speaking, we believe that our conclusion would apply very well to speech that achieves or approaches telephone quality. In extremely low-quality delta modulation (such as may be used in special applications), on the other hand, the intelligibility of speech will be a critical criterion; and in such a situation, depending on other factors like ambient noise at a transmitter, slope overload may very well become a more important perceptual attribute.

REFERENCES

1. de Jager, F., "Delta Modulation, A Method of PCM Transmission Using 1-Unit Code," Phillips Research Reports, 7, No. 6 (December 1952), pp. 442-446.
2. Winkler, M. K., "High Information Delta Modulation," IEEE International Convention Record, pt. 8, 1963, pp. 260-265.
3. Greefkes, J. A., and de Jager, F., "Continuous Delta Modulation," Phillips Research Reports, 23, No. 2 (April 1968), pp. 233-246.
4. Jayant, N. S., "Adaptive Delta Modulation with a One-Bit Memory," B.S.T.J., 49, No. 3 (March 1970), pp. 321-342.
5. Levitt, H., McGonegal, C. A., and Cherry, L. L., "Perception of Slope-Overload Distortion in Delta-Modulated Speech Signals," IEEE Transactions on Audio and Electro-Acoustics, AU-18, No. 3 (September 1970), pp. 240-247.

Some Considerations of Error Bounds in Digital Systems

By V. K. PRABHU

(Manuscript received June 22, 1971)

Simple upper and lower bounds on the distribution function of the sum of two random variables are presented in terms of the marginal distribution functions of the variables. These bounds are then used to obtain upper and lower bounds to the error probability of a coherent digital system in the presence of intersymbol interference and additive gaussian noise. The bounds are expressed in terms of the error probability obtained with a finite pulse train, and the bounds to the marginal distribution function of the residual pulse train. Since the difference between the upper and lower bounds can be shown to be a monotonically decreasing function of the number of pulses in the finite pulse train, the bounds can be used to compute the error probability of the system with arbitrarily small error. Also when the system performance is evaluated by simulation techniques, the methods presented in our paper can be utilized to estimate the error caused by using a finite pulse train approximation.

I. INTRODUCTION

In digital transmission systems the transfer characteristics of the transmitting and receiving filters are far from ideal, and the real transmission channel usually exhibits some form of time dispersion.^{1,2} When an ideal digital signal is passed through such filters or is transmitted through such a channel, the successive pulses overlap; this form of distortion is usually known as intersymbol interference. Intersymbol interference may also result from the choice of nonoptimum sampling instants, imperfect demodulating-carrier phase, improper pulse design, etc. In addition the signal may be corrupted by thermal noise, co-channel and adjacent channel interference, and other forms of noise that may be present in the channel or in the system used to transmit the information.

In digital transmission systems, one of the main performance char-

acteristics is the probability of error; this probability of error can often be expressed as a finite weighted sum of one or more distribution functions.

Various authors have tried to evaluate this probability of error by a variety of methods,²⁻¹⁴ but this highly complex probability distribution can seldom be exactly computed.

Simulation techniques that may be used to solve this and other similar problems are never exact since one is constrained to use only a finite number of pulses and no bounds to the truncation error have been derived.*

Another method is an analysis by means of a worst-case or "eye pattern" analysis. Since the probability of occurrence of a worst sequence may be very small, this analysis usually leads to very pessimistic results and suboptimum system design.

Recently, some authors have derived⁷⁻⁹ several different upper bounds on the probability of error when the system is subject to both intersymbol interference and additive gaussian noise. Some of these bounds make use of the Chernoff inequality in their derivation, and hence are often more useful than the worst-case bound.⁸ However, since these bounds, in certain cases, can be shown to be loose,¹¹ and since no useful lower bounds have been derived, they are not as useful in system design as the evaluation of the exact error rate of the system.

The third method consists in using the finite pulse train approximation and calculating the error probability either by the direct enumeration of all possible sequences² or by the series expansion method.¹⁰⁻¹¹ The series expansion method, which involves the computation of the moments of the intersymbol interference, is a convenient method but is still inexact as no truncation error bounds due to the residual pulse train have been derived. Note that in this method the number of terms in the finite pulse train is gradually increased until the change in probability of error is less than a given number ϵ .¹¹

In this paper we first present simple upper and lower bounds to the distribution function of the sum of two random variables z_N and z_R in terms of their marginal distribution functions. If the spread or dispersion¹⁵ of the random variable z_R is smaller than the spread of the

* In simulation techniques the number N of pulses are usually chosen so that the computed probability of error stops changing by less than ϵ when the number N is increased by 1. Noting that the series $\sum_{n=1}^{\infty} 1/n$ diverges, and that the difference between two successive partial sums of this series can be made less than any given number ϵ , one concludes that this technique of choosing N is mathematically unsound.

random variable z_N , one can show that these two bounds are fairly close to each other and that one can evaluate the distribution function of the sum of the variables in terms of the distribution function of z_N and the bounds on the distribution function of z_R .

We then use these bounds to obtain upper and lower bounds on the error probability of a binary coherent digital system in the presence of intersymbol interference and additive gaussian noise. Since the difference between the upper and lower bounds can be shown to be a monotone decreasing function of the number N of pulses in the finite pulse train, the bounds can be used to compute the error probability of the system with arbitrarily small error.

Also when the system performance is evaluated by simulation techniques, the methods presented in our paper can be utilized to estimate the error caused by using a finite pulse train approximation.

If the symbols are equally likely, we also show that another set of upper and lower bounds can be derived for the probability of error of a system subject to intersymbol interference and additive gaussian noise.

The usefulness of the bounds is illustrated by two examples.

II. DISTRIBUTION FUNCTION AND ITS EVALUATION

Let us assume that a random variable z is the sum of two random variables z_N and z_R ,

$$z = z_N + z_R, \quad (1)$$

and that we are interested in the distribution function of z

$$F_z(a) = \Pr [z \leq a] = \Pr [z_N + z_R \leq a]. \quad (2)$$

In this section we shall also assume that z_N and z_R are statistically independent random variables.

The probability of error of a large number of digital systems subject to various forms of noise can often be expressed as a weighted sum of $F_z(a)$'s. If z is the sum of an infinite number of random variables, and if z_N represents its partial sum of the first N terms, we sometimes can evaluate $F_{z_N}(a)$, but $F_z(a)$ can seldom be computed exactly. In such a case it is often advantageous to obtain upper and lower bounds to $F_z(a)$ in terms of $F_{z_N}(a)$ and some known parameters associated with the random variable z_R , the sum of the remaining terms in z . If the difference between the two bounds is a strictly monotone-decreasing function of N , we can then calculate $F_z(a)$ with arbitrarily small error.

Without loss of generality we shall assume that the mean of z_R is

zero. From (2) we can write (see Fig. 1)

$$F_z(a) = \int_{-\infty}^{\infty} \int_{-\infty}^{a-y} f_{z_N, z_R}(x, y) dx dy \quad (3)$$

if the joint probability density function $f_{z_N, z_R}(x, y)$ exists; and

$$F_z(a) = \int_{-\infty}^{\infty} \int_{-\infty}^{a-y} dF_{z_N}(x) dF_{z_R}(y) = \int_{-\infty}^{\infty} F_{z_N}(a - y) dF_{z_R}(y), \quad (4)$$

or

$$F_z(a) = \langle F_{z_N}(a - y_{z_R}) \rangle_{z_R}. \quad (5)$$

Let us now select an interval $(-\Delta l, \Delta u)$ from the range of the random variable z_R . From (4) we can write

$$F_z(a) = I_1 + I_2 + I_3 \quad (6)$$

where

$$I_1 \equiv \int_{-\infty}^{-\Delta l} F_{z_N}(a - y) dF_{z_R}(y), \quad (7)$$

$$I_2 \equiv \int_{-\Delta l}^{\Delta u} F_{z_N}(a - y) dF_{z_R}(y), \quad (8)$$

and

$$I_3 \equiv \int_{\Delta u}^{\infty} F_{z_N}(a - y) dF_{z_R}(y). \quad (9)$$

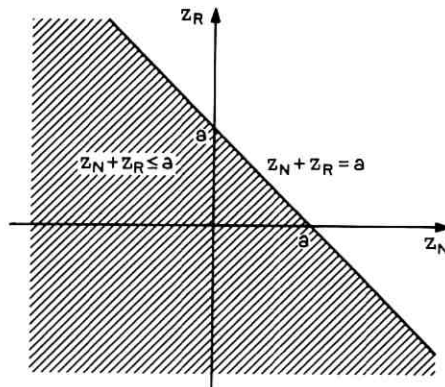


Fig. 1—Distribution function of $z = z_N + z_R$.

One can show (see Fig. 2) that

$$0 \leq I_1 \leq \int_{-\infty}^{-\Delta l} dF_{z_R}(y) = F_{z_R}(-\Delta l), \quad (10)$$

$$\begin{aligned} 0 \leq I_3 &\leq F_{z_N}(a - \Delta u) \int_{\Delta u}^{\infty} dF_{z_R}(y) = F_{z_N}(a - \Delta u)\{1 - F_{z_R}(\Delta u)\} \\ &\leq F_{z_N}(a + \Delta l)\{1 - F_{z_R}(\Delta u)\}, \end{aligned} \quad (11)$$

$$I_2 \geq F_{z_N}(a - \Delta u) \int_{-\Delta l}^{\Delta u} dF_{z_R}(y) = F_{z_N}(a - \Delta u)\{F_{z_R}(\Delta u) - F_{z_R}(-\Delta l)\}, \quad (12)$$

and

$$I_2 \leq F_{z_N}(a + \Delta l) \int_{-\Delta l}^{\Delta u} dF_{z_R}(y) = F_{z_N}(a + \Delta l)\{F_{z_R}(\Delta u) - F_{z_R}(-\Delta l)\}. \quad (13)$$

Combining (6) with (10)–(13), we have

$$\begin{aligned} F_{z_N}(a - \Delta u)[F_{z_N}(\Delta u) - F_{z_N}(-\Delta l)] \\ \leq F_z(a) \leq F_{z_R}(-\Delta l) + F_{z_N}(a + \Delta l)[1 - F_{z_R}(-\Delta l)] \\ \leq F_{z_R}(-\Delta l) + F_{z_N}(a + \Delta l). \end{aligned} \quad (14)$$

In general it is not easy to compute $F_{z_R}(y)$. However we may be able to bound $F_{z_R}(y)$ so that

$$0 \leq F_{z_R}(-\Delta l) = \Pr [z_R \leq -\Delta l] \leq L_{z_R}(-\Delta l) \leq 1, \quad (15)$$

$$0 \leq 1 - F_{z_R}(\Delta u) = \Pr [z_R > \Delta u] \leq U_{z_R}(\Delta u) \leq 1, \quad (16)$$

and

$$\begin{aligned} 1 \geq F_{z_R}(\Delta u) - F_{z_R}(-\Delta l) &= \Pr [-\Delta l < z_R \leq \Delta u] \\ &\geq 1 - L_{z_R}(-\Delta l) - U_{z_R}(\Delta u) \geq 0. \end{aligned} \quad (17)$$

If these bounds can be found, (14)–(17) can be made to yield

$$\begin{aligned} F_{z_N}(a - \Delta u)[1 - L_{z_R}(-\Delta l) - U_{z_R}(\Delta u)] &\leq F_z(a) \\ &\leq F_{z_N}(a + \Delta l) + L_{z_R}(-\Delta l). \end{aligned} \quad (18)$$

These are the basic bounds that we shall use in the rest of this paper.

If the mass of the distribution of z_R is very much concentrated around $y = 0$, our technique of computing $F_z(a)$ from (18) relies on the assumption that we can find two numbers Δu and Δl such that

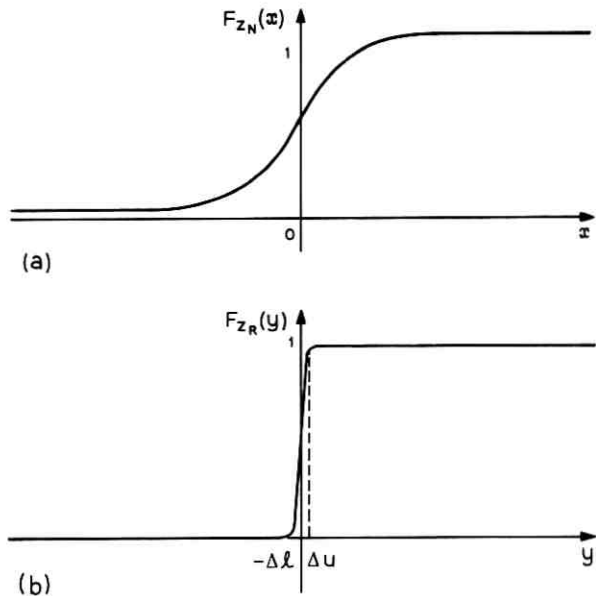


Fig. 2a—Distribution function $F_{z_N}(x)$.

Fig. 2b—Distribution function $F_{z_R}(y)$. The interval $(-\Delta l, \Delta u)$ is contained in the range of z_R , and for all practical purposes the mass of z_R is contained in $(-\Delta l, \Delta u)$.

$\Delta u \ll |a|$, $\Delta l \ll |a|$, $L_{z_R}(-\Delta l) \ll F_{z_N}(a)$, $U_{z_R}(\Delta u) \ll F_{z_N}(a)$, and $F_{z_N}(a - \Delta u) \approx F_{z_N}(a + \Delta l)$.

The difference $D(\Delta u, \Delta l)$ between the upper and lower bounds can be written as

$$D(\Delta u, \Delta l) = \Pr[a - \Delta u < z_N \leq a + \Delta l] \\ + F_{z_N}(a - \Delta u)[L_{z_R}(-\Delta l) + U_{z_R}(\Delta u)] + L_{z_R}(-\Delta l). \quad (19)$$

If Δu and Δl can be so chosen that they are strictly monotone-decreasing functions of N , $\Delta u \rightarrow 0$, $\Delta l \rightarrow 0$, as $N \rightarrow \infty$, and if the bounds on the distribution of z_R are such that, for sufficiently large N , $L_{z_R}(-\Delta l)$ and $U_{z_R}(\Delta u)$ can be made smaller than any given number ϵ_1 , we can estimate $F_z(a)$ from (18) with arbitrarily small error.*

For any given N even though Δu and Δl can be chosen by optimizing the bounds in (18), this optimization leads to very complex equations. Hence we think that an algorithm should be developed to choose Δu and Δl for any given z_N and z_R . The development of this algorithm will be illustrated by an example in Section IV.

* We assume that $\Pr[a - 0 < a_N \leq a + 0] = 0$.

2.1 Lower Bound Evaluation with Convex $F_{z_N}(a)$

We shall now derive a simpler lower (upper) bound to $F_z(a)$ if $F_{z_N}(a)$ is a convex (concave) function and if z_R is an even random variable, or

$$F_z(-t) = 1 - F_z(t). \quad (20)$$

From (20) one can show that the mean m of z is zero, and that its probability density $f_z(t)$, if it exists, satisfies the equation

$$f_z(-t) = f_z(t). \quad (21)$$

If z_R is an even random variable, we shall set $\Delta u = \Delta l$ in (18).

Let us now assume that z_R is an even random variable and that $F_{z_N}(a)$ is convex over the range $(a - \Delta u, a + \Delta u)$ where $(-\Delta u, \Delta u)$ is the range of z_R . Since z_R is an even random variable

$$F_z(a) = \langle F_{z_N}(a - y_{z_R}) \rangle_{z_R} = \langle F_{z_N}(a + y_{z_R}) \rangle_{z_R} \quad (22)$$

or

$$F_z(a) = \langle \frac{1}{2}[F_{z_N}(a - y_{z_R}) + F_{z_N}(a + y_{z_R})] \rangle_{z_R}. \quad (23)$$

Since $F_{z_N}(a)$ is convex over the range $(a - \Delta u, a + \Delta u)$,¹⁶

$$\frac{1}{2}[F_{z_N}(a - y_{z_R}) + F_{z_N}(a + y_{z_R})] \geq F_{z_N}(a). \quad (24)$$

From (23) and (24) we have

$$F_z(a) \geq F_{z_N}(a). \quad (25)$$

Since this bound does not contain Δu and Δl , it is simpler to calculate than that given in (18). It is also tighter than the lower bound in (18). In this case we then have

$$F_{z_N}(a) \leq F_z(a) \leq F_{z_N}(a + \Delta l) + L_{z_R}(-\Delta l). \quad (26)$$

If $F_{z_N}(a)$ is concave over the domain $(a - \Delta l, a + \Delta u)$ and if z_R is an even random variable, we can similarly show that

$$F_{z_N}(a) \geq F_z(a) \geq F_{z_N}(a - \Delta u)[1 - L_{z_R}(-\Delta l) - U_{z_R}(\Delta u)]. \quad (27)$$

2.2 Evaluation of Another Upper Bound to $F_z(a)$

Often we find that z contains a gaussian random variable n and can be written as

$$z = n + w_N + z_R = z_N + z_R, \quad z_N = n + w_N, \quad (28)$$

where n , w_N , and z_R are statistically independent random variables.

We have already assumed that the mean of w_N is zero. Without loss of generality we shall now assume that the mean of n is zero, and its variance is σ^2 .

From (28) one can show that

$$F_{w_N}(a) = \frac{1}{2} \left\langle \operatorname{erfc} \left(\frac{-a + x_{w_N}}{\sigma\sqrt{2}} \right) \right\rangle_{w_N}, \quad (29)$$

where

$$\operatorname{erfc}(x) \equiv \frac{2}{\sqrt{\pi}} \int_x^\infty \exp(-t^2) dt. \quad (30)$$

Hence we have^{17,18}

$$F_{w_N}(a) = \frac{1}{2} \operatorname{erfc} \left(\frac{-a}{\sigma\sqrt{2}} \right) + \frac{1}{\sqrt{\pi}} \exp[-a^2/2\sigma^2] \cdot \sum_{k=1}^{\infty} (-1)^k H_{k-1}(-a/\sigma\sqrt{2}) (1/\sigma\sqrt{2})^k \mu_k/k!, \quad (31)$$

where $H_k(x)$ is the k th order Hermite polynomial and μ_k is the k th moment of w_N ,

$$\mu_k = \int_{-\infty}^\infty x^k dF_{w_N}(x). \quad (32)$$

If the range $(-\Omega_l, \Omega_u)$ of w_N is finite and if Ω denotes the maximum absolute value that can be attained by w_N , we can show that

$$|\mu_{k+s}| \leq m_k \Omega^s, \quad k \geq 0, s \geq 0, \quad (33)$$

$$m_k = \int_{-\infty}^\infty |x|^k dF_{w_N}(x). \quad (34)$$

m_k is called the k th absolute moment of w_N .

If the first K moments are used in estimating $F_{w_N}(a)$ from (31), the truncation error T_K is given by

$$T_K = \frac{1}{\sqrt{\pi}} \exp(-a^2/2\sigma^2) \sum_{k=K+1}^{\infty} (-1)^k H_{k-1}(-a/\sigma\sqrt{2}) (1/\sigma\sqrt{2})^k \mu_k/k!. \quad (35)$$

Since it can be shown¹⁹ that

$$|H_n(t)| < b 2^{n/2} \sqrt{n!} \exp(t^2/2), \quad b \approx 1.086435, \quad (36)$$

one can show from (35)–(36) that

$$|T_K| < (b/\sqrt{2\pi}) \exp(-a^2/4\sigma^2) \frac{m_K}{\sigma^K} \frac{(\Omega/\sigma)}{(K+1)\sqrt{K!}} \cdot \left[1 - \frac{\Omega}{\sigma\sqrt{K+1}}\right]^{-1}, \frac{\Omega}{\sigma\sqrt{K+1}} < 1. \quad (37)$$

From (31) and (37) one may observe that $F_{z_N}(a)$ may be estimated with as great an accuracy as desired if the range of w_N is finite and if the moments of w_N are known.

If w_N is an even random variable, we can also show that^{10,18}

$$\mu_{2k-1} = 0, \quad k \geq 1 \quad (38)$$

$$F_{z_N}(a) = \frac{1}{2} \operatorname{erfc}(-a/\sigma\sqrt{2}) + \frac{1}{\sqrt{\pi}} \exp(-a^2/2\sigma^2) \cdot \sum_{k=1}^{\infty} H_{2k-1}(-a/\sigma\sqrt{2})(1/\sigma\sqrt{2})^{2k} \mu_{2k}/(2k)! \quad (39)$$

$$|T_{2K}| < \frac{b}{\sqrt{2\pi}} \exp(-a^2/4\sigma^2) \frac{\mu_{2K}}{\sigma^{2K}} \frac{(\Omega/\sigma)^2}{(2K+2)\sqrt{(2K+2)(2K+3)}} \cdot [1 - (\Omega/\sigma)^2/\sqrt{(2K+2)(2K+3)}]^{-1}, \\ (\Omega/\sigma)^2/[(2K+2)(2K+3)]^{1/2} < 1. \quad (40)$$

By using the inequality¹⁹

$$|H_{2k+1}(t)| \leq |t| \exp(t^2/2)(2k+2)/(k+1)!, \quad (41)$$

we can also show that

$$|T_{2K}| \leq \frac{|a|}{\sigma\sqrt{2\pi}} \exp(-a^2/4\sigma^2) \frac{\mu_{2K}}{\sigma^{2K}} \frac{(\Omega/\sigma)^2}{(K+1)!} [1 - (\Omega/\sigma)^2/(K+2)]^{-1}, \\ (\Omega/\sigma)^2/(K+2) < 1. \quad (42)$$

If z_R is an even random variable, we have

$$F_z(a) = \frac{1}{4} \langle \operatorname{erfc} [(-a + x_{w_N} + y_{z_R})/\sigma\sqrt{2}] \rangle_{w_N, z_R} \\ + \frac{1}{4} \langle \operatorname{erfc} [(-a + x_{w_N} - y_{z_R})/\sigma\sqrt{2}] \rangle_{w_N, z_R}. \quad (43)$$

Since one can show (see Appendix A) that

$$\frac{1}{2} \operatorname{erfc}(x+\lambda) + \frac{1}{2} \operatorname{erfc}(x-\lambda) \geq \operatorname{erfc}(x), \quad x \geq 0, \quad (44)$$

we can write

$$F_z(a) \geq \frac{1}{2} \langle \operatorname{erfc} [(-a + x_{w_N})/\sigma\sqrt{2}] \rangle_{w_N}, \quad -a + x_{w_N} \geq 0, \\ = F_{z_N}(a), \quad -a + x_{w_N} \geq 0, \quad \forall x_{w_N}. \quad (45)$$

Now from (28) we can write

$$F_z(a) = \frac{1}{2} \langle \eta_{w_N, z_R} \rangle_{w_N, z_R}, \quad (46)$$

where

$$\begin{aligned} \eta_{w_N, z_R} &= \operatorname{erfc}(x_1), x_1 = (-a + x_{w_N} + y_{z_R})/\sigma\sqrt{2}, \\ &= \frac{2}{\sqrt{\pi}} \int_{x_2}^{\infty} \exp \{-(s + y_{z_R}/\sigma\sqrt{2})^2\} ds, x_2 = (-a + x_{w_N})/\sigma\sqrt{2}. \end{aligned} \quad (47)$$

Since

$$\exp [-(y_{z_R}/\sigma\sqrt{2})^2] \leq 1, \quad \forall y_{z_R}, \quad (48)$$

we have

$$\eta_{w_N, z_R} \leq \frac{2}{\sqrt{\pi}} \int_{x_2}^{\infty} \exp [-s^2 - s(\sqrt{2}/\sigma)y_{z_R}] ds, \quad (49)$$

$$F_z(a) \leq \frac{1}{\sqrt{\pi}} \left\langle \int_{x_2}^{\infty} \exp [-s^2 - s(\sqrt{2}/\sigma)y_{z_R}] ds \right\rangle_{w_N, z_R} \quad (50)$$

$$= \frac{1}{\sqrt{\pi}} \left\langle \int_{x_2}^{\infty} \exp (-s^2) \Phi_{z_R}(-s\sqrt{2}/\sigma) ds \right\rangle_{w_N}, \quad (51)$$

where

$$\Phi_{z_R}(t) = \int_{-\infty}^{\infty} \exp (ty) dF_{z_R}(y) \quad (52)$$

is the moment-generating function of the random variable z_R .

If we can find two numbers m_R and σ_R^2 such that

$$\Phi_{z_R}(t) \leq \exp [tm_R + \sigma_R^2 t^2/2], \quad \forall t, \quad (53)$$

one can show from (51) that

$$\begin{aligned} F_z(a) &\leq B_{z_N}(a, m_R, \sigma_R^2) = (1 - \sigma_R^2/\sigma^2)^{-1/2} \exp [m_R^2/\{2\sigma^2(1 - \sigma_R^2/\sigma^2)\}] \\ &\cdot \frac{1}{2} \left\langle \operatorname{erfc} \left[\frac{-a + m_R/(1 - \sigma_R^2/\sigma^2) + x_{w_N}}{\sigma 2^{1/2}(1 - \sigma_R^2/\sigma^2)^{-1/2}} \right] \right\rangle_{w_N}, \quad \sigma_R^2/\sigma^2 < 1. \end{aligned} \quad (54)$$

The derivation of the upper bound in (54) is based on results given in Ref. 20.

In this case we then have

$$\begin{aligned} F_{z_N}(a) &\leq F_z(a) \leq B_{z_N}(a, m_R, \sigma_R^2), \\ &-a + x_{w_N} \geq 0, \quad \sigma_R^2/\sigma^2 < 1, \quad \forall x_{w_N}. \end{aligned} \quad (55)$$

Since the lower bound in (55) may not be valid if $-a + x_{w_N}$ can be nonpositive for some value of x_{w_N} , and if the maximum absolute value of x_{w_N} is a monotone-increasing function of N , we note that there is an upper bound N_{\max} to N that can be used in estimating the lower bound in (55). If this upper bound $N_{\max} < \infty$, we may not be able to estimate $F_z(a)$ from (55) with arbitrarily small error. However if there is no finite upper bound to N such that $-a + x_{w_N}$ is nonpositive (system with an "open eye pattern") and if $|m_R|$ and σ_R^2 are strictly monotone-decreasing functions of N , it is clear that we can estimate $F_z(a)$ from (55) with any desired accuracy.

III. BOUNDS ON THE TAILS OF PROBABILITY DISTRIBUTIONS

To use the bounds given in (18), it is necessary to determine $L_{z_R}(\Delta l)$ and $U_{z_R}(\Delta u)$. There are several methods (including numerical methods) of determining these parameters, and here we shall discuss two of them.

From Chebyshev-Bienayme bounds^{15,21} we have

$$\Pr [z_R \leq -\Delta l] \leq \frac{(\mu_{2n})_{z_R}}{(\Delta l)^{2n}}, \quad (56)$$

$$\Pr [z_R > \Delta u] \leq \frac{(\mu_{2n})_{z_R}}{(\Delta u)^{2n}}, \quad (57)$$

where

$$(\mu_{2n})_{z_R} = \langle y_{z_R}^{2n} \rangle. \quad (58)$$

Hence we can set

$$L_{z_R}(-\alpha) = U_{z_R}(\alpha) = \frac{(\mu_{2n})_{z_R}}{\alpha^{2n}}. \quad (59)$$

Also in communication problems, bounds of the Chernoff type have been used on the tails of the probability distributions, and these Chernoff bounds are often tighter than the Chebyshev-Bienayme bounds.^{7-9,21-23}

One can show²³ that

$$\begin{aligned} \Pr [z_R \leq -\Delta l] &\leq \exp(-\lambda \Delta l) \langle \exp(-\lambda y_{z_R}) \rangle \\ &= \exp(-\lambda \Delta l) \Phi_{z_R}(-\lambda), \quad \lambda \geq 0, \end{aligned} \quad (60)$$

$$\Pr [z_R > \Delta u] \leq \exp(-\lambda \Delta u) \Phi_{z_R}(\lambda), \quad \lambda \geq 0. \quad (61)$$

The parameter λ is arbitrary and is chosen so as to optimize the bounds in (60) and (61).

If we can find two functions $\psi_{z_R}(-\lambda)$ and $\Psi_{z_R}(\lambda)$ such that

$$0 \leq \Phi_{z_R}(-\lambda) \leq \psi_{z_R}(-\lambda), \quad \lambda \geq 0, \quad (62)$$

and

$$0 \leq \Phi_{z_R}(\lambda) \leq \Psi_{z_R}(\lambda), \quad \lambda \geq 0, \quad (63)$$

and then optimize $\exp(-\lambda \Delta l)\psi_{z_R}(-\lambda)$ and $\exp(-\lambda \Delta u)\Psi_{z_R}(\lambda)$, we can make

$$L_{z_R}(-\Delta l) = \exp(-\lambda_{opt} \Delta l)\psi_{z_R}(-\lambda_{opt}), \quad (64)$$

and

$$U_{z_R}(\Delta u) = \exp(-\lambda_{opt} \Delta u)\Psi_{z_R}(\lambda_{opt}). \quad (65)$$

The functions $\psi_{z_R}(-\lambda)$ and $\Psi_{z_R}(\lambda)$ are often chosen so that (64) and (65) have the desired functional forms for optimization.^{7,9,24} From (52) one may note that it is not necessary to determine (explicitly) $\Phi_{z_R}(\lambda)$ to get $\psi_{z_R}(-\lambda)$ and $\Psi_{z_R}(\lambda)$. Bounds can be used to determine these functions. Also one may make use of the semi-invariant moment-generating function of z_R in determining $\Psi_{z_R}(-\lambda)$ and $\psi_{z_R}(\lambda)$.

If z_R is an even random variable, note also that

$$\Phi_{z_R}(-\lambda) = \Phi_{z_R}(\lambda), \quad \lambda \geq 0, \quad (66)$$

and we can make

$$\psi_{z_R}(-\lambda) = \Psi_{z_R}(\lambda), \quad \lambda \geq 0, \quad (67)$$

$$L_{z_R}(-\alpha) = U_{z_R}(\alpha) = \exp(-\alpha \lambda_{opt})\Psi_{z_R}(\lambda_{opt}). \quad (68)$$

IV. ERROR BOUNDS WITH INTERSYMBOL INTERFERENCE AND ADDITIVE GAUSSIAN NOISE

The methods presented in Section II are now applied to the analysis of a binary coherent digital system subject to intersymbol interference and additive gaussian noise. Various methods have been proposed to evaluate this error probability.¹⁻¹¹ They provide either an upper bound to the error rate or error rate with a finite pulse train approximation.

Let us now assume that the signal at the input to the receiver detector (see Fig. 3) can be represented as

$$y(t) = \sum_{l=-\infty}^{\infty} a_l p(t - lT) + n(t), \quad (69)$$

where $n(t)$ is a gaussian random variable with mean zero and variance σ^2 . We shall also assume that $\{a_l\}$ is a sequence of independent random variables, and $a_l = \pm 1$ with equal probability.

If the zeroth transmitted symbol is $a_0 = 1$ and if it is detected by

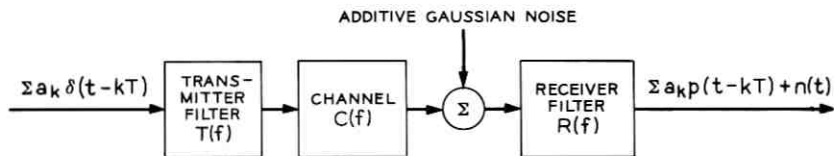


Fig. 3—Simplified block diagram of a coherent digital communication system. $C(f)$, $T(f)$, and $R(f)$ denote respectively the transfer functions of the channel, and transmitting and receiving filters. T is the signaling interval.

sampling $y(t)$ at $t = t_0$, we can show that

$$y(t_0) = p(t_0) + \sum' a_l p(t_0 - lT) + n(t_0), \quad (70)$$

where \sum' does not include the term $l = 0$. Assuming that the slicing level of the system is zero, and that there are no other imperfections in the system, we can show that the probability of error P_2 can be written as

$$P_2 = \Pr [n + \sum' a_l p_l < -p_0], \quad (71)$$

where

$$p_l = |p(t_0 - lT)|, \quad (72)$$

and

$$n = n(t_0). \quad (73)$$

Without loss of generality we shall now reorder sequence $\{p_l\}$ in such a way that the terms of the sequence are nonincreasing with increasing l , and let us denote this new sequence by $\{r_k\}$. Hence we can write

$$P_2 = \Pr \left[n + \sum_1^{\infty} a_k r_k < -p_0 \right] \quad (74)$$

or

$$P_2 = \Pr [z < -p_0] = F_z(-p_0), \quad (75)$$

$$z \equiv n + \sum_1^{\infty} a_k r_k = z_N + z_R, \quad (76)$$

$$z_N \equiv n + \sum_{k \in \xi_N} a_k r_k, \quad \xi_N = \{1, 2, 3, \dots, N\}, \quad (77)$$

$$w_N = z_N - n, \quad (78)$$

$$z_R = \sum_{k \notin \xi_N} a_k r_k. \quad (79)$$

Since z_N and z_R are statistically independent random variables, (18) gives bounds to $F_z(-p_0)$. Let us first determine $F_{z_N}(a)$ where $a = -p_0 + \Delta u$ or $a = -p_0 - \Delta l$. Methods given in Section 2.2 can be used in determining $F_{z_N}(a)$.* We would like to note here that (31) must be used in determining $F_{z_N}(a)$ when +1 and -1 do not occur with equal probability.

The recurrence relation given in Ref. 10 to calculate the even order moments μ_{2n} 's is to be used with care since the summation in the recurrence relation contains both positive and negative terms. In Appendix B we give another recurrence relation to compute μ_{2l} 's (and μ_{2l+1} 's, $l \geq 0$). Since the new recurrence relation for μ_{2n} 's contains the summation of positive terms only, we consider this method of computing μ_{2n} 's preferable to that given in Ref. 10.

We used (31) and our new method for computing μ_{2n} 's to calculate $F_{z_N}(a)$.

We shall now determine $L_{z_R}(-\Delta l)$ and $U_{z_R}(\Delta u)$. Since z_R is an even random variable, we will set $\Delta u = \Delta l$, $L_{z_R}(-\Delta u) = U_{z_R}(\Delta u)$. Also one can show⁷ that

$$\begin{aligned}\Phi_{z_R}(\lambda) &= \prod_{k \in \Lambda^c} \cosh \lambda r_k \\ &\leq \exp \left[\lambda \sum_{l \in \Lambda} r_l + \frac{\lambda^2}{2} \sum_{l \in \Lambda^c} r_l^2 \right], \quad \Lambda + \Lambda^c = \xi_N.\end{aligned}\quad (80)$$

From (68) we have

$$U_{z_R}(\Delta u) = \exp \left[-\frac{\{\Delta u - \sum_{\Lambda} r_l\}^2}{2 \sum_{\Lambda^c} r_l^2} \right], \quad \Delta u - \sum_{\Lambda} r_l \geq 0, \quad \Lambda \subset \xi_N^c. \quad (81)$$

Equation (18) now yields

$$\begin{aligned}F_{z_N}(-p_0 - \Delta u) &\leq 1 - 2 \exp \left\{ -\frac{[\Delta u - \sum_{\Lambda} r_l]^2}{2 \sum_{\Lambda^c} r_l^2} \right\} \\ &\leq F_z(-p_0) \leq F_{z_N}(-p_0 + \Delta u) + \exp \left[-\frac{[\Delta u - \sum_{\Lambda} r_l]^2}{2 \sum_{\Lambda^c} r_l^2} \right].\end{aligned}\quad (82)$$

For any given N , an optimum Δu can be chosen to minimize the difference between the upper and lower bounds in (82). This is often

* Other methods (including simulation) can also be used in determining $F_{z_N}(a)$.

found to be difficult and tedious and relies heavily on the search methods given in Ref. 7.

Here we assume that

$$\Lambda = \zeta_N^c, \quad (83)$$

and we write

$$\begin{aligned} F_{z_N}(-p_0 - \Delta u)[1 - 2 \exp\{-(\Delta u)^2/2\beta_R^2\}] \\ \leq F_z(-p_0) \leq F_{z_N}(-p_0 + \Delta u) + \exp[-(\Delta u)^2/2\beta_R^2], \end{aligned} \quad (84)$$

$$\beta_R^2 = \sum_{\zeta_N^c} r_t^2. \quad (85)$$

Note that any number $\beta_R^2 \geq \sum_{\zeta_N^c} r_t^2$ can be used in computing the bounds in (84). This may be done to simplify computing $\sum_{\zeta_N^c} r_t^2$.

The difference $D_N(\Delta u, \Delta u)$ between the upper and lower bounds can be written as

$$\begin{aligned} D_N(\Delta u, \Delta u) = \Pr[-p_0 - \Delta u < z_N \leq -p_0 + \Delta u] \\ + \exp[-(\Delta u)^2/2\beta_R^2]\{1 + 2F_{z_N}(-p_0 - \Delta u)\}. \end{aligned} \quad (86)$$

Since β_R^2 is a strictly monotone-decreasing function of N , $D_N(\Delta u, \Delta u)$ can be made smaller than any given number ϵ . Hence we can calculate $F_z(-p_0)$ from (84).

Several different algorithms can be developed to compute $F_z(-p_0)$. One of our algorithms is as follows. Let us assume that we have to calculate $F_z(-p_0)$ with a fractional error less than ϵ_1 .

Since $F_z(-p_0) \leq 1$, we assume that there exists an N such that

$$|F_{z_N}(-p_0) - F_{z_{N+1}}(-p_0)| < \epsilon_2, \quad (87)$$

where

$$\epsilon_2 \leq \frac{1}{2}\epsilon_1 \min\{F_{z_N}(-p_0), F_{z_{N+1}}(-p_0)\}. \quad (88)$$

For this N we calculate β_R^2 and choose Δu so that

$$\exp[-(\Delta u)^2/2\beta_R^2] = \epsilon_2/3. \quad (89)$$

We then calculate $D_N(\Delta u, \Delta u)$ and compare it with

$$\chi_N = \epsilon_1 F_{z_N}(-p_0 - \Delta u)[1 - 2 \exp\{-(\Delta u)^2/2\beta_R^2\}]. \quad (90)$$

We increase N so that

$$D_{N'}(\Delta u, \Delta u) \leq \chi_{N'}, \quad N' \geq N. \quad (91)$$

It is not necessary to increase N in steps of one. The step size can be chosen to suit particular examples.

From (18) and (91) we can write

$$A_{N'}(-p_0) \leq F_z(-p_0) \leq B_{N'}(-p_0), \quad (92)$$

$$A_{N'}(-p_0) \equiv F_{z_N}(-p_0 - \Delta u)[1 - 2 \exp\{-(\Delta u)^2/2\beta_R^2\}], \quad (93)$$

$$B_{N'}(-p_0) \equiv F_{z_N}(-p_0 + \Delta u) + \exp\{-(\Delta u)^2/2\beta_R^2\}, \quad (94)$$

$$B_{N'}(-p_0) - A_{N'}(-p_0) \leq \epsilon_1 A_{N'}(-p_0). \quad (95)$$

It is evident from (92) and (95) that $F_z(-p_0)$ is equal to $A_{N'}(-p_0)$ or $B_{N'}(-p_0)$ with an error less ϵ_1 .

We have programmed this algorithm on a digital computer and we have been very successful in evaluating $F_z(-p_0)$ from this algorithm.

4.1 Applications

Let us now assume that $p(t)$ is obtained by passing a square pulse through a single-pole RC-filter or that

$$p(t) = 0, \quad t < 0 \quad (96)$$

$$p(t) = 1 - \exp(-2\pi Wt), \quad 0 \leq t \leq T, \quad (97)$$

$$p(t) = \exp[-2\pi W(t - T)] - \exp[-2\pi Wt], \quad t \geq T. \quad (98)$$

For this pulse we can write

$$p_0 = 1 - \exp(-2\pi Wt_0), \quad 0 \leq t_0 \leq T, \quad (99)$$

and

$$r_k = [1 - \exp(-2\pi WT)] \exp[-2\pi W\{t_0 + (k-1)T\}], \quad k \geq 1. \quad (100)$$

For $2WT = 0.5$, and $t_0 = T$, we plot in Fig. 4 $F_z(-p_0)$ with an error less than 0.2 percent. In this figure we also plot N' , the number of terms required in estimating $F_z(-p_0)$. $F_{z_N}(-p_0)$ is calculated from (31) with a truncation error of less than 0.01 percent.

Let us now consider the ideal bandlimited pulse $p(t)$ where

$$p(t) = \frac{\sin \pi t/T}{\pi t/T}, \quad (101)$$

$$p_0 = \frac{\sin \pi \delta}{\pi \delta}, \quad \delta = t_0 T < 1, \quad t_0 \geq 0, \quad (102)$$

$$r_{2k-1} = \frac{\sin \pi \delta}{\pi [k - \delta]}, \quad k \geq 1, \quad (103)$$

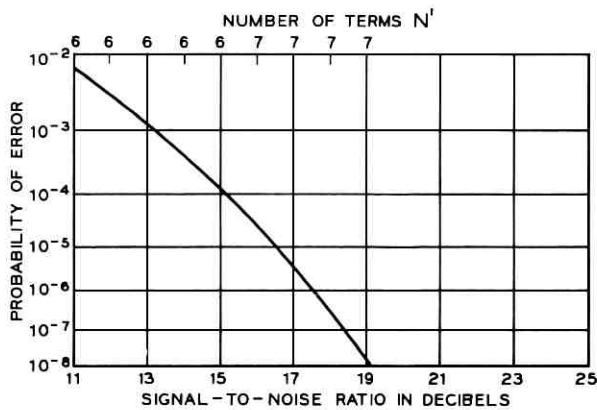


Fig. 4—Probability of error of binary coherent digital system with intersymbol interference and additive gaussian noise. The received pulse is an exponential pulse, and $2WT = 0.5$. The upper bound $B_{N'}(-p_0)$ is plotted in this figure and N was increased in steps of one. $[B_{N'}(-p_0) - F_z(-p_0)]/F_z(-p_0) < 0.002$. The truncation error is less than 0.01 percent.

$$r_{2k} = \frac{\sin \pi \delta}{\pi[k + \delta]}, \quad k \geq 1. \quad (104)$$

We shall assume that we take an even number of terms in w_N in estimating $F_{z_N}(-p_0)$.

We have

$$\begin{aligned} \beta_R^2 &= \sum_{l=2N+1}^{\infty} r_l^2 \\ &= \sum_{k=N+1}^{\infty} \frac{\sin^2 \pi \delta}{\pi^2} \left[\frac{1}{(k - \delta)^2} + \frac{1}{(k + \delta)^2} \right] \\ &\leq 2 \frac{(1 + \delta^2)}{(1 - \delta^2)^2} \frac{\sin^2 \pi \delta}{\pi^2} \left[\frac{\pi^2}{6} - \sum_{l=1}^N \frac{1}{l^2} \right] = \alpha_R^2. \end{aligned} \quad (105)$$

Since α_R^2 is more easily computed than β_R^2 , we shall use α_R^2 in (84).

For $\delta = 0.05$ we plot in Fig. 5, $F_z(-p_0)$ with an error less than 50 percent when $F_z(-p_0) \geq 2 \times 10^{-6}$ and less than 100 percent when $F_z(-p_0) < 2 \times 10^{-6}$. In this figure we also plot N' the number of terms required in estimating $F_z(-p_0)$. Since α_R^2 is a slowly decreasing function of N , the number of terms required for estimating $F_z(-p_0)$ is much larger than that in the earlier example.

Since z_N contains a gaussian random variable and since z_R is an even

random variable, (55) can also be used to obtain upper and lower bounds to $F_z(-p_0)$. Equations (53) and (80) can be shown to yield

$$m_R = \sum_{\Lambda^c} r_i , \quad (106)$$

$$\sigma_R^2 = \sum_{\Lambda^c} r_i^2 . \quad (107)$$

By choosing $\Lambda^c = \zeta_N^c$, we obtain the bounds given in Ref. 20.

Here we would like to note that the relative merits of the two sets of bounds cannot be compared as the bounds in (55) may not be applicable when the system has a closed eye pattern. The lower bound in (55) can be shown to be tighter than that in (18) but is not applicable to a system with a noneven z_R . The random variable z_R is noneven if +1 and -1 do not occur with equal probability. From the point of view of computation, tightness, and applicability, we think that specific problems should determine the set of bounds best suited to them.

The extension of this analysis to m -ary coherent digital systems, $m > 2$, and binary coherent phase-shift keyed systems is obvious from

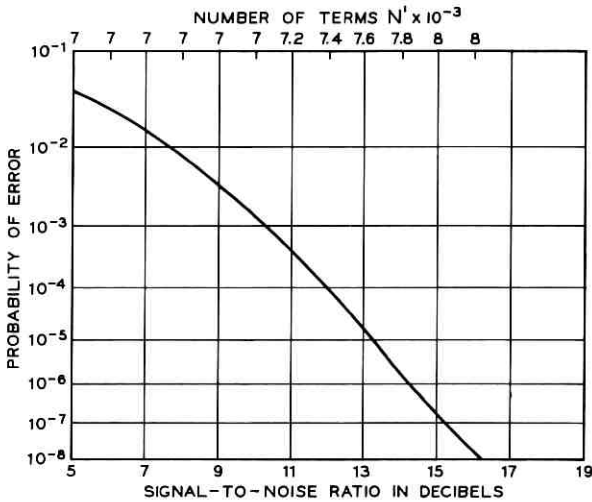


Fig. 5—Probability of error of binary coherent digital system with intersymbol interference and additive gaussian noise. The received pulse is an ideal bandlimited pulse, and it is sampled at t_0 , $t_0 T = 0.05$. The upper bound $B_{N'}(-p_0)$ is plotted in this figure and N was increased in steps of 100. $[B_{N'}(-p_0) - F_z(-p_0)]/F_z(-p_0) < 0.5$, $F_z(-p_0) \geq 2 \times 10^{-6}$, $[B_{N'}(-p_0) - F_z(-p_0)]/F_z(-p_0) < 1$, $F_z(-p_0) < 2 \times 10^{-6}$. The truncation error is less than 0.1 percent.

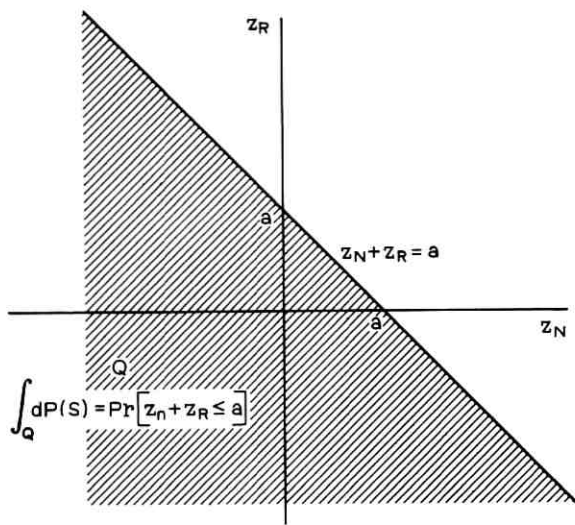


Fig. 6—Distribution function $F_z(a) = \Pr[z_N + z_R \leq a]$.

Refs. 7 and 9. The analysis for higher-order phase-shift keyed systems needs extensive modification and will be treated in a future publication.

V. DISTRIBUTION FUNCTION $F_z(a)$ WITH ARBITRARY z_N AND z_R

Consider two one-dimensional random variables z_N and z_R . The joint probability distribution of z_N and z_R is a distribution in Ω^2 , or a two-dimensional distribution.

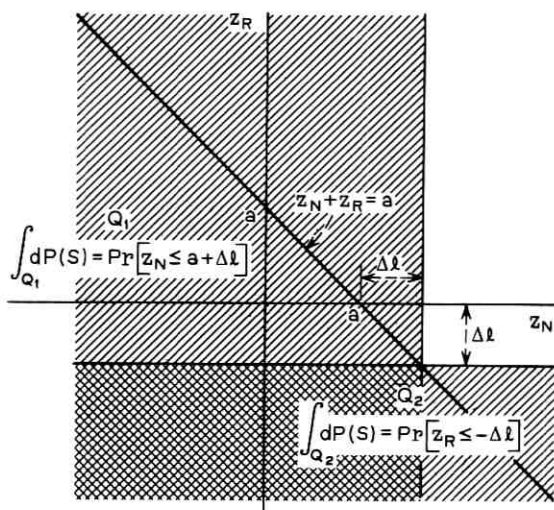
Now the probability distribution of $z = z_N + z_R$ is given by (see Fig. 6)

$$\begin{aligned} F_z(a) &= \Pr [z_N + z_R \leq a] \\ &= \int_Q dP(S), \quad (x, y) \in Q \quad \text{if } x + y \leq a \end{aligned} \quad (108)$$

and $P(S)$ is the probability function of z_N and z_R .¹⁵ $P(S)$ represents the probability of the relation $(x, y) \subset S$.

Since $dP(S) \geq 0$, note that (see Fig. 7)

$$\begin{aligned} \int_Q dP(S) &\leq \int_{Q_1} dP(S) + \int_{Q_2} dP(S), \quad (x, y) \in Q_1 \quad \text{if } x \leq a + \Delta l, \\ &\quad (x, y) \in Q_2 \quad \text{if } y \leq -\Delta l. \end{aligned} \quad (109)$$

Fig. 7—Upper bound on distribution function $F_z(a)$.

Since

$$\int_{Q_1} dP(S) = \Pr [z_N \leq a + \Delta l] = F_{z_N}(a + \Delta l), \quad (110)$$

$$\int_{Q_2} dP(S) = \Pr [z_R \leq -\Delta l], \quad (111)$$

$$F_z(a) \leq F_{z_N}(a + \Delta l) + \Pr [z_R \leq -\Delta l]. \quad (112)$$

Also we have (see Fig. 8)

$$\begin{aligned} \int_Q dP(S) &\geq \int_{Q_3} dP(S) - \int_{Q_4} dP(S), \quad (x, y) \in Q_3 \quad \text{if } x \leq a - \Delta u, \\ &\quad (x, y) \in Q_4 \quad \text{if } y \geq \Delta u. \end{aligned} \quad (113)$$

Since

$$\int_{Q_3} dP(S) = \Pr [z_N \leq a - \Delta u] = F_{z_N}(a - \Delta u), \quad (114)$$

$$\int_{Q_4} dP(S) = \Pr [z_R \geq \Delta u], \quad (115)$$

$$F_z(a) \geq F_{z_N}(a - \Delta u) - \Pr [z_R \geq \Delta u]. \quad (116)$$

From (112) and (116) we can write

$$\begin{aligned} F_{z_N}(a - \Delta u) &= \Pr [z_R \geq \Delta u] \\ &\leq F_z(a) \leq F_{z_N}(a + \Delta l) + \Pr [z_R \leq -\Delta l]. \end{aligned} \quad (117)$$

Equation (117) is valid even when z_N and z_R are statistically dependent random variables.

If the distribution of z_R is very much concentrated around some point $y = y_0$, it was shown in Sections II and IV that $F_z(a)$ can be evaluated with arbitrarily small error if z_N and z_R are statistically independent random variables and if we can bound $F_{z_R}(\lambda)$. If z_N and z_R are statistically dependent random variables, equation (117) shows that the same techniques can be used to compute $F_z(a)$ if the distribution of z_R is very much concentrated around some point $y = y_0$.

VI. CONCLUSIONS

We have presented simple upper and lower bounds on the distribution function of the sum of two random variables in terms of the marginal distribution functions of the variables.

We have also derived several other bounds when one of the random variables is a gaussian random variable or when one of the distribution functions is convex or concave.

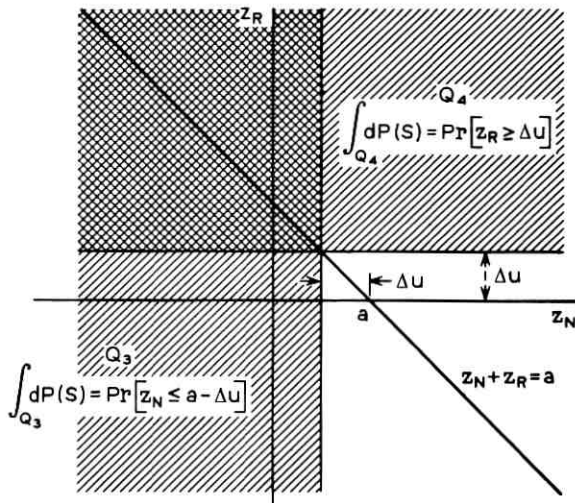


Fig. 8—Lower bound on distribution function $F_z(a)$.

These bounds are then applied to the error rate analysis of a binary coherent digital system subject to intersymbol interference and additive gaussian noise. Since the difference between the upper and lower bounds is a monotone decreasing function of the number of pulses in the finite pulse train, the bounds can be used to compute the error probability with arbitrarily small error. Application of these bounds is illustrated by two examples. Relative merits of the bounds are also briefly discussed.

Many other applications including the analysis of co-channel and adjacent channel interference in communication systems will be evident to the reader. Some such novel applications will be given in a future publication.

APPENDIX A

Let us write

$$G(\alpha) = \frac{1}{2} \operatorname{erfc}(x + \alpha) + \frac{1}{2} \operatorname{erfc}(x - \alpha). \quad (118)$$

If $x = 0$, one can easily show that

$$\frac{1}{2} \operatorname{erfc}(\alpha) + \frac{1}{2} \operatorname{erfc}(-\alpha) = 1 = \operatorname{erfc}(x). \quad (119)$$

We shall now assume that $x \neq 0$. Also since $G(\alpha)$ is an even function of α , we shall consider $\alpha \geq 0$. From (31) and (118) we can write

$$G'(\alpha) = \frac{1}{\sqrt{\pi}} [\exp\{-(x - \alpha)^2\} - \exp\{-(x + \alpha)^2\}]. \quad (120)$$

Note that $G'(0) = 0$ and that there are no other finite stationary points of $G(\alpha)$, $x \neq 0$. Further one can show that

$$G'(\alpha) > 0, \quad x > 0, \quad \alpha > 0. \quad (121)$$

$$G'(\alpha) < 0, \quad x < 0, \quad \alpha > 0. \quad (122)$$

From (118), (121), and (122) we then have

$$\frac{1}{2} \operatorname{erfc}(x + \alpha) + \frac{1}{2} \operatorname{erfc}(x - \alpha) \geq \operatorname{erfc}(x), \quad x \geq 0, \quad (123)$$

$$\frac{1}{2} \operatorname{erfc}(x + \alpha) + \frac{1}{2} \operatorname{erfc}(x - \alpha) \leq \operatorname{erfc}(x), \quad x \leq 0. \quad (124)$$

For the sake of completeness we would like to note here that $\operatorname{erfc}(x)$ is a convex function for $x \geq 0$ and is concave for $x \leq 0$. Hence we can also show that

$$\begin{aligned} p \operatorname{erfc}(x + \alpha) + (1 - p) \operatorname{erfc}(x - \alpha) \\ \geq \operatorname{erfc}(x), \quad x + \alpha \geq 0, \quad x - \alpha \geq 0, \quad 0 \leq p \leq 1, \end{aligned} \quad (125)$$

and

$$\begin{aligned} p \operatorname{erfc}(x + \alpha) + (1 - p) \operatorname{erfc}(x - \alpha) \\ \leq \operatorname{erfc}(x), \quad x + \alpha \leq 0, \quad x - \alpha \leq 0, \quad 0 \leq p \leq 1. \end{aligned} \quad (126)$$

Observe that (125) is not sufficient to prove (123).

APPENDIX B

Let η_k denote the partial sum $\sum_{i=1}^k \xi_i$ where

$$w_N = \sum_{i=1}^N \xi_i, \quad (127)$$

and ξ_i 's are statistically independent random variables. From (32) and (127) we can write

$$\mu_n = \langle x_{w_N}^n \rangle = \theta_n(N) \quad (128)$$

where

$$\theta_n(i) \equiv \langle \eta_i^n \rangle, \quad n \geq 1, \quad \theta_0(i) = 1. \quad (129)$$

Now

$$\theta_n(k) = \langle [\eta_{k-1} + \xi_k]^n \rangle, \quad k > 1, \quad (130)$$

or

$$\theta_n(k) = \sum_{p=0}^n \binom{n}{p} \theta_p(k-1) \alpha_{n-p}(k), \quad k > 1, \quad (131)$$

where

$$\alpha_{n-p}(k) = \langle \xi_k^{n-p} \rangle, \quad \alpha_0(k) = 1, \quad k \geq 1. \quad (132)$$

Since

$$\theta_n(1) = \langle \eta_1^n \rangle = \langle \xi_1^n \rangle = \alpha_n(1), \quad (133)$$

and since we shall assume that all $\alpha_{n-p}(k)$'s are known or can be evaluated, we have a recurrence relation in (131) to compute μ_n .

Often ξ_k 's are even random variables, and in this case we can show that

$$\mu_{2l+1} = 0, \quad l \geq 0, \quad (134)$$

$$\mu_{2n} = \theta_{2n}(N), \quad (135)$$

$$\theta_{2n}(k) = \sum_{p=0}^{2n} \binom{2n}{2p} \theta_{2p}(k-1) \alpha_{2n-2p}(k). \quad (136)$$

The recurrence relation (136) contains only the sum of positive terms, and hence can easily be used to compute μ_{2n} 's.

In Section IV, $\xi_k = a_k r_k$, $\mu_{2l+1} = 0$, $l \geq 0$ and $\alpha_{2i}(k) = r_k^{2i}$, $i \geq 0$. All even order moments of w_N can therefore be easily calculated from (136).

In Refs. 18 and 25 methods have been developed to calculate μ_{2n} of the random variable θ where

$$\theta = \sum_{i=1}^K R_i \cos \theta_i \quad (137)$$

and θ_i 's are independently distributed random variables uniformly distributed over the range $[0, 2\pi]$. Most of these methods use an infinite series expansion, and often the accuracy obtained from these methods is questionable.²⁵

Noting that we can set $\xi_i = R_i \cos \theta_i$, $\mu_{2l+1} = 0$, $l \geq 0$, and

$$\alpha_{2i}(j) = \langle (R_i \cos \theta_i)^{2i} \rangle$$

or

$$\alpha_{2i}(j) = R_i^{2i} \frac{(2i)!}{2^{2i}(i!)^2}, \quad (138)$$

all even order moments μ_{2n} 's can be calculated by using (136) and (138).

This method of calculating μ_{2n} 's can be shown to be analogous to that given in Ref. 26 and is preferable to that in Refs. 18 and 25.

REFERENCES

1. Lucky, R. W., Salz, J., and Weldon, E. J., Jr., *Principles of Date Communication*, New York: McGraw-Hill Book Co., 1968, pp. 59-63.
2. Aaron, M. R., and Tufts, D. W., "Intersymbol Interference and Error Probability," IEEE Trans. Inform. Theory, *IT-12*, January 1966, pp. 26-34.
3. Aein, J. M., and Hancock, J. C., "Reducing the Effects of Intersymbol Interference with Correlation Receivers," IEEE Trans. Inform. Theory, *IT-9*, July 1963, pp. 167-175.
4. Calandruo, L., Crippa, G., and Immovilli, G., "Intersymbol Interference in Binary and Quaternary PSK and DCPSK Systems," Alta Frequenza, *38*, May 1969, pp. 337-344.
5. Tufts, D. W., "Summary of Certain Intersymbol Interference Results," IEEE Trans. Inform. Theory, *IT-10*, October 1964, p. 380.
6. Saltzberg, B. R., "Error Probabilities for Binary Signal Perturbed by Intersymbol Interference and Gaussian Noise," IEEE Trans. Com. Sys., *CS-12*, March 1964, pp. 17-120.
7. Saltzberg, B. R., "Intersymbol Interference Error Bounds with Application to Ideal Bandlimited Signaling," IEEE Trans. Inform. Theory, *IT-14*, July 1968, pp. 563-568.
8. Lugannani, R., "Intersymbol Interference and Probability of Error in Digital Systems," IEEE Trans. Inform. Theory, *IT-15*, November 1970, pp. 686-688.

9. Prabhu, V. K., "Performance of Coherent Phase-Shift Keyed Systems with Intersymbol Interference," *IEEE Trans. Inform. Theory, IT-17*, No. 4 (July 1971), pp. 418-431.
10. Ho, E. Y., and Yeh, Y. S., "A New Approach for Evaluating the Error Probability in the Presence of Intersymbol Interference and Additive Gaussian Noise," *B.S.T.J.*, 49, No. 9 (November 1970), pp. 2249-2266.
11. Celebiler, M. I., and Shimbo, O., "Intersymbol Interference Considerations in Digital Communications," *ICC Record*, June 1970, pp. 8.1-8.10.
12. Shimbo, O., and Celebiler, M. I., "The Probability of Error Due to Intersymbol Interference and Gaussian Noise in Digital Communication Systems," *IEEE Trans. on Com. Tech., COM-19*, No. 2 (April 1971), pp. 113-119.
13. Mullins, J. H., "A Computer Program Simulating the Two-Level Millimeter Wave Waveguide Communication System," unpublished work.
14. Tu, P. J., "A Study of the System Impairments for the Two-Level FM-DCPSK WT-4 Transmission System," unpublished work.
15. Cramer, H., *Mathematical Methods of Statistics*, Princeton University Press, Princeton, N. J., 1957.
16. Wagner, H. M., *Principles of Operations Research*, Englewood Cliffs, N. J.: Prentice-Hall, 1969, pp. 592-596.
17. Pagones, M. J., "Error Probability Upper Bound of a Coherently Detected PSK Signal Corrupted by Interference and Gaussian Noise," unpublished work.
18. V. K. Prabhu, "Error Rate Considerations for Coherent Phase-Shift Keyed Systems with Co-Channel Interference," *B.S.T.J.*, 48, No. 3 (March 1969), pp. 743-767.
19. Abramowitz, M., and Stegun, I. A., *Handbook of Mathematical Functions*, Washington, D. C.: National Bureau of Standards, 1967, p. 787.
20. Yeh, Y. S., and Ho, E. Y., "Improved Intersymbol Interference Error Bounds in Digital Systems," *B.S.T.J.*, 50, No. 8 (October 1971), pp. 2585-2598.
21. Algazi, V. R., "Bounds on the Spectra of Angle-Modulated Waves," *IEEE Trans. Com. Tech., COM-16*, No. 4 (August 1968), pp. 561-566.
22. Chernoff, H., "A Measure of Asymptotic Efficiency for Tests of a Hypothesis Based on a Sum of Observations," *Ann. Math. Stat.*, 23, April 1952, pp. 493-507.
23. Bennett, G., "On the Probability of Large Deviations from the Expectation for Sums of Bounded, Independent, Random Variables," *Biometrika*, 50, 1963, pp. 528-535.
24. Prabhu, V. K., "Error-Probability Upper Bound for Coherently Detected PSK Signals with Co-Channel Interference," *Elec. Letters*, 5, August 1969, pp. 383-385.
25. Rosenbaum, A. S., "Binary PSK Error Probabilities with Multiple Co-Channel Interferences," *IEEE Trans. Com. Tech., COM-18*, No. 3 (June 1970), pp. 241-253.
26. Goldman, J., "Moments of the Sum of Circularly Symmetric Random Variables," to be published.



Optical Fiber Joining Technique

By D. L. BISBEE

(Manuscript received July 15, 1971)

*This paper describes a method of thermally fusing clad glass fibers, end to end, to obtain a good mechanical joint with low transmission loss. Methods of preparing fiber ends and aligning them for joining are discussed. Two sizes of fibers were joined (10.8- μm core and 20- μm core clad fibers with outside diameters of 75 μm and 150 μm respectively).**

I. INTRODUCTION

There is a great deal of interest in using glass fibers as optical waveguides to carry information in much the same way as wires or metallic waveguides do. If glass fibers are to be used in this way, they will need to be joined just as wires and metallic waveguides must be joined.

A method for joining single fibers was developed. Clad glass fibers were joined which had cores of 10.8- μm and 20- μm diameters and overall diameters of 75 μm and 150 μm respectively. The cores were Schott SSK-1 glass and the cladding of Schott SK-14 glass which have glass transition temperatures of 621°C and 649°C respectively. Good mechanical joints which can be made quickly with transmission losses as low as 11.5 percent were obtained, but lower losses should be possible with a little more effort.

II. FIBER END PREPARATION

To get a good joint, good fiber ends are needed. Polishing or etching the fiber ends has been suggested, but we have found that if a fiber is broken properly it will have an end that is suitably flat over most of its surface and perpendicular to the axis of the fiber as seen under a microscope. Figure 1 shows two good ends of 10.8- μm core, 75- μm o.d. fibers magnified 500X. The break can be made by scoring the fiber with a razor blade and breaking it or by laying the fiber across a sharp metallic edge and positioning a Tesla coil so that its discharge is con-

* The fibers were manufactured by DeBell and Richardson, Inc., of Hazardville, Connecticut.

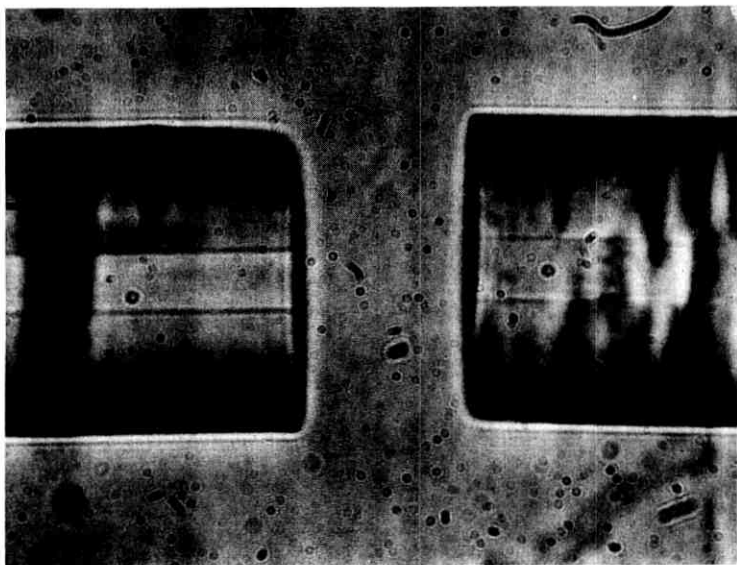


Fig. 1—Two cleanly broken ends of 10.8- μm core, 75- μm o.d. fibers magnified 500X.

centrated at the point where the fiber touches the metal, then breaking it by bending or pulling. The sparking must continue for several seconds with greater time for greater fiber diameter. To prevent the deposition of metal on the fiber because of the electrical discharge, platinum wire was used as the metallic contact. Fibers of 250- μm o.d. or greater can be scored with a file or diamond before breaking.

If the fiber is bent to the breaking point after it is scored or treated with an electrical discharge, one end will have a lip protruding and the other end will have a corresponding absence of material. This can be seen in Fig. 2. This lip is sometimes as long as the diameter of the fiber and would prevent the end from being brought close enough to another fiber end to permit joining them. If the fiber is pulled instead of bent until it breaks, the lip is not produced on most occasions, so this is the recommended procedure.

Very small fibers will sometimes soften and bend from the heat when the discharge from the Tesla coil strikes them, but with care, fibers as small as 25- μm o.d. have been broken with good ends suitable for joining.

III. ALIGNMENT

After the ends of the fiber have been prepared, they must be mounted so that they can be aligned. Teflon-coated tweezers to hold the fiber ends were mounted, one on a general purpose 3-dimensional micromanipulator and one on a precision 3-dimensional micromanipulator with a positioning resolution of $0.127\text{ }\mu\text{m}$.

The Teflon-coated tweezers are gentle with the fiber and allow it to slip when the fiber contracts after having been heated, as will be discussed later.

From measurements of light output versus fiber end displacement we find that a misalignment of less than $2\text{ }\mu\text{m}$ in the $10.8\text{-}\mu\text{m}$ core fiber gives 10 percent less transmission than when the ends are aligned. Losses due to fiber offsets are covered in detail in Ref. 1.

One can determine when the ends are aligned by viewing them through a microscope and assuming that the core is concentric with the outside of the cladding. To get two perpendicular views of the fiber, a mirror can be mounted so the fiber can be viewed directly from the front and

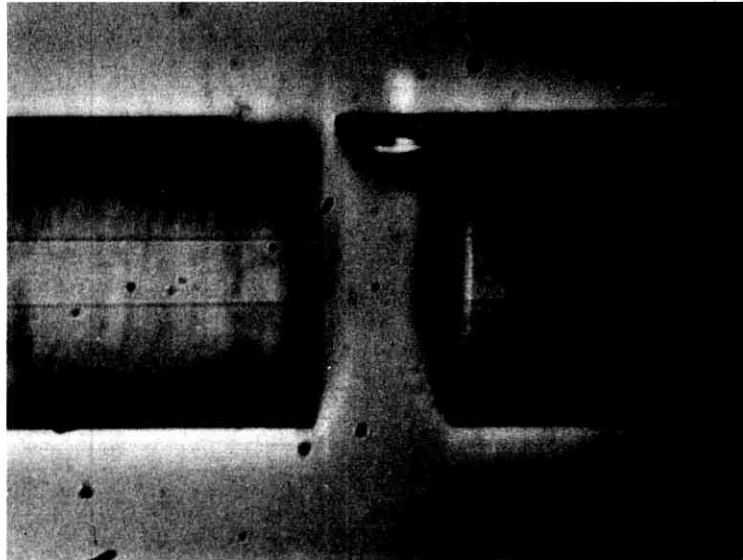


Fig. 2—A characteristic break in a $10.8\text{-}\mu\text{m}$ core, $75\text{-}\mu\text{m}$ o.d. fiber showing the protruding lip.

through the mirror from the side. Two problems in this method of alignment are, first, the core and cladding may not be concentric, and second, rather sophisticated optics are needed to see an alignment error of 1 μm or less. If the core and cladding are made concentric and if a microscope of 200X or greater is used, one can probably align them well enough by this means.

Another method we have used of determining optimum alignment is to send laser light down the fiber to a detector and adjust the fiber ends for maximum transmission. A problem with this method is that if the end of the fiber is broken at an angle with respect to the normal to the fiber axis, the maximum transmission will be obtained when the fiber ends are misaligned to compensate for the offset in the beam direction caused by the angle of refraction at the nonnormal surface. This offset is y in Fig. 3. This error is small, though, if the angle is small. With a fiber of 80- μm diameter, core index of 1.6, and a surface at the end that is 10 degrees from the normal, the ends of the fibers would have to be offset 0.73 μm to correct for the beam misalignment. This would introduce about 5 percent loss in our 10.8- μm core fiber. An angle of 10 degrees is large, so one should be able to do much better than that.

IV. JOINING THE FIBERS

Several unsuccessful attempts were made to join fibers with epoxy alone and epoxy in a glass sleeve. When using epoxy alone, the resultant joint was too weak to keep the fiber ends aligned when transverse pressure was applied. When using sleeves, the tolerance between sleeve i.d. and fiber o.d. had to be very close, of the order of 1 μm to keep the fibers aligned properly, and this tolerance is hard to obtain. Further, a bubble formed at the fiber junction inside several sleeve joints. Thus, this method was considered limited in practicality.

A method that worked was the fusing of the fiber ends. Number 24 nichrome wire was wound around two metal posts so as to leave an

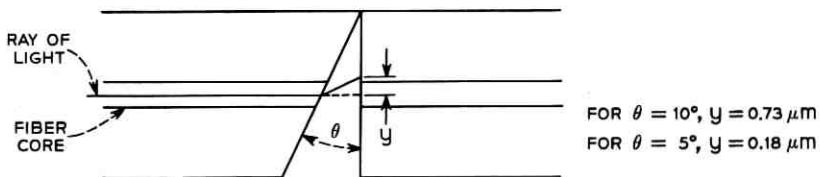


Fig. 3—Beam refraction at a nonnormal fiber end.



Fig. 4—Heating wire with fiber ends held in place by Teflon coated tweezers.

opening between the wires through which the fiber ends could pass as shown in Fig. 4.

The fiber ends were aligned, leaving a space of about $15\text{ }\mu\text{m}$ between them for thermal expansion. About 14 amperes of current were passed through the nichrome wire which surrounded the fiber ends causing the wire to heat up and fuse the fiber ends together. The longitudinal expansion of the fiber when heated closed the $15\text{-}\mu\text{m}$ gap that was left between the fiber ends. Of course, when the fiber cooled it shrank again, but the fiber could slip in the Teflon-coated tweezers when shrinking. The ends fused together in about 30 seconds after the heat was applied. To tell when the ends were fused, a lamp was placed so that the specular reflection from the fiber ends could be seen in the microscope. Disappearance of the reflection indicated the surface had vanished and the ends were fused. Figure 5 is a microphotograph of a fused joint in a $10.8\text{-}\mu\text{m}$ core, $75\text{-}\mu\text{m}$ o.d. fiber, at $500X$ magnification. Such joints exhibited losses as low as 11.5 percent.

JOINT



Fig. 5—A thermally fused joint in 10.8- μm core, 75- μm o.d. fiber.

V. CONCLUSIONS

After two fiber ends are carefully broken and properly aligned, they can be fused together by means of a heated wire to give a good mechanical joint with an acceptable amount of loss. Fibers of 10.8- μm core were joined and gave losses as low as 11.5 percent, but with a little more effort it is believed that joints could be made with considerably lower loss than this.

REFERENCES

1. Bisbee, D. L., "Measurements of Loss Due to Offsets and End Separations of Optical Fibers," B.S.T.J., this issue, pp. 3159-3168.

Measurements of Loss Due to Offsets and End Separations of Optical Fibers

By D. L. BISBEE

(Manuscript received June 23, 1971)

If fibers are to be coupled together by means of detachable connectors, there is a need to know how much light will be lost by misalignment or axial separation of the fiber ends.

Measurements were made of coupling efficiency from one fiber to another versus offset and end separation with and without index-matching liquid between the ends for a single-mode and a multimode fiber at $\lambda = 0.6328 \mu\text{m}$. Graphs are presented for offsets as great as 3 radii and for end separations up to 127 μm . Maximum coupling efficiency of 97 percent was obtained, and about 50 percent was obtained with an offset of 1 radius.

I. INTRODUCTION

Coupling of glass fibers, end to end, for transmitting optical signals requires critical alignment at each coupling point. Coupling can be accomplished by permanently fusing the fibers together,¹ by using permanently bonded sleeves, or by using detachable connectors.

This paper presents experimental data for the coupling efficiency of light from one fiber end into another as a function of offsets and axial separation which will be present in detachable connectors and to a lesser extent in fused joints and sleeve joints.

Measurements of coupling efficiency versus end separation and translation were made and plotted for a multimode fiber with core diameter of 10.8 μm and a single-mode fiber with a core diameter of 3.7 μm .*

Several people^{2,3,4} have studied the problem of launching efficiency from a Gaussian beam into a fiber, both theoretically and experimentally. A comparison will be made between the theory and our experimental data.

* The 10.8- μm core fiber was manufactured by DeBell and Richardson, Inc., of Hazardville, Connecticut, and the 3.7- μm core fiber was made by Corning Glass Co.

II. EXPERIMENT

2.1 Equipment

Figure 1 is a sketch of the measuring apparatus. The light from a He-Ne laser operating in the single transverse TEM_{00} mode that gives a Gaussian distribution was chopped, then focused down by a 10X microscope objective into a fiber that we call the launching fiber. The output end of the launching fiber was mounted on a precision 3-dimensional micromanipulator with positioning resolution of $0.127 \mu\text{m}$. The output of this fiber was launched into a fiber that we call the receiving fiber. The output of the receiving fiber was detected by a solar cell immersed in index-matching liquid, measured by a lock-in amplifier, and recorded on a chart recorder. Mode strippers (not shown) were used on both launching and receiving fibers to eliminate the light traveling in the cladding. These were made by cutting an S-shaped groove about 0.25 mm wide and deep in a piece of plexiglass about 30 cm long and placing the fiber in the groove, then filling it with index-matching oil of a slightly higher index than the fiber cladding. None of these dimensions are critical, and the same effect could probably be obtained by making the stripper much smaller.

2.2 Method

(i) Coupling efficiency versus fiber end separation was measured by first aligning the fiber ends axially and then bringing them into contact

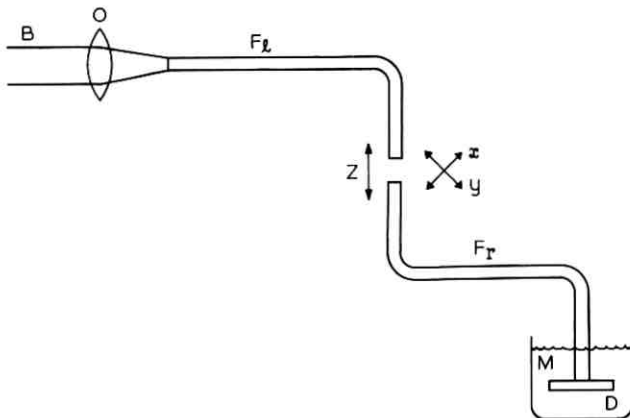


Fig. 1—Schematic diagram of light coupling measuring apparatus: B, chopped beam from laser; O, microscope objective; F_L , launching fiber; F_R , receiving fiber; M, index-matching oil; D, detector.

with each other for the measurement at zero separation. One fiber was then separated from the other by known amounts and the output of the receiving fiber was recorded. This was repeated several times for each case and the mean of the readings was plotted. These measurements were made for the 10.8- μm and 3.7- μm -diameter core fibers with and without index-matching oil in the gap. A reliable measurement could not be made at zero separation without oil because of interference effects.

(ii) Coupling efficiency versus fiber lateral displacement was measured and plotted for both fibers with and without matching oil between them. These measurements were made for fiber end separations of 5.08 μm , 10.16 μm , 25.4 μm , and 50.8 μm . The smallest separation for which scanning measurements were made was 5.08 μm because they could not be made at zero separation as one fiber would rub against the other, and also because of the interference effects mentioned above. In each case the scanning was begun with the fibers out of alignment on one side of the fiber axis so as to give approximately zero transmission, then one fiber was translated past the axis of the other reaching a maximum transmission, and continuing on until approximately zero transmission was reached again. This operation was repeated four times, once each in the plus and minus x and y directions of Fig. 1 for each separation. The mean of these four readings was then plotted.

(iii) The coupling efficiency expressed in percent was calculated from the power levels measured at the ends of the launching and receiving fibers and from the transmission loss in the second fiber. Absolute values of the data presented could be in error by as much as 3 percent.

2.3 Results

2.3.1 Multimode 10.8- μm -Diameter Core Fiber

For this fiber $r = 5.4 \mu\text{m}$, $\lambda = 0.6328 \mu\text{m}$, the core index is 1.6171, and the cladding index is 1.6038. From this data we find that the fiber is capable of propagating 67 modes.⁵

It would be difficult to mathematically predict the light coupling loss due to offsets or fiber end separation from such a multimode fiber, so no comparison was made between theory and experimental data on this fiber.

The coupling efficiency at 2.54- μm separation without oil in the gap was measured to be 88.8 percent, and at zero separation with oil in the gap it was 97.06 percent. These values appear as points on the curves of Fig. 2. The data in graph B was taken with index-matching oil

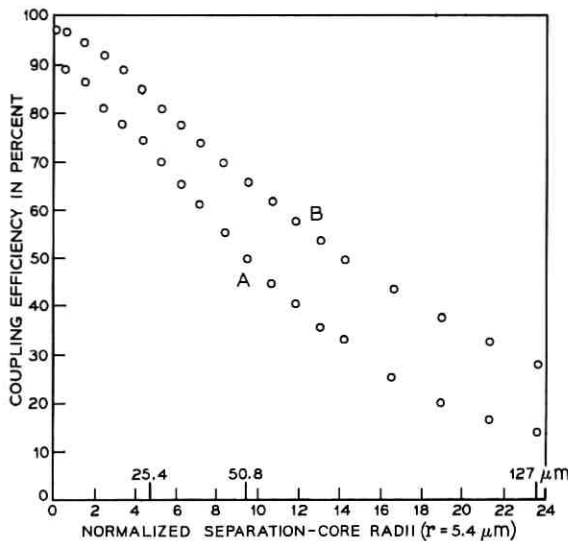


Fig. 2—Curves of coupling efficiency versus fiber end separation for 10.8- μm -diameter core fiber: A, without index-matching oil in the gap; B, with matching oil in the gap.

($n = 1.6204$) in the gap between the fiber ends, and in graph A without oil. A reliable reading could not be taken at zero separation without oil in the gap because of the interference between the transmitted and reflected beams between the plane parallel surfaces of the fiber ends, but all the readings for each graph at 2.54- μm (approximately 0.5 radius) separation were within ± 0.5 percent of each other.

The Fresnel reflection loss at the two core-air interfaces is 11.2 percent (neglecting resonance effects). If we subtract this from 100 percent we get 88.8 percent which is the coupling efficiency that was measured at 2.54- μm separation without oil in the gap. This implies that all the light except that reflected is coupled into the receiving fiber.

When oil of index $n = 1.6204$ was put between the fiber ends eliminating the core-air interfaces, the amount of light coupled increased by about 8 percent to 97 percent, which was less than the 11.2 percent increase predicted.

Figure 3 shows the coupling efficiency versus offset for four different fiber end separations without index-matching liquid in the gap. Figure 4 has the same set of curves with index-matching oil in the gap.

We see that only 50 percent of the light is transmitted with perfect axial alignment for fibers separated by 50.8 μm without matching oil

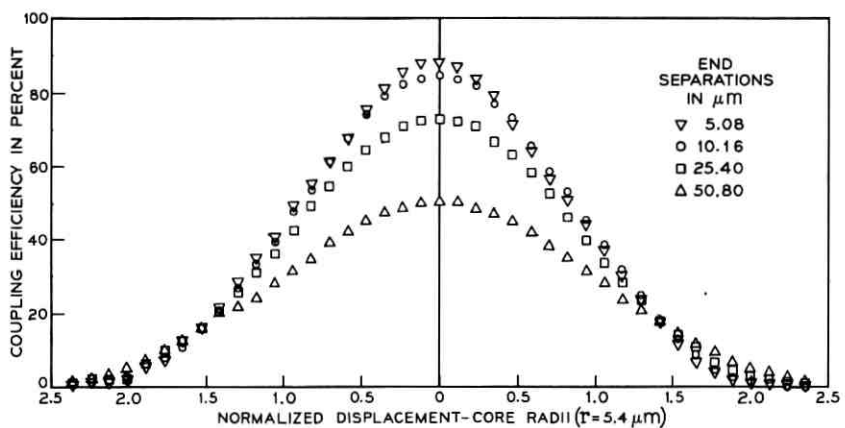


Fig. 3—Coupling efficiency versus displacement of 10.8- μm -diameter core fiber without index-matching oil in the gap.

between them. It can be seen also that all the curves are coincident at about 20 percent efficiency at a little less than 1.5 radii translation both with and without index-matching liquid in the gap.

2.3.2 Single-Mode 3.7- μm -Diameter Core Fiber

For this fiber, the fiber characteristic term⁶

$$R = \frac{2\pi a}{\lambda} (n_1^2 - n_2^2)^{\frac{1}{2}}$$

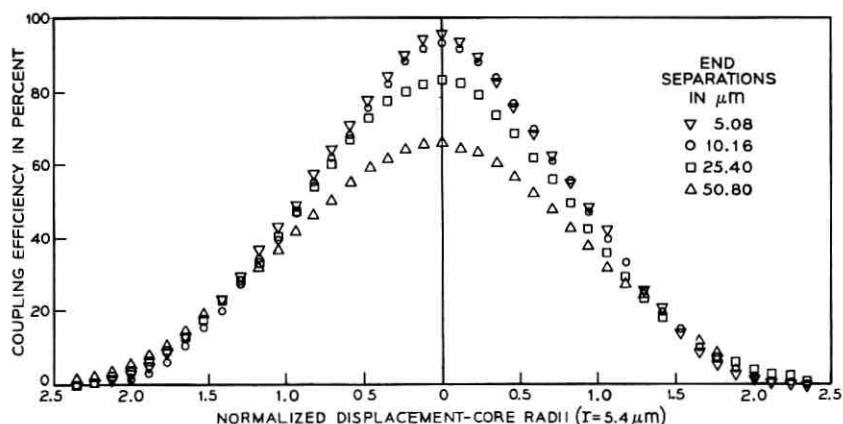


Fig. 4—Coupling efficiency versus displacement of 10.8- μm -diameter core fiber with index-matching oil in the gap.

is 2.2 at $\lambda = 0.6328 \mu\text{m}$, where a is the radius of the core, n_1 is the refractive index of the core, n_2 is the index of the cladding, and λ is the wavelength of the light. Only the HE_{11} mode can propagate because all other modes are cut off in a fiber with $R < 2.405$.

Coupling efficiency versus fiber end separation is plotted in Fig. 5. The coupling efficiency at $2.54\text{-}\mu\text{m}$ separation without oil in the gap was found to be 90 percent. This is shown in curve A, and when this curve is extrapolated to zero separation, we find the coupling efficiency at zero separation is approximately 91 percent. This compares with 90 percent for the multimode fiber at zero separation without oil. With oil in the gap at zero separation the coupling efficiency was 97 percent. Thus, the matching oil increased efficiency by 6 percent. This is the same efficiency as was found for the multimode fiber with oil in the gap at zero separation.

There are no striking differences between the coupling efficiency versus fiber end separation curves of the two fibers which are shown in Figs. 2 and 5. It has been noted that at zero separation the efficiencies are virtually the same, but at $127\text{-}\mu\text{m}$ separation, which is almost 70 radii for the $3.7\text{-}\mu\text{m}$ -diameter core fiber though less than 24 radii for the $10.8\text{-}\mu\text{m}$ -diameter core fiber, we see some small differences. Without oil at this separation the $10.8\text{-}\mu\text{m}$ core fiber has 14.5 percent efficiency and the $3.7\text{-}\mu\text{m}$ core fiber has 13 percent showing the multimode fiber more efficient by 1.5 percent. With index-matching oil at this separation, coupling into the single-mode fiber is more efficient by 5 percent, than into the multimode fiber. At about $50\text{-}\mu\text{m}$ separation both with and without oil in the gap, coupling efficiency is about 10 percent less in the single-mode fiber than in the multimode fiber.

Figures 6 and 7 show curves of coupling efficiency versus fiber translation for the single-mode fiber. Figure 6 shows curves of coupling efficiency versus fiber translation for four end separations without matching oil in the gap and Fig. 7 shows the same curves with oil in the gap. These curves are comparable to the corresponding ones for the multimode fiber in Figs. 3 and 4, except for the above-noted lower efficiency for the single-mode fiber at greater end separations. We see also that the efficiency does not drop to zero as quickly with respect to displacement with the single-mode fiber as with the multimode one. This is understandable in that with the single-mode fiber, the field extends into the cladding, but in the other fiber the field is rather sharply restricted to the core.

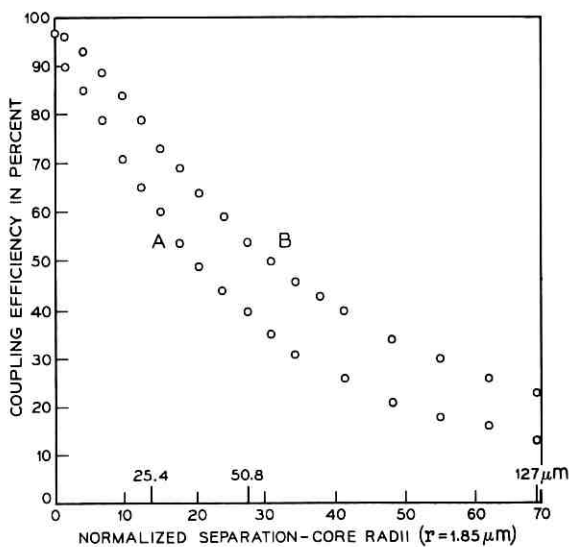


Fig. 5—Coupling efficiency versus fiber end separation of 3.7- μm -diameter core fiber: A, without index-matching oil in the gap; B, with index-matching oil.

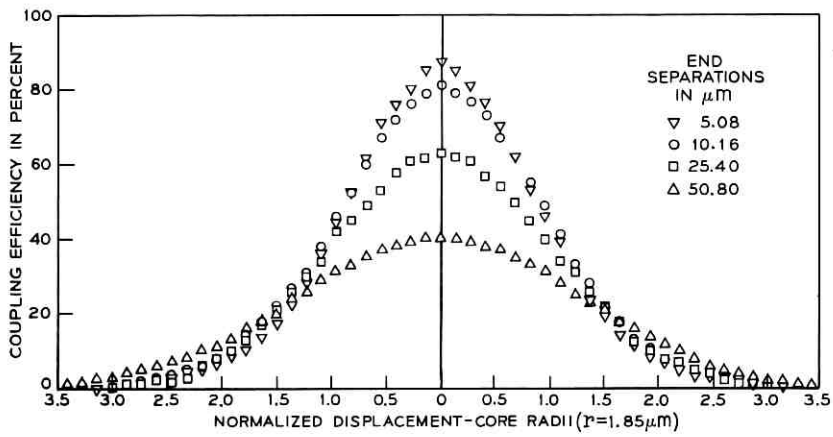


Fig. 6—Coupling efficiency versus displacement of 3.7- μm -diameter core fiber without index-matching oil in the gap.

III. COMPARISON WITH THEORY

In the absence of irregularities such as nonflat fiber ends and index mismatch, the coupling efficiency from one fiber to another at zero separation should be 100 percent.

Launching efficiencies of nearly 100 percent for the HE₁₁ mode from an incident Gaussian beam have been predicted theoretically by J. R. Stern and R. B. Dyott,² and D. Marcuse.³ The field profile of the HE₁₁ mode is similar to a Gaussian distribution, thus the theory which predicts the launching efficiency from a Gaussian beam into a fiber should approximately predict the coupling efficiency from our single HE₁₁ mode launching fiber into the corresponding receiving fiber. Marcuse calculated the theoretical curve of coupling efficiency versus translation in Fig. 8 using the parameters of our single-mode fiber. The experimental data for our fiber with index-matching oil in the gap at 5.08-μm separation was modified to represent a curve of zero separation and is plotted in Fig. 8 for comparison. At the top of the curve we launched only 97 percent of the incident light where theoretically almost 100 percent could have been launched. In the middle the curves are coincident and at the lower end the discrepancy between the curves is probably due to the fact that the edge of the HE₁₁ mode is not well approximated by the Gaussian beam.

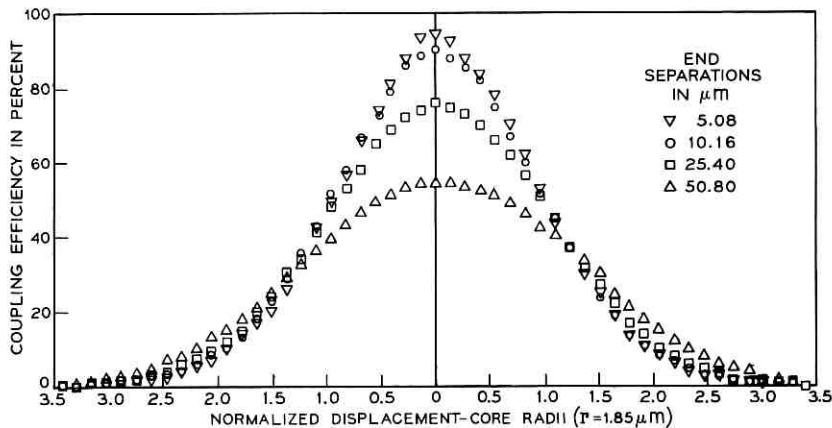


Fig. 7—Coupling efficiency versus displacement of 3.7-μm-diameter core fiber with index-matching oil in the gap.

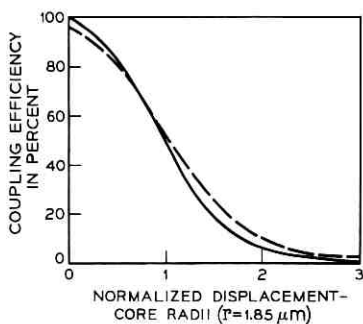


Fig. 8—Coupling efficiency versus translation of 3.7- μm -diameter core fiber: solid line is theoretical, broken line experimental.

IV. CONCLUSIONS

With matching oil in the gap between two fiber ends with zero separation, 97 percent of the light from one fiber was coupled into the other in either single-mode or multimode fibers. The light coupled from a single-mode fiber into another single-mode fiber follows closely the theory for light coupled from a Gaussian beam into a single-mode fiber when one fiber is offset with respect to the other. For fiber ends separated up to 25 μm , a lateral displacement of one radius reduces the coupling efficiency to about 50 percent if there is index-matching liquid between the fiber ends, and to about 40 percent if there is none. The coupling efficiency was reduced by 10 percent with end separation of about 3 radii for the multimode fiber and about 7 radii for the single-mode fiber.

V. ACKNOWLEDGMENT

The author wishes to thank D. Marcuse for making the theoretical calculations reported.

REFERENCES

1. Bisbee, D. L., "Optical Fiber Joining Technique," *B.S.T.J.*, this issue, pp. 3153-3158.
2. Stern, J. R., and Dyott, R. B., "Launching into Single Mode Optical Fiber Waveguide," *IEE Conference Publication 71*, 1970, pp. 191-196.
3. Marcuse, D., "Excitation of the Dominant Mode of a Round Fiber by a Gaussian Beam," *B.S.T.J.*, *49*, No. 8 (October 1970), pp. 1695-1703.

4. Heyke, H. J., "Launching of Fiber Modes by Gaussian Beams," AEU, 24, No. 11 (November 1970), pp. 521-522.
5. Gloge, D., "Weakly Guiding Fibers," to be published in Applied Optics.
6. Kapany, N. S., *Fiber Optics—Principles and Applications*, New York: Academic, 1967, p. 55, Eq. 3.20.

Zero Loss Transfer Across Gaps in a CCD

By R. H. KRAMBECK

(Manuscript received July 19, 1971)

When a charge-coupled device is made with a single layer of metallization, adjacent electrodes must be placed several micrometers apart. As a result there may be some difficulty in moving the charge from one electrode to another. In this paper it will be shown that, for any substrate material, there is a wide range of interface charge for which complete transfer can be achieved regardless of electrode separation. It will further be shown that for a p-substrate with a doping of less than $10^{15}/\text{cm}^3$, the natural charge found in a good quality thermally grown layer of SiO_2 is always of the appropriate sign and magnitude to ensure complete transfer. Therefore, for simple fabrication of a CCD with one layer of metal, this substrate material is the appropriate choice.

I. INTRODUCTION

In a charge-coupled device,¹ charge is transferred from a potential well under one metallization to a deeper potential well under an adjacent metal. Since the metals cannot touch one another, this process involves passing through an interelectrode gap. If the potential pattern is such that there is a potential barrier or a potential well in the space at the end of transfer, then complete charge transfer is impossible. If two layers of metallization are used (which are separated by an insulating layer of 1000 Å), no barrier or well can form. This requires a more complex technology, so it would be desirable to make a CCD with one layer of metallization.

In this paper the effect of interface charge and substrate doping on potential well and barrier formation will be analyzed. It will be shown that, for any given substrate doping and drive voltages, there is an interface charge for which neither well nor barrier forms. The calculations in this paper will assume an infinitely long gap which will ensure that no yield losses will result from small variations in gap width or surface charge magnitude.

II. ANALYSIS

The objective of this analysis will be to find the conditions which will permit complete charge transfer. It is therefore necessary to examine the state of the CCD at the end of the transfer of only the largest ONE that can be accommodated. That is, if the largest ONE is transferred without loss, then any piece of information could be transferred with no loss of charge. Our objective then is to find free-carrier density vs position at the end of transfer. If there is neither a peak nor a minimum of free-charge density in the space, then the space is not interfering with transfer.

To find free-carrier density on the surface, we must find total surface charge density and subtract fixed charge density. The first part of the problem is to find charge density vs position at the end of transfer. This is simplified by the fact that at the end of transfer of the largest possible ONE, the semiconductor surface is an equipotential (the movement of free charge will not stop until an equipotential is achieved).

The geometry of the interelectrode space is shown in Fig. 1. Just below the semiconductor surface the field is uniform because the surface is an equipotential. The displacement field is given by

$$D_s = \sqrt{2N\epsilon_s Vq} \quad (1)$$

where N is the semiconductor doping, ϵ_s is the semiconductor dielectric constant, V is the surface potential, and q is the electronic charge. Just above the surface the field is

$$D_{ox} = D_s + qn - Q_{ss} \quad (2)$$

where n is the free-electron density (cm^{-2}) and Q_{ss} is the density of charged states either in the oxide or at the semiconductor surface (p-type substrate has been assumed with electrons as free carriers). From equations (1) and (2)

$$qn = D_{ox} - \sqrt{2N\epsilon_s Vq} + Q_{ss}. \quad (3)$$

Since Q_{ss} and V are constants, differences in electron density from one point to another are directly related to changes in D_{ox} by

$$\Delta n = \frac{\Delta D_{ox}}{q}. \quad (4)$$

This means that if D_{ox} varies monotonically from the region under one electrode to the region under the adjacent electrode, then electron density also varies monotonically and no barrier or well exists. In Fig. 2

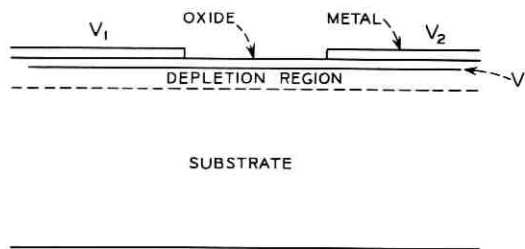


Fig. 1—Cross section of a charge-coupled device showing the interelectrode gap

the three possible variations of D_{ox} with position are shown. First, in Fig. 2a $V < V_1$ and $V < V_2$ where V_1 and V_2 are the voltages applied to the two metals. In this case, D_{ox} is positive under both metals but drops to zero in between (for sufficiently large separation). This means electron density is lower in the space between the electrodes than it is under either of them, and as a result a barrier must be holding back charge. Second, in Fig. 2b $V > V_1$ and $V > V_2$. Here D_{ox} is negative under each electrode but is again zero in the gap. This means electron density is higher in the space than under either electrode, so a potential

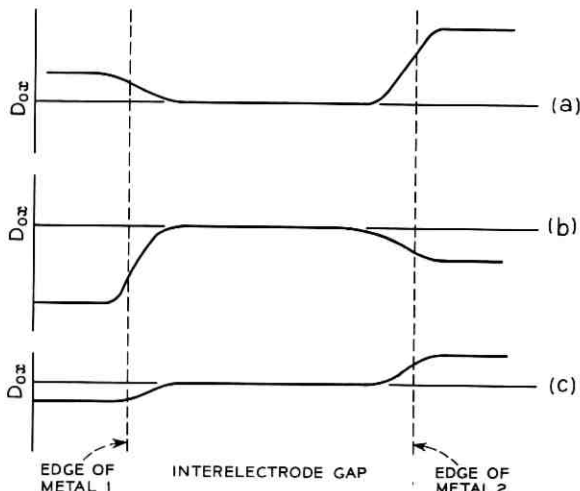


Fig. 2—The variation of oxide field at the surface of the semiconductor, D_{ox} , vs position along the surface when the interelectrode gaps are arbitrarily large. The curves are for three combinations of applied voltages, V_1 and V_2 , and surface potential, V : (a) $V < V_1$, $V < V_2$, (b) $V > V_1$, $V > V_2$, (c) $V \geq V_1$, $V \leq V_2$.

well must be present. Finally, in Fig. 2c $V \geq V_1$ and $V \leq V_2$. Here $D_{ox} \leq 0$ under metal 1, $D_{ox} \geq 0$ under metal 2, and $D_{ox} = 0$ somewhere in between. This is the situation desired. It is therefore necessary to find only what value of Q_{ss} will cause the surface potential at the end of transfer to be in between the two metal voltages.

Let us assume metal 1 is giving its charge to metal 2. Then at the end of transfer free-electron density under metal 1 is zero. Therefore from equation (3)

$$D_{ox_1} = \sqrt{2Ne_s V q} - Q_{ss}. \quad (5)$$

Also the difference between V_1 and V is given by

$$V_1 - V = \frac{D_{ox_1}}{\epsilon_{ox}} \delta \quad (6)$$

where δ is the oxide thickness. Since we need $V \geq V_1$, $D_{ox_1} < 0$. Therefore

$$Q_{ss} \geq \sqrt{2Ne_s V q}. \quad (7)$$

The minimum value of Q_{ss} is obtained when $V = V_1 (D_{ox_1} = 0)$ which gives:

$$Q_{ss} \geq \sqrt{2Ne_s V_1 q}. \quad (8)$$

As an example, with $N = 10^{14}/\text{cm}^3$, $\epsilon_s = 10^{-12} \text{ F/cm}$, and $V_1 = 1 \text{ volt}$, $Q_{ss}/q \geq 3.5 \times 10^{10}/\text{cm}^2$.

This specifies the minimum for N_{ss} . Any lesser value would give rise to a barrier. To prevent formation of a well, we have $V \leq V_2$. Under electrode 2

$$D_{ox_2} = D_s - Q_{ss} + qn$$

$$D_{ox_2} \geq 0.$$

Therefore

$$Q_{ss} \leq \sqrt{2Ne_s V q} + qn. \quad (9)$$

If the largest allowable Q_{ss} is being used, $D_{ox_2} = 0$ and $V = V_2$. Also, from equation (4)

$$D_{ox_2} - D_{ox_1} = qn.$$

Therefore

$$V_2 - V_1 = \frac{qn}{\epsilon_{ox}} \delta$$

where ϵ_{ox} is the oxide dielectric constant. The maximum value of Q_{ss} is therefore

$$Q_{ss} \leq \sqrt{2N\epsilon_s V_2 q} + \frac{\epsilon_{ox}}{\delta} (V_2 - V_1). \quad (10)$$

Using $V_2 = 10$ volts and the same numbers as above for the other parameters gives

$$\frac{Q_{ss}}{q} \leq 2.0 \times 10^{12}/\text{cm}^2.$$

Equations (8) and (10) specify the allowable range for Q_{ss} , which is the result needed.

III. DISCUSSION

The previous section showed that a specific range of Q_{ss} is appropriate for any given substrate doping and pair of driving voltages. In this section the attainability of this range will be discussed. The range is shown graphically in Fig. 3 for the driving voltages $V_1 = 1$ volt and $V_2 = 10$ volts.

It turns out that for a thermally grown oxide on silicon Q_{ss}/q in

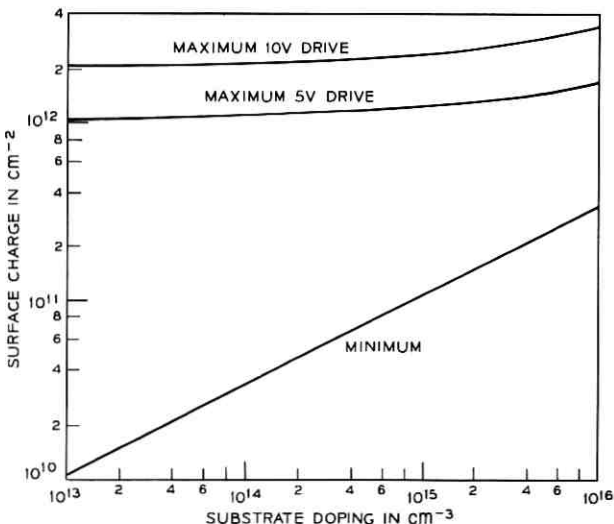


Fig. 3—Minimum and maximum surface charge vs substrate doping for $V_1 = 1$ volt and for $V_2 = 5$ volts and 10 volts.

the oxide is normally in the range 10^{11} to $6 \times 10^{11}/\text{cm}^2$. Therefore for a p-type substrate any doping under $10^{15}/\text{cm}^3$ will ensure complete transfer. For other substrates and oxides some doping must be introduced. Probably the easiest way would be a uniform ion implant chosen so the total charge including oxide charge lies in the allowed range.

An important point about Fig. 3 is the width of the allowed range. For drive voltages of 1 volt and 10 volts the allowed range of charge extends over at least one order of magnitude for any substrate doping below $10^{16}/\text{cm}^3$ which ensures that a proper amount of charge can be obtained even with substantial slice-to-slice variations in charge. It also means that aging effects are unlikely to change the amount of charge to a value outside of the desired range.

In the analysis it was assumed there is sufficient time for complete transfer to occur. An appropriate question is how much longer transfer takes if a gap separates the metals. R. J. Strain and N. L. Schryer² have shown that in a CCD the rate of carrier flow is inversely proportional to the sum of the capacitances between surface and substrate and between surface and metal. Since this sum is much higher when the surface is covered by a metal, the low capacitance gap will not significantly increase transfer time as long as the gap is shorter than the metal.

IV. CONCLUSIONS

From the above discussion it can be seen that the simplest way to obtain complete transfer in a charge-coupled device, with a thermal SiO_2 layer used as insulator, is to use as substrate material p-type silicon with a doping of less than $10^{15}/\text{cm}^3$.

It can be further concluded that for other substrate materials and for other insulators an appropriate charge range always exists, and that this charge range can be obtained by ion implantation over the entire surface of the slice without use of a photographic masking step. Selective implantation of the region between the metals and the regions under the edges of the metals could also eliminate potential barriers and wells. However, because of fringing fields, this can be achieved only by extension of the tail of the charge distribution for a specific distance under each metal, but this would be a more difficult way to achieve complete transfer.

Summarizing, it should be clear that potential barriers and wells in the spaces between electrodes in charge-coupled devices can be eliminated easily. Therefore the possibility of incomplete charge transfer

should not be cited as a reason for spacing electrodes abnormally closely or using two layers of metallization. For most applications future CCD's should be made on p-type substrates with less than $10^{15}/\text{cm}^3$ doping since the proper charge is automatically obtained.

REFERENCES

1. Boyle W. S., and Smith, G. E., "Charge Coupled Semiconductor Devices," *B.S.T.J.*, 49, No. 4 (April 1970), pp. 587-593.
2. Strain, R. J., and Schryer, N. L., unpublished work.

A General Class of Rate-Change Circuits

By S. V. AHAMED

(Manuscript received June 3, 1971)

Rate changing is encountered in data transmission, distributing, collating, encoding, and decoding. It entails the transformation of data at one rate to data at another predefined rate. It is the object of this paper to investigate a special class of circuits that accomplish such a transformation quite mechanically and methodically when only one clock is available to propagate all the binary bits of information. These circuits can be implemented by magnetic domains, by charge transfer and charge-coupled devices, or by any other technology which permits (i) propagation of binary bits of information by a certain modular "period" or "distance" in a modular unit of time and (ii) gating of preselected bits of information from one branch into one or the other branches of three branch nodes in a circuit. The generalization of rate-changing circuits to distributing, collating, reversing, and reversing-with-rate-changing is also presented in the paper.

I. INTRODUCTION

Algebraic coding schemes¹ increase the length of the information block. Shortened codes^{2,3} obtained from such coding schemes further alter the length. When these codes are transmitted uniformly over the telephone networks, a change of rate from the received rate to the transmitted rate is essential. Further, channels carry coded information at different rates. If it is necessary to obtain information at a uniform rate, encode it with a general coding scheme and transmit it over any general channel, decode it to its original rate and refurbish it, then many stages of rate changing are necessary.

To collate bursts of information from many sources onto a signal channel also entails a rate-change process. Distributing circuits which select and uniformly distribute a given number of information bits from longer blocks of uniformly received information are special cases of rate-change circuits. It is the object of this paper to report a set of circuits which perform (i) general rate changing, (ii) general collating and sorting, and finally (iii) reversing and reversing-with-rate-changing

functions. They operate methodically, and mechanically when only one clock source is available for propagation of information bits. This condition exists specifically in magnetic domain technology^{4,5} with field access propagation and to a less stringent measure in charge-transfer⁶ and charge-coupled^{7,8} device technologies. In general, the circuits presented can be implemented by any technology that permits (i) all binary bits of information to be shifted from one location to the adjoining location within one clock cycle and (ii) the channeling of information bits to one or the other branch of a node within a circuit.

For clarity of exposition, the following terms are defined. A "period" is a unit of distance or location by which a binary bit of information may be moved in one unit of time. A "clock cycle" is the smallest unit of time. It is also the time required to propagate one binary bit of information by one period. A "gate" is a device which channelizes a selected number of information bits into one or another branch at a node in a circuit. Such functions can be readily accomplished^{5,9,10} in the various technologies^{4,6,8} presently under development in the Bell System.

The paper is divided into five sections. After the introduction, Section II describes a general class of rate-change circuits. These circuits become an important element in the collating and distributing circuits described in Section III, and Section IV discusses reversing circuits by which the order of incoming data bits may be reversed. Section V is devoted to conclusions.

II. GENERAL RATE-CHANGE CIRCUITS

The principle of rate changing is explained by two examples in this section. The generality of the principle is proved in Appendix A.

2.1 Rate-Reducing Circuits

Example 1. Consider a block of data 8 bits long to be expanded by a ratio of 2, yielding a new rate that is half the original rate. Figure 1 represents a circuit in which the data arrives at the clock rate. The incoming polynomial may be written as

$$u_0 = a_0 + a_1X + a_2X^2 + a_3X^3 + a_4X^4 + a_5X^5 + a_6X^6 + a_7X^7.$$

The four data positions corresponding to the first four terms of u_0 are diverted into the upper part of stage 1 containing N_1 periods, and the second four data positions are diverted in the lower half of stage 1 containing $N_1 + 4$ periods. Gate g_2 diverts the first two data positions into the upper half of stage 2, the next two data positions into the lower

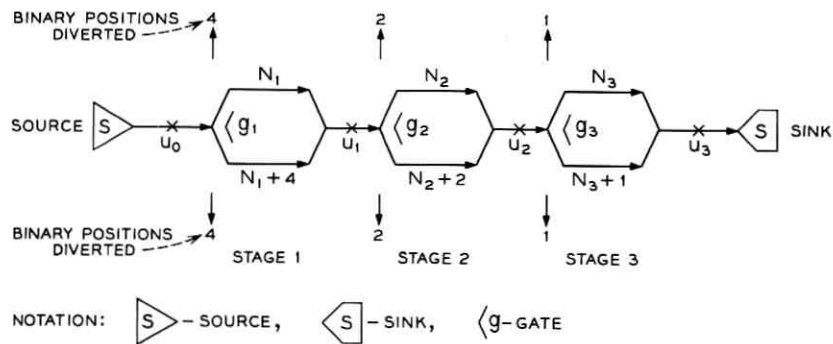


Fig. 1—A simple example of a 2:1 rate-reducing circuit for an 8-bit data block.

half, and so on, so that

$$\begin{aligned} u_1 &= X^{N_1}(a_0 + a_1X + a_2X^2 + a_3X^3) \\ &\quad + X^{N_1+4}(a_4X^4 + a_5X^5 + a_6X^6 + a_7X^7) \\ &= X^{N_1}\{X^0(a_0 + a_1X + a_2X^2 + a_3X^3) \\ &\quad + X^8(a_4 + a_5X + a_6X^2 + a_7X^3)\}. \end{aligned}$$

Similarly

$$\begin{aligned} u_2 &= X^{N_1}\{X^{N_2}\{X^0(a_0 + a_1X) + X^2(a_2X^2 + a_3X^3) \\ &\quad + X^0(a_4X^8 + a_5X^9) + X^2(a_6X^{10} + a_7X^{11})\} \\ &= X^{N_1+N_2}\{X^0(a_0 + a_1X) + X^4(a_2 + a_3X) \\ &\quad + X^8(a_4 + a_5X) + X^{12}(a_6 + a_7X)\} \end{aligned}$$

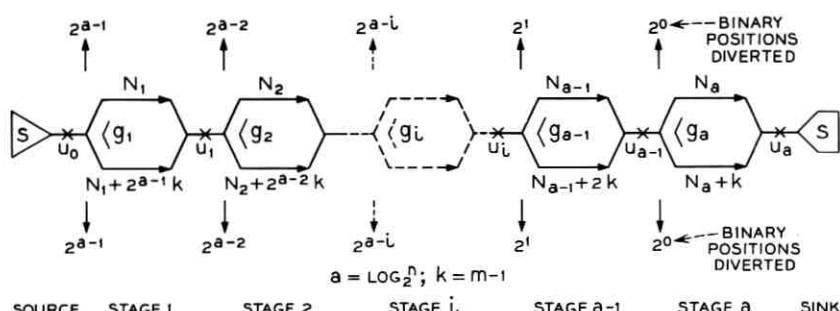


Fig. 1a—General rate-reducing circuit for an n -bit data block and rate ratio of $m:1$.

and

$$u_3 = X^{N_1 + N_2 + N_3} \cdot \{a_0 + a_1 X^2 + a_2 X^4 + a_3 X^6 + a_4 X^8 + a_5 X^{10} + a_6 X^{12} + a_7 X^{14}\}.$$

The rate of the polynomial u_3 corresponds to half the rate of the input polynomial u_0 . The output polynomial u_3 has a delay of $(N_1 + N_2 + N_3)$ clock cycles corresponding to the sum of periods in the upper section of the rate-change circuit. In charge-transfer and charge-coupled¹⁰ devices $(N_1 + N_2 + N_3)$ can be made zero. In magnetic domain circuits a certain minimum value for $(N_1 + N_2 + N_3)$ is foreseen.

In general it can be seen from Appendix A that the number of stages in a rate-reducing circuit is determined by the number of bit positions in the data block. The differences in periods between the upper half and the lower half of each of the stages are determined by the rate-change ratio. Table I contains the characteristics of a general circuit (Fig. 1a) for an n -bit data stream. The rate-change ratio is m . In Table I, a , denoting the number of stages, is an integer which satisfies the equation

$$2^a \geq n \quad \text{or} \quad a \geq \log_2^n, \quad (1)$$

and k is an integer obtained as

$$k = m - 1. \quad (2)$$

The delay in the circuit can be computed as $(N_1 + N_2 + N_3 \cdots N_a)$ clock cycles (see Fig. 1a) from the normal polynomial calculations presented in Appendix A.

2.2 Rate-Increasing Circuits

Rate-increasing circuits are derived as inversions of rate-reducing circuits. If the data flow is reversed in a rate-reduction circuit, a rate increase results. The process is investigated in the following example.

Example 2. A block of data 16 bits long, each bit arriving every four clock cycles, is to be condensed to a data block of 16 clock cycles thus

TABLE I—CHARACTERISTICS OF A GENERAL RATE-REDUCING CIRCUIT

Ratio of Input Rate to Output Rate	Number of Bit Positions Diverted by Gates					Difference in Periods in the Stages				
	g_1	g_2	\cdots	g_{a-1}	g_a	1	2	\vdots	$a-1$	a
m	2^{a-1}	2^{a-2}	\cdots	2^1	2^0	$2^{a-1}k$	$2^{a-2}k$	\vdots	$2k$	k

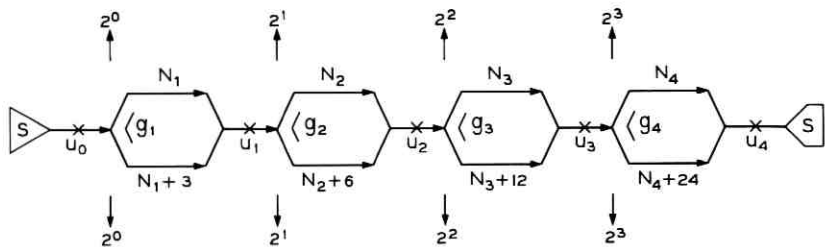


Fig. 2—A 1:4 rate-increasing circuit for a 16-bit data block.

enhancing the rate four times. Figure 2 represents a rate-increasing circuit for the 16-bit data block. The incoming polynomial is

$$u_0 = \sum_{i=0}^{i=15} a_i X^{4^i}, \quad (3)$$

and

$$\begin{aligned} u_1 &= X^{N_1} \{X^3(a_0 + a_1 X) + X^{11}(a_2 + a_3 X) \\ &\quad + X^{19}(a_4 + a_5 X) + \cdots X^{59}(a_{14} + a_{15} X)\} \\ u_2 &= X^{N_1+N_2} \{X^9(a_0 + a_1 X + a_2 X^2 + a_3 X^3) \\ &\quad + X^{25}(a_4 + a_5 X + a_6 X^2 + a_7 X^3) + \cdots \\ &\quad + X^{57}(a_{12} + a_{13} X + a_{14} X^2 + a_{15} X^3)\} \\ u_3 &= X^{N_1+N_2+N_3} \{X^{21}(a_0 + a_1 X + \cdots a_7 X^7) \\ &\quad + X^{53}(a_8 + a_9 X + a_{10} X^2 \cdots a_{15} X^7)\} \\ u_4 &= X^{N_1+N_2+N_3+N_4} \{X^{45}(a_0 + a_1 X + a_2 X^2 \cdots a_{15} X^{15})\}. \end{aligned} \quad (4)$$

The X^{45} term indicates the delay for the first bit which passes through the extra

$$(3 + 6 + 12 + 24) = (m - 1) \sum_0^{a-1} 2^i$$

periods corresponding to the four stages of the rate-change circuit. (See also Appendix B.) Table II shows a circuit characteristic for an n -bit data stream where the rate change is $1:m$. The polynomial calculations are presented in Appendix B. When it is desired to change the rate by a fraction $(m_1:m_2)$, a combination of rate-increasing and rate-decreasing circuits may be used in series. It is then necessary to choose the main clock frequency (f_c) which corresponds to the lowest multiple of m_1 , m_2 , and the incoming data frequency (f_{in}). The first section of

the combined circuit will enhance the frequency from f_{in} to f_c , and the second section will reduce from f_c to the desired frequency of $f_{in}m_2/m_1$. For instance if the input rate is 2400 baud and it is desired to obtain 3600 baud, then a clock rate of 7200 cycles per second will be necessary. The entire circuit for this example is shown in Fig. 3 for a data block 32 bits long.

2.3 Fractional Ratio Rate-Changing Circuits

It is sometimes possible to combine the two independent circuits into one circuit and accomplish fractional ratio rate changing. It becomes necessary however to perform a special function of delaying selected bit positions by a fractional cycle. An example of this circuit is presented for a 2:3 rate-change circuit.

Example 3. A block of data 8 bits long which arrives uniformly during 12 clock cycles is to be condensed to a data block of 8 clock cycles. The incoming data polynomial u_0 in Fig. 3a is

$$u_0 = a_0X^0 + a_1X^{3/2} + a_2X^3 + a_3X^{9/2} + a_4X^6 + a_5X^{15/2} \\ + a_6X^9 + a_7X^{21/2}. \quad (5)$$

The polynomial u_1 after delaying alternate bit positions by half a cycle is

$$u_1 = X^{1/2}\{(a_0 + a_1X) + X^3(a_2 + a_3X) \\ + X^6(a_4 + a_5X) + X^9(a_6 + a_7X)\}. \quad (6)$$

After the first stage of the circuit in which the gate g_1 diverts the two data positions for three clock cycles into the lower half of the stage and the two data positions for the next three cycles into the top half of the stage, the polynomial u_2 may be written as

$$u_2 = X^{1/2}\{X^{N_1+1}(a_0 + a_1X) + X^{N_1}(X^3(a_2 + a_3X)) \\ + X^{N_1+1}(X^6(a_4 + a_5X)) + X^{N_1}(X^9(a_6 + a_7X))\} \\ = X^{N_1+3/2}\{(a_0 + a_1X + a_2X^2 + a_3X^3) \\ + X^6(a_4 + a_5X + a_6X^2 + a_7X^3)\}, \quad (7)$$

TABLE II—CHARACTERISTICS OF A GENERAL RATE-INCREASING CIRCUIT

Ratio of Input Rate to Output Rate	Number of Bit Positions Diverted by Gates					Difference in Periods in the Stages				
	g_1	g_2	g_3	\dots	g^a	1	2	—	$a - 1$	a
1: m	2^0	2^1	2^2	\dots	2^{a-1}	k	$2k$	—	$2^{a-2}k$	$2^{a-1}k$

and similarly

$$\begin{aligned}
 u_3 &= X^{N_1+3/2} \{ X^{N_2+2} (a_0 + a_1 X + a_2 X^2 + a_3 X^3) \\
 &\quad + X^{N_2+6} (a_4 + a_5 X + a_6 X^2 + a_7 X^3) \} \\
 &= X^{N_1+N_2+7/2} \{ a_0 + a_1 X + a_2 X^2 + a_3 X^3 \\
 &\quad + a_4 X^4 + a_5 X^5 + a_6 X^6 + a_7 X^7 \}. \quad (8)
 \end{aligned}$$

The magnetic domain technology is especially suitable for creating an effect obtained by delaying the alternate bit position by half a clock cycle. The peculiarities of the T-bar circuits⁴ may be exploited in achieving this effect. Figure 3b shows two generators, G_1 and G_2 , excited by the same generating current in the coil. The "seed bubbles" (see Ref. 4) of both the generators rotate with the main driving field in synchronism. When the coil is excited every $3/2$ cycles, G_1 and G_2 generate bubbles corresponding to the alternate binary bits. The distance between the bubbles in section A or section B of the circuit will be three T-bar periods. At the junction of A and B, the effect of the split Tee will add a quarter period (i.e., $X^{1/4}$) for the bubbles in section B and subtract a quarter period (i.e., $X^{-1/4}$) for bubbles in section A, and the net effect will be to delay the alternate bubble position by half a cycle ($X^{1/2}$). The polynomial in section C of the circuit will already have a form identical to u_1 in (6).

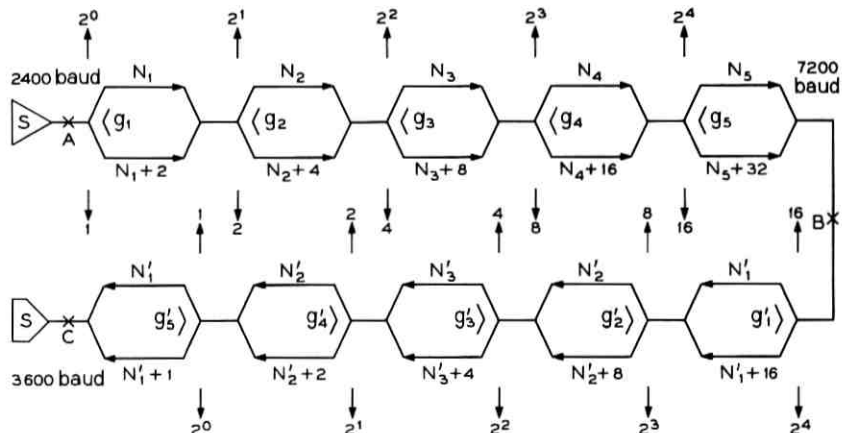


Fig. 3—An example of combination rate-reducing and rate-increasing circuits for a 2:3 rate-change circuit for a data block 32 bits long.

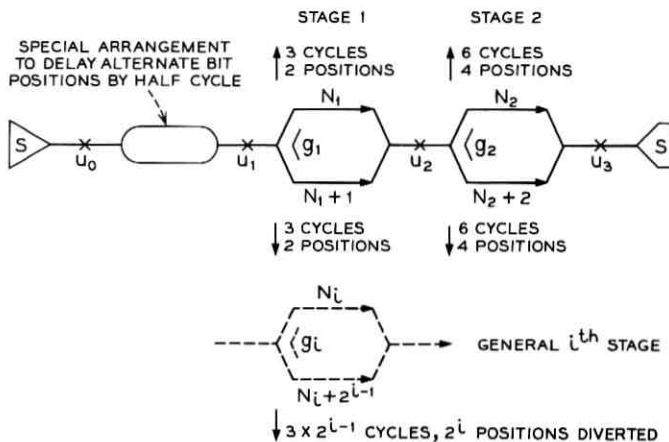


Fig. 3a—A circuit arrangement for a 2:3 ratio rate change for an 8-bit data stream. It is possible to add more stages for longer data streams.

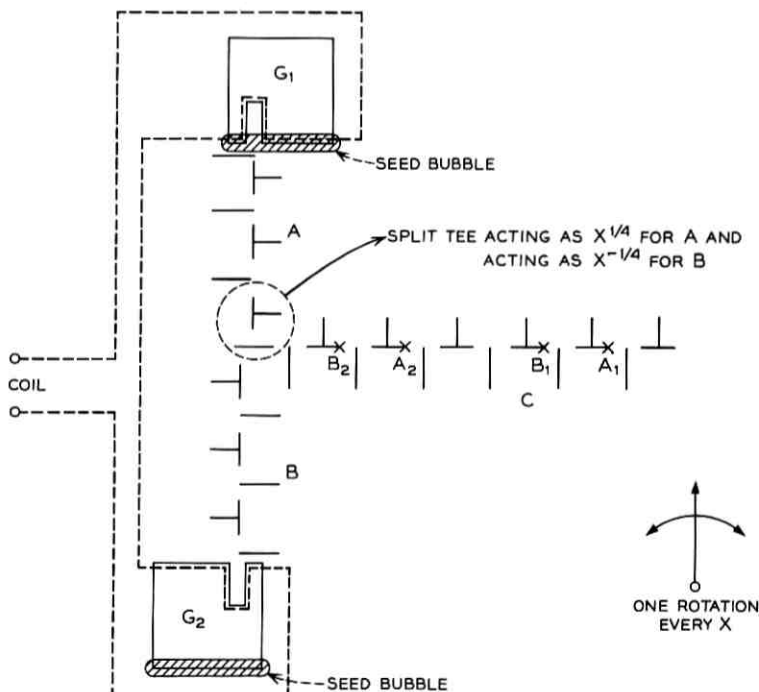


Fig. 3b—Two generators, G_1 and G_2 , excited by the same coil, generate alternate bit positions; i.e., G_1 generates a_0, a_2, a_4 —and G_2 generates a_1, a_3, a_5 .

III. COLLATING AND DISTRIBUTING CIRCUITS

To avoid undue complications in the polynomial algebra, one example of collating circuit and one example of distributing circuit are presented in this section. It is possible to generalize the polynomial calculations for any general incoming polynomial u_0 .

Example 4. Four 4-bit inputs from channels 1, 2, 3, and 4 are to be collated onto one channel (see Fig. 4). Let the incoming polynomials be

$$\begin{aligned} u_1 &= a_0 X^0 + a_1 X + a_2 X^2 + a_3 X^3, \\ u_2 &= a_4 X^4 + a_5 X^5 + a_6 X^6 + a_7 X^7, \\ u_3 &= a_8 X^8 + a_9 X^9 + a_{10} X^{10} + a_{11} X^{11}, \end{aligned}$$

and

$$u_4 = a_{12} X^{12} + a_{13} X^{13} + a_{14} X^{14} + a_{15} X^{15}, \quad (9)$$

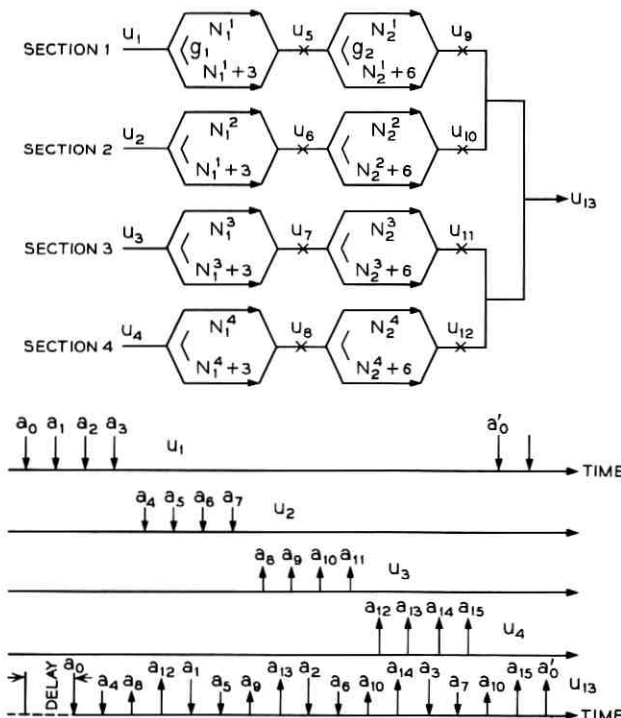


Fig. 4—A typical 4-input, 4-bit collating circuit.

then each of the sections 1, 2, 3, and 4 must accomplish a rate reduction of 1:4. Let

N_1^1 and N_2^1 be the number of periods in top sections of 1,
 N_1^2 and N_2^2 be the number of periods in top sections of 2,
 N_1^3 and N_2^3 be the number of periods in top sections of 3, and
 N_1^4 and N_2^4 be the number of periods in top sections of 4.

According to Section II, the lower halves of sections 1, 2, 3, and 4 are $(N_1^1 + 3)$, $(N_2^1 + 6)$, and so on. The polynomial u_5 between the two stages of the first section is

$$u_5 = X^{N_1^1} \{ (a_0 + a_2 X^2) + X^4 (a_1 + a_3 X^2) \}, \quad (10)$$

and so on. The polynomials u_9 , u_{10} , u_{11} , and u_{12} may be calculated as

$$\begin{aligned} u_9 &= X^{N_1^1 + N_2^1} \{ a_0 + a_1 X^4 + a_2 X^8 + a_3 X^{12} \} \\ u_{10} &= X^{N_1^2 + N_2^2 + 4} \{ a_4 + a_5 X^4 + a_6 X^8 + a_7 X^{12} \} \\ u_{11} &= X^{N_1^3 + N_2^3 + 8} \{ a_8 + a_9 X^4 + a_{10} X^8 + a_{11} X^{12} \} \\ u_{12} &= X^{N_1^4 + N_2^4 + 12} \{ a_{12} + a_{13} X^4 + a_{14} X^8 + a_{15} X^{12} \}. \end{aligned} \quad (11)$$

The periods in sections 1, 2, 3, and 4 are chosen such that

$$\begin{aligned} N_1^1 + N_2^1 &= N_1^4 + N_2^4 + 9 \\ N_1^2 + N_2^2 &= N_1^4 + N_2^4 + 10 \\ N_1^3 + N_2^3 &= N_1^4 + N_2^4 + 11. \end{aligned} \quad (12)$$

If the technology for implementation permits $N_1^4 + N_2^4 = 0$, then

$$\begin{aligned} u_9 &= X^9 (a_0 + a_1 X^4 + a_2 X^8 + a_3 X^{12}) \\ u_{10} &= X^{10} (a_4 + a_5 X^4 + a_6 X^8 + a_7 X^{12}) \\ u_{11} &= X^{11} (a_8 + a_9 X^4 + a_{10} X^8 + a_{11} X^{12}) \\ u_{12} &= X^{12} (a_{12} + a_{13} X^4 + a_{14} X^8 + a_{15} X^{12}). \end{aligned} \quad (13)$$

The output polynomial u_{13} can be written as:

$$\begin{aligned} u_{13} &= X^9 \{ a_0 + a_4 X + a_8 X^2 + a_{12} X^3 \\ &\quad + a_1 X^4 + a_5 X^5 + a_9 X^6 + a_{13} X^7 \\ &\quad + a_2 X^8 + a_6 X^9 + a_{10} X^{10} + a_{14} X^{11} \\ &\quad + a_3 X^{12} + a_7 X^{13} + a_{11} X^{14} + a_{15} X^{15} \}; \end{aligned} \quad (14)$$

and X^9 corresponds to the minimum delay in the circuit. It can be seen

that $N_1^4 + N_2^4$ need not equal zero. However, equations (12) must be satisfied. Under these conditions a fixed delay between the input and output results. Further, it is to be noted that equations (12) must be chosen with care to ascertain that the output polynomial u_{13} has each of its term $a_b X^b$ satisfying the equation

$$(\text{minimum delay}) + c \geq b \quad (15)$$

where b is the power of X in any one of the terms $a_b X^b$ in the input polynomial. Physically relation (15) implies that no term in the output appears before it has been received at the input terminal. In equations (12), as b varies between 0 and 15, the corresponding values of c in equation (14) satisfy relation (15).

Other generalizations of this circuit can be readily obtained by changing the number of stages (depending upon the number of bits in $u_1, u_2 \dots$ etc.) and the number of inputs to be collated. Reversing the direction of propagation yields a reversal of input and output polynomials leading to the distributing circuit.

Example 5. A typical distributing circuit is shown in Fig. 5. The input polynomial is

$$u_0 = a_0 X^0 + a_1 X + a_2 X^2 + \dots + a_{15} X^{15}. \quad (16)$$

The binding conditions on this circuit imply that

$$N_1^1 + N_2^1 + N_3^1 = N_1 + N_2 + N_3 + 7.* \quad (17)$$

The polynomial calculations lead to the output polynomial

$$\begin{aligned} u_7 = X^7 \{ & a_0 + a_2 X + a_4 X^2 + a_6 X^3 + a_8 X^4 + a_{10} X^5 + a_{12} X^6 + a_{14} X^7 \\ & + a_1 X^8 + a_3 X^9 + a_5 X^{10} + a_7 X^{11} + a_9 X^{12} + a_{11} X^{13} \\ & + a_{13} X^{14} + a_{15} X^{15} \}. \end{aligned} \quad (18)$$

It can be seen that if the direction of propagation is reversed, the circuit performs a collating function.

IV. REVERSING CIRCUITS

These circuits are capable of changing the order of data bits in an incoming polynomial. If the input polynomial is $u_0 = \sum_0^n a_i X^i$, then the output of the circuit can be written as $u_a = X^d \sum_0^n a_{n-i} X^i$. To

* Alternatively the lower half of the entire circuit may be designed to have seven additional periods if

$$N_1^1 + N_2^1 + N_3^1 = N_1 + N_2 + N_3.$$

Under these conditions the gating at g_2, g_3 , and g_4 is somewhat simplified.

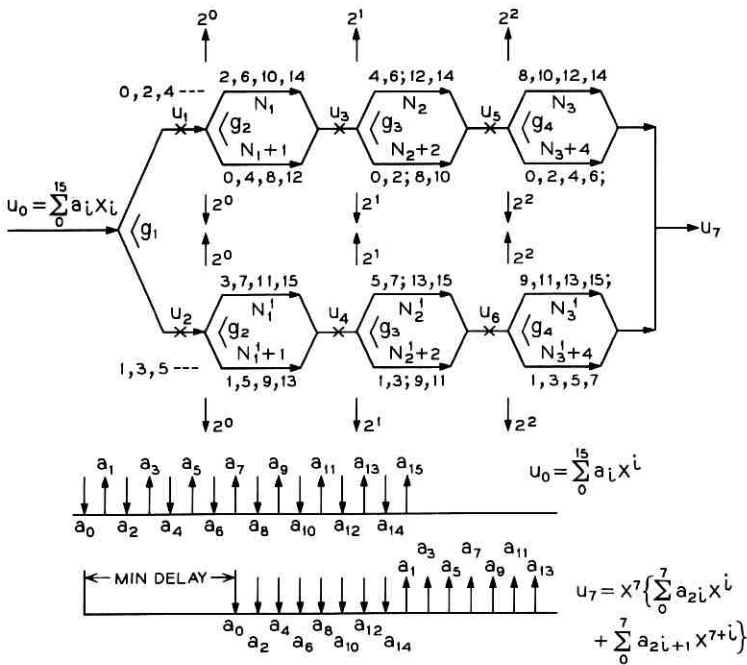


Fig. 5.—An example of a distributing circuit.

satisfy the physical constraint that no term of the output polynomial appears at the output before it is received at the input

$$d \geq n. \quad (19)$$

A specific example of reversing an 8-bit data block is presented in this section. The generality of this type of circuit is proved in Appendix C.

Example 6. It is desired to reverse an 8-bit data block represented as

$$\begin{aligned} u_0 = & a_0 X^0 + a_1 X + a_2 X^2 + a_3 X^3 \\ & + a_4 X^4 + a_5 X^5 + a_6 X^6 + a_7 X^7. \end{aligned} \quad (20)$$

After this data block is processed by the first stage in the circuit (Fig. 6)

$$\begin{aligned} u_1 = & X^{N_1} \{ X(a_1 + a_0 X) + X^3(a_3 + a_2 X) \\ & + X^5(a_5 + a_4 X) + X^7(a_7 + a_6 X) \}. \end{aligned}$$

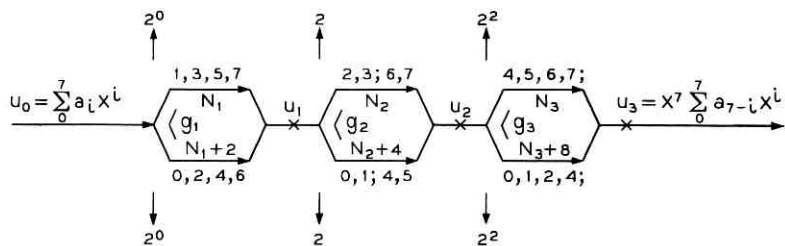


Fig. 6—An example of a reversing circuit (the general reversing circuits are presented in Figs. 8 and 9).

Further, u_2 and u_3 can be written as

$$\begin{aligned} u_2 &= X^{N_1+N_2} \{ X^3(a_3 + a_2X + a_1X^2 + a_0X^3) \\ &\quad + X^7(a_7 + a_6X + a_5X^2 + a_4X^3) \} \\ u_3 &= X^{N_1+N_2+N_3} \{ X^7(a_7 + a_6X + a_5X^2 + a_4X^3 \\ &\quad + a_3X^4 + a_2X^5 + a_1X^6 + a_0X^7) \}. \end{aligned}$$

If the technology for implementation permits $N_1 + N_2 + N_3 = 0$, then

$$\begin{aligned} u_3 &= X^7 \{ a_7 + a_6X + a_5X^2 + a_4X^3 \\ &\quad + a_3X^4 + a_2X^5 + a_1X^6 + a_0X^7 \}. \quad (21) \end{aligned}$$

V. CONCLUSIONS

The techniques presented in this paper indicate simple combinations of gating and propagation functions to yield any general rate-changing, collating, distributing, and reversing of data streams. All the necessary gates are generally driven by one binary clock diverting $2^0, 2, 2^2, \dots$ binary position (or "domains") from one branch into one or the other branches of three branch nodes distributed systematically in the circuit. Further, the circuit configurations are optimal within the constraints of the problem to the extent that a minimum number of gates are necessary to accomplish any one of the rate changing, distributing, collating, or reversing functions. For this general reason the control circuitry necessary for implementation of these configurations is reduced to a minimum.

Bubble technology, charge-transfer, or charge-coupled device technology each lends itself to the implementation of such circuits.

APPENDIX A

Generalized Calculation for a Rate-Decreasing Circuit

Let m be the ratio of the incoming data rate to the desired rate and n be the number of data bits in the data stream. For initial calculations let us choose n to be 2^a where a is an integer. The incoming polynomial can be represented as

$$u_0 = a_0 X^0 + a_1 X + a_2 X^2 + a_3 X^3 + \cdots + a_{n-1} X^{n-1}.$$

After the first stage of the general circuit shown in Fig. 1a,

$$\begin{aligned} u_1 = X^{N_1} [& X^0 \{ a_0 X^0 + a_1 X + \cdots + a_{n'-1} X^{n'-1} \} \\ & + X^{n^k} \{ a_{n'} X^{n'} + \cdots + a_{n-1} X^{n-1} \}] \end{aligned}$$

where $n' = 2^{a-1}$ and $k = m - 1$. Or u_1 can be written as

$$\begin{aligned} u_1 = X^{N_1} [& X^0 (a_0 X^0 + a_1 X + \cdots + a_{n'-1} X^{n'-1}) + X^{n'(k+1)} \\ & (a_{n'} X^0 + a_{n'+1} X + \cdots + a_{n-1} X^{n'-1})]. \end{aligned}$$

After the second stage of the general circuit

$$\begin{aligned} u_2 = X^{N_1+N_2} [& X_0 (a_0 X^0 + a_1 X + \cdots + a_{n'-1} X^{n'-1}) \\ & + X^{n''(k+1)} \{ a_{n''} X^0 + \cdots + a_{n'-1} X^{n'-1} \} \\ & + X^{n'(k+1)} (a_{n'} X^0 + \cdots + a_{n'+n'-1} X^{n'-1}) \\ & + X^{(n''+n')(k+1)} (a_{n'+n''} X^0 + \cdots + a_{n-1} X^{n'-1})] \end{aligned}$$

where $n'' = 2^{a-2}$.

After the $(a - 1)$ st stage

$$\begin{aligned} u_{a-1} = X^{N_1+N_2+\cdots+N_{a-1}} [& X_0 (a_0 X^0 + a_1 X) \\ & + X^{2m} (a_2 + a_3 X + \cdots + X^{(n-2)m} (a_{n-2} + a_{n-1} X)] \end{aligned}$$

and after the a th stage

$$\begin{aligned} u_a = X^{\sum_1^a N_i} [& a X^0 + a_1 X^m + a_2 X^{2m} \\ & + a_3 X^{3m} + \cdots + a_{n-2} X^{(n-2)m} + a_{n-1} X^{m(n-1)}] \end{aligned}$$

since $m = k + 1$ and $a = \log_2 n$. It can be seen that the rate for the u_a polynomial is $(1/m)$ th the rate of the incoming polynomial u_0 . When the number of data bits n does not equal a number 2^a , the general polynomial calculations become more complicated, but the difference

of elements in the two branches is still the same, and the gates can still be driven by binary counters. When the circuit is used on a repetitive basis, the gating sequence of the various gates $g_1, g_2 \dots g_a$ must be altered to adjust for the value of n . One such sequence of a gate operation for a 26-bit, 2:1 rate-decreasing circuit (shown in Fig. 7) is presented in Table III.

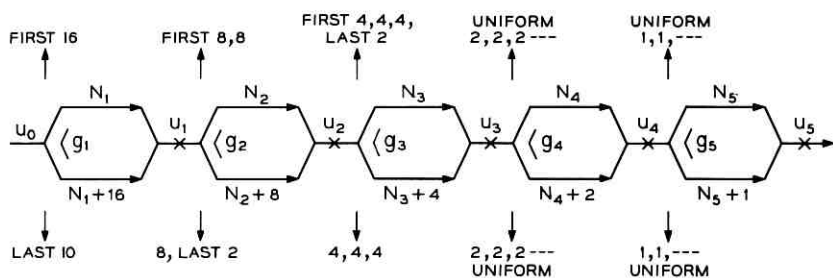


Fig. 7—A typical 2:1 rate-decreasing circuit for a 26-bit data block.

APPENDIX B

Generalized Calculation for a Rate-Increasing Circuit

Let m be the rate increase desired and n be the number of bits in the data stream. For initial calculation let us choose n as a 2^a where a is an integer. The incoming data polynomial may be written as

$$u_0 = a_0 X^0 + a_1 X^m + a_2 X^{2m} + a_3 X^{3m} \dots a_{n-1} X^{(n-1)m}.$$

After the first stage of the general rate-increasing circuit (Fig. 8),

$$u_1 = X^{N_1} \{ X^{m-1} (a_0 + a_1 X) + X^{3m-1} (a_2 + a_3 X) \dots a^{(n-1)m-1} (a_{n-2} + a_{n-1} X) \}.$$

TABLE III—SEQUENCE OF GATE OPERATION FOR A 26-BIT DATA STREAM

Number of Bit Positions Diverted by Gates					Difference in Periods in Different Stages				
g_1	g_2	g_3	g_4	g_5	1	2	3	4	5
16, 10;	; 8, 8, 8, 2;	; 4, 4, 4, 4, 4, 4, 2; ... 2, 2;	; 2, 2, 2, 2;	; 1, 1, 1, 1;	16	8	4	2	1

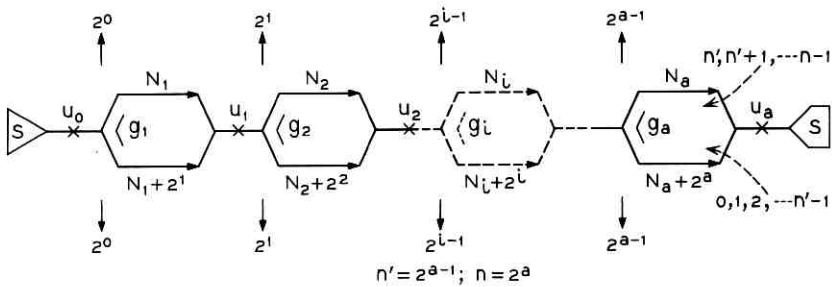


Fig. 8—A general reversing circuit for an n -bit data block.

After the second stage

$$\begin{aligned} u_2 &= X^{N_1+N_2} \{ X^{3m-3}(a_0 + a_1X + a_2X^2 + a_3X^3) + \dots \\ &\quad + X^{(n-1)m-3}(a_{n-4} + a_{n-3}X + a_{n-2}X^2 + a_{n-1}X^3) \} \\ &= X^{\sum_1^2 N_i} \{ X^{\sum_0^{2^i(m-1)} (a_0 + a_1X + a_2X^2 + a_3X^3)} + \dots \\ &\quad + X^{(n-1)m - \sum_0^{2^i(m-1)} (a_{n-4} + a_{n-3}X + a_{n-2}X^2 + a_{n-1}X^3)} \}. \end{aligned}$$

After the a th stage,

$$u_a = X^{\sum_1^a N_i} \{ X^{\sum_0^{a-1} (a_0 + a_1X + a_2X^2 + \dots + a_{n-1}X^{n-1})} \}.$$

When it is necessary to cover the case in which n is not 2^a but any given number, it is essential to choose an integer number, a , such that

$$2^a \geq n.$$

The functioning of the rate-increasing circuit can be proved in the following way:

The power of X associated with any term a_i in the converted polynomial u_a can be written as the delay d' which the circuit introduces and

$$d' = \sum_{i=0}^{j=a-1} 2^i(m-1) + i.$$

(See the expression for u_a in this appendix and assume $\sum_1^a N_i = 0$). The first term a_0 of the incoming polynomial u_0 must be delayed by $((n-1)m - (n-1))$ clock cycles to ascertain that a_0 is $(n-1)$ clock cycles ahead of a_{n-1} , the last term in u_0 . After the conversion to u_a the i th term will have to be i clock cycles behind a_0 in u_a . This leads to the total delay d'' for i th term as

$$d'' = ((n-1)m - (n-1)) + i \text{ clock cycles}$$

$$\begin{aligned}
 &= (n - 1)(m - 1) + i \\
 &= (2^a - 1)(m - 1) + i \\
 &= \sum_{i=0}^{i=a-1} 2^i(m - 1) + i.
 \end{aligned}$$

This corresponds to the delay d' in the polynomial u_a .

APPENDIX C

Generalized Calculation for a Reversing Circuit

Consider a block of binary data with n -bit positions and a reversing circuit shown in Fig. 8. To simplify the nature of equations let us assume that $n = 2^a$ where a is an integer. This constraint can, however, be easily relaxed in practice as shown in Appendix A.

$$u_0 = a_0 X^0 + a_1 X^1 + a_2 X^2 + \cdots + a_{n-1} X^{n-1}$$

$$u_1 = X^{N_1} \{ (a_0 X^2 + a_1 X) + (a_2 X^4 + a_3 X^3) + \cdots + a_{n-2} X^{n+1} + a_{n-1} X^{n-1} \}$$

$$u_1 = X^{N_1} \{ X(a_1 + a_0 X) + X^3(a_3 + a_2 X) + \cdots + X^{n-1}(a_{n-1} + a_{n-2} X) \}.$$

Similarly

$$\begin{aligned}
 u_{a-1} = X^{\sum_{i=1}^{a-1} N_i} &\{ X^{n'-1}(a_{n'-1} + a_{n'-2} X + \cdots + a_0 X^{n'-1}) \\
 &+ X^{n'-1}(a_{n-1} + a_{n-2} X + \cdots + a_{n-n'} X^{n'-1}) \}
 \end{aligned}$$

where $n' = 2^{a-1}$; $n' = n/2$ and finally

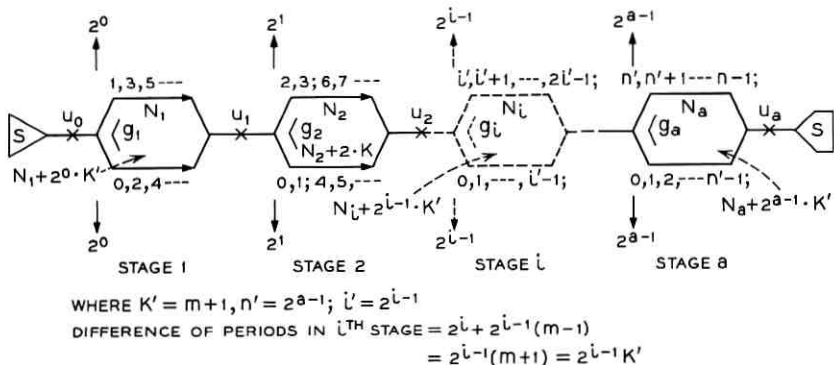
$$u_a = X^{\sum_{i=1}^a N_i} \{ X^{n-1}(a_{n-1} + a_{n-2} X + a_{n-3} X^2 + \cdots + a_0 X^{n-1}) \}.$$

The order of the polynomial u_a is reversed. The minimum delay that is essential in the circuit is $(n - 1)$ cycles to satisfy the physical constraint that a_{n-1} appear at the output only after it is received by the circuit. The delay of $\sum_i^a N_i$ depends on the nature of the basic vehicle for implementation. With magnetic domain circuits a certain minimum is deemed necessary. With charge-transfer or charge-coupled devices the value can be made zero.

When a rate change and reversing are both desired, the number of periods in the lower section of any stage i should become

$$(N_i + a^i + a^{i-1} \cdot k)$$

where $k = m - 1$ and m is the rate change desired. The general circuit for a combination reversing-rate change circuit is shown in Fig. 9. The

Fig. 9—A combined reversing and $1:m$ rate-change circuit.

polynomial calculations are very similar to those presented in Appendixes A and B.

REFERENCES

- Peterson, W. W., *Error-Correcting Codes*, Cambridge, Massachusetts: MIT Press, 1961.
- Berlekamp, E. R., *Algebraic Coding Theory*, New York: McGraw-Hill Book Company, 1968.
- Lucky, R. W., Salz, J., and Weldon, E. J., *Principles of Data Communication*, New York: McGraw-Hill Book Company, 1968.
- Bobbeck, A. H., Fischer, R. F., and Perneski, A. J., "A New Approach to Memory and Logic Cylindrical Domain Devices," Proc. FJCC, 1969, pp. 489-498.
- Bonygard, P. I., Danylchuk, I., Kish, D. E., and Smith, J. L., "Application of Bubble Devices," IEEE Trans. Magnetics, MAG-6, No. 3 (September 1970), pp. 447-451.
- Waaben, S., "Charge-Transfer Electronics—Tandem Matrix Semiconductor Memory Selection," 1971 IEEE, Int. Solid-State Circuits Conf., Digest of Technical Papers, XIV, February 1971, pp. 84-85.
- Berglund, C. N., and Boll, H. J., "Performance Limitation of the IGFET Bucket Brigade Shift Register," Int. Electron Device Meeting, Washington, D.C., October 1970.
- Boyle, W. S., and Smith, G. E., "Charge Coupled Devices," B.S.T.J., 49, No. 4 (April 1970), pp. 587-593.
- Waaben, S., private communication.
- Berglund, C. N., private communication.

The Overflow Distribution for Constant Holding Time

By P. J. BURKE

(Manuscript received July 20, 1971)

An infinite trunk group split into a finite first-choice group and an overflow group is studied. The equilibrium distribution, at an arbitrary instant, of the number of busy trunks in the overflow is obtained for the case of Poisson input and constant holding time. Some numerical comparisons of variances and distributions for exponential and constant holding time are given. The variance of the overflow was found to be always the greater for constant holding time, and in the case of one trunk in the first-choice group this inequality is proven to be true analytically. In some cases studied, the variances differ markedly—by as much as 50 percent. Implications of these results for the traffic engineering of overflow groups with nonexponential holding time are discussed.

I. INTRODUCTION

We consider an infinite trunk group which is split into a finite first-choice group and an overflow group. Calls that find all trunks busy in the first-choice group are placed on the overflow group. It is assumed that the input is Poisson and that the system is in equilibrium. Under these conditions the distributions of the number of calls in the total group and of that in the first-choice group are known and, for a given load, are independent of the holding-time distribution. For the case of exponential holding time the distribution of the number of calls in existence at an arbitrary instant in the overflow group is also known, having been found by Kosten in 1937.¹ The latter distribution, in particular its second moment, is basic to the method of engineering overflow groups, often called the "equivalent random" method, pioneered by Wilkinson and Bretschneider. (See Ref. 2 for a description of this method.) If this distribution were also independent of the holding-time distribution, then the equivalent random method could be applied

with uniform validity regardless of the underlying holding-time distribution.

It is indeed tempting to speculate that the overflow distribution has this independence property, since the number of busy trunks in the overflow group is the difference between two random variables: the number of busy trunks in the total group and that in the first-choice group, each of which is independent of the holding-time distribution.

Unfortunately the simple example of constant holding time studied here proves that the overflow distribution does in fact depend on the holding-time distribution. This result is reminiscent of that of Tånge and Wikell,³ who found that the blocking probability in a grading depends on the form of the holding-time distribution. In the case of the grading the differences between the blocking probabilities for constant and exponential holding times are too small to be of practical significance. In contrast, the differences between the respective overflow distributions, as measured by the relative differences between variances, can be quite large, running close to 50 percent in some cases.

Unpublished work by N. P. Archer indicates, nevertheless, that when the equivalent random method is based on constant holding time, the results of engineering a first-stage overflow group are essentially the same as when the method is based on exponential holding time. That is, for a given configuration of first-choice groups and Poisson offered loads the equivalent random method, consistently applied, results in the same size overflow group for a given loss probability whether the holding time is taken to be constant or exponential. Thus the computing aids—that is, algorithms, tables, and graphs used in the application of the equivalent random method—which are based on exponential-holding-time theory can be used without change, as a practical matter, for the purpose of engineering a single overflow group even when the holding time is constant. A word of caution, however, is in order. It should be obvious that the substitution of an exponential for a constant holding-time distribution must be done throughout the procedure, in the calculation both of the overflow variances and of the size of the equivalent group. If exponential theory is used for the overflow variances and constant theory for dimensioning the equivalent group, there will be a bias toward too few trunks in the overflow group and the service may be significantly worse than that aimed for. If the opposite error is made and the overflow variances are based on a constant holding-time assumption while the exponential charts are used for estimating the size of the equivalent group, the overflow group will be over-engineered. The latter erroneous result will occur also if constant-

holding-time overflow variances are estimated by actual measurements of overflow traffic rather than, as is done presently, from theoretical considerations only, and if consideration is not given to the effect of the holding-time distribution on the overflow variance.

It is fortunate that the constant-holding-time case is tractable, since constant holding-time represents an extreme point in the set of holding-time distributions when these are ordered according to their coefficients of variation. It is reasonable to conjecture, for example, that an overflow variance for any holding-time distribution whose coefficient of variation is less than unity will differ less from that for exponential holding time than does the overflow variance for constant holding time. Thus, if the equivalent random method is applicable in the case of constant holding time, it is *a fortiori* so when the coefficient of variation of the holding time distribution is between zero and one. Furthermore, the fact that a constant-holding-time equivalent random procedure yields results which are almost indistinguishable from those for exponential holding time lends support to the conjecture that in the application of the procedure the form of the holding-time distribution may be ignored even when its coefficient of variation is greater than unity.

Although the chief purpose of this study was to gain information about the extent of the dependence of the parameters of overflow distributions on holding-time distributions, the original motivation was provided otherwise. In fact the present investigation was sparked by the observation that the formula for the decomposition of the variance of overflow traffic resulting from a superposition of independent Poisson input streams offered to the same first-choice group, derived rigorously by A. Descloux for exponential holding time in unpublished work, is valid for any holding-time distribution. This formula is

$$\text{Var}(y_i) = p_i^2 \text{Var}(y) + p_i(1 - p_i)\text{E}(y), \quad (1)$$

where

y_i = the number of calls in the overflow belonging to the i th stream,
 p_i = the proportion of the offered load in the i th stream,

and

$$y = \sum_i y_i.$$

The question immediately arises whether the observation that (1) is independent of the holding-time distribution has any application, since it involves $\text{Var}(y)$, which was known heretofore only for the exponential case. To settle this question, a characterization of the overflow traffic

in nonexponential cases is required. As it turns out, in the constant-holding-time case not only the variance but also the distribution itself may be found exactly.

Kosten's formula for the probability of y trunks busy in the overflow for an offered load of a erlangs offered to c trunks may be written, after some simplification, as

$$w_{y}^{(E)} = \frac{a^y}{y!} \sum_{i=0}^{\infty} \frac{(-a)^i}{j!} \frac{1}{\sum_{i=0}^c \binom{y+j+i-1}{i} \frac{(c)_i}{a^i}} \quad (2)$$

where $(c)_0 = 1$ and $(c)_i = c(c-1) \cdots (c-i+1)$.

The corresponding formulas for the constant case are

$$w_y = \frac{e^{-a}}{\sum_{i=0}^c \frac{a^i}{i!}} \frac{a^{c+y}}{(c+y+1)!} \sum_{h=0}^c \frac{a^h}{h!} (c+y-h+1)(c-h+1), \quad y > 0, \quad (3)$$

and

$$w_0 = \frac{e^{-a}}{\sum_{i=0}^c \frac{a^i}{i!}} \left\{ \sum_{h=0}^c \frac{(2a)^h}{h!} + \sum_{h=c+1}^{2c} \frac{a^h}{h!} \cdot \left[\sum_{i=h-c}^c \binom{h}{i} - \binom{h}{c+1} (2c-h+1) \right] \right\}. \quad (4)$$

(A brief outline of the derivation of (3) and (4) is given in Section II. Algebraic details of the derivations of these and subsequent formulas are given in the Appendix.)

It might be remarked that the state probability formulas in the constant case are the simpler for computational purposes, since they involve only finite sums of positive terms.

With respect to complexity, the formulas for the moments are another story. The means, of course, are equal and are given by

$$M_1 = aE_{1,c}(a) = \frac{a^{c+1}}{c!} \left[\sum_{i=0}^c \frac{a^i}{i!} \right]^{-1}. \quad (5)$$

Although the variance is the second-order moment of direct interest, the second factorial moment is equivalent for our purpose and will be given here since it is simpler. For exponential service time this moment may be written

$$F_2^{(E)} = a^2 \left[(c+1-a) \sum_{i=1}^c \frac{(c)_i}{a^i} + c+1 \right]^{-1}. \quad (6)$$

(From this expression it is immediate that $F_2^{(E)} = c + 1$ for $a = c + 1$, a fact that was found useful in checking computer programs.) For constant holding time the second factorial moment is

$$F_2 = \frac{1}{\sum_{i=0}^c \frac{(c)_i}{a^i}} \left\{ a^2 - ac - \sum_{j=0}^c \frac{(c)_j}{a^j} [j(j+3) - 2c] + e^{-a} \sum_{k=0}^{2c-2} \frac{a^{k-c} c!}{k!} \cdot \sum_{h=\lfloor k-c \rfloor +}^{\min\{k,c\}} \binom{k}{h} (c+1-h)(c-2k+3h) \right\}. \quad (7)$$

In all the numerical cases studied, it turns out that $F_2 > F_2^{(E)}$. In the case $c = 1$, the formulas are simple enough to allow an easy analytic proof that this relationship is true uniformly in a . The fact that $F_2 > F_2^{(E)}$ implies that the correlation between the number of busy trunks in the overflow group and that in the first-choice group is lower in the constant than in the exponential case. This fact is perhaps less surprising to the intuition than is the result that the overflow is more variable for constant than for exponential holding time.

II. OUTLINE OF THE DERIVATION

Owing to the constancy of the holding time, taken here and below to be of unit length, the calls present in the overflow group at an arbitrary instant, t_0 , are precisely those that overflowed during the preceding time interval of length unity. The number of calls present in the first-choice group at the instant $t_0 - 1$ is known to have the truncated Poisson distribution (also known as Erlang's first distribution). We condition first on the number of calls present in the first-choice group at $t_0 - 1$. Next, we condition on the number of arrivals during the interval $[t_0 - 1, t_0]$, which, of course, has the ordinary Poisson distribution. We now observe that the hang-up or departure instants together with the arrival instants, as conditioned, are mutually-independently, uniformly distributed on the unit interval. This observation enables us to complete the calculation by an application of a ballot theorem.

Let

c = number of trunks in the first-choice group

a = offered load in erlangs

π_i = probability of i calls on the first-choice group at an arbitrary instant

p_j = probability of j arrivals during a unit of time; $p_j = e^{-a} a^j / j!$

w_{xy} = probability of x calls on the first-choice group and y calls on the overflow group at an arbitrary instant

$w_{\cdot y}$ = probability of y calls on the overflow group at an arbitrary instant

$f(y; i, j)$ = probability of y overflows during a unit interval at whose initial instant there are i calls on the first-choice group and during which j new calls arrive.

Then we may write

$$w_{x0} = p_x \sum_{i=0}^c \pi_i f(0; i, x) \quad (8)$$

and

$$w_{xy} = p_{x+y} \sum_{i=c-x}^c \pi_i f(y; i, x + y), \quad y > 0; \quad (9)$$

and, with a reversal of the order of summation, we have

$$w_{\cdot 0} = \sum_{i=0}^c \pi_i \sum_{j=0}^c p_j f(0; i, j), \quad (10)$$

and

$$w_{\cdot y} = \sum_{i=0}^c \pi_i \sum_{j=c-i+y}^{c+y} p_j f(y; i, j), \quad y > 0. \quad (11)$$

The distribution of the number of calls on the first-choice group at an arbitrary instant is independent of the holding-time distribution and is given by

$$\pi_i = (a^i / i!) \left[\sum_{h=0}^c (a^h / h!) \right]^{-1}, \quad i = 0, \dots, c, \quad (12)$$

while the remaining service times of these i calls are independently and identically distributed according to the equilibrium excess distribution; that is, the remaining service time of each call has the distribution function

$$F(t) = \int_0^t (1 - H(u)) du \quad (13)$$

where $H(u)$ is the service-time distribution function (with unit mean). The last two results have been published by several authors; an elementary proof has been given by L. Takács,⁴ whose paper includes a bibliography on the problem.

The implication of (13) in the present case is that the remaining service times of the calls initially on the first-choice trunks are inde-

pendently uniformly distributed on the unit interval. Furthermore, it is well-known that when the number of Poisson arrivals during a fixed time interval is given, the individual arrival instants are independently uniformly distributed over this interval. Hence any specific sequence of the i departures and j arrivals during the interval $[t_0 - 1, t_0)$ has the same probability, namely $1/{i+j \choose i}$.

The quantity $f(0; i, j)$ is the probability that a sequence of arrivals and departures has the property that at all times the excess of the accumulated arrivals over the accumulated departures is strictly less than one more than the initial number of idle trunks, i.e., less than $c - i + 1$. Thus the problem of calculating $f(0; i, j)$ can be recognized as a "ballot" problem. Successive arrivals and departures are called "events," and we denote by α_r and β_r , respectively, the accumulated number of arrivals and departures at the r th event. With this notation,

$$f(0; i, j) = \Pr \{ \alpha_r < \beta_r + c - i + 1, \quad r = 1, \dots, i + j \}. \quad (14)$$

The required probability is given as a solution to exercise 3 of Chapter 1 of Ref. 5. We have, with the usual conventions concerning binomial coefficients,

$$f(0; i, j) = 1 - \frac{{j \choose c-i+1}}{{c+1 \choose c-i+1}}, \quad j \leq c, \\ = 0, \quad j > c. \quad (15)$$

Similarly,

$$f(y; i, j) = \Pr \{ \alpha_r < \beta_r + c - i + y + 1, r = 1, \dots, i + j \} \\ - \Pr \{ \alpha_r < \beta_r + c - i + y, r = 1, \dots, i + j \}, \quad y > 0, \quad (16)$$

and thus for $j \leq c + y$,

$$f(y; i, j) = \frac{{j \choose c-i+y}}{{c+y \choose c-i+y}} - \frac{{j \choose c-i+y+1}}{{c+y+1 \choose c-i+y+1}}. \quad (17)$$

We are particularly interested in the marginal overflow state probabilities, namely the quantities denoted $w_{..0}$ and $w_{..y}$. These may be put into a form suitable for numerical calculation by substituting the values of the expressions π_i , p_i , and $f(y; i, j)$ into (10) and (11). The final results,

obtained after a small amount of manipulation, are shown as (3) and (4). (See Appendix.)

III. MOMENTS

The results (3) and (4) are considerably simpler than their analogs for exponential holding time, shown in (2), which was obtained from equation (38) of Ref. 1. It does not follow, however, that the moments of the distribution defined by (3) and (4) are simpler in form than those for exponential holding time. In fact, although in principle each of the moments can be written as a finite sum, it seems to be a rather tedious task to obtain closed-form expressions for them. Since only the first two moments of overflow distributions are presently of practical interest, we shall confine our attention to the two lowest-order moments for the case of constant holding time.

The mean of the distribution $\{w_{.y}; y = 0, 1, \dots\}$ is obviously the same as that for exponential holding time. Nevertheless, a direct calculation of the mean from the expression for the state probabilities is useful as a check on the accuracy of the algebraic manipulation indicated previously. That is, as a check, the equation

$$\sum_{y=1}^{\infty} y w_{.y} = \frac{a^{c+1}}{c!} \left[\sum_{i=0}^c \frac{a^i}{i!} \right]^{-1} \quad (18)$$

should be shown to be an identity, as indeed it is. (See Appendix.)

The calculation of the second factorial moment was done by direct summation. The details are given in the Appendix.

It was remarked above that a simple proof that $F_2 > F_2^{(E)}$ can be given for $c = 1$. To do this, we observe that by substituting $c = 1$ into (7) we obtain

$$F_2 = \frac{1}{1+a} \{a^3 - a^2 + 2a - 2 + 2e^{-a}\}. \quad (19)$$

By substituting $c = 1$ into (6), we obtain

$$F_2^{(E)} = \frac{a^3}{2+a}. \quad (20)$$

Thus we must prove

$$\frac{a^3 - a^2 + 2a - 2 + 2e^{-a}}{1+a} > \frac{a^3}{2+a}. \quad (21)$$

After cross-multiplying and simplifying, there results, equivalently,

$$(2 + a)e^{-a} > 2 - a \quad (22)$$

or

$$e^{-a} > \frac{1 - \frac{a}{2}}{1 + \frac{a}{2}}, \quad (23)$$

which is true for a positive (take logarithms).

IV. NUMERICAL RESULTS

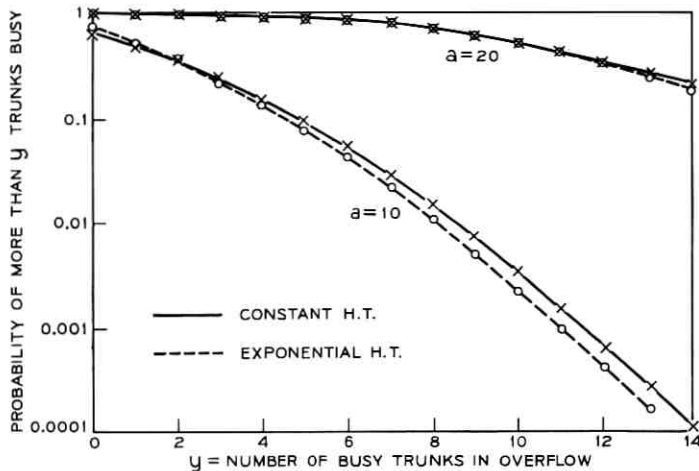
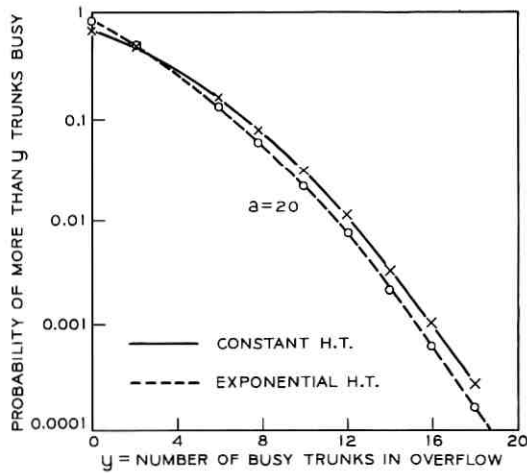
A comparison of the overflow variances from first-choice trunk group sizes ranging from 1 to 100 is shown in Table I. These numbers were calculated on the basis of (6) and (7). The starred entries, for low offered loads and high values of c , were calculated separately because of a loss of accuracy in (7) at these values. It should be noted that (3), having no subtractions, does not suffer from loss of accuracy from this cause and hence was used to obtain the variance by direct numerical summation.

The distributions of tails for several trunk-group sizes and offered loads are shown in Figs. 1 and 2. It should be observed that even when the variances differ noticeably, as for example for $c = a$, where in both cases shown the variance difference is greater than 20 percent, the tails distributions are very close at all probabilities of practical interest.

Since the (almost indistinguishable) curves for $c = 10$, $a = 20$ are truncated at a high probability level, it may be well to point out that they differ negligibly even at low values. Thus the probability of exceeding 25 busy trunks in the overflow is 0.0096 for exponential and 0.0109 for constant holding time. A negligible difference in the state probability distributions, as seen in the case of $c = 10$, $a = 20$, was also seen in other cases for which $a = 2c$ and $c > 10$. For $c = 20$ and $a = 40$, however, a comparison could not be made because of a complete loss of accuracy in (2). Since the relative difference in the variances is even less in this case than for c small, it is reasonable to conjecture that (3) provides an excellent approximation to (2) in this case. This suggests that (3) is useful as an approximation to (2) for $a \gg c$, precisely in the range where (2) is unsatisfactory for numerical computations.

TABLE I—COMPARISON OF VARIANCES OF OVERFLOW FOR CONSTANT HOLDING TIME AND EXPONENTIAL HOLDING TIME

e	a	Mean M1	Exp Var VE	Const Var VD	VE/M1	VD/M1	(VD/VE) — 1
1	0.40	0.1143	0.1279	0.1331	1.1190	1.1647	0.0408
	0.60	0.2250	0.2575	0.2704	1.1442	1.2017	0.0503
	0.80	0.3556	0.4120	0.4351	1.1587	1.2236	0.0560
	1.00	0.5000	0.5833	0.6179	1.1667	1.2358	0.0592
	1.20	0.6545	0.7661	0.8127	1.1705	1.2416	0.0607
	1.40	0.8167	0.9568	1.0152	1.1716	1.2431	0.0611
	1.60	0.9846	1.1529	1.2228	1.1709	1.2419	0.0606
	1.80	1.1571	1.3529	1.4334	1.1692	1.2387	0.0595
	2.00	1.3333	1.5556	1.6458	1.1667	1.2343	0.0580
	2	0.80	0.1208	0.1478	0.1595	1.2240	1.3211
2	1.20	0.2959	0.3778	0.4132	1.2767	1.3966	0.0939
	1.60	0.5278	0.6873	0.7562	1.3021	1.4327	0.1003
	2.00	0.8000	1.0489	1.1555	1.3111	1.4443	0.1016
	2.40	1.1006	1.4425	1.5864	1.3106	1.4413	0.0997
	2.80	1.4218	1.8551	2.0330	1.3048	1.4299	0.0959
	3.20	1.7579	2.2784	2.4858	1.2961	1.4140	0.0910
	3.60	2.1054	2.7075	2.9392	1.2860	1.3960	0.0856
	4.00	2.4615	3.1392	3.3902	1.2753	1.3773	0.0800
	5	2.00	0.0734	0.1040	0.1198	1.4176	1.6319
5	3.00	0.3302	0.5186	0.6078	1.5707	1.8409	0.1720
	4.00	0.7963	1.3013	1.5284	1.6342	1.9194	0.1745
	5.00	1.4243	2.3332	2.7210	1.6381	1.9104	0.1662
	6.00	2.1624	3.4864	4.0166	1.6123	1.8575	0.1521
	7.00	2.9730	4.6819	5.3164	1.5748	1.7882	0.1355
	8.00	3.8321	5.8806	6.5798	1.5346	1.7170	0.1189
	9.00	4.7242	7.0661	7.7970	1.4957	1.6504	0.1034
	10.00	5.6395	8.2327	8.9712	1.4598	1.5908	0.0897
	10	4.00	0.0212	0.0329	0.0399	1.5485	1.8816
10	6.00	0.2589	0.4872	0.6044	1.8821	2.3349	0.2406
	8.00	0.9733	1.9857	2.4530	2.0402	2.5203	0.2354
	10.00	2.1458	4.3624	5.2907	2.0330	2.4656	0.2128
	12.00	3.6231	7.0710	8.3540	1.9516	2.3058	0.1815
	14.00	5.2820	9.7876	11.2465	1.8530	2.1292	0.1491
	16.00	7.0490	12.4046	13.8965	1.7598	1.9714	0.1203
	18.00	8.8826	14.9080	16.3490	1.6783	1.8407	0.0967
	20.00	10.7592	17.3130	18.6671	1.6091	1.7350	0.0782
	20	8.00	0.0013	0.0021	0.0027	1.6141	2.1127
20	12.00	0.1175	0.2584	0.3401	2.1986	2.8935	0.3161
	16.00	1.0306	2.7028	3.5055	2.6226	3.4015	0.2970
	20.00	3.1778	8.2920	10.3872	2.6093	3.2686	0.2527
	24.00	6.1700	14.8143	17.7126	2.4010	2.8708	0.1956
	28.00	9.5977	20.9311	23.9282	2.1808	2.4931	0.1432
	32.00	13.2464	26.4675	29.2087	1.9981	2.2050	0.1036
	36.00	17.0146	31.5567	33.9567	1.8547	1.9957	0.0761
	40.00	20.8522	36.3397	38.4213	1.7427	1.8426	0.0573
	50	20.00	0.0000	0.0000	0.0000*	1.6452	2.2408*
50	30.00	0.0066	0.0161	0.0230	2.4215	3.4727	0.4341
	40.00	0.7476	2.7343	3.7810	3.6573	5.0574	0.3828
	50.00	5.2393	19.7746	25.5769	3.7743	4.8817	0.2934
	60.00	12.9671	40.9397	48.5749	3.1572	3.7460	0.1865
	70.00	21.9661	57.8384	64.1752	2.6331	2.9216	0.1096
	80.00	31.4446	71.6558	76.4680	2.2788	2.4318	0.0672
	90.00	41.1339	83.8760	87.5797	2.0391	2.1291	0.0442
	100.00	50.9303	95.2624	98.2036	1.8704	1.9282	0.0309
	100	60.00	0.0000	0.0001	0.0001*	2.4634	3.6885*
100	80.00	0.3194	1.4158	2.0681	4.4331	6.4758	0.4608
	100.00	7.5700	38.5958	50.7901	5.0985	6.7094	0.3180
	120.00	23.5523	89.6717	103.9455	3.8073	4.4134	0.1592
	140.00	42.1741	123.6750	133.0991	2.9325	3.1559	0.0762
	160.00	61.5406	149.8224	156.0855	2.4345	2.5363	0.0418

Fig. 1—Tails distributions, $c = 10$.Fig. 2—Tails distributions, $c = 20$.

APPENDIX

A.1 Formulas for the Overflow State Probabilities

The probability of zero calls in the overflow group is given by (10), which, after substitution of the values of π_i and p_i , becomes

$$w_{.0} = \sum_{i=0}^c \frac{a^i / i!}{\sum_{h=0}^c a^h / h!} \sum_{j=0}^c e^{-a} \frac{a^j}{j!} f(0; i, j). \quad (24)$$

For brevity, let

$$f(a) = e^{-a} \left[\sum_{h=0}^c \frac{a^h}{h!} \right]^{-1}. \quad (25)$$

Then, replacing $f(0; i, j)$ by its value as given in (15), we may write

$$\begin{aligned} w_{.0} &= f(a) \sum_{i,j=0}^c \frac{a^{i+j}}{i! j!} \left[1 - \frac{\binom{j}{c-i+1}}{\binom{c+1}{c-i+1}} \right] \\ &= f(a) \sum_{i,j=0}^c \frac{a^{i+j}}{i! j!} \left[1 - \frac{i! j!}{(i+j-(c+1))! (c+1)!} \right]. \end{aligned} \quad (26)$$

Setting $i + j = h$ and multiplying the numerator and denominator of each term by $h!$,

$$\begin{aligned} w_{.0} &= f(a) \left[\sum_{h=0}^c \frac{a^h}{h!} \sum_{i=0}^h \frac{h!}{i! (h-i)!} \right. \\ &\quad \left. + \sum_{h=c+1}^{2c} \frac{a^h}{h!} \sum_{i=h-c}^c \left(\frac{h!}{i! (h-i)!} - \frac{h!}{(h-(c+1))! (c+1)!} \right) \right] \end{aligned} \quad (27)$$

$$w_{.0} = f(a) \sum_{h=0}^c \frac{a^h}{h!} \cdot 2^h + \sum_{h=c+1}^{2c} \frac{a^h}{h!} \left[\sum_{i=h-c}^c \binom{h}{i} - (2c-h+1) \binom{h}{c+1} \right]. \quad (28)$$

Use of (25) now yields (4).

The probability of y calls in the overflow group is given by (11). We first simplify $f(y; i, j)$, as given by (17). We have

$$\begin{aligned} f(y; i, j) &= \frac{i! j!}{[i+j-(c+y)]! (c+y)!} \\ &\quad - \frac{i! j!}{[i+j-(c+y+1)]! (c+y+1)!}. \end{aligned} \quad (29)$$

Thus, from (11),

$$\begin{aligned} w_{.y} &= \sum_{i=0}^c \frac{a^i / i!}{\sum_{h=0}^c \frac{a^h}{h!}} \sum_{j=c-i+y}^{c+y} \frac{e^{-a} \frac{a^j}{j!}}{[i+j-(c+y)]! (c+y)!} \left[\frac{i! j!}{[i+j-(c+y)]! (c+y)!} \right. \\ &\quad \left. - \frac{i! j!}{[i+j-(c+y+1)]! (c+y+1)!} \right] \end{aligned} \quad (30)$$

$$\begin{aligned} w_{.y} &= f(a) \sum_{i=0}^c \sum_{j=c-i+y}^{c+y} a^{i+j} \left[\frac{1}{(i+j-(c+y))! (c+y)!} \right. \\ &\quad \left. - \frac{1}{(i+j-(c+y+1))! (c+y+1)!} \right]. \end{aligned} \quad (31)$$

Setting $h = i + j - (c + y)$, reversing the order of summation, and

factoring yields

$$w_{.y} = f(a) \sum_{h=0}^c \sum_{i=h}^c \frac{a^{h+c+y}}{h! (c+y+1)!} (c+y+1-h), \quad (32)$$

$$w_{.y} = f(a) \frac{a^{c+y}}{(c+y+1)!} \sum_{h=0}^c \frac{a^h}{h!} \sum_{i=h}^c (c+y+1-h), \quad (33)$$

and (3) follows.

A.2 Proof That (18) Is an Identity

Let the mean of the overflow distribution be denoted by M . From (3),

$$M/f(a) = \sum_{y=1}^{\infty} \frac{ya^{c+y}}{(c+y+1)!} \sum_{j=0}^c \frac{a^j}{j!} (c-j+1)(c+y+1-j) \quad (34)$$

$$\begin{aligned} M/f(a) &= \sum_{i=0}^c \frac{a^i}{j!} (c-j+1) \sum_{y=1}^{\infty} (c+y+1) \frac{ya^{c+y}}{(c+y+1)!} \\ &\quad - \sum_{j=0}^c \frac{ja^j}{j!} (c-j+1) \sum_{y=1}^{\infty} \frac{ya^{c+y}}{(c+y+1)!} \end{aligned} \quad (35)$$

$$\begin{aligned} M/f(a) &= \sum_{i=0}^c \frac{a^i}{j!} (c-j+1) \sum_{y=1}^{\infty} \frac{ya^{c+y}}{(c+y)!} \\ &\quad - \sum_{j=1}^c \frac{a^{j-1}}{(j-1)!} (c-j+1) \sum_{y=1}^{\infty} \frac{ya^{c+y+1}}{(c+y+1)!}. \end{aligned} \quad (36)$$

After changing the indices in the subtracted sums by replacing j by $j+1$ and y by $y-1$, we obtain

$$\begin{aligned} M/f(a) &= \sum_{i=0}^c \frac{a^i}{j!} (c-j+1) \sum_{y=1}^{\infty} \frac{ya^{c+y}}{(c+y)!} \\ &\quad - \sum_{i=0}^c \frac{a^i}{j!} (c-j) \sum_{y=1}^{\infty} (y-1) \frac{a^{c+y}}{(c+y)!}. \end{aligned} \quad (37)$$

Simplification yields

$$M/f(a) = \sum_{i=0}^c \frac{a^i}{j!} \sum_{y=1}^{\infty} \frac{ya^{c+y}}{(c+y)!} + \sum_{i=0}^c \frac{a^i}{j!} (c-j) \sum_{y=1}^{\infty} \frac{a^{c+y}}{(c+y)!}. \quad (38)$$

Putting $h = y + c$ and adding and subtracting terms, we have

$$\begin{aligned} M/f(a) &= \sum_{i=0}^c \frac{a^i}{j!} \left[\sum_{h=0}^{\infty} (h-c) \frac{a^h}{h!} - \sum_{h=0}^c (h-c) \frac{a^h}{h!} \right] \\ &\quad + \sum_{i=0}^c \frac{a^i}{j!} (c-j) \left[\sum_{h=0}^{\infty} \frac{a^h}{h!} - \sum_{h=0}^c \frac{a^h}{h!} \right]. \end{aligned} \quad (39)$$

We notice that the finite series vanish and the infinite series combine to give

$$M/f(a) = \left[\sum_{i=0}^c \frac{a^{i+1}}{j!} - \sum_{i=0}^{c-1} \frac{a^{i+1}}{j!} \right] \sum_{h=0}^{\infty} \frac{a^h}{h!} = \frac{a^{c+1}}{c!} e^a. \quad (40)$$

Replacing $f(a)$ by its explicit expression, we have

$$M = \frac{a^{c+1}}{c!} \left(\sum_{i=1}^c \frac{a^i}{i!} \right)^{-1}. \quad (41)$$

A.3 Derivation of the Formula for the Second Factorial Moment of the Constant-Holding-Time Overflow Distribution

From (3),

$$\begin{aligned} F_2/f(a) &= \sum_{y=2}^{\infty} y(y-1) \frac{a^{c+y}}{(c+y+1)!} \\ &\quad \cdot \sum_{i=0}^c \frac{a^i}{j!} (c+y+1-j)(c-j+1) \end{aligned} \quad (42)$$

$$\begin{aligned} F_2/f(a) &= \sum_{i=0}^c \frac{a^i}{j!} (c-j+1) \sum_{y=2}^{\infty} y(y-1)(c+y+1) \frac{a^{c+y}}{(c+y+1)!} \\ &\quad - \sum_{i=0}^c \frac{ja^i}{j!} (c-j+1) \sum_{y=2}^{\infty} y(y-1) \frac{a^{c+y}}{(c+y+1)!}. \end{aligned} \quad (43)$$

Again replacing j by $j+1$ and y by $y-1$ in the subtracted sums in (43), we obtain

$$\begin{aligned} F_2/f(a) &= \sum_{i=0}^c \frac{a^i}{j!} (c-j+1) \sum_{y=2}^{\infty} y(y-1) \frac{a^{c+y}}{(c+y)!} \\ &\quad - \sum_{i=0}^c \frac{a^i}{j!} (c-j) \sum_{y=2}^{\infty} (y-1)(y-2) \frac{a^{c+y}}{(c+y)!} \end{aligned} \quad (44)$$

$$\begin{aligned} F_2/f(a) &= \sum_{i=0}^c \frac{a^i}{j!} \sum_{y=2}^{\infty} y(y-1) \frac{a^{c+y}}{(c+y)!} \\ &\quad + 2 \sum_{i=0}^c \frac{a^i}{j!} (c-j) \sum_{y=2}^{\infty} (y-1) \frac{a^{c+y}}{(c+y)!}. \end{aligned} \quad (45)$$

Letting $h = c+y$ and adding and subtracting terms allows us to write

$$F_2/f(a) = \sum_{i=0}^c \frac{a^i}{j!} \left\{ \sum_{h=0}^{\infty} (h-c)(h-c-1) \frac{a^h}{h!} \right\}$$

$$-\sum_{h=0}^c \frac{a^h}{h!} (h-c)(h-c-1) \Big\} + 2 \sum_{j=0}^c \frac{a^j}{j!} (c-j) \\ \cdot \left\{ \sum_{h=0}^{\infty} (h-c-1) \frac{a^h}{h!} - \sum_{h=0}^c \frac{a^h}{h!} (h-c-1) \right\} \quad (46)$$

$$F_2/f(a) = \sum_{h=0}^{\infty} [h(h-1) - 2hc + c(c+1)] \frac{a^h}{h!} \sum_{i=0}^c \frac{a^i}{j!} \\ + \sum_{h=0}^{\infty} 2[hc - c(c+1)] \frac{a^h}{h!} \sum_{i=0}^c \frac{a^i}{j!} \\ - \sum_{h=0}^{\infty} [2ah - 2a(c+1)] \frac{a^h}{h!} \sum_{i=0}^{c-1} \frac{a^i}{j!} \\ - \sum_{i=0}^c \frac{a^i}{j!} \sum_{h=0}^c \frac{a^h}{h!} (c-h)(c+1+h) \\ + 2 \sum_{i=0}^c \frac{a^i}{j!} (c-i) \sum_{h=0}^c \frac{a^h}{h!} (c+1-h). \quad (47)$$

After substituting k for $h+j$ in the finite sums and substituting e^a for its series expansion, we obtain

$$F_2/f(a) = e^a \left\{ [2a(c+1) - a^2 - c(c+1)] \right. \\ \cdot \sum_{i=0}^c \frac{a^i}{j!} + [2a^2 - 2a(c+1)] \frac{a^c}{c!} \Big\} \\ + \sum_{k=0}^{2c-1} \frac{a^k}{k!} \sum_{h=\lfloor k-c \rfloor^+}^{\min\{k,c\}} \binom{k}{h} (c+1-h)(c-2k+3h). \quad (48)$$

It turns out that the second sum vanishes for $k = 2c-1$, and thus after deleting the vanishing term and writing the coefficient of e^a as a polynomial in a , we have

$$F_2/f(a) = e^a \left\{ \frac{a^{c+2}}{c!} = \frac{a^{c+1}}{(c-1)!} \right. \\ - \sum_{i=0}^c \frac{a^i}{j!} [j(j-1) - 2j(c+1) + c(c+1)] \Big\} \\ + \sum_{k=0}^{2c-2} \frac{a^k}{k!} \sum_{h=\lfloor k-c \rfloor^+}^{\min\{k,c\}} \binom{k}{h} (c+1-h)(c-2k+3h). \quad (49)$$

Finally, after substituting the value of $f(a)$, given by (25), transposing

the limits of summation in the first sum on the right-hand side, and some minor simplification, we obtain (7).

REFERENCES

1. Kosten, L., "Über Sperrungswahrscheinlichkeiten bei Staffelschaltungen," Elek Nachr. Tech., 14, 1937, pp. 5-12.
2. Wilkinson, R. I., "Theories for Toll Traffic Engineering in the U.S.A.," B.S.T.J., 35, No. 2 (March 1956), pp. 421-514.
3. Tånge, F. I., and Wikell, G., "Comparative Studies of Congestion Values Obtained in Gradings When Holding-Times are Constant Respectively Follow the Negative Exponential Distribution Law," Fourth International Teletraffic Congress, London, July 1964.
4. Takács, L., "On Erlang's Formula," Ann. Math. Statist., 40, 1969, pp. 71-78.
5. Takács, L., *Combinatorial Methods in the Theory of Stochastic Processes*, New York: John Wiley & Sons, 1967.

Statistical Behavior of a Fading Signal

By S. H. LIN

(Manuscript received July 22, 1971)

A general analysis of the statistical behavior of the envelope of a fading signal $V(t)e^{i\phi(t)}$ is presented in this paper. The statistics include the probability $P(V \leq L)$ that the amplitude $V(t)$ will fade below a specified signal level L ; the expected number $N(L)$ of fades of $V(t)$ below L per unit time; and the average duration $\bar{t}(L)$ of fades below L . The model for the fading signal is a constant vector plus a random interfering vector which represents the resultant of all the received extraneous signals and noise. The theoretical results agree with three empirically observed power relationships obtained in deep fades of nondiversity signals: $P(V \leq L) \propto L^2$, $N(L) \propto L$ and $\bar{t}(L) \propto L$. The theoretical results are applicable to a wide class of fading problems. The analysis includes the previous works of Rice, Nakagami, Norton, Vogler, Mansfield, and Short as special cases.

I. INTRODUCTION

A general analysis of the statistical behavior of the envelope $V(t)e^{i\phi(t)}$ of a fading signal is presented in this paper. Our principal interests are the probability, $P(V \leq L)$, that the amplitude $V(t)$ will fade below a specified signal level L^* ; the expected number, $N(L)$, of fades per unit time below the specified level L ; and the average duration, $\bar{t}(L)$, of fades below L . These statistics are all functions of the signal level L .

The theory presented herein has been developed to complement and extend the empirical results developed by my colleagues at Bell Telephone Laboratories¹⁻⁶ from their extensive experimental experience. Published data of other workers have also been considered.

The previous theoretical works on the statistics of a fading signal often assume a complex Gaussian model for the fading signal. The theoretical support for this assumption is that, by the central limit theorem, the real and the imaginary parts of the sum of a large number of independent interfering signals will be approximately Gaussian.

* More precisely speaking, in a long time period containing a large number of fades, the distribution $P(V \leq L)$ represents the expected fraction of this long time period that the signal amplitude V will fade below L .

For tropospheric radio links, this model seems to be satisfactory. However, for line-of-sight radio links, the results of a short pulse experiment⁷ and the angle-of-arrival measurements^{8,9,10} indicate that the number of interfering signals is usually fairly small. Ray tracing theory also indicates that for typical line-of-sight radio links the number of paths contributing to multipath propagation is unlikely to be large. Furthermore, the theoretical results of the complex Gaussian model do not agree well with the experimental data on the statistics of fading signals of line-of-sight radio links, especially for certain overwater paths with severe fading.

In this paper, we do not impose the restrictive assumptions of the complex Gaussian model. Rather, we simply model the fading signal $Ve^{i\phi}$ as a constant vector plus an interfering random vector; i.e.,

$$Ve^{i\phi} = 1 + Re^{i\phi} = 1 + \alpha + j\beta, \quad (1)$$

where R , θ , α , and β are the amplitude, phase, real part, and imaginary part respectively of the interfering vector. The interfering vector is described by the joint probability density function $f(\alpha, \beta)$ and represents the resultant of all the received extraneous signals, echoes, rays, and noise. The analysis applies for R and θ either dependent or independent; θ uniformly or nonuniformly distributed; α and β either Gaussian or nonGaussian. Thus, the results of this analysis may be applied to a wide class of fading problems.

This paper treats the problem in three parts: The first is concerned with the amplitude distribution of V . The second considers the number of fades $N(L)$ and the average fade duration $\bar{t}(L)$. The final section investigates several special topics including m -distributions, chi-distributions, the Rayleigh distribution, Rice distribution, log-normal distribution and the sum of n unit random vectors.

Appendix A is a list of symbols and their definitions.

II. SUMMARY OF RESULTS

- (i) In spite of great variations in fading environment and test conditions, the experimental data^{1-6,11-14,15-17} on $P(V \leq L)$, $N(L)$, and $\bar{t}(L)$ of most nondiversity* fading signals obey the following three prevailing power laws of deep fades:

* The diversity signal is the output signal of a diversity combining system with two or more input signals. A "nondiversity fading signal" is a fading signal that is not a diversity signal.

$$\left. \begin{aligned} P(V \leq L) &\propto L^2 \\ N(L) &\propto L \end{aligned} \right\} \quad (2)$$

$$\left. \begin{aligned} N(L) &\propto L \\ l(L) &\propto L \end{aligned} \right\} \text{ for small } L. \quad (3)$$

$$\left. \begin{aligned} l(L) &\propto L \end{aligned} \right\} \quad (4)$$

The theoretical analysis shows that if the probability density function $f(\alpha, \beta)$ of the resultant interfering vector, $Re^{i\theta} = \alpha + j\beta$, is a smooth function which is neither singular nor zero at the deep fade point ($\alpha = -1, \beta = 0$), then the statistics $P(V \leq L)$, $N(L)$, and $l(L)$ of deep fades follow the three prevailing power laws (2), (3), and (4). The easily satisfied condition, $\infty > f(-1, 0) > 0$, is sufficient to obtain these functional relationships.

- (ii) The set of power laws (2), (3), and (4) apply for R and θ either independent or dependent, θ either uniformly or nonuniformly distributed, (or, α and β either Gaussian or nonGaussian, either independent or dependent) as long as $f(\alpha, \beta)$ is smooth.
- (iii) If $f(\alpha, \beta)$ is singular at ($\alpha = -1, \beta = 0$), then the theory predicts that for small L

$$\left. \begin{aligned} P(V \leq L) &\propto L^{2\mu} \\ N(L) &\propto L^{2\mu-1} \end{aligned} \right\} \quad (5)$$

$$\left. \begin{aligned} N(L) &\propto L^{2\mu-1} \\ l(L) &\propto L \end{aligned} \right\} \quad 1 > \mu > \frac{1}{2}. \quad (6)$$

$$\left. \begin{aligned} l(L) &\propto L \end{aligned} \right\} \quad (7)$$

The exceptional behavior (5) consistent with $\mu = 1/2$ has been observed experimentally on certain overwater radio links with severe fading. In this case, the resultant interfering vector contains the strong water-reflected ray as a dominant component. Therefore, the probability density function $f(\alpha, \beta)$ has a singularity at the position of the dominant component vector.*

- (iv) If $f(\alpha, \beta)$ has a zero at ($\alpha = -1, \beta = 0$) or is negligibly small at ($\alpha = -1, \beta = 0$), the theory predicts that for small L :

$$\left. \begin{aligned} P(V \leq L) &\propto L^{2\mu} \\ N(L) &\propto L^{2\mu-1} \end{aligned} \right\} \quad (8)$$

$$\left. \begin{aligned} N(L) &\propto L^{2\mu-1} \\ l(L) &\propto L \end{aligned} \right\} \quad \mu > 1 \quad (9)$$

$$\left. \begin{aligned} l(L) &\propto L \end{aligned} \right\} \quad (10)$$

The composite fading signals of diversity combining systems obey the set of power laws (8), (9), and (10). For overland radio

* The complex Gaussian model, which assumes that $f(\alpha, \beta)$ is a two-dimensional normal density function, is unable to explain the exceptional behavior (5) and (6).

links, the parameter μ is equal to the order of diversity. In our experiments, the nondiversity fading signal of a relatively short* radio link with path length 15.87 miles has also shown the exceptional behavior described by (8), (9), and (10).

- (v) The theoretical results (4), (7), and (10) indicate that the power law, $\bar{t}(L) \propto L$, for the average fade duration is more universal than those of $P(V \leq L)$ and $N(L)$. This prediction agrees with available experimental data.
- (vi) In general, the relationship between $f(\alpha, \beta)$ and the amplitude distribution $P(V \leq L)$ is not unique. As an example, this non-uniqueness shows that specifying the Rayleigh distribution for the amplitude of a fading signal does not necessarily imply that α and β are Gaussian, nor does it necessarily imply a large number of interfering signals.

* At 4-GHz operating frequency, the average path length of line-of-sight radio links is about 27 miles.

Part 1. Amplitude Distribution

<i>Contents</i>	<i>Page</i>
I. Introduction and Summary.....	3215
II. Fading Signal Model.....	3218
III. General Formulation of Amplitude Distribution.....	3220
IV. Probability Density Function of Interfering Vector.....	3221
V. Power Series Representation of Amplitude Distribution.....	3222
VI. Prevailing Square Law of Deep Fades.....	3223
VII. A Dominant Component Interfering Signal.....	3225
VIII. Diversity Systems.....	3226
IX. One-Echo Model.....	3226

I. INTRODUCTION AND SUMMARY

In the study of fading signals due to multipath interference, the experimental data on the cumulative amplitude distribution, $P(V \leq L)$, of deep fades are often plotted on a graph paper where the fade depth is expressed in dB and the probability of fade is expressed on a log scale as shown in Fig. 1. The consensus based on large amounts of experimental data^{1-6,11-14,15-17} is that the cumulative amplitude distribution of most nondiversity fading signals in the deep-fade region can well be represented by a straight line with a prevailing inverse slope of 10 dB per decade of probability.

The equation which describes this typical distribution on Fig. 1 is

$$P(V \leq L) = \epsilon \cdot L^2, \quad \text{for } L_{\text{up}} \geq L \geq 0 \quad (11)$$

where V is the envelope voltage of the random fading signal normalized to its nonfaded signal level, L is any specified signal level, ϵ is a parameter depending on fading environment, and L_{up} is the upper bound of signal level below which the straight-line representation of $P(V \leq L)$ on Fig. 1 is valid.

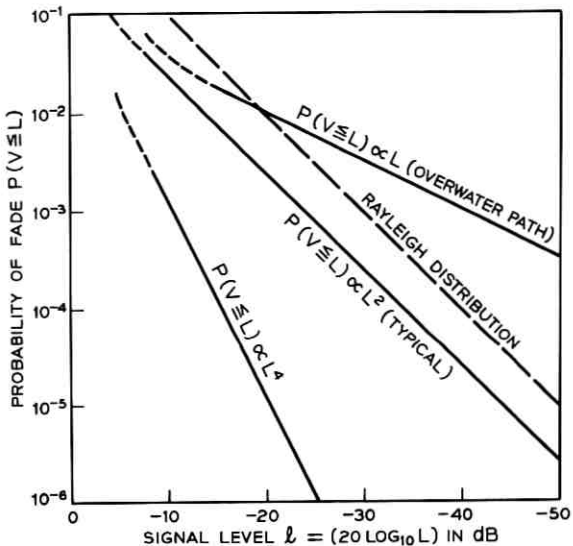


Fig. 1—Cumulative amplitude distributions of fading signals.

The empirical result (11) means that the amplitude distributions of most nondiversity fading signals obey the following square law of deep fades

$$P(V \leq L) \propto L^2, \quad L_{\text{up}} \geq L \geq 0 \quad (12)$$

in spite of the great variations of fading environment and test condition. However, there are some exceptional cases. The most profound exception occurs on certain overwater radio links with severe fading. In these instances, the probability of fades, $P(V \leq L)$, decreases very slowly as the signal level L decreases and is characterized by an inverse slope of 20 dB per decade of probability as shown in Fig. 1, implying a power law

$$P(V \leq L) \propto L \quad (13)$$

in the deep-fade region.

Another kind of exception occurs on certain radio links with relatively little multipath fading. The probability of fades, $P(V \leq L)$, decreases very rapidly with L and is characterized by an inverse slope of 5 dB per decade of probability as shown in Fig. 1. This kind of distribution follows the power law

$$P(V \leq L) \propto L^4 \quad (14)$$

in the deep-fade region. For example, at 4-GHz operating frequency, the average path length of line-of-sight radio links is about 27 miles. The behavior (14) has been observed to occur on a relatively short path with path length of 15.87 miles.

The theoretical amplitude distributions previously derived were based on a complex Gaussian model and predict a square-law dependence, $P(V \leq L) \propto L^2$, in the deep-fade region. For example, the Nakagami distributions,¹⁸ which include Hoyt distribution,^{18,19} Rice distribution,¹⁸ and Rayleigh distribution as special cases, all are square law in the deep-fade region. The explicit expression of Nakagami distribution can be found in Equation (4.6-28) of Reference 18. Figure 1 also includes Rayleigh distribution (dashed line) for comparison with the experimental data.

The small number of interfering signals in line-of-sight radio links suggests that the assumption of a complex Gaussian model may be unjustified. One of the main objectives of this paper is to determine the weakest set of assumptions under which the square law (12) is obtained, and the condition for which the exceptional case such as (13) or (14) will occur.

In summary:

- (i) The theoretical model for the fading signal, $Ve^{i\phi}$, is a constant unit vector plus a resultant interfering vector

$$Ve^{i\phi} = 1 + Re^{i\theta} = 1 + \alpha + j\beta.$$

The resultant interfering vector $Re^{i\theta} = \alpha + j\beta$, with joint probability density function $f(\alpha, \beta)$, represents the sum of all the received extraneous signals, echoes, rays, and noise.

- (ii) An infinite fade (i.e., $V = 0$) occurs whenever $\alpha = -1$ and $\beta = 0$. At this point $R = 1$ and $\theta = \pi$. Therefore, the behavior of $f(\alpha, \beta)$ near the infinite fade point ($\alpha = -1, \beta = 0$) is closely related to the power law of amplitude distribution $P(V \leq L)$ in the deep-fade region.
- (iii) For most radio links, the interfering signals and noise may be considered random, so that the joint probability density function $f(\alpha, \beta)$ of the resultant interfering vector is a smooth function near the infinite fade point ($\alpha = -1, \beta = 0$). The analysis shows that if $f(\alpha, \beta)$ is a smooth function which is neither singular nor zero at ($\alpha = -1, \beta = 0$), then $P(V \leq L) \propto L^2$ for small L . The simple condition $\infty > f(-1, 0) > 0$ is easily satisfied by most radio links. The validity of this square law does

not require that $f(\alpha, \beta)$ be a normal density function. Therefore, the number of interfering signals does not have to be large.

- (iv) The analysis shows that if $f(\alpha, \beta)$ is not smooth, but is singular at $(\alpha = -1, \beta = 0)$, then for small L ,

$$P(V \leq L) \propto L^{2\mu}, \quad 1 > \mu \geq \frac{1}{2}.$$

A physical example for this case is the overwater radio link where the water-reflected ray is almost as stable as the direct ray. The resultant interfering vector in this case contains the water-reflected ray which is "not very random." In other words, the joint probability density function $f(\alpha, \beta)$ has a high peak at the position of the dominant, stable component, and may be considered singular at that point.

- (v) If $f(\alpha, \beta)$ is zero or is negligibly small at the infinite fade point $(\alpha = -1, \beta = 0)$, then the analysis shows that for small L

$$P(V \leq L) \propto L^{2\mu}, \quad \mu > 1.$$

A physical example for this case is the short radio link where the phase differences among the multipath propagations are all small. Then the value of $f(-1, 0)$ is negligibly small because the phase, θ , of the resultant interfering vector is generally small. Another example for this case is the composite signal of the output of a diversity combining system where the artificial active combining device serves to create a zero of $f(\alpha, \beta)$ at $(\alpha = -1, \beta = 0)$.

II. FADING SIGNAL MODEL

The received fading signal is modeled as a constant vector plus an interfering random vector as shown in Fig. 2. The latter represents the resultant of all the received extraneous signals, echoes, rays, and noise. The received fading signal normalized to the magnitude of the constant vector can be written as

$$V(t)e^{i\phi(t)} = 1 + R(t)e^{i\theta(t)}, \quad (15)$$

where $R(t)$ and $\theta(t)$ are the normalized magnitude and the phase of the interfering random vector respectively; $V(t)$ and $\phi(t)$ are the normalized magnitude and the phase of the received fading signal respectively.

Let $x(t)$ and $y(t)$ be the real part and the imaginary part of the complex fading signal $Ve^{i\phi}$, i.e.,

$$V(t)e^{i\phi(t)} = x(t) + jy(t); \quad (16)$$

and let $\alpha(t)$ and $\beta(t)$ be the real part and the imaginary part of the complex interfering random vector $Re^{i\theta}$, i.e.,

$$R(t)e^{i\theta(t)} = \alpha(t) + j\beta(t). \quad (17)$$

V , ϕ , R , θ , x , y , α and β are all real random variables. The normalized output power is

$$V^2 = 1 + 2R \cos \theta + R^2 = (1 + \alpha)^2 + \beta^2. \quad (18)$$

The relative phase, $\theta(t)$, between the interfering vector and the constant vector can be taken to have values from 0 to 2π because θ and $(\theta \pm 2n\pi)$ for any integer n are indistinguishable to the received signal at an operating frequency.

A geometrical interpretation of equations (15) to (18) shows that deep fades (i.e., small V) occur when R and θ are near the infinite fade point, $(1, \pi)$, in the (R, θ) plane or equivalently when α and β are near the infinite fade point, $(-1, 0)$, in the (α, β) plane.

For line-of-sight radio links, notice that as far as the received signal $V(t)e^{i\phi(t)}$ is concerned, scintillation, atmospheric divergence, and earth bulge effects may also be replaced by a mathematically equivalent interfering signal $R(t)e^{i\theta(t)}$ which when combined with the constant vector gives the received fluctuating signal.

Therefore, the model described by equations (15) to (18) includes many possible fading mechanisms which may occur individually or simultaneously on a fading environment.

Going one step further, this model also includes the situations where no physical constant vector* exists because the mathematical decomposition (15) is applicable to any arbitrary fading signal. For such situations, the constant vector may represent the average signal level. The fluctuation of the signal is considered to be caused by an equivalent resultant interfering vector $Re^{i\theta}$.

For radio links subjected to multipath interference, the number of incoming component waves is usually more than two. Thus the resultant interfering vector $Re^{i\theta}$ consists of more than one echo and should not be interpreted as a simple physical echo. The main distinction is that the magnitude and the time delay of a physical echo are not functions of operating frequency whereas the magnitude R and the equivalent time delay, $\xi_e = \theta/\omega$, of a resultant interfering vector consisting of more than one echo, are functions of operating frequency (i.e., are dispersive).

* For beyond-the-horizon radio links, there is no direct radio path between the transmitter and the receiver.

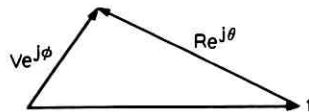


Fig. 2—Fading signal model.

III. GENERAL FORMULATION OF AMPLITUDE DISTRIBUTION

Equation (18) shows that the probability that the random signal V be faded below a specified signal level L is equal to the probability that α and β fall within the circular region

$$(1 + \alpha)^2 + \beta^2 \leq L^2 \quad (19)$$

in the (α, β) plane as shown in Fig. 3. Let $f(\alpha, \beta)$ be the joint probability function of α and β . Then $P(V \leq L)$ is the integral of $f(\alpha, \beta)$ over the circular region (19); i.e.,

$$P(V \leq L) = \int_{\beta=-L}^{\beta=L} \int_{\alpha=-1-\sqrt{L^2-\beta^2}}^{\alpha=-1+\sqrt{L^2-\beta^2}} f(\alpha, \beta) d\alpha d\beta. \quad (20)$$

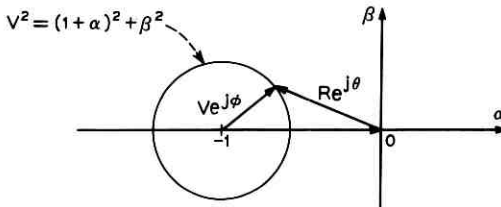
The statistical behavior of the interfering vector, $Re^{j\theta} = \alpha + j\beta$, is sometimes described by the joint probability density function $q(R, \theta)$ of the magnitude R and the phase θ of the interfering vector. A similar derivation in terms of R and θ yields

$$P(V \leq L) = \int_{R=1-L}^{R=1+L} \int_{\theta=\pi-\theta_L}^{\theta=\pi+\theta_L} q(R, \theta) d\theta dR, \quad (21)$$

where

$$\theta_L = \cos^{-1} \left(\frac{1 + R^2 - L^2}{2R} \right). \quad (22)$$

Most of the following analysis is in terms of α and β . An equivalent result in terms of R and θ is given in Appendix B.

Fig. 3—Fading signal model on (α, β) plane.

IV. PROBABILITY DENSITY FUNCTION OF INTERFERING VECTOR

Equation (18) indicates that the infinite fade (i.e., $V = 0$) occurs when $\alpha = -1, \beta = 0$. For most overland radio links, the interfering signals and the noise vary continuously in a random manner, so that the joint probability density function $f(\alpha, \beta)$ of the resultant vector is a smooth function. On the other hand, there are some paths for which $f(\alpha, \beta)$ may not be smooth, but singular. For example, for overwater radio links, the water-reflected ray near the grazing angle is comparable in magnitude and stability to the direct ray. Therefore, the resultant interfering vector contains a dominant component and the probability density function $f(\alpha, \beta)$ has a sharp peak (i.e., singular) at this point. If the heights of the antennas and the path length are such that the average phase of the water-reflected ray is equal to π , then the singularity of $f(\alpha, \beta)$ occurs at the infinite fade point ($\alpha = -1, \beta = 0$).

These discussions suggest that in the general analysis of deep fades, one should consider not only the case with smooth $f(\alpha, \beta)$ but also the case where $f(\alpha, \beta)$ is singular at ($\alpha = -1, \beta = 0$). A general probability density function $f(\alpha, \beta)$, which is useful in our study, is^{*†}

$$f(\alpha, \beta) = [(1 + \alpha)^2 + \beta^2]^{(\mu-1)} \cdot H(\alpha, \beta) \quad (23)$$

$$= V^{2(\mu-1)} \cdot H(\alpha, \beta). \quad (24)$$

where $H(\alpha, \beta)$ is an arbitrary smooth function. In the range $1 > \mu \geq 1/2$, the density function $f(\alpha, \beta)$ has a singularity of order $2|\mu - 1|$ at ($\alpha = -1, \beta = 0$).

On the other hand, in the range $\infty > \mu > 1$, the density function has a zero of order $2(\mu - 1)$ at ($\alpha = -1, \beta = 0$). For convenience, we shall call the parameter, μ , the smoothness index of $f(\alpha, \beta)$.

Since the possible singularity or zero of $f(\alpha, \beta)$ at ($\alpha = -1, \beta = 0$) is taken care of by the factor $[(1 + \alpha)^2 + \beta^2]^{\mu-1}$, we shall assume that

$$\infty > H(-1, 0) > 0. \quad (25)$$

Thus, the density function $f(\alpha, \beta)$ given by equation (23) is neither singular nor zero at ($\alpha = -1, \beta = 0$) if, and only if, $\mu = 1$ because the condition $\mu = 1$ implies $f(\alpha, \beta) = H(\alpha, \beta)$, and vice versa.

In equations (23) and (24), the smoothness index μ can be either an

* The reason for the use of the factor $(\mu - 1)$ instead of a simple power index in equations (23) and (24) is for the convenience of notation in Section IV of Part 3 when we investigate the m -distributions.

† The cases where the singularity of $f(\alpha, \beta)$ occurs at positions other than the infinite fade point ($\alpha = -1, \beta = 0$) will not be analyzed in this paper. A brief discussion is included in Section VII of this part.

integer or a noninteger. The only restriction on μ is that

$$\mu \geq \frac{1}{2}. \quad (26)$$

The reason for this constraint on μ is that in Section V of Part 2 we find that if $\mu < 1/2$, then the expected number of fades $N(L)$ approaches infinity as the fade depth L approaches zero. This seems to be nonphysical. Therefore, we require that $\mu \geq 1/2$.*

Since $H(\alpha, \beta)$ is an arbitrary smooth function and μ can range from $1/2$ to ∞ , then the probability density function $f(\alpha, \beta)$, as given by equation (23), includes a large variety of fading environments.

V. POWER SERIES REPRESENTATION OF AMPLITUDE DISTRIBUTION

We shall assume that $H(\alpha, \beta)$ is sufficiently smooth so that the two-dimensional Taylor series²⁰ expansion of $H(\alpha, \beta)$ is applicable in the neighborhood of $\alpha = -1$, and $\beta = 0$. Several situations, where the Taylor series expansion of $H(\alpha, \beta)$ is not applicable, will be discussed in Section IX and Appendix C.

The Taylor series²⁰ expansion of $H(\alpha, \beta)$ gives

$$\begin{aligned} H(\alpha, \beta) &= \sum_{n=0}^{n=\infty} \left[\frac{1}{n!} \sum_{r=0}^{r=n} C_r H_{n-r,r}(-1, 0)(1 + \alpha)^{n-r} \beta^r \right] \\ &= H(-1, 0) + H_{1,0}(-1, 0)(1 + \alpha) + H_{0,1}(-1, 0)\beta \end{aligned} \quad (27)$$

$$\begin{aligned} &+ \frac{1}{2!} [H_{2,0}(-1, 0)(1 + \alpha)^2 + 2H_{1,1}(-1, 0)(1 + \alpha)\beta + H_{0,2}(-1, 0)\beta^2] \\ &+ \dots, \end{aligned} \quad (28)$$

where

$$H_{n-r,r}(-1, 0) = \left. \frac{\partial^n}{\partial \alpha^{n-r} \partial \beta^r} H(\alpha, \beta) \right|_{\substack{\alpha=-1 \\ \beta=0}} \quad (29)$$

$$C_r^n = \frac{n!}{r!(n-r)!}. \quad (30)$$

Substituting (27) and (23) into (20) for $P(V \leq L)$ and carrying out the integration (Appendix D) yields

$$P(V \leq L) = \sum_{s=0}^{\infty} d_{2s+2} L^{2s+2\mu} \quad (31)$$

* Notice that the unity total probability requires that the singularity of $f(\alpha, \beta)$ be integrable (i.e., $\mu > 0$). The constraint $\mu \geq \frac{1}{2}$ does not violate this condition.

$$= d_2 L^{2\mu} + \sum_{S=1}^{\infty} d_{2S+2} L^{2S+2\mu}, \quad (32)$$

where

$$d_2 = \frac{\pi H(-1, 0)}{\mu}, \quad (33)$$

$$d_{2S+2} = \frac{\pi}{S! (S + \mu) 2^{2S}} \sum_{\nu=0}^{S} \frac{H_{2S-2\nu, 2\nu}(-1, 0)}{(\nu!) (S - \nu)!}, \quad (34)$$

$$S! = S(S - 1)(S - 2) \dots 3 \cdot 2 \cdot 1.$$

The corresponding amplitude probability density function $p(L)$ is

$$p(L) = \frac{\partial}{\partial L} P(V \leq L) = \sum_{S=0}^{S=\infty} (2S + 2\mu) d_{2S+2} L^{2S+2\mu-1}. \quad (35)$$

In the deep-fade region where L is small, the limiting forms of $P(V \leq L)$ and $p(L)$ are

$$P(V \leq L) \xrightarrow[L \rightarrow 0]{} \frac{\pi H(-1, 0)}{\mu} L^{2\mu} \quad (36)$$

and

$$p(L) \xrightarrow[L \rightarrow 0]{} 2\pi H(-1, 0) L^{2\mu-1}, \quad (37)$$

where $\mu \geq 1/2$. The power law of deep fades for the three different cases (i) $\mu = 1$, (ii) $1 > \mu \geq 1/2$, and (iii) $\mu > 1$ with their physical fading environments will be discussed in the following sections (VI, VII, and VIII respectively).

VI. PREVAILING SQUARE LAW OF DEEP FADES

For the nondiversity fading signals of most radio links, $f(\alpha, \beta)$ is neither singular nor zero at $(\alpha = -1, \beta = 0)$. Then $\mu = 1$ and $f(\alpha, \beta) = H(\alpha, \beta)$. Equations (31) to (37) under this situation become

$$P(V \leq L) = \sum_{S=0}^{\infty} d_{2S+2} L^{2S+2}, \quad (38)$$

$$= \pi f(-1, 0) L^2 + d_4 L^4 + d_6 L^6 + \dots, \quad (39)$$

$$f(\alpha, \beta) = H(\alpha, \beta), \quad (40)$$

$$d_2 = \pi f(-1, 0) = \pi H(-1, 0), \quad (41)$$

$$d_{2S+2} = \frac{\pi}{(S + 1)! 2^{2S}} \sum_{\nu=0}^{S} \frac{f_{2S-2\nu, 2\nu}(-1, 0)}{(\nu!) (S - \nu)!}, \quad (42)$$

$$f_{2S-2\nu, 2\nu}(-1, 0) = \frac{\partial^{2S}}{\partial \alpha^{2S-2\nu} \partial \beta^{2\nu}} f(\alpha, \beta) \Big|_{\substack{\alpha=-1 \\ \beta=0}}, \quad (43)$$

$$p(L) = \sum_{S=0}^{\infty} (2S+2) d_{2S+2} L^{2S+1}, \quad (44)$$

$$P(V \leq L) \xrightarrow[L \rightarrow 0]{} \pi f(-1, 0) L^2, \quad (45)$$

and

$$p(L) \xrightarrow[L \rightarrow 0]{} 2\pi f(-1, 0) L. \quad (46)$$

Equation (45) means that as long as $f(\alpha, \beta)$ is neither singular nor zero at $(\alpha = -1, \beta = 0)$, then the cumulative amplitude distribution in the deep-fade region always obeys the square law

$$P(V \leq L) \propto L^2, \quad L_{\text{up}} \geq L \geq 0. \quad (12)$$

Notice that this conclusion does not depend on any specific probability density function $f(\alpha, \beta)$ for the interfering vector as long as $f(\alpha, \beta)$ is smooth and $\infty > f(-1, 0) > 0$. The conclusion applies for α and β either normal or not, either dependent* or independent, either with zero mean or with nonzero means. The magnitude R and the phase θ of the interfering vector can be either dependent* or independent and θ can be either uniformly or nonuniformly distributed. Therefore, this conclusion covers a wide class of signal fading problems.

Apparently the simple condition, $\infty > f(-1, 0) > 0$, is appropriate to the nondiversity fading signals of most radio links because the square law of deep fades is representative of the experimental data.^{1-6, 11-14, 15-16†}

Notice that the first terms of equations (39) and (45), πL^2 , are the area of the two-dimensional region on (α, β) plane bounded by the circle, $L^2 = (1 + \alpha)^2 + \beta^2$, in which $V \leq L$, as shown in Fig. 3.

The coefficient $f(-1, 0)$ in equation (45) has been observed to depend upon path length, operating frequency, path profile, and geographical factors. From the experimental data of a large number of radio links, it is possible to deduce an empirical formula of $f(-1, 0)$ as a function of these parameters.^{22, 23, 24, 25}

In equation (12), the upper bound, L_{up} , of signal level below which

* This conclusion does not hold if the correlation coefficient between α and β or between R and θ is unity because the joint probability density $f(\alpha, \beta)$ becomes singular.

† This theoretical result also explains an experimental fact that the observed amplitude distributions of atmospheric radio noise are also characterized by the square law (12) in the small amplitude region.²¹

the square law applies also depends upon fading environment. Our experimental data show that L_{up} of most line-of-sight microwave radio links is above 0.3 (i.e., above -10 dB).

If $f(-1, 0)$ is negligibly small, so that the first term in the power series (39) can be neglected, then the second term, $d_4 L^4$, dominates, with the result that the amplitude distribution follows the power law $P(V \leq L) \propto L^4$. We have observed this behavior on a short radio link in the signal range from -10 dB to -20 dB (i.e., $0.3 \geq L \geq 0.1$). For fade depths deeper than -20 dB (i.e., $0.1 > L \geq 0$) the quadratic term of (39) again dominates; and the transition region between $P(V \leq L) \propto L^2$ and $P(V \leq L) \propto L^4$ occurs at about -20 dB for this short path.

An obvious reason that $f(-1, 0)$ is small for short radio links is that the multipath length differences are mostly less than a half-wavelength.

VII. A DOMINANT COMPONENT INTERFERING SIGNAL

For this case, μ is bounded by $1 > \mu \geq 1/2$. By equation (36)

$$P(V \leq L) \xrightarrow[L \rightarrow 0]{} \frac{\pi H(-1, 0)}{\mu} L^{2\mu}, \quad 1 > \mu \geq \frac{1}{2}, \quad (47)$$

and the corresponding power law of deep fades is

$$P(V \leq L) \propto L^{2\mu}, \quad 1 > \mu \geq \frac{1}{2}. \quad (48)$$

Since μ is less than unity for this case, then as $L \rightarrow 0$, the probability of deep fades decreases more slowly than square law (12). Physically, this means that the deep-fade problem for these links is more severe. The experimental data of two oversea paths (shown as curve 2 in Fig. 16.5a and as curve 1 in Fig. 16.5b of Reference 15) follow this power law (48) of severe fading.

It is true, however, that some overwater radio links still obey the square law (12) rather than (48).^{15,17} The reason is that because of the geometry of the radio link, the singularity in the density function $q(R, \theta)$ may occur, if it exists at all, at a position far away from the infinite fade point ($R = 1, \theta = \pi$). Then in the neighborhood of the infinite fade point ($R = 1, \theta = \pi$), the density function $q(R, \theta)$ (or equivalently $f(\alpha, \beta)$) may still be a smooth function.

For overland paths, it is possible that an exceptionally calm and stratified atmosphere would also create a stable, dominant interfering signal over a sustained period. Then the joint probability density function $f(\alpha, \beta)$ may also be singular at the position of this stable,

dominant interfering signal. Therefore, the results of this section on the power law of severe fading may also occur on an overland radio link.

VIII. DIVERSITY SYSTEMS

When $\mu > 1$, the power law of deep fades is

$$P(V \leq L) \xrightarrow[L \rightarrow 0]{} \frac{\pi H(-1, 0)}{\mu} L^{2\mu}, \quad \mu > 1, \quad (49)$$

$$P(V \leq L) \propto L^{2\mu}, \quad \mu > 1. \quad (50)$$

As L decreases, the probability of deep fades decreases faster than those following the square law (12). Physically, this means the problem of fading for this case is less severe than those following the square law (12).

The experimental data^{1,2,5} of composite signals of the outputs of diversity combining systems show that the amplitude distributions of composite signals in the deep-fade region obey the power-law equation (50) rather than the square-law equation (12).

Since $\mu > 1$ implies $f(\alpha, \beta)$ has a zero at the deep-fade point ($\alpha = -1, \beta = 0$), these results show that the artificial active combining devices of diversity combining systems serve to create a zero at ($\alpha = -1, \beta = 0$) of order $2(\mu - 1)$ of the density function $f(\alpha, \beta)$ of the equivalent interfering vector of the output composite signal. The value of μ depends on the order of diversity. By comparing the power law (50) to the experimental data^{1,2,5} and the theoretical results on the diversity systems, we find that for most overland paths, the value of μ for the composite signal is equal to the order of diversity.

IX. ONE-ECHO MODEL

In the model described by equation (15) for the fading signal, if there is only one echo and if the magnitude of this echo is a constant, then $R \equiv A$ is a constant rather than a random variable. For this idealized case, the joint probability density function $q(R, \theta)$ of R and θ contains a delta function

$$q(R, \theta) = \delta(R - A)W(\theta), \quad (51)$$

where $W(\theta)$ is the probability density function of the random relative phase θ between the echo $Ae^{i\theta}$ and the constant vector.

For convenience, we shall call this specialized model the one-echo model. (In the literature, it is also known as the two-ray model.)

In the analysis, we shall assume that $A \leq 1$. The case where $A > 1$

can be treated similarly simply by switching the roles of echo and the constant vector.

Since the joint probability density function of the interfering vector of the one-echo model does not belong to the class of $f(\alpha, \beta)$ discussed in Section IV of this part, the results of previous sections are not directly applicable. Nevertheless, substituting the density function (51) into the general formulation (21) for $P(V \leq L)$ and integrating over R (see Fig. 4) yields

$$P(V \leq L) = \int_{\pi - \theta_L}^{\pi + \theta_L} W(\theta) d\theta, \quad (52)$$

where

$$\theta_L = \cos^{-1} \left(\frac{1 + A^2 - L^2}{2A} \right), \quad (1 + A) \geq L \geq (1 - A). \quad (53)$$

Since the behavior of $W(\theta)$ in the neighborhood of $\theta = \pi$ is important for the analysis of deep fades, we shall assume that $W(\theta)$ is smooth in this neighborhood so that the Taylor series expansion of $W(\theta)$ is applicable. Then

$$W(\theta) = W(\pi) + W_1(\pi)(\theta - \pi) + \frac{W_2(\pi)}{2!} (\theta - \pi)^2 + \dots, \quad (54)$$

where

$$W_n(\pi) = \frac{d^n}{d\theta^n} W(\theta) \Big|_{\theta=\pi}, \quad n = 1, 2, 3, \dots. \quad (55)$$

Substituting equation (54) into equation (52) and carrying out the integration yields

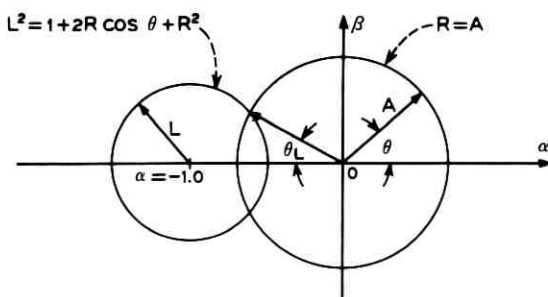


Fig. 4—The range of phase, $(\pi - \theta_L) \leq \theta \leq (\pi + \theta_L)$, in which $V \leq L$.

$$P(V \leq L) = 2 \sum_{s=0}^{\infty} \frac{W_{2s}(\pi)}{(2s+1)!} \left[\cos^{-1} \left(\frac{1+A^2-L^2}{2A} \right) \right]^{2s+1},$$

$$(1+A) \geq L \geq (1-A). \quad (56)$$

If the magnitudes of the two vectors are equal, then $A = 1$, and equation (56) becomes

$$P(V \leq L) = 2 \sum_{s=0}^{\infty} \frac{W_{2s}(\pi)}{(2s+1)!} \left[\cos^{-1} \left(1 - \frac{L^2}{2} \right) \right]^{2s+1}, \quad 2 \geq L \geq 0.$$

$$(57)$$

Since

$$\cos^{-1} \left(1 - \frac{L^2}{2} \right) = \sin^{-1} \left[L \left(1 - \frac{L^2}{4} \right)^{\frac{1}{2}} \right]; \quad (58)$$

$$\therefore \cos^{-1} \left(1 - \frac{L^2}{2} \right) \xrightarrow[L \rightarrow 0]{} L \quad (59)$$

Then the behavior of $P(V \leq L)$ given by equation (57) in the deep-fade region is

$$P(V \leq L) \xrightarrow[L \rightarrow 0]{} 2W(\pi)L; \quad (60)$$

$$\therefore p(L) \xrightarrow[L \rightarrow 0]{} 2W(\pi). \quad (61)$$

This result shows that as long as the probability density function $W(\theta)$ of the random phase θ is neither singular nor zero at $\theta = \pi$, then the cumulative amplitude distribution of the one-echo model with $R \equiv 1$ always obeys the power law

$$P(V \leq L) \propto L \quad (62)$$

in the deep-fade region no matter whether $W(\theta)$ is uniform or not. Equation (57) shows that the nonuniform part of $W(\theta)$ contributes only to the high-order terms of $P(V \leq L)$ and does not affect the behavior of $P(V \leq L)$ in the deep fade region.

If the distribution of the random relative phase is uniform in $(0, 2\pi)$, then

$$W(\theta) = \frac{1}{2\pi} \quad (63)$$

$$W_n(\pi) = 0, \quad n \geq 1.$$

Equation (56) specialized to this case is

$$P(V \leq L) = \frac{1}{\pi} \cos^{-1} \left(\frac{1+A^2-L^2}{2A} \right). \quad (64)$$

If $A = 1$, then equation (64) becomes

$$P(V \leq L) = \frac{1}{\pi} \cos^{-1} \left(1 - \frac{L^2}{2} \right). \quad (65)$$

As far as the deep-fade region is concerned, equation (57) can also be written as

$$P(V \leq L) = 2W(\pi)L + O(L^{1+\eta}), \quad \eta > 0; \quad (66)$$

$$\therefore p(L) = 2W(\pi) + O(L^\eta), \quad (67)$$

where $O(L^\eta)$ is a symbol to denote the component which goes to zero at a rate equal to or faster than that of L^η as $L \rightarrow 0$.

Although the one-echo model of this section and the other two cases discussed in Appendix C do not exhaust all the situations where $H(\alpha, \beta)$ is not analytic, the main objective is to show that the assumption of Taylor series expansion of $H(\alpha, \beta)$ in Section V of this part is not strictly necessary for the derivation of the power law of deep fades.

To unify the representations for all the cases considered in this paper, we shall rewrite equations (66) and (67) as

$$P(V \leq L) = 2W(\pi)L^{2\mu} + O(L^{2\mu+\eta}) \quad (68)$$

and

$$p(L) = 2W(\pi)L^{2\mu-1} + O(L^{2\mu-1+\eta}), \quad \mu = \frac{1}{2}, \quad \eta > 0. \quad (69)$$

Then the amplitude distributions of deep fades of all the cases discussed in Part 1 can be summarized as

$$P(V \leq L) = d_2 L^{2\mu} + O(L^{2\mu+\eta}) \quad (70)$$

and

$$p(L) = 2\mu d_2 L^{2\mu-1} + O(L^{2\mu-1+\eta}), \quad \mu \geq \frac{1}{2}, \quad \eta > 0. \quad (71)$$

If $H(\alpha, \beta)$ is continuous at $(\alpha = -1, \beta = 0)$, then $d_2 = \pi H(-1, 0)/\mu$. If $H(\alpha, \beta)$ is discontinuous at $(\alpha = -1, \beta = 0)$, then $d_2 = \pi \bar{H}(-1, 0)/\mu$. For a one-echo model, $d_2 = 2W(\pi)$ and $\mu = 1/2$.

Part 2. Expected Number of Fades and Average Fade Duration

<i>Contents</i>	<i>Page</i>
I. Introduction and Summary.....	3230
II. General Formulation for Number of Fades.....	3233
III. General Formulation for Average Fade Duration.....	3234
IV. Assumption on Conditional Average Positive Derivative.....	3235
V. Power Series Form of $N(L)$	3237
5.1 Prevailing Power Law of Number of Deep Fades.....	3237
VI. Average Duration of Deep Fades.....	3238
VII. Invariance of Power Law of Average Fade Duration.....	3238
VIII. Incompatibility Between One-Echo Model and Overland Radio Links..	3239
IX. Approximate Average Positive Derivative $\bar{V}_+(L)$ of Line-of-Sight Microwave Radio Links.....	3241
X. Generalized Assumption on $\bar{V}_+(L)$	3241

I. INTRODUCTION AND SUMMARY

In Part 1 we investigated the amplitude distribution of a fading signal. In a long time period, the cumulative amplitude distribution $P(V \leq L)$ tells us the expected fraction of this time period that the signal will fade below any specified signal level L . However, $P(V \leq L)$ does not tell us anything about the dynamic aspects of the fading signal. For example, a large number of short fades and a small number of long fades may have the same amplitude distribution.

Some communication systems may tolerate the short fades but not the long fades. Furthermore, in the design of a diversity combining device, a distortion equalizer, or an automatic gain controlling device

to combat the fading problem, one needs information on the dynamic behavior of the fading signal.

In Part 2 we present the results of our investigation on the expected number $N(L)$ per unit time that the signal $V(t)$ fades below a given signal level L ; and the average duration $\bar{t}(L)$ of fades below L .

The analysis is based on the general integral formulation of $N(L)$ by Rice^{26,27} and Vigants⁴ and our results for $P(V \leq L)$ in Part 1. Again, we do not impose the restrictive assumption of the complex Gaussian model so that the theoretical results may be applied to a wide class of fading problems.

In the study of $N(L)$ and $\bar{t}(L)$, the experimental data¹⁻⁶ for $N(L)$ or $\bar{t}(L)$ are often plotted on a log scale as shown in Figs. 5 and 6. It is an experimental fact that the data for $N(L)$ and $\bar{t}(L)$ can be well represented by straight lines on this kind of graph paper for fade depth deeper than -10 dB, as shown in Figs. 5 and 6. The slopes of these straight lines are directly related to the power laws of $N(L)$ and $\bar{t}(L)$ in the deep-fade region. The experimental observations of $N(L)$ and $\bar{t}(L)$ are summarized below:

- (i) The experimental data show that $N(L)$ for most nondiversity fading signals obeys the power law, $N(L) \propto L$, in the deep-fade region.
- (ii) For a short radio link from Villa Rica to Palmetto, Georgia, the $N(L)$ of a nondiversity signal follows the cubic power law, $N(L) \propto L^3$, in the deep-fade region.

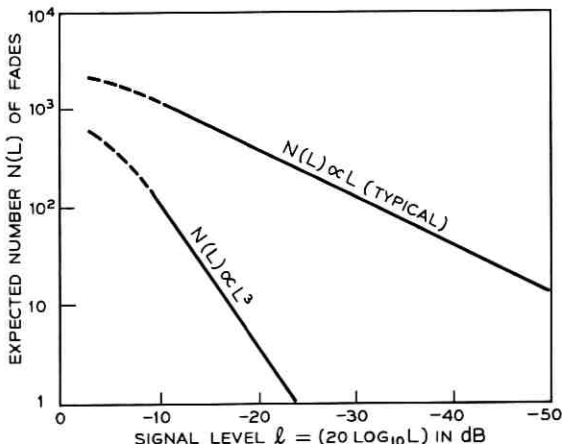


Fig. 5—Number of fades below signal level L .

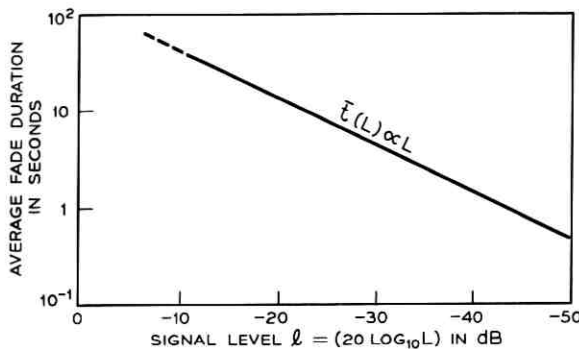


Fig. 6—Average duration of fades below signal level L .

- (iii) The experimental data of $N(L)$ of composite fading signals of most dual diversity systems also follows the cubic power law, $N(L) \propto L^3$, in the deep-fade region.
- (iv) The available experimental data on average fade duration $\bar{t}(L)$ all obey the universal power law, $\bar{t}(L) \propto L$, in the deep-fade region. This includes the fading signals of nondiversity systems, diversity systems, long radio links, and short radio links.

In summary:

- (i) Our theory indicates that if the joint probability density function $f(\alpha, \beta)$ of the resultant interfering vector, $Re^{i\theta} = \alpha + j\beta$, is a smooth function which is neither singular nor zero at the infinite fade point ($\alpha = -1, \beta = 0$), then for small L

$$N(L) \simeq \pi a_o f(-1, 0) L \propto L,$$

where a_o is a constant approximately equal to the average positive derivative of the amplitude of the fading signal in the deep-fade region.

- (ii) If $f(\alpha, \beta)$ is singular or zero at ($\alpha = -1, \beta = 0$) then

$$N(L) \simeq \pi H(-1, 0) a_o L^{2\mu-1} \propto L^{2\mu-1}$$

for $\mu \geq 1/2$ and small L . The cubic power law, $N(L) \propto L^3$, of dual diversity systems and short radio links can be explained by this result when $\mu = 2$, which means $f(-1, 0)$ is zero or is negligibly small.

- (iii) The theory predicts that the average fade duration always obeys the power law $\bar{t}(L) \propto L$ for small L no matter whether $f(\alpha, \beta)$ is

smooth, singular or zero at ($\alpha = -1, \beta = 0$). This means the power law, $t(L) \propto L$, is invariant with respect to variations of fading environment and diversity combinations of fading signals. This prediction agrees with the available experimental data.

- (iv) The theoretical results on $N(L)$ and $\bar{t}(L)$ for the one-echo model are shown to be incompatible with the experimental data of most overland microwave radio links. Therefore, the one-echo model is not suitable for the study of the statistics of fading signals of these radio links.
- (v) For line-of-sight radio links at 4 GHz and 6 GHz, the average positive derivative of the amplitude of the fading signal is estimated to range from 2×10^{-3} to 4×10^{-3} times V_{ref} per second, where V_{ref} is the signal level when there is no interference.

II. GENERAL FORMULATION FOR NUMBER OF FADES

The general expression for the expected number of fades per unit time of a random signal $V(t)$, below signal level L has been shown^{26,27,4} to be

$$N(L) = \int_{\dot{V}=0}^{\dot{V}=\infty} \dot{V} p(\dot{V}, V) |_{V=L} d\dot{V}, \quad (72)$$

where $\dot{V} = dV/dt$, and $p(\dot{V}, V)$ is the joint probability density of \dot{V} and V . For the sake of completeness, a brief derivation of (72) is included in Appendix E.

The joint probability density function $p(\dot{V}, V)$ can be written in terms of conditional probability²⁸ as

$$p(\dot{V}, V) = p_1(\dot{V} | V)p_2(V), \quad (73)$$

where $p_1(\dot{V} | V)$ is the conditional probability density of \dot{V} under the condition that the signal level is V ; and $p_2(V)$ is the probability density of V . Substituting (73) into (72) yields

$$N(L) = p_2(L) \int_{\dot{V}=0}^{\dot{V}=\infty} \dot{V} p_1(\dot{V} | L) d\dot{V}. \quad (74)$$

Let us define

$$\bar{V}_+(L) = 2 \int_{\dot{V}=0}^{\dot{V}=\infty} \dot{V} p_1(\dot{V} | L) d\dot{V}. \quad (75)$$

The physical meaning of the definition (75) is that $\bar{V}_+(L)$ is the conditional average positive derivative of V under the condition $V = L$.

The factor 2 in (75) is based upon the assumption that $p_1(\dot{V} | L)$ is symmetric about $\dot{V} = 0$.

Since $V(t)$ is a random fading signal, at a given signal level L , the value of its time derivative \dot{V} is also random. In general, the conditional average positive derivative $\bar{V}_+(L)$ is a function of signal level L .

By using definition (75), equation (74) becomes

$$N(L) = \frac{1}{2}\bar{V}_+(L)p_2(L). \quad (76)$$

Or, equivalently,

$$N(L) = \frac{1}{2}\bar{V}_+(L) \frac{\partial}{\partial L} P(V \leq L), \quad (77)$$

which indicates $N(L)$ proportional to the conditional average positive derivative of the fading signal and to the probability density of fades at $V = L$.

III. GENERAL FORMULATION FOR AVERAGE FADE DURATION

In a long time interval, T , containing a large number of fades,* the expected total length of time that the random signal $V(t)$ spends below a specified signal level L is

$$t(L) = TP(V \leq L). \quad (78)$$

The expected number of fades below L in this interval T is $TN(L)$. Therefore, the average duration of fades below L is

$$\bar{t}(L) = \frac{t(L)}{TN(L)} = \frac{P(V \leq L)}{N(L)}. \quad (79)$$

Substituting (77) into (79) yields

$$\bar{t}(L) = \frac{1}{\bar{V}_+(L)} \frac{2P(V \leq L)}{\frac{\partial}{\partial L} P(V \leq L)}. \quad (80)$$

Equation (80) shows that the average fade duration is inversely proportional to the conditional average positive derivative of the fading signal at $V = L$.

* In our experiment on line-of-sight radio links, the typical time interval T is a whole summer of more than 100 days in which there are more than 500 fades below -10 dB relative to the nonfaded signal level.

IV. ASSUMPTION ON CONDITIONAL AVERAGE POSITIVE DERIVATIVE

Most existing theoretical work on $N(L)$ assumes that V and \dot{V} are independent so that $\bar{V}_+(L)$ becomes a constant which is independent of signal level L . In this paper we include the situation for which V and \dot{V} are dependent and assume that $\bar{V}_+(L)$ can be expanded into a Taylor series in the deep-fade region (i.e., small L); then

$$\bar{V}_+(L) = a_0 + a_1 L + a_2 L^2 + a_3 L^3 + \dots, \quad (81)$$

where

$$a_0 = \lim_{L \rightarrow 0^+} \bar{V}_+(L) = \bar{V}_+(0^+), \quad (82)$$

$$a_1 = \lim_{L \rightarrow 0^+} \frac{\partial}{\partial L} \bar{V}_+(L), \quad (83)$$

$$a_2 = \frac{1}{2!} \lim_{L \rightarrow 0^+} \frac{\partial^2}{\partial L^2} \bar{V}_+(L), \quad \text{etc.} \quad (84)$$

The justification for this assumption is not trivial, and includes the following considerations:

- (i) The theoretical results based on this assumption agree with the available experimental data.
- (ii) For a complex Gaussian model, the conditional probability density function $p_1(\dot{V} | L)$ is known. Then with the help of the work of Rice^{26,27} the integration indicated in (75) for $\bar{V}_+(L)$ can be carried out in closed form. These explicit expressions are discussed in Section III of Part 3. The results of this model show that if the power spectrum of the Gaussian noise is symmetric with respect to the frequency of the sine wave (i.e., the constant unit vector), then $\bar{V}_+(L) \equiv a_0$ is a constant independent of L . On the other hand, if the power spectrum of the Gaussian noise is asymmetric with respect to the signal frequency, then $\bar{V}_+(L)$ is a function of L and the nonconstant terms in equation (81) cannot be omitted.

The theoretical work of Clarke,²⁹ Ossanna,³⁰ and Gans³¹ on mobile radio indicate that the power spectrum of the fading signal is generally asymmetric with respect to the received carrier frequency unless the straight line joining the base station and the mobile antenna is perpendicular to the velocity of the mobile and the antenna pattern is symmetric with respect to this line. Therefore, the work on asymmetric power spectrum, and hence nonconstant $\bar{V}_+(L)$, is not purely academic.

- (iii) It is known¹⁸ that the correlation between any real random variable $\epsilon(t)$ at instant t and its time derivative $\dot{\epsilon}(t + \xi)$ at instant $(t + \xi)$ vanishes if $\xi = 0$. This is often used to support the assumption that V and \dot{V} are independent and hence $\bar{V}_+(L)$ is a constant. However, we know that the vanishing of correlation between $V(t)$ and $\dot{V}(t + \xi)$ at $\xi = 0$ does not imply the independency of V and \dot{V} unless V is normally distributed. Including high-order terms in equation (81) removes the assumption of independency of V and \dot{V} and enlarges the applicable scope of this theory.
- (iv) In equations (82), (83), and (84) we define those coefficients of the Taylor series as the limits of $\bar{V}_+(L)$ and its L -derivatives at $L = 0^+$ from the positive side. The reason is that $V(t)$ is the absolute value of a fluctuating complex signal; i.e.,

$$V(t) = |x + jy| = |Ve^{j\phi}|.$$

When the complex fluctuating signal $V(t)e^{j\phi(t)}$ crosses zero, its absolute value $V(t)$ may have a cusp at $V = 0$ as shown in Fig. 7. Therefore, the derivatives of $V(t)$ may not be well defined at $V = 0$. However, the limits of the derivatives at $V = 0^+$ from the positive side are well defined.

- (v) Fig. 7 also shows that although $V = 0$ is a minimum of $V(t)$,

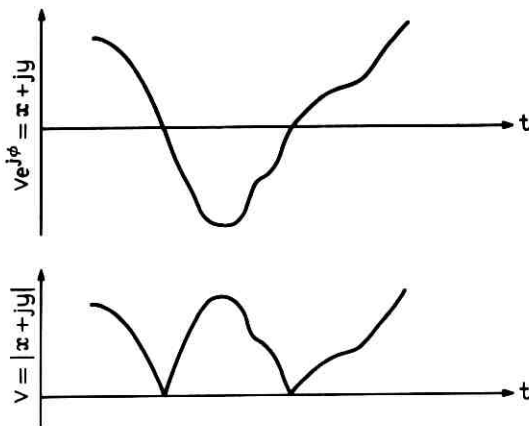


Fig. 7—The amplitude $V(t)$ may have a cusp at $V = 0$ even though the complex fading signal is a smooth time function. For convenience, the complex fading signal is plotted as a real function in this example.

$\dot{V}(t) = d/dt V(t)$ may not be zero at $V = 0^+$. Therefore, in equation (81), the constant term $a_0 = \bar{V}_+(0^+)$ does not vanish for most cases, and cannot be omitted from equation (81).

V. POWER SERIES FORM OF $N(L)$

Substituting the power series (35) for $(\partial/\partial L) P(V \leq L)$ of Part 1 and the power series (81) for $\bar{V}_+(L)$ into equation (77) yields

$$N(L) = \pi H(-1, 0)a_0 L^{2\mu-1} + \pi H(-1, 0)a_1 L^{2\mu} + \dots \quad (85)$$

In the deep-fade region, the leading term dominates the power series (85). Therefore,

$$N(L) \cong \pi H(-1, 0)a_0 L^{2\mu-1}, \quad \text{for small } L; \quad (86)$$

$$\therefore N(L) \propto L^{2\mu-1}, \quad \text{for small } L. \quad (87)$$

Equations (85) and (86) show that if $a_0 \neq 0$ and if $\mu < 1/2$, then $N(L) \rightarrow \infty$ as $L \rightarrow 0$. This seems to be nonphysical. Therefore, we require that $\mu \geq 1/2$. This is the reason we impose this condition on the order of singularity of $f(\alpha, \beta)$ in Section IV of Part 1.*

5.1 Prevailing Power Law of Number of Deep Fades

For the nondiversity fading signals of most radio links, the probability density function $f(\alpha, \beta)$ of the resultant interfering signal is a smooth function which is neither singular nor zero at $(\alpha = -1, \beta = 0)$. Then $\mu = 1$ and $f(\alpha, \beta) = H(\alpha, \beta)$. Equations (85), (86), and (87) under this condition become

$$N(L) = \pi f(-1, 0)a_0 L + \pi f(-1, 0)a_1 L^2 + [2a_0 d_4 + \pi f(-1, 0)a_2]L^3 + \dots \quad (85')$$

$$N(L) \cong \pi f(-1, 0)a_0 L, \quad \text{for small } L. \quad (86')$$

$$N(L) \propto L, \quad \text{for small } L. \quad (87')$$

It is seen that as long as $\infty > f(-1, 0) > 0$, then the expected number $N(L)$ of deep fades always obeys the prevailing power law (86'). With reference to Fig. 5, the straight lines corresponding to the power law (87') have inverse slopes of 20 dB per decade.

* If we assume that $a_0 = 0$, then the only constraint on μ is $\mu > 0$ due to the unity total probability. However, assuming $a_0 = 0$ implies that the time derivative of \bar{V} is always zero at $V = 0$. Such an assumption is unreasonable for multipath interference fading, but may be useful if the effects of random circuit interruptions, such as equipment failure, are included in the signal fading problem.

Apparently, the simple condition is easily satisfied by the nondiversity fading signals of most microwave radio links because the experimental¹⁻⁶ data of $N(L)$ are mostly characterized by the inverse slope of 20 dB per decade in the deep-fade region.

As L increases from zero towards unity, equation (85') indicates that there may be a transition point beyond which high-order terms become significant and the slope begins to deviate.

For most microwave radio links, the transition points of $N(L)$ seem to be well above -10 dB. However, our latest experimental data show that the first transition point of $N(L)$ of a relatively short path (path length 15.87 miles, $f = 4$ GHz) is below -20 dB. The inverse slope of $N(L)$ in the region from -10 dB to -20 dB is approximately 20/3 dB per decade of number of fades. This indicates that the third term $[2a_0 d_4 + \pi a_2 f(-1, 0)]L^3$ dominates in the region $0.3 > L > 0.1$ for this path.

VI. AVERAGE DURATION OF DEEP FADES

Substituting the power series (31) of $P(V \leq L)$ of Part 1 and the power series (85) of $N(L)$ into equation (79) yields

$$\bar{t}(L) = \frac{\frac{\pi H(-1, 0)}{\mu} L^{2\mu} + d_4 L^{2\mu+2} + d_6 L^{2\mu+4} + \dots}{\pi H(-1, 0) a_0 L^{2\mu-1} + \pi H(-1, 0) a_1 L^{2\mu} + \dots}. \quad (88)$$

In the deep-fade region, equation (88) becomes

$$\bar{t}(L) \cong \frac{1}{\mu a_0} L, \quad \text{for small } L; \quad (89)$$

$$\therefore \bar{t}(L) \propto L, \quad \text{for small } L. \quad (90)$$

On Fig. 6, the straight lines corresponding to the power law (90) have an inverse slope of 20 dB per decade of fade duration. The experimental data¹⁻⁶ agree with this conclusion on the slope of $\bar{t}(L)$ when plotted on Fig. 6.

VII. INVARIANCE OF POWER LAW OF AVERAGE FADE DURATION*

Equations (36), (87), and (90) show that in general $P(V \leq L)$, $N(L)$, and $\bar{t}(L)$ obey the following set of power laws of deep fades:

* In equation (26) of Ref. 32, Rice has already predicted that the power law $\bar{t}(L) \propto L$ for small L may be applicable to cases more general than the complex Gaussian model even though most of his work in Ref. 32 is devoted to the statistics of a sine wave plus a narrowband Gaussian noise.

$$\left. \begin{aligned} P(V \leq L) &\propto L^{2\mu} \\ N(L) &\propto L^{2\mu-1} \end{aligned} \right\} \quad (91)$$

$$\text{for } \mu \geq \frac{1}{2} \text{ and small } L. \quad (92)$$

$$\bar{l}(L) \propto L \quad (93)$$

It is seen that the power laws of $P(V \leq L)$ and $N(L)$ depend on the value of μ which depends on whether $f(\alpha, \beta)$ is smooth, singular, or zero at $(\alpha = -1, \beta = 0)$. On the other hand, the power law (93) for the average fade duration is invariant with respect to μ . Since the behavior of $f(\alpha, \beta)$, and hence the value of μ , depends on fading environment, we conclude that the power law (93) for the average fade duration is insensitive to the fading environment in contrast to the power laws of $P(V \leq L)$ and $N(L)$.

In equation (89), notice that μa_o , and hence $\bar{l}(L)$, does depend on the fading environment. However, it is the *power law*, $\bar{l}(L) \propto L$, which is insensitive to the fading environment.

Vigants,^{4,5,6} Crawford, Hogg, and Kummer¹² have investigated the effects of diversity on $P(V \leq L)$, $N(L)$ and $\bar{l}(L)$. The theoretical results and the experimental results of these authors show that in the deep-fade region, the diversity drastically changes the power laws of $P(V \leq L)$ and $N(L)$ but does not affect the power law $\bar{l}(L) \propto L$. For example, the results of Vigants are shown in Table I. From this table it is seen that the power laws of $P(V \leq L)$ and $N(L)$ depend on the diversity combination of fading signals, whereas the power law, $\bar{l}(L) \propto L$, of average fade duration is invariant.

VIII. INCOMPATIBILITY BETWEEN ONE-ECHO MODEL AND OVERLAND RADIO LINKS

Equations (60), (61), (91), (92), and (93) show that $p(L)$, $N(L)$, and $\bar{l}(L)$ of the one-echo model (with equal magnitudes, $A = 1$) in the

TABLE I—EFFECTS OF DIVERSITY ON POWER LAWS OF DEEP FADES

	Nondiversity	Diversity
$P(V \leq L)$	L^2	$(1/q) L^4$
$N(L)$	cL	$(2c/q) L^3$
$\bar{l}(L)$	$(1/c) L$	$(1/2c) L$

Remark: In this table, the parameter, c , as defined by Vigants, is equal to a_0 of this paper; and the parameter, q , as defined by Vigants, is equal to $2/\pi H(-1, 0)$ of this paper.

deep-fade region are

$$\left. \begin{aligned} p(L) &\propto L^0 \\ N(L) &\propto L^0 \end{aligned} \right\} \quad (94)$$

$$l(L) \propto L \quad (95)$$

$$(L) \propto L \quad (96)$$

On the other hand, the long-term experimental data of a nondiversity signal of most overland microwave radio links indicate that

$$p(L) \propto L \quad (97)$$

$$\left. \begin{aligned} N(L) &\propto L \\ l(L) &\propto L \end{aligned} \right\} \quad \text{for small } L. \quad (98)$$

$$(L) \propto L \quad (99)$$

The experimental results (97) and (98) disagree with (94) and (95) of the one-echo model.

In view of this disagreement, we may want to check the effect of the assumption (81) of $\bar{V}_+(L)$ on the theoretical results of the one-echo model. Although we know that the constant term a_0 of (78) generally does not vanish, yet we may deliberately set $a_0 = 0$ and see what kind of theoretical results we get.

If we do so, the theoretical results of the one-echo model become

$$\left. \begin{aligned} p(L) &\propto L^0 \\ N(L) &\propto L \end{aligned} \right\} \quad (100)$$

$$l(L) \propto L \quad (101)$$

$$(L) \propto L^0 \quad (102)$$

Under this modified assumption, $p(L)$ and $\bar{l}(L)$ of the one-echo model disagree with the experimental results (97) and (99). Similarly, forcing the coefficients of other higher order terms of (81) to zero also yields theoretical results which disagree with the experimental results. Therefore, we conclude that the one-echo model is not suitable for the study of the fading signals of most overland microwave radio links.

However, we emphasize that the experimental data mentioned in this section are restricted to the long-term data of overland microwave radio links. Therefore, the incompatibility of the one-echo model with these data does not necessarily exclude the use of this model for the study of other fading problems.

IX. APPROXIMATE AVERAGE POSITIVE DERIVATIVE \bar{V}_+ OF LINE-OF-SIGHT MICROWAVE RADIO LINKS

For line-of-sight microwave radio links, let V_{ref} be the signal level when there is no interference, and $V_{fad}(t)$ be the random fading signal when the interference appears. In our analysis

$$V(t) = \frac{V_{fad}(t)}{V_{ref}} \quad (103)$$

is a normalized fading signal.

By comparing the experimental data of $\bar{t}(L)$ and the theoretical equation (89) for $\bar{t}(L)$, we can estimate the value of a_o of the radio link. The value of μ in equation (89) can be determined from the experimental data on the power laws (36) and (86) for $P(V \leq L)$ and $N(L)$ of the same radio link.

Our experimental data of several line-of-sight microwave radio links in Ohio and Georgia indicate that the value of a_o ranges from 2×10^{-3} to 4×10^{-3} . In the deep-fade region where L is small, equation (81) shows that $\bar{V}_+(L) \cong a_o$.

$$\left| \frac{d}{dt} V(t) \right|_{\text{average}} \cong a_o = 2 \times 10^{-3} \sim 4 \times 10^{-3}. \quad (104)$$

Substituting (103) into (104) yields

$$\left| \frac{d}{dt} V_{fad}(t) \right|_{\text{average}} \cong (2 \times 10^{-3} \sim 4 \times 10^{-3}) \cdot V_{ref}. \quad (105)$$

Thus, the average positive derivative of the unnormalized fading signal, $V_{fad}(t)$, of these microwave radio links ranges from 2×10^{-3} to 4×10^{-3} times V_{ref} per second.

These approximate values of average positive derivative are valid only in the deep-fade region because they are deduced from the experimental data of deep fades. The path length of these radio links ranges from 15 miles to 36 miles. The operating frequencies are in 4-GHz and 6-GHz bands.

X. GENERALIZED ASSUMPTION ON $\bar{V}_+(L)$

In Part 1, we indicated that the assumption of the Taylor series expansion of $H(\alpha, \beta)$ is not strictly necessary for the validity of the power law of $P(V \leq L)$ deduced from the experimental data. In this section, we point out that the assumption of the Taylor series expansion

of $\bar{V}_+(L)$ in Section IV of this part is also not strictly necessary for the validity of the power laws of $N(L)$ and $\bar{t}(L)$. From a theoretical viewpoint, the assumption of $\bar{V}_+(L)$ can be generalized to the following form:

$$\bar{V}_+(L) = a_0 + O(L^\eta), \quad \eta > 0 \quad (106)$$

where $O(L^\eta)$ is a symbol to denote the component which goes to zero at a rate equal to or faster than that of L^η as $L \rightarrow 0$.

In assumption (106), we do not require the existence of the limits in equations (83), (84), etc. Therefore, the assumption (106) is less restrictive than the assumption (81). It can be shown that the power laws of $N(L)$ and $\bar{t}(L)$ of deep fades based on (106) are the same as those based on (81). However, at the present time, we do not have any practical evidence to necessitate the use of (106). Therefore, we merely point out the possibility but do not explicitly carry out this generalized analysis.

Part 3. Special Topics on Statistics of a Fading Signal

Contents

	<i>Page</i>
I. Introduction and Summary.....	3243
II. Sum of n Unit Vectors with Uniform Random Phases.....	3245
III. A Sine Wave Plus a Gaussian Noise.....	3247
3.1 Amplitude Distribution of Deep Fades.....	3248
3.2 Symmetric Power Spectrum and Constant $\bar{V}_+(L)$	3248
3.3 Asymmetric Power Spectrum and Nonconstant $\bar{V}_+(L)$	3250
IV. m -Distributions, Chi-Distributions, and Rayleigh Distribution.....	3251
4.1 Log Normal Behavior of m -Distribution Near the RMS Value.....	3252
V. Nonunique Relation Between Amplitude Distribution and $f(\alpha, \beta)$	3253
VI. Physical Model and Rayleigh Distribution.....	3254
6.1 Number of Interfering Signals.....	3254
6.2 Mean values of x and y	3255

I. INTRODUCTION AND SUMMARY

In Parts 1 and 2, the analysis was oriented towards an explanation of the experimentally observed common behavior of a fading signal $Ve^{i\phi}$. The basic assumptions of the theoretical model are kept to a minimum in order to include the widest possible variation in practical fading environments. During the development of this general analysis, we have gained a new insight into several topics related to fading signals as investigated by previous authors.

Part 3 of this paper is a collection of theoretical treatments of several special topics relating our generalized analysis to the work of previous authors. These topics include the sum of n unit vectors with random phases; a sine wave plus Gaussian noise, m -distributions, chi-distribution, Rayleigh distribution, and log normal distribution.

In summary:

- (i) In Section II of this part, the results of Part 1 are applied to find the amplitude distribution of the sum of n unit vectors with uniformly distributed random phases. For $n \geq 3$, the analysis shows that the amplitude distribution always follows the square law $P(V \leq L) \propto L^2$ for small L . On the other hand, when $n = 2$, the amplitude distribution follows the power law $P(V \leq L) \propto L$ for small L .
- (ii) In Section III, we investigate the model of a sine wave plus a narrowband Gaussian noise for the fading signal. By using the closed-form solutions of Rice, it is shown that if the power spectrum of the Gaussian noise is symmetric with respect to the frequency of the sine wave, then the amplitude V and its time derivative \dot{V} are independent; and the conditional average positive derivative $\bar{V}_+(L)$ is a constant. On the other hand, if the power spectrum is not symmetric, then V and \dot{V} are dependent; and the conditional average positive derivative $\bar{V}_+(L)$ is a function of signal level $V = L$.

As an example, the fading signal spectral density of a mobile radio is generally not symmetric with respect to the received carrier frequency. Therefore, in the analysis of $N(L)$ and $\bar{t}(L)$, it is not safe to assume that V and \dot{V} are always independent.

- (iii) In Section IV, we investigate the theoretical condition (147) on the joint probability density function $f(\alpha, \beta)$ of the interfering vector such that the amplitude distribution of the fading signal belongs to the family of m -distributions which includes normal distribution, Rayleigh distribution, Maxwell distribution, and all of chi-distributions as special cases.

It is also shown that the set of m -distributions behave like a log normal distribution within a small range (148) of signal level near its rms value. This result shows that in the interpretation of the experimental data, one must be cautious in attempting to estimate the tails of the distribution by an extension from the middle section of the distribution.

- (iv) We find that in general, the integral transformation (20) from

$f(\alpha, \beta)$ into $P(V \leq L)$ is not unique. Physically this means the signals of fading environments with different $f(\alpha, \beta)$ can have the same amplitude distribution $P(V \leq L)$. As an example, this nonuniqueness shows that specifying a Rayleigh distribution for $P(V \leq L)$ does not necessarily imply that there are a large number of interfering signals; nor does it necessarily imply that the real and imaginary parts of the fading signal are normally distributed with zero mean.

II. SUM OF n UNIT VECTORS WITH UNIFORM RANDOM PHASES

The amplitude distribution of the sum of two unit vectors with uniformly distributed random relative phase has been shown in Section IX of Part 1 to be, for $0 \leq L \leq 2$,

$$P(V \leq L) = \frac{1}{\pi} \cos^{-1} \left(1 - \frac{L^2}{2} \right), \quad (107)$$

and

$$p(L) = \frac{\partial}{\partial L} P(V \leq L) = \frac{1}{\pi} \frac{1}{\left[1 - \left(1 - \frac{L^2}{2} \right)^2 \right]^{\frac{1}{2}}}. \quad (108)$$

In the deep-fade region where L is small, this amplitude distribution obeys the power law

$$P(V \leq L) \propto L. \quad (109)$$

The sum of n unit vectors with uniformly distributed random phases has been investigated previously by many authors.^{33,34-37} The mathematics involved in obtaining the amplitude distribution for any arbitrary $n \geq 3$ is fairly complicated. Computer numerical integration is needed to show the distribution explicitly. In this section, we shall avoid the complicated mathematics and shall apply the results of Part 1 to show that the amplitude distribution for any arbitrary $n \geq 3$ in the deep-fade region always follows the square law:

$$P(V \leq L) \propto L^2, \quad \text{for small } L. \quad (110)$$

The sum of n unit vectors with random phases can be written as

$$Ve^{i\phi} = \sum_{i=1}^{i=n} e^{i\theta_i} \quad (111)$$

$$= \left[1 + \sum_{i=2}^{i=n} e^{i(\theta_i - \theta_1)} \right] e^{i\theta_1} \quad (112)$$

$$= [1 + Re^{i\theta}]e^{i\theta_1}, \quad (113)$$

where

$$Re^{i\theta} = \sum_{i=2}^{i=n} e^{i(\theta_i - \theta_1)}. \quad (114)$$

Rosenbaum³⁸ has indicated that if all the phases $\{\theta_i\}_{i=1}^{i=n}$ of the unit vectors are independently and uniformly distributed in $(0, 2\pi)$, then $Ve^{i\phi}$ and $Re^{i\theta}$ have circular symmetric probability density functions; i.e., the amplitude and the phase are independent and the phase is uniformly distributed in $(0, 2\pi)$.

It then follows that the random signal represented by equation (113) for any arbitrary $n \geq 3$ is a special case of Appendix B. The case for $n = 2$ is an exception because the joint probability density function $g(R, \theta)$ contains a delta function whereas the $g(R, \theta)$ in Appendix B is assumed to be a smooth function.

The sum of three unit vectors can be considered as a unit vector suffering interference by a random vector $R(t)e^{i\theta(t)}$ which is the sum of the other two unit vectors. The amplitude distribution $g(R)$ of $R(t)$ is given by equation (108) except for the replacement of the notation L by R . Equation (108) implies

$$g(1) = \frac{2}{\pi\sqrt{3}}. \quad (115)$$

Therefore, $g(R)$ for this case is a smooth function which is neither singular nor zero at $R = 1$. Then equation (165) shows that

$$P(V \leq L) \cong \frac{1}{2}g(1)L^2 = \frac{1}{\pi\sqrt{3}}L^2 \propto L^2. \quad (116)$$

The sum of n unit vectors, $n \geq 3$, can be considered as a unit vector suffering interference for a random vector $R(t)e^{i\theta(t)}$ which is the sum of the other $(n - 1)$ unit vectors. It is obvious that $g(1) \neq 0$ simply because each of the $(n - 1)$ unit vectors has unity amplitude. Then, the results (see Appendix B) imply

$$P(V \leq L) \propto L^2, \quad \text{for small } L \text{ and } n \geq 3. \quad (117)$$

On a log-versus-dB graph paper, as shown in Fig. 1, the power law (109) implies a straight line with an inverse slope of 20 dB per decade of probability whereas the square law (117) implies a straight line with the same inverse slope of 10 dB per decade of probability as that of Rayleigh distribution.

Therefore, we conclude that for $n = 2$, the distribution of deep fades

is characterized by the inverse slope of 20 dB per decade of probability whereas for any $n \geq 3$, the distribution of deep fades is always characterized by the inverse slope of 10 dB per decade of probability. This conclusion agrees with the numerical results of Norton, et al., in Fig. 2 of Reference 33.

III. A SINE WAVE PLUS A GAUSSIAN NOISE

The statistical behavior of a sine wave plus narrowband Gaussian random noise has been investigated in great detail by Rice.^{26-27,32} In this section we shall apply our general analysis to this case to show the consistency of our results with the work of Rice. Furthermore, we shall also use the closed-form solution of $N(L)$ and $\bar{t}(L)$ obtained by Rice to show that the conditional average positive derivative $\bar{V}_+(L)$ can be either a constant or a function of signal level L , depending on whether the power spectrum of the noise is symmetric or asymmetric with respect to the frequency of the sine wave.

In this model, the interfering vector, $Re^{i\theta} = \alpha + j\beta$, represents the envelope of a narrowband Gaussian noise; the constant vector represents the sine wave with a constant amplitude and frequency f_a . The joint probability density function $f(\alpha, \beta)$ is a two-dimensional normal density function; i.e.,

$$f(\alpha, \beta) = \frac{1}{2\pi b_0} \exp [-(\alpha^2 + \beta^2)/2b_0], \quad (118)$$

where α and β are assumed to be independent normal random variables with the same variance b_0 and zero mean.

The well known Rice distribution for the amplitude of this model is

$$p(L) = \frac{\partial}{\partial L} P(V \leq L) = \frac{L}{b_0} I_0\left(\frac{QL}{b_0}\right) \exp\left(\frac{-L^2 - Q^2}{2b_0}\right), \quad (119)$$

where $I_o(\sim)$ is the modified Bessel function of zeroth order, and Q is the magnitude of the sine wave. In our analysis, $Q = 1$ because all the signals are normalized to the magnitude of the constant vector.

Rice²⁷ has also shown that the joint probability density function $p(\dot{V}, V)$ for this model is

$$\begin{aligned} p(\dot{V}, V) = & \frac{V}{(2\pi)^{\frac{3}{2}} \sqrt{Bb_0}} \int_{-\pi}^{\pi} \exp \left\{ \frac{-1}{2Bb_0} [B(V^2 - 2VQ \cos \phi + Q^2) \right. \\ & \left. + (b_0 \dot{V} + b_1 Q \sin \phi)^2] \right\} d\phi, \end{aligned} \quad (120)$$

where ϕ is the phase of the resultant fading signal $Ve^{i\phi}$; f_a is the frequency of the sine wave, $w(f)$ is the power spectrum of the Gaussian noise, and

$$b_n = (2\pi)^n \int_0^\infty w(f)(f - f_a)^n df, \quad n = 0, 1, 2, \quad (121)$$

$$B = b_0 b_2 - b_1^2. \quad (122)$$

3.1 Amplitude Distribution of Deep Fades

The normal density function (118) is obviously a smooth function which is neither singular nor zero at the infinite fade point ($\alpha = -1$, $\beta = 0$). Then the results of Section VI of Part 1 predict that the amplitude distribution of the fading signal in the deep-fade region is

$$P(V \leq L) \cong \pi f(-1, 0) L^2 \quad (123)$$

$$\cong \frac{1}{2b_0} \exp\left(\frac{-1}{2b_0}\right) \cdot L^2. \quad (124)$$

On the other hand, the limiting form of the Rice distribution for small L is

$$p(L) \cong \frac{L}{b_0} \exp\left(\frac{-Q^2}{2b_0}\right); \quad (125)$$

$$\therefore P(V \leq L) \cong \frac{1}{2b_0} \exp\left(\frac{-Q^2}{2b_0}\right) \cdot L^2, \quad \text{for } L \ll Q = 1. \quad (126)$$

It is seen that our result (124) agrees with the Rice distribution in the deep-fade region.

The square law (124) implies that on a log-versus-dB graph paper, the Rice distribution in the deep-fade region is always characterized by the prevailing inverse slope of 10 dB per decade of probability. The numerical results of Norton, et al., in Fig. 5 of Reference 33 agree with this prediction.

3.2 Symmetric Power Spectrum and Constant $\bar{V}_+(L)$

If the power spectrum $w(f)$ of the Gaussian noise is symmetric about f_a , then $b_1 = 0$ and the integration of (120) under this condition yields

$$p(\dot{V}, V) = \left\{ \frac{1}{\sqrt{2\pi b_2}} \exp\left[\frac{-\dot{V}^2}{2b_2}\right] \right\} \left\{ \frac{V}{b_0} I_0\left(\frac{QV}{b_0}\right) \exp\left[\frac{-V^2 - Q^2}{2b_0}\right] \right\} \quad (127)$$

$$= p_1(\dot{V} | V)p_2(V) \quad (128)$$

$$= p_3(\dot{V})p_2(V), \quad (129)$$

where

$$p_2(V) = \frac{V}{b_0} I_0\left(\frac{QV}{b_0}\right) \exp\left[\frac{-V^2 - Q^2}{2b_0}\right] \quad (130)$$

is the Rice distribution for V ;

$$p_3(\dot{V}) = \frac{1}{\sqrt{2\pi b_2}} \exp\left[\frac{-\dot{V}^2}{2b_2}\right] \quad (131)$$

is a normal density function for \dot{V} ; and

$$b_2 = \frac{B}{b_0} = \dot{V}_{rms}^2 \quad \text{when } b_1 = 0. \quad (132)$$

Equations (127) and (129) show that if the power spectrum is symmetric about f_a , then the envelope V and its time derivative \dot{V} are independent, and \dot{V} is normally distributed.

Substituting (131) and (132) into the definition (75) for $\bar{V}_+(L)$ yields

$$\bar{V}_+(L) = \frac{2\dot{V}_{rms}}{\sqrt{2\pi}} = a_0 = \text{constant}. \quad (133)$$

Therefore, the conditional average positive derivative $\bar{V}_+(L)$ for this model is a constant if the power spectrum is symmetric about f_a .

Substituting (130) and (133) into the general expression (76) for $N(L)$ yields

$$N(L) = \frac{\dot{V}_{rms}}{\sqrt{2\pi}} \frac{L}{b_0} I_0\left(\frac{QL}{b_0}\right) \exp\left[\frac{-L^2 - Q^2}{2b_0}\right] \quad (134)$$

$$= \frac{1}{2} a_0 p_2(L). \quad (135)$$

Then

$$l(L) = \frac{P(V \leq L)}{N(L)} = \frac{2 \int_0^L p_2(V) dV}{a_0 p_2(L)}. \quad (136)$$

In the deep-fade region where $L \ll Q = 1$,

$$N(L) \cong \frac{\dot{V}_{rms}}{\sqrt{2\pi}} \frac{1}{b_0} \exp\left[\frac{-Q^2}{2b_0}\right] \cdot L \quad (137)$$

$$\cong \pi a_0 f(-1, 0) L, \quad (138)$$

$$l(L) \cong \frac{1}{a_0} L. \quad (139)$$

It is seen that equations (138) and (139) agree with equations (86') and (89) of Part 2.

3.3 Asymmetric Power Spectrum and Nonconstant $\bar{V}_+(L)$

If the power spectrum $w(f)$ is not symmetric about f_a , then V and \dot{V} are dependent and $b_1 \neq 0$. The joint probability density function $p(V, \dot{V})$ for this case cannot be written as the product of the individual probability density functions of V and \dot{V} . For this case, Rice²⁷ has obtained $N(L)$ by substituting (120) into the general expression (72) and carrying out the integration. This gives

$$N(L) = \frac{p_2(L) \sqrt{\frac{B}{b_0}}}{\sqrt{2\pi} I_0\left(\frac{QL}{b_0}\right)} \sum_{n=0}^{n=\infty} \frac{1}{2^n \cdot n!} \left(\frac{-b_0 \gamma^2}{QL}\right)^n \\ \cdot \left[I_n\left(\frac{QL}{b_0}\right) + \frac{b_0 \gamma^2}{QL} I_{n+1}\left(\frac{QL}{b_0}\right) \right], \quad (140)$$

where $I_n(\sim)$ is the modified Bessel function of order n , and

$$\gamma^2 = \frac{b_1 Q^2}{B b_0}. \quad (141)$$

Comparing equation (140) and the general expression (76) for $N(L)$ shows that

$$\bar{V}_+(L) = \frac{2\left(\frac{B}{2\pi b_0}\right)}{I_0\left(\frac{QL}{b_0}\right)} \sum_{n=0}^{n=\infty} \frac{1}{2^n \cdot n!} \left(\frac{-b_0 \gamma^2}{QL}\right)^n \\ \cdot \left[I_n\left(\frac{QL}{b_0}\right) + \frac{b_0 \gamma^2}{QL} I_{n+1}\left(\frac{QL}{b_0}\right) \right]. \quad (142)$$

It is seen that when V and \dot{V} are dependent, then the conditional average positive derivative $\bar{V}_+(L)$ is a function of signal level $V = L$.

The expected number of fades $N(L)$ and the average fade duration $\bar{t}(L)$ for this case in the deep-fade region are

$$N(L) \cong \pi a_0 f(-1, 0) L \\ \cong \frac{a_0}{2b_0} \exp\left(\frac{-Q^2}{2b_0}\right) \cdot L \\ \bar{t}(L) \cong \frac{1}{a_0} L,$$

where

$$a_0 = \lim_{L \rightarrow 0^+} \bar{V}_+(L) = \left(\frac{2B}{\pi b_0} \right)^{\frac{1}{2}} \sum_{n=0}^{\infty} \frac{(-\gamma^2)^n}{(2^n \cdot n!)^2} \left[1 + \frac{\gamma^2}{2(n+1)} \right].$$

The work of Clarke,²⁹ Ossanna,³⁰ and Gans³¹ on mobile radio indicates that the power spectrum of the fading signal is generally not symmetric with respect to the received carrier frequency unless the straight line joining the base station and the mobile antenna is perpendicular to the velocity of the mobile and the antenna pattern is symmetric with respect to this straight line. Therefore, in the theoretical work of $N(L)$ and $\bar{t}(L)$, it is not safe to assume that V and \dot{V} are always independent.

IV. *m*-DISTRIBUTIONS, CHI-DISTRIBUTIONS, AND RAYLEIGH DISTRIBUTION

In the study of the experimental data of amplitude distributions of short-term high-frequency long-distance propagations, Nakagami³² found that the set of experimental data can well be described by a family of *m*-distributions:^{*}

$$p(L) = \frac{2 \cdot m^m}{\Gamma(m) \Omega^m} L^{2m-1} \exp \left[\frac{-mL^2}{\Omega} \right], \quad (143)$$

where Ω is the mean square value of the fading signal. The operating frequency ranged from 10 MHz to 20 MHz and the path length from 1500 kilometers to 9000 kilometers. Nakagami indicated that these results were obtained from short records of data from three to seven minutes in length in order to avoid the effects of slow fading on the distribution of rapid fading.

The various properties of the *m*-distributions have been investigated in detail by Nakagami.³³ It is easily shown that the set of chi-distributions²⁸ is a subset of *m*-distributions by setting $2m =$ any positive integer in (143). This means the normal distribution, Rayleigh distribution, and Maxwell distribution are also special cases of *m*-distributions when $m = 1/2, 1$, and $3/2$ respectively. On Rayleigh paper, all the *m*-distributions appear to be straight lines passing through the common point of 50 percent at 0 dB, with different slopes which depend on the value of *m*. The graphical representation of *m*-distributions can be seen in Reference 39.

However, in Reference 39, one does not know the theoretical condition under which the amplitude distribution of a fading signal will

* To avoid possible confusion, we emphasize that the Nakagami distribution mentioned in Section I of Part 1 is not the *m*-distribution discussed in this section.

belong to this family of m -distributions. In this section we shall find the condition on the joint probability density function $f(\alpha, \beta)$ of the interfering vector such that the amplitude distribution $P(V \leq L)$ will belong to m -distributions.

Expanding the exponential function in equation (143) into a power series gives

$$p(L) = \frac{2 \cdot m^m}{\Gamma(m)\Omega^m} \sum_{s=0}^{S=\infty} \frac{1}{S!} \left(\frac{-m}{\Omega} \right)^s \cdot L^{2s+2m-1}. \quad (144)$$

Comparing equation (144) and the general power series (35) for $p(L)$ shows that

$$\mu = m, \quad (145)$$

$$(2S + 2\mu) d_{2s+2} = \frac{2(-1)^s}{\left(\frac{\Omega}{\mu} \right)^{s+\mu} \Gamma(\mu) \cdot S!}. \quad (146)$$

Substituting (34) into (146) gives

$$\frac{\pi}{2^{2s}} \sum_{\nu=0}^{\nu=S} \frac{H_{2s-2\nu, 2\nu}(-1, 0)}{(\nu!)(S-\nu)!} = \frac{(-1)^s}{\left(\frac{\Omega}{\mu} \right)^{s+\mu} \cdot \Gamma(\mu)}, \quad S = 0, 1, 2, \dots \quad (147)$$

Thus, equations (145) and (147) are the general conditions on the interfering vector such that $P(V \leq L)$ is an m -distribution.

In Section V of Part 2 we showed that $\mu \geq 1/2$ which implies $m \geq 1/2$. Nakagami³⁹ has also found this condition on the parameter m by a different approach. Since m can be any value $\geq 1/2$, equation (143) represents an infinitely large family of distributions.

4.1 Log Normal Behavior of m -Distribution Near the RMS Value

The experimental data of optical propagation⁴⁰⁻⁴² and line-of-sight radio links show that the distributions of the signal scintillation near its average value are approximately log normal. Usually the accuracy of experimental data is best in the middle section of the distribution and deteriorates towards the tails. It is quite tempting to estimate the tails of the distribution by an extension from the middle section. The deviations of the experimental data at the tails are often attributed to the experimental error.

However, de Wolf⁴⁰ and Deltz and Wright⁴² have pointed out that the use of the middle section of a log normal paper may not be a reliable test of the log normal distribution. The differentiation between the log

normal distribution and certain other distributions may be significant only at the tails rather than the middle section of these distributions.

Nakagami³⁹ has pointed out that all the m -distributions behave like a log normal distribution for the fading signal $V(t)$ in the neighborhood of its rms value $\sigma_R = \sqrt{\Omega}$. The explicit bounds on the signal level within which this approximation holds are:

$$20 \left| \log_{10} \frac{L}{\sqrt{\Omega}} \right| \ll 4.3 \text{ dB}. \quad (148)$$

It is shown in Appendix F that the m -distribution within the signal range (148) is approximately equal to

$$p(L) = \left[\frac{2m^m}{L \cdot \Gamma(m)} e^{-m} \right] \exp [-2m(\ln L - \ln \sqrt{\Omega})^2], \quad (149)$$

which is a log normal distribution for the signal level L .

Therefore, the m -distributions, including the normal distribution, Rayleigh distribution, Maxwell distribution, and chi-distributions, all behave like a log normal distribution within the signal range (148). This result points out that in the interpretation of the experimental data, one must examine the behavior of the data not only inside but also outside of the range (148) in order to assert their distribution.

V. NONUNIQUE RELATION BETWEEN AMPLITUDE DISTRIBUTION AND $f(\alpha, \beta)$

From the general integral relation (20) between $P(V \leq L)$ and $f(\alpha, \beta)$, it is seen that any component of $f(\alpha, \beta)$ that is antisymmetric with respect to $(1 + \alpha)$ and/or β will cancel out in the integration (20), and contributes nothing to $P(V \leq L)$. This means that there are many different $f(\alpha, \beta)$'s, with the same symmetric* part and different anti-symmetric* part, which correspond to the same amplitude distribution $P(V \leq L)$.

Mathematically, this means the integral transformation (20) from $f(\alpha, \beta)$ into $P(V \leq L)$ is not unique. Physically, this means the fading signals in fading environments with different $f(\alpha, \beta)$ can have the same amplitude distribution.

Furthermore, even if we restrict $f(\alpha, \beta)$ to functions symmetric with respect to $(1 + \alpha)$ and β , the relation between $f(\alpha, \beta)$ and $P(V \leq L)$ is still not unique. We shall demonstrate this nonunique relation specifically by using the results for the m -distributions previously discussed. We notice that for each S , equation (147) is an algebraic equation

* With respect to $(1 + \alpha)$ and β .

for $(S + 1)$ unknowns $\{H_{2s-2v, 2v}(-1, 0)\}_{v=0}^{v=S}$. It is then obvious that there are infinitely many different sets of $\{H_{2s-2v, 2v}(-1, 0)\}_{v=0}^{v=S}$ which will satisfy equation (147) because there is only one equation for $(S + 1)$ unknowns. This nonuniqueness gives a great freedom for the wide variations of the individual term, $H_{2s-2v, 2v}(-1, 0)$, which is the even-order partial derivative of $H(\alpha, \beta)$ at $(\alpha = -1, \beta = 0)$. From the Taylor series (27), it is seen that $H_{2s-2v, 2v}(-1, 0)$ is the coefficient of the even-order term $(1 + \alpha)^{2s-2v}\beta^{2v}$ which is symmetric with respect to $(1 + \alpha)$ and β . Therefore, the relation between $f(\alpha, \beta)$ and $P(V \leq L)$ is not unique even if $f(\alpha, \beta)$ is symmetric with respect to $(1 + \alpha)$ and β .

A more detailed discussion of this nonunique relation in polar coordinates is given in Appendix G.

VI. PHYSICAL MODEL AND RAYLEIGH DISTRIBUTION

In this section, we shall show that specifying a Rayleigh distribution for the amplitude of a complex fading signal $Ve^{i\phi}$ does not necessarily imply that there is a large number of interfering signals; nor does it necessarily imply that the real part and the imaginary part of the fading signal are normal with zero mean.

Let x and y be the real part and the imaginary part respectively of the complex fading signal $Ve^{i\phi}$, and let $F(x, y)$ be the joint probability density function of x and y . Since $V^2 = x^2 + y^2$, then the probability of $V \leq L$ is the probability of x and y falling within the circular region

$$x^2 + y^2 \leq L^2. \quad (150)$$

Therefore, $P(V \leq L)$ is the integration of $F(x, y)$ over the circular region (150); i.e.,

$$P(V \leq L) = \int_{y=-L}^{y=L} \int_{x=-\sqrt{L^2-y^2}}^{x=\sqrt{L^2-y^2}} F(x, y) dx dy. \quad (151)$$

6.1 Number of Interfering Signals

In the most common derivation of the Rayleigh distribution, the fading signal is assumed to consist of a large number of random, independent interfering signals,

$$Ve^{i\phi} = \sum_{i=1}^n E_i e^{i\theta_i} = x + jy. \quad (152)$$

Furthermore, it is assumed that none of the components $\{E_i\}_{i=1}^{i=n}$ predominates in the summation (152). Then by the central limit theorem, one argues that as the number, n , of interfering signals approaches

infinity, the real part x and the imaginary part y of the fading signal $Ve^{i\phi}$ become independent normal random variables with the same variance and zero mean. This implies that V and ϕ are independent and ϕ is uniformly distributed in $(0, 2\pi)$. Under this condition, the distribution of the random amplitude V is Rayleigh.

However, by an observation similar to those in Section V of Part 3 and Appendix G, we realize that the transformation (151) from $F(x, y)$ into $P(V \leq L)$ is not unique. Given an amplitude distribution $P(V \leq L)$, there correspond infinitely many different $F(x, y)$'s. In other words, the independent normal distribution for x and y with the same variance and zero mean is only a sufficient condition but is not a necessary condition for the amplitude V to have a Rayleigh distribution. Since x and y do not have to be normal, then the number n of the interfering signals does not have to be large.

In Appendix G, we have shown that the relation between $P(V \leq L)$ and $F(x, y)$ becomes unique if the following two additional conditions are imposed;

- (i) V and ϕ are independent, and
- (ii) ϕ is uniformly distributed in $(0, 2\pi)$.

For long radio links such as beyond-the-horizon radio links, the conditions *i* and *ii* seem to be applicable. However, for line-of-sight radio links, our experience indicate that the phase ϕ has much higher tendency of wide variation during the deep fade where V is small. This means for short radio links, V and ϕ may not be independent and ϕ may not be uniform. Therefore, in our general analysis we do not impose the conditions *i* and *ii*.

6.2 Mean Values of x and y

In the integral relation (151) the antisymmetric part of $F(x, y)$ contributes nothing to the amplitude distribution $P(V \leq L)$, but does affect the mean value of x and y . Then by adding a suitable* antisymmetric function to $F(x, y)$, the mean values of x and y can be changed arbitrarily without affecting the amplitude distribution $P(V \leq L)$ of the fading signal $Ve^{i\phi}$.

In other words, given an amplitude distribution $P(V \leq L)$ of a complex fading signal $Ve^{i\phi}$, the mean values and the higher moments

* The probability density function $F(x, y)$ must be ≥ 0 for any x and y ; therefore, the symmetric part of $F(x, y)$ must be \geq |antisymmetric part of $F(x, y)$ | when the antisymmetric part is negative.

of x and y are not unique. (However, the moments of the amplitude V are unique.)

Therefore, specifying a Rayleigh distribution for the amplitude V does not necessarily imply that the mean values of x and y are zero. Physically if there is a direct path between the transmitter and the receiver of a radio link, then the mean values of x and y may not be zero. However, the results of this section show that the mere nonzero means of x and y do not necessarily exclude the Rayleigh distribution for the amplitude of the fading signal.

ACKNOWLEDGMENTS

The foundation of this theoretical work is the large amount of experimental data from the work of my colleagues in Bell Laboratories. I wish to express appreciation to W. T. Barnett, A. Vigants, and C. H. Menzel who processed and analyzed the experimental data; and to G. A. Zimmerman who designed the Multiple Input Data Acquisition System for the experiment. I would also like to thank K. Bullington, W. T. Barnett, A. Vigants, and S. O. Rice for many valuable suggestions and discussions. The interest and support of K. Bullington were invaluable.

APPENDIX A

List of Symbols and Their Definitions

A	The constant amplitude of the echo in the one-echo model.
a_0	The zero th order term of the Taylor Series expansion of $\bar{V}_+(L)$ defined in equation (81).
a_n	The coefficient of the n th order term of the Taylor series expansion $\bar{V}_+(L)$ defined in equation (81).
B	$= b_0 b_2 - b_1^2$ as defined in equation (122).
$b_n, n = 0, 1, 2$	Defined by equation (121).
C_4	The coefficient of the fourth order term L^4 of $P(V \leq L)$ in equations (161) and (163).
C_r^n	Defined by equation (30).
d_{2s+2}	The coefficient of the power series representation of $P(V \leq L)$ defined in equations (31) and (34).
$f(\alpha, \beta)$	Joint probability density function of α and β .
$F(x, y)$	Joint probability density function of the real part x and the imaginary part y of the fading signal.
f_a	The frequency of the sine wave.
$g(R)$	The probability density function of the amplitude R of the interfering vector.
$g_n(R)$	The n th order derivative of $g(R)$.
$H(\alpha, \beta)$	The smooth part of $f(\alpha, \beta)$ as defined in equation (23).
$H_{n,m}(\alpha, \beta)$	The partial derivative of $H(\alpha, \beta)$ as defined in equation (29).
$H(-1, 0)$	The value of $H(\alpha, \beta)$ at $(\alpha = -1, \beta = 0)$.
$\bar{H}(-1, 0)$	The average value of $H(\alpha, \beta)$ at $(\alpha = -1, \beta = 0)$ if $H(\alpha, \beta)$ is discontinuous at this point.
$I_n(\sim)$	Modified Bessel function of order n .
L	An arbitrarily specified signal level in the study of the statistics $P(V \leq L)$, $N(L)$ and $\bar{I}(L)$.
m	An integer.
n	An integer.
$N(L)$	Expected number of fades per unit time below the specified signal level L .
$0(L^\eta)$	A symbol to denote a function which goes to zero at a rate equal to or faster than L^η as $L \rightarrow 0$ where $\eta > 0$.
$P(V \leq L)$	Probability that the amplitude V of a fading signal fades below a specified signal level L .

$p(L)$	Probability density of the amplitude V at the specified signal level L .
$p_2(V)$	Probability density function of V . $p_2(V) = p(V)$.
$p(\dot{V}, V)$	Joint probability density function of \dot{V} and V .
$p_1(\dot{V} L)$	Conditional probability density of \dot{V} under the condition $V = L$.
Q	The constant magnitude of the sine wave in the specialized model of a sine wave plus a Gaussian noise. In this paper, $Q = 1$ because of the normalization of the signal level.
$q(R, \theta)$	Joint probability density function of R and θ .
R	The amplitude of the resultant interfering vector $Re^{i\theta}$ of the fading signal model.
$Re^{i\theta}$	The resultant complex interfering vector.
r	An integer.
S	An integer.
t	A variable representing time.
$\bar{t}(L)$	Average duration of fades below L .
V	The amplitude of the envelope of a complex fading signal normalized to the nonfaded value V_{ref} .
\dot{V}	The time derivative of the normalized amplitude V of the fading signal.
$Ve^{i\phi}$	The envelope of the fading signal.
\dot{V}_{rms}	The rms value of the time derivative of V .
$V_{fad}(t)$	The unnormalized amplitude of the random fading signal.
V_{ref}	The nonfaded signal level when there is no interference.
$\dot{V}_+(L)$	Conditional average positive derivative of V as defined in equation (75).
$W(\theta)$	Probability density function of the random relative phase θ of one-echo model.
$W_n(\theta)$	The n th order derivative of the probability density function $W(\theta)$.
x	The real part of the fading signal $Ve^{i\phi}$.
y	The imaginary part of the fading signal $Ve^{i\phi}$.
α	The real part of the interfering vector $Re^{i\theta}$.
β	The imaginary part of the interfering vector $Re^{i\theta}$.
$\Gamma(\sim)$	Gamma function.
γ^2	Defined by equation (141).
η	An arbitrary constant > 0 .
θ	The phase of the resultant interfering vector $Re^{i\theta}$.

θ_L	Defined by equation (53).
μ	($1 - \mu$)/2 is the order of singularity of the joint probability density function $f(\alpha, \beta)$ at ($\alpha = -1, \beta = 0$) as defined in equation (23).
ν	An integer.
$\rho(V, \phi)$	Joint probability density function of the amplitude V and the phase ϕ of the fading signal.
$\sigma(V, \phi)$	A function of V and ϕ satisfying the homogeneous integral equation (207).
ϕ	The phase of the envelope of the complex fading signal.
Ω	The mean square value of an m -distributed random variable.

APPENDIX B

Amplitude Distribution In Polar Coordinates

Since the results of $P(V \leq L)$ for $\mu = 1$ cover a large class of fading problems and since the statistical behavior of the interfering vector is sometimes described by the joint probability density function $q(R, \theta)$ of the interfering vector, we shall also obtain the power series representation of $P(V \leq L)$ in terms of $q(R, \theta)$ when $\mu = 1$. By using the relations:

$$\alpha = R \cos \theta, \quad (153)$$

$$\beta = R \sin \theta, \quad (154)$$

and the Jacobian relation²⁸ between $f(\alpha, \beta)$ and $q(R, \theta)$ one can represent the coefficients $\{d_{2s+2}\}$ of (42) in terms of $q(R, \theta)$. This gives

$$P(V \leq L) = \pi q(1, \pi) L^2 + d_4 L^4 + d_6 L^6 + \dots \quad (155)$$

where

$$d_2 = \pi q(1, \pi) = \pi f(-1, 0), \quad (156)$$

$$d_4 = \frac{\pi}{8} [q(1, \pi) - q_{1,0}(1, \pi) + q_{2,0}(1, \pi) + q_{0,2}(1, \pi)] \text{ etc.,} \quad (157)$$

$$q_{n,m}(R, \theta) = \frac{\partial^{n+m}}{\partial R^n \partial \theta^m} q(R, \theta). \quad (158)$$

In the deep-fade region,

$$P(V \leq L) \xrightarrow[L \rightarrow 0]{} \pi q(1, \pi) L^2, \quad (159)$$

and

$$p(L) \xrightarrow[L \rightarrow 0]{} 2\pi q(1, \pi)L. \quad (160)$$

B.1 Circular Symmetric Probability Density Function

In this subsection, we consider a special case where the interfering random vector, $Re^{i\theta}$, has a circular symmetric probability density function $q(R, \theta)$; i.e., R and θ are independent and θ is uniformly distributed in $(0, 2\pi)$. For this case, let $g(R)$ be the probability density function of the magnitude R of the interfering vector, then

$$P(V \leq L) = \frac{1}{2}g(1)L^2 + C_4L^4 + C_6L^6 + \dots, \quad (161)$$

$$q(R, \theta) = g(R) \frac{1}{2\pi}, \quad (162)$$

$$C_4 = \frac{1}{16} [g(1) - g_1(1) + g_2(1)] \text{ etc.,} \quad (163)$$

$$g_n(1) = \frac{d^n}{dR^n} g(R) |_{R=1}. \quad (164)$$

In the deep-fade region

$$P(V \leq L) \xrightarrow[L \rightarrow 0]{} \frac{1}{2}g(1)L^2. \quad (165)$$

These results are used in Part 3 where we discuss the relation between our generalized analysis and the existing theoretical work.

APPENDIX C

Nonanalytic $H(\alpha, \beta)$

In Section V of Part 1, the analysis is carried out based on the assumption that $H(\alpha, \beta)$ can be expanded into a two-dimensional Taylor series. In this appendix, we shall investigate two cases where $H(\alpha, \beta)$ cannot be expanded into the two-dimensional Taylor series. The objective is to show that from a theoretical viewpoint, the assumption of the Taylor series expansion of $H(\alpha, \beta)$ is not strictly necessary for the validity of the power laws of deep fades discussed in this paper.

C.1 Continuous $H(\alpha, \beta)$ With Unbounded Derivatives

If $H(\alpha, \beta)$ is continuous at $(\alpha = -1, \beta = 0)$ but its first-order partial derivatives and/or its higher order partial derivatives are unbounded at $(\alpha = -1, \beta = 0)$, then $H(\alpha, \beta)$ in the neighborhood of $\alpha = -1$ and

$\beta = 0$ can be written as

$$H(\alpha, \beta) = H(-1, 0) + 0\{[(1 + \alpha)^2 + \beta^2]^{\eta/2}\}, \quad (166)$$

where $1 > \eta > 0$, and

$$0\{[(1 + \alpha)^2 + \beta^2]^{\eta/2}\}$$

is a symbol to denote the component which goes to zero at a rate equal to or faster than that of

$$[(1 + \alpha)^2 + \beta^2]^{\eta/2} \quad \text{as} \quad [(1 + \alpha)^2 + \beta^2] \rightarrow 0.$$

It is obvious that $H(\alpha, \beta)$ given by (166) cannot be expanded into Taylor series because the derivatives of $H(\alpha, \beta)$ are unbounded (i.e., singular) at $(\alpha = -1, \beta = 0)$.

Substituting equations (166) and (23) into the general formulation (20) for $P(V \leq L)$, and carrying out the integration yields

$$P(V \leq L) = \frac{\pi H(-1, 0)}{\mu} L^{2\mu} + O(L^{2\mu+\eta}), \quad (167)$$

$$p(L) = 2\pi H(-1, 0)L^{2\mu-1} + O(L^{2\mu-1+\eta}), \quad (168)$$

where $O(L^{2\mu+\eta})$ is a symbol to denote the high-order terms which go to zero at a rate equal to or faster than that of $L^{2\mu+\eta}$ as $L \rightarrow 0$. Since $\eta > 0$, then in the deep-fade region

$$P(V \leq L) \xrightarrow[L \rightarrow 0]{} \frac{\pi H(-1, 0)}{\mu} L^{2\mu}, \quad (169)$$

which is the same as equation (36). Then the discussions and conclusions in Sections VI, VII, and VIII of Part 1 on the power laws of deep fades for $\mu = 1$, $1 > \mu \geq 1/2$ and $\mu > 1$ are readily applicable to the present case even though the derivatives of $H(\alpha, \beta)$ are unbounded at $(\alpha = -1, \beta = 0)$.

c.2 Discontinuous $H(\alpha, \beta)$

Suppose $H(\alpha, \beta)$ and its derivatives are bounded but are discontinuous at $\beta = 0$ so that

$$\lim_{\beta \rightarrow 0^+} H_{n,m}(\alpha, \beta) \neq \lim_{\beta \rightarrow 0^-} H_{n,m}(\alpha, \beta); \quad (170)$$

i.e.,

$$H_{n,m}(\alpha, 0^+) \neq H_{n,m}(\alpha, 0^-)$$

$$n = 0, 1, 2, \dots, \quad m = 0, 1, 2, \dots. \quad (171)$$

Then on each side of $\beta = 0$, the one-sided Taylor series expansion of $H(\alpha, \beta)$ is applicable. One for $\beta > 0$ and another for $\beta < 0$. Substituting these two Taylor series and equation (23) into the general formulation (20) for $P(V \leq L)$ and carrying out the integration, one can show that

$$P(V \leq L) \xrightarrow[L \rightarrow 0]{} \frac{\pi \bar{H}(-1, 0)}{\mu} L^{2\mu}, \quad (172)$$

$$p(L) \xrightarrow[L \rightarrow 0]{} 2\pi \bar{H}(-1, 0) L^{2\mu-1}, \quad (173)$$

where

$$\bar{H}(-1, 0) = \frac{1}{2}[H(-1, 0^+) + H(-1, 0^-)] \quad (174)$$

is the average value of the discontinuous $H(\alpha, \beta)$ at $(\alpha = -1, \beta = 0)$.

It is seen that equation (172) is also the same as equation (36) except for the proper interpretation of $\bar{H}(-1, 0)$ when $H(\alpha, \beta)$ is discontinuous at $(\alpha = -1, \beta = 0)$. Therefore, the discussions and conclusions of Sections VI, VII, and VIII of Part 1 are also applicable to the present case.

APPENDIX D

Integration for Power Series of Amplitude Distribution

Substituting (27) and (23) into (20) gives

$$P(V \leq L) = \sum_{n=0}^{n=\infty} \frac{1}{n!} \sum_{r=0}^{r=n} C_r^n H_{n-r,r}(-1, 0) I_{n-r,r}, \quad (175)$$

where

$$I_{n-r,r} = \int_{\beta=-L}^{\beta=L} \int_{\alpha=-1-\sqrt{L^2-\beta^2}}^{\alpha=-1+\sqrt{L^2-\beta^2}} [(1+\alpha)^2 + \beta^2]^{\mu-1} (1+\alpha)^{n-r} \beta^r d\alpha d\beta. \quad (176)$$

From (176) it is seen that if either $(n - r)$ or r is an odd integer, then $I_{n-r,r}$ vanishes because the integrand is antisymmetric. Therefore, $I_{n-r,r}$ does not vanish only when both $(n - r)$ and r are even integers. Then let $n = 2S$ and $r = 2\nu$. Equation (176) becomes

$$\begin{aligned} I_{2S-2\nu, 2\nu} &= \int_{\beta=-L}^{\beta=L} \int_{\alpha=-1-\sqrt{L^2-\beta^2}}^{\alpha=-1+\sqrt{L^2-\beta^2}} [(1+\alpha)^2 + \beta^2]^{\mu-1} (1+\alpha)^{2S-2\nu} \beta^{2\nu} d\alpha d\beta \\ &= \frac{2\Gamma(S-\nu+\frac{1}{2})\Gamma(\nu+\frac{1}{2})}{(2S+2\mu)\Gamma(S+1)} L^{2S+2\mu}. \end{aligned} \quad (177)$$

Combining (175) and (177) gives

$$P(V \leq L) = \sum_{S=0}^{S=\infty} L^{2S+2\mu} \cdot \left[\frac{2}{(2S)!} \sum_{\nu=0}^{\nu=S} \frac{C_{2\nu}^{2S} \Gamma(S - \nu + \frac{1}{2}) \Gamma(\nu + \frac{1}{2})}{(2S + 2\mu) \Gamma(S + 1)} H_{2S-2\nu, 2\nu}(-1, 0) \right] \quad (178)$$

$$= \sum_{S=0}^{S=\infty} d_{2S+2} L^{2S+2\mu}, \quad (179)$$

where

$$d_{2S+2} = \frac{2}{(2S)!} \sum_{\nu=0}^{\nu=S} \frac{C_{2\nu}^{2S} \Gamma(S - \nu + \frac{1}{2}) \Gamma(\nu + \frac{1}{2})}{(2S + 2\mu) \Gamma(S + 1)} H_{2S-2\nu, 2\nu}(-1, 0). \quad (180)$$

APPENDIX E

Derivation for Expected Numbers of Fades

Suppose $T = t_2 - t_1$ is the time interval in which we want to find the expected number of times that the random fluctuating signal $V(t)$ crosses the signal level $V = L$. This interval is divided into a large number of smaller intervals of width Δt so short that each contains no more than one level crossing. We first consider the expected number of upward level crossings. The downward level crossings can be treated similarly.

In an infinitesimal interval Δt , the conditions for an upward level crossing of $V(t)$ are

$$\dot{V}(t) = \frac{\partial V(t)}{\partial t} > 0 \quad (181)$$

$$\dot{V}(t) \Delta t > [L - V(t)] > 0 \quad (182)$$

These two conditions are shown graphically in Fig. 8. On a \dot{V} versus V plane, the region in which \dot{V} and V satisfy conditions (181) and (182) are shown as the shaded area in Fig. 9. The integration of the joint probability density $p(\dot{V}, V)$ over this range will give the probability that $V(t)$ will have an upward level crossing in Δt ,

$$P_{\Delta t}(L) = \int_{\dot{V}=0}^{\dot{V}=\infty} \int_{V=L-\dot{V}\Delta t}^L p(\dot{V}, V) dV d\dot{V} \quad (183)$$

$$\cong \Delta t \int_{\dot{V}=0}^{\dot{V}=\infty} \dot{V} p(\dot{V}, V) \Big|_{V=L} d\dot{V}. \quad (184)$$

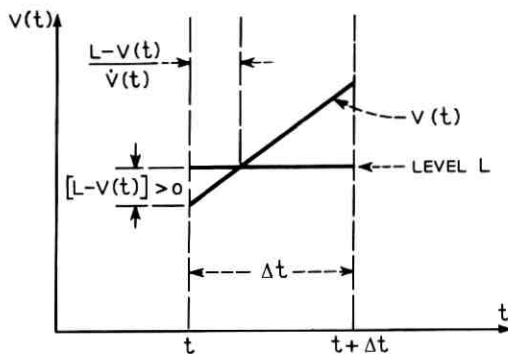


Fig. 8—The conditions for an upward level crossing of $V(t)$ in an interval Δt .

The expected number $N_{\text{up}}(L)$ of upward level crossings per unit time is

$$N_{\text{up}}(L) = \frac{P_{\Delta t}(L)}{\Delta t} = \int_{\dot{V}=0}^{\dot{V}=\infty} \dot{V} p(\dot{V}, V) \Big|_{v=L} d\dot{V}. \quad (185)$$

Similarly, the expected number of downward level crossings per unit time is

$$N_{\text{down}}(L) = \int_{\dot{V}=-\infty}^{\dot{V}=0} |\dot{V}| p(\dot{V}, V) \Big|_{v=L} d\dot{V}. \quad (186)$$

The total expected number of level crossings per unit time is

$$\begin{aligned} N_c(L) &= N_{\text{up}}(L) + N_{\text{down}}(L) \\ &= \int_{\dot{V}=-\infty}^{\dot{V}=\infty} |\dot{V}| p(\dot{V}, V) \Big|_{v=L} d\dot{V}. \end{aligned} \quad (187)$$

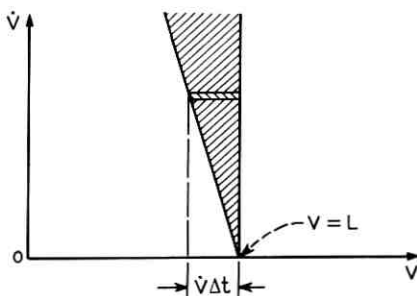


Fig. 9—The region in which \dot{V} and V satisfy the conditions for an upward level crossing.

The expected number of fades per unit time below $V = L$ is

$$\begin{aligned} N(L) &= \frac{1}{2}N_c(L) = N_{\text{up}}(L) = N_{\text{down}}(L) \\ &= \int_{V=0}^{\dot{V}=\infty} \dot{V} p(\dot{V}, V) \Big|_{V=L} d\dot{V}. \end{aligned} \quad (188)$$

APPENDIX F

Log Normal Behavior of M-Distributions Near the RMS Value

Let

$$Z = 20 \log_{10} \left(\frac{L}{\sqrt{\Omega}} \right) = 20[\log_{10} L - \log_{10} \sqrt{\Omega}] \quad (189)$$

be the signal level in dB with respect to its rms value $\sqrt{\Omega}$. Equation (189) implies

$$\frac{Z}{M} = \ln \left(\frac{L}{\sqrt{\Omega}} \right), \quad (190)$$

$$\frac{L}{\sqrt{\Omega}} = \exp \left(\frac{Z}{M} \right), \quad (191)$$

$$\frac{\partial L}{\partial Z} = \frac{\sqrt{\Omega}}{M} \exp \left(\frac{Z}{M} \right) = \frac{L}{M}, \quad (192)$$

where

$$M = 20 \log_{10} e = 8.686 \text{ dB.} \quad (193)$$

Then the probability density functions of L and Z are related by the Jacobian relation:^{28,18}

$$h(Z) = p(L) \left| \frac{\partial L}{\partial Z} \right| = \frac{L}{M} p(L). \quad (194)$$

Substituting the m -distribution (143) and equation (191) into (194) yields the following probability density of Z :

$$\begin{aligned} h(Z) &= \frac{2m_m}{M\Gamma(m)} \left(\frac{L}{\sqrt{\Omega}} \right)^{2m} \exp \left[\frac{-mL^2}{\Omega} \right] \\ &= \frac{2m^m}{M\Gamma(m)} \exp \left\{ m \left[\frac{2Z}{M} - \exp \left(\frac{2Z}{M} \right) \right] \right\}. \end{aligned} \quad (195)$$

Substituting the following power series

$$\exp \left(\frac{2Z}{M} \right) = \sum_{n=0}^{\infty} \frac{1}{n!} \left(\frac{2Z}{M} \right)^n \quad (196)$$

into (195) gives

$$h(Z) = \left[\frac{2m^m}{M\Gamma(m)} e^{-m} \right] \exp \left\{ -m \left[2\left(\frac{Z}{M}\right)^2 + \sum_{n=3}^{\infty} \frac{1}{n!} \left(\frac{2Z}{M}\right)^n \right] \right\}. \quad (197)$$

If the signal level L is very close to its rms value $\sqrt{\Omega}$, then

$$\left| \frac{L}{\sqrt{\Omega}} - 1 \right| \ll 1, \quad (198)$$

$$\left| \frac{2Z}{M} \right| = 2 \left| \ln \frac{L}{\sqrt{\Omega}} \right| \ll 1, \quad (199)$$

for

$$\begin{aligned} |Z| &\ll M/2 \\ &= 4.3 \text{ dB} \end{aligned}$$

Under this condition, we have

$$\sum_{n=3}^{\infty} \frac{1}{n!} \left(\frac{2Z}{M}\right)^n \ll 2\left(\frac{Z}{M}\right)^2. \quad (200)$$

Then $h(Z)$ in equation (197) becomes

$$h(Z) \cong \left[\frac{2m^m}{M\Gamma(m)} e^{-m} \right] \exp \left[-2m\left(\frac{Z}{M}\right)^2 \right], \quad (201)$$

which is a normal distribution for Z . Substituting (190) and (201) into (194) yields

$$p(L) \cong \left[\frac{2m^m}{L\Gamma(m)} e^{-m} \right] \exp [-2m(\ln L - \ln \sqrt{\Omega})^2], \quad (202)$$

which is a log normal distribution for L . Therefore, within the range $|z| \ll M/2 = 4.3 \text{ dB}$, all the m -distributions for any $m \geq 1/2$ behave like a log normal distribution given by (202).

APPENDIX G

Nonunique Relation Between $P(V \leq L)$ and $f(\alpha, \beta)$

In the definition of the fading signal model discussed in Section II of Part 1, the four random variables V , ϕ , α , and β are related by

$$\begin{cases} 1 + \alpha = V \cos \phi \\ \beta = V \sin \phi \end{cases}. \quad (203)$$

Let $\rho(V, \phi)$ be the joint probability density function of the amplitude V and the phase ϕ of the fading signal. By the Jacobian^{28,18} of the transformation (203), it is easily shown that

$$\rho(V, \phi) = \sqrt{(1 + \alpha)^2 + \beta^2} f(\alpha, \beta) = V f(V \cos \phi, V \sin \phi). \quad (204)$$

In this appendix we shall show that the relation between $P(V \leq L)$ and $\rho(V, \phi)$ is not unique. This then implies that the relation between $P(V \leq L)$ and $f(\alpha, \beta)$ is also nonunique because of the simple algebraic relation (204) between $\rho(V, \phi)$ and $f(\alpha, \beta)$.

In the study of the amplitude distribution $P(V \leq L)$ of a complex fading signal $Ve^{i\phi}$, it is often assumed that V and ϕ are independent with ϕ uniformly distributed in $(0, 2\pi)$. However, in the study of interference, distortion, FM radio system, radio navigation system, etc., many authors^{27,43,44,19} have investigated the distribution of the random phase, $\phi(t)$. These results show that the distribution of phase is not always uniform. Furthermore, when the signal is weak (i.e., V is small), the phase is more likely to vary over wider range. This means the random variables V and ϕ are somewhat correlated. Therefore, V and ϕ generally can be either dependent or independent and ϕ can be either uniformly or nonuniformly distributed.

By definition,^{28,18} the probability density $p(V)$ of V is the integration of $\rho(V, \phi)$ over the entire range of ϕ ; i.e.,

$$p(V) = \int_{\phi=0}^{\phi=2\pi} \rho(V, \phi) d\phi. \quad (205)$$

Furthermore, the cumulative amplitude distribution $P(V \leq L)$ is the integration of $p(V)$ from $V = 0$ to $V = L$. Therefore,

$$P(V \leq L) = \int_{V=0}^{V=L} \int_{\phi=0}^{\phi=2\pi} \rho(V, \phi) d\phi dV. \quad (206)$$

Given a joint probability density function $\rho(V, \phi)$, then $P(V \leq L)$ can be calculated by (206).

On the other hand, given an amplitude distribution $P(V \leq L)$, equation (206) is an integral equation to solve for $\rho(V, \phi)$. An immediate question arising in solving the integral equation (206) is the uniqueness of the solution. A procedure to test the uniqueness of the solution is to consider the following homogeneous equation

$$0 = \int_{V=0}^{V=L} \int_{\phi=0}^{\phi=2\pi} \sigma(V, \phi) d\phi dV. \quad (207)$$

If the homogeneous equation (207) has a nontrivial solution, then the

solution of (206) is not unique because, given any particular solution $\rho_P(V, \phi)$ of (206), then

$$\rho(V, \phi) = \rho_P(V, \phi) + c\sigma(V, \phi) \quad (208)$$

is also a solution of (206) where c is an arbitrary constant.*

It is obvious that all of the following functions

$$\sigma_n(V, \phi) = \xi_n(V) \sin(n\phi) + \zeta_n(V) \cos(n\phi); \quad n = \pm 1, \pm 2, \pm 3, \dots \quad (209)$$

are nontrivial solutions of the homogeneous equation (207) where $\xi_n(V)$ and $\zeta_n(V)$ are arbitrary functions of V . Notice that the nontrivial solutions (209) contain both symmetric and antisymmetric functions of ϕ . Furthermore, any arbitrary linear combination of $\{\sigma_n(V, \phi)\}$ is also a solution of the homogeneous equation (207). By the experience of Fourier series synthesis technique, we know that the linear combination of the set $\{\sigma_n(V, \phi)\}$ is able to represent a very large class of either simple or complicated functions of V and ϕ .

Therefore, given an amplitude distribution $P(V \leq L)$, the integral equation (206) has infinitely many different solutions.

On the other hand, in equation (206), if one imposes the following two additional conditions:

- (i) V and ϕ are independent, and
- (ii) ϕ is uniformly distributed in $(0, 2\pi)$,

then

$$\rho(V, \phi) = \frac{1}{2\pi} p(V) = \frac{1}{2\pi} \frac{\partial}{\partial L} P(V \leq L) \Big|_{L=V} \quad (210)$$

is the only possible solution of (206).

REFERENCES

1. Barnett, W. T., "Microwave Line-of-Sight Propagation With and Without Frequency Diversity," B.S.T.J., 49, No. 8, part 2 (October 1970), pp. 1827-1871.
2. Barnett, W. T. and Lin, S. H., unpublished work on the experimental data of microwave line-of-sight propagation.
3. Vigants, A., "Number and Duration of Fades at 6 and 4 GHz," B.S.T.J., 50, No. 3 (March 1971), pp. 815-841.
4. Vigants, A., "The Number of Fades in Space Diversity Reception," B.S.T.J., 49, No. 7, part 2 (September 1970), pp. 1513-1530.
5. Vigants, A., "Space-Diversity Performance as a Function of Antenna Separation," IEEE Trans. Commun. Tech., COM-16 (December 1968), pp. 831-836.

* Since the probability density function $\rho(V, \phi)$ must be ≥ 0 for any V and ϕ , then $\rho_p(V, \phi)$ must be $\geq |\sigma(V, \phi)|$ when $\sigma(V, \phi)$ is negative.

6. Vigants, A., "The Number of Fades and Their Durations on Microwave Line-of-Sight Links With and Without Space Diversity," Conf. Record, 1969 Int. Conf. Commun. (June 9-11, 1969), Boulder, Colorado, pp. 3-7 to 3-11.
7. DeLange, O. E., "Propagation Studies at Microwave Frequencies by Means of Very Short Pulses," B.S.T.J., 31, No. 1 (January 1952), pp. 91-103.
8. Sharpless, W. M., "Measurement of the Angle of Arrival of Microwaves," Proc. IRE, 34 (November 1946), pp. 837-845.
9. Crawford, A. B. and Sharpless, W. M., "Further Observations of the Angle of Arrival of Microwaves," Proc. IRE, 34 (November 1946), pp. 845-848.
10. Crawford, A. B. and Jakes, W. C., "Selective Fading of Microwaves," B.S.T.J., 31, No. 1 (January 1952), pp. 68-90.
11. Pearson, K. W., "Method for the Prediction of the Fading Performance of a Multisection Microwave Link," Proc. IEE (London), 112, No. 7 (July 1965), pp. 1291-1300.
12. Crawford, A. B., Hogg, D. C., and Kummer, W. H., "Studies in Tropospheric Propagation Beyond the Horizon," B.S.T.J., 38, No. 5, part 2 (September 1959), pp. 1067-1178.
13. Harkless, E. T. and Lenzing, H. F., "Excitation of Higher Order Antenna Modes by Multipath Propagation," IEEE Trans. Comm. Tech., COM-15, No. 4 (August 1967), pp. 597-603.
14. Makino, H. and Morita, K., "Design of Space Diversity Receiving and Transmitting Systems for Line-of-Sight Microwave Links," IEEE Trans. Comm. Tech., COM-15, No. 4 (August 1967), pp. 603-614.
15. Beckmann, P. and Spizzichino, A., *The Scattering of Electromagnetic Waves from Rough Surfaces*, London/New York: Pergamon [Macmillan], 1963.
16. Jelonek, Z., Fitch, E., and Chalk, J. H. H., "Diversity Reception; Statistical Evaluation of Possible Gain," Wireless Engineer (February 1947), pp. 54-62.
17. Gudmandsen, P. and Larsen, B. F., "Statistical Data for Microwave Propagation Measurements on Two Overseas Paths in Denmark," IRE Trans. Ant. Prop., AP-5, (July 1957), pp. 255-259.
18. Beckmann, P., *Probability in Communication Engineering*, New York: Harcourt, Brace and World, Inc., 1967.
19. Hoyt, R. S., "Probability Functions for the Modulus and Angle of Normal Complex Variate," B.S.T.J., 26, No. 2 (April 1947), pp. 318-359.
20. Fulks, W., *Advanced Calculus*, New York: John Wiley and Sons, Inc., 1961.
21. Beckmann, P., "Amplitude Probability Distribution of Atmospheric Radio Noise," Radio Science, J. Research, NBS, 68D, No. 6 (June 1964), pp. 723-736.
22. Barnett, W. T., "Occurrence of Selective Fading as a Function of Path Length, Frequency, and Geography," 1969 USNC/URSI Spring Meeting, Washington, D. C. (April 21-24, 1969).
23. Barnett, W. T., "Multipath Fading as a Function of Frequency from the 1966, Ohio Data," private communication.
24. Barnett, W. T. and Vigants, A., "Occurrence of Multipath Fading in the United States and Japan," to be published in Proceedings of the IEEE.
25. Morita, K., "Prediction of Rayleigh Fading Occurrence Probability of Line-of-Sight Microwave Links," Review Electr. Commun. Lab. (Japan), 18, No. 11-12 (November-December 1970), pp. 810-822.
26. Rice, S. O., "Mathematical Analysis of Random Noise," B.S.T.J., 23, No. 3 (July 1944), pp. 282-332, and 24, No. 1 (January 1945), pp. 46-156.
27. Rice, S. O., "Statistical Properties of a Sine Wave Plus Random Noise," B.S.T.J., 27, No. 1 (January 1948), pp. 109-157.
28. Papoulis, A., *Probability, Random Variables, and Stochastic Processes*, New York: McGraw-Hill Book Co., 1965.
29. Clarke, R. H., "A Statistical Theory of Mobile Radio Reception," B.S.T.J., 47, No. 6, part 1 (July-August 1968), pp. 957-1000.
30. Ossanna, J. F. Jr., "A Model for Mobile Radio Fading Due to Building Reflections: Theoretical and Experimental Fading Waveform Power Spectra," B.S.T.J., 43, No. 6, part 3 (November 1964), pp. 2935-2971.
31. Gans, M. J., "A Power Spectral Theory of Mobile Radio Propagation," unpublished work.

32. Rice, S. O., "Distribution of the Duration of Fades on Radio Transmission," *B.S.T.J.*, *37*, No. 3, part 1 (May 1958), pp. 581-635.
33. Norton, K. A., Vogler, L. E., Mansfield, W. V., and Short, P. J., "The Probability Distribution of the Amplitude of a Constant Vector and a Rayleigh Distributed Vector," *Proc. IRE*, *43* (October 1955), pp. 1354-1361.
34. Bennet, W. R., "Distribution of the Sum of Randomly Phased Components," *Quart. Appl. Math.*, *5*, No. 4 (January 1948), pp. 385-393.
35. Rice, S. O., "Distribution of a Sum of n Sine Waves," *Quart. Appl. Math.*, *12* (January 1955), pp. 375-381.
36. Greenwood, J. A. and Durand, D., "The Distribution of Length and Components of the Sum of n Random Unit Vectors," *Ann. Math. Stat.*, *26* (June 1955), pp. 233-246.
37. Slack, M., "The Probability Distributions of Sinusoidal Oscillations Combined in Random Phase," *J.I.E.E.*, Pt. III, *93*, 1946, pp. 76-82.
38. Rosenbaum, A. S., "Binary PSK Error Probabilities With Multiple Cochannel Interferences," *IEEE Trans. Comm. Tech.*, *COM-18*, No. 3 (June 1970), pp. 241-253.
39. Nakagami, M., "The m -Distribution—A General Formula of Intensity Distribution of Rapid Fading," *Statistical Methods in Radio Wave Propagation*, W. C. Hoffman (ed.), Oxford, Pergamon, 1960, pp. 3-36.
40. DeWolf, A. A., "Saturation of Irradiance Fluctuations due to Turbulent Atmosphere," *J. Opt. Soc. Amer.*, *58* (1968), pp. 461-466.
41. Fried, D. L., Mevers, G. E. and Keister, M. P. Jr., "Measurements of Laser Beam Scintillation in the Atmosphere," *J. Opt. Soc. Amer.*, *57*, No. 6 (June 1967), pp. 787-797.
42. Deitz, P. H. and Wright, N. J., "Saturation of Scintillation Magnitude in Near Earth Optical Propagation," *J. Opt. Soc. Amer.*, *59*, No. 5 (May 1969), pp. 527-535.
43. Norton, K. A., Shultz, E. L. and Yarbrough, H., "The Probability Distribution of the Phase of the Resultant Vector Sum of a Constant Vector Plus a Rayleigh Distributed Vector," *J. Appl. Phys.*, *23*, No. 1 (January 1952), pp. 137-141.
44. Goldman, J., "The Probability Density Function of the Phase Angle of a Cosinusoid Plus Interference and Noise with Application to PSK Systems," unpublished work.

Contributors to This Issue

SYED V. AHAMED, B.E., 1957, University of Mysore, India; M.E., 1958, Indian Institute of Science; Ph.D., 1962, University of Manchester, U.K.; Post Doctoral Research Fellow, 1963, University of Delaware; Assistant Professor, 1964, University of Colorado; Bell Telephone Laboratories, 1966—. Mr. Ahamed was working in Computer Aided Engineering Analysis and Software Design at Whippany. Presently he is investigating the applications of Algebraic Techniques for Domain Circuits.

DAN L. BISBEE, B.S., 1965, Monmouth College; Bell Telephone Laboratories, 1955—. Mr. Bisbee has worked with the design and measurement of millimeter waveguide components. At present he is engaged in the study and measurement of optical transmission losses in bulk glass and optical fiber waveguides.

PAUL J. BURKE, B.S., 1940, City College of New York; Ed. M., 1950, Harvard University; Ph.D., 1966, Columbia University; Bell Telephone Laboratories, 1953—. Mr. Burke's work is in the field of telephone traffic theory and its applications. Member, Phi Beta Kappa, Phi Delta Kappa, Sigma Xi, Operations Research Society of America, Institute of Mathematical Statistics.

NUGGEHALLY S. JAYANT, B.Sc., 1962, University of Mysore (India); B. E. (Distinction), 1965, and Ph.D., 1970, Indian Institute of Science, Bangalore; Research Associate, 1967–68, Stanford Electronics Laboratories; Bell Telephone Laboratories, 1968—. Mr. Jayant has worked on digital communication in the presence of burst-noise, and on the detection of fading signals. His current interests include source encoding and pattern discrimination. Member, IEEE.

ROBERT H. KRAMBECK, B.E., 1965, City College of New York; M.S.E.E., 1966, and Ph.D., 1969, Carnegie-Mellon University; Bell Telephone Laboratories, 1968—. Mr. Krambeck has been engaged in the analysis and development of new types of memory elements. Member, IEEE.

SING-HSIUNG LIN, B.S.E.E., 1963, National Taiwan University; M.S.E.E., 1966, and Ph.D., 1969, University of California, Berkeley;

Bell Telephone Laboratories, 1969—. Mr. Lin is working on propagation effects, such as multipath interference and rain attenuation, on radio transmission systems. Member, IEEE, Sigma Xi.

S. D. PERSONICK, B.E.E., 1967, City College of New York; S.M. in E.E., 1968, E.E., 1969, and Sc.D., 1969, Massachusetts Institute of Technology; Bell Telephone Laboratories, 1967—. Mr. Personick is engaged in studies of optical communication systems and cable transmission systems.

V. K. PRABHU, B.E. (Dist.), 1962, Indian Institute of Science, Bangalore, India; S.M., 1963, and Sc.D., 1966, Massachusetts Institute of Technology; Bell Telephone Laboratories, 1966—. Mr. Prabhu has been concerned with various theoretical problems in solid-state microwave devices, noise, and optical communication systems. Member, IEEE, Eta Kappa Nu, Sigma Xi, Tau Beta Pi, AAAS.

LAWRENCE R. RABINER, S.B. and S.M., 1964, and Ph.D. (E.E.), 1967, Massachusetts Institute of Technology; Bell Telephone Laboratories, 1962–1964, 1967—. Mr. Rabiner has worked on digital circuitry, military communications problems, and problems in binaural hearing. Since 1967, he has been engaged in research on speech communication, signal analysis, digital filtering, and techniques for waveform processing. Member, Eta Kappa Nu, Sigma Xi, Tau Beta Pi, IEEE; Fellow, Acoustical Society of America. He is chairman of the IEEE Technical Committee on Digital Signal Processing, and member of the technical committees on speech communication of both the IEEE and the Acoustical Society.

A. E. ROSENBERG, S.B. and S.M. in E.E., 1960, Massachusetts Institute of Technology; Ph.D., 1964, University of Pennsylvania; Bell Telephone Laboratories, 1964—. Mr. Rosenberg is a member of the Acoustics Research Department currently engaged in studies in speech perception and speaker verification. Member, IEEE, Acoustical Society of America.

RONALD W. SCHAFER, B.S. (E.E.), 1961, and M.S. (E.E.), 1962, University of Nebraska; Ph.D., 1968, Massachusetts Institute of Technology; Bell Telephone Laboratories, 1968—. Mr. Schafer has been engaged in research on digital waveform processing techniques and

speech communication. He is a member of the IEEE Technical Committees on Digital Signal Processing and Speech Communication. Member, Phi Eta Sigma, Eta Kappa Nu, Sigma Xi, IEEE, Acoustical Society of America.

